MINISTRY OF EDUCATION
AND TRAINING

VIETNAM ACADEMY
OF SCIENCE AND TECHNOLOGY

GRADUATE UNIVERSITY OF SCIENCE AND TECHNOLOGY

BÙI MINH HUỆ

STUDY OF ISOMERIC RATIO AND RELATED EFFECTS IN PHOTONUCLEAR AND NEUTRON CAPTURE REACTIONS

ATOMIC AND NUCLEAR PHYSICS DOCTORAL THESIS

Ha Noi – 2023

BỘ GIÁO DỤC VÀ ĐÀO TẠO

VIỆN HÀN LÂM KHOA HỌC
VÀ CÔNG NGHỆ VIỆT NAM

HỌC VIỆN KHOA HỌC VÀ CÔNG NGHỆ

BÙI MINH HUỆ

NGHIÊN CỨU TỶ SỐ ĐỒNG PHÂN VÀ CÁC HIỆU ỨNG LIÊN QUAN TRONG PHẢN ỨNG QUANG HẠT NHÂN VÀ PHẢN ỨNG BẮT NEUTRON

LUẬN ÁN TIẾN SỸ VẬT LÝ NGUYÊN TỬ VÀ HẠT NHÂN

Hà Nội – 2023

BỘ GIÁO DỤC
VÀ ĐÀO TẠO

VIỆN HÀN LÂM KHOA HỌC
VÀ CÔNG NGHỆ VIỆT NAM

HỌC VIỆN KHOA HỌC VÀ CÔNG NGHỆ

Bùi Minh Huệ

NGHIÊN CỨU TỶ SỐ ĐỒNG PHÂN VÀ CÁC HIỆU ỨNG LIÊN QUAN TRONG PHẢN ỨNG QUANG HẠT NHÂN VÀ PHẢN ỨNG BẮT NEUTRON

LUẬN ÁN TIẾN SĨ VẬT LÝ NGUYÊN TỬ VÀ HẠT NHÂN

Mã số: 9440106

Xác nhận của Học viện Khoa học và Công nghệ	Người hướng dẫn 1	Người hướng dẫn 2
KT. GIÁM ĐỐC PHÓ GIÁM ĐỐC HỌC VIỆN KHOA HỌC VÀ CÔNG NGHỆ Nguyễn Thị Trung	GS.TS. Trần Đức Thiệp	TS. Sergey Mikhailovich Lukyanov

Hà Nội - 2023

MINISTRY OF EDUCATION
AND TRAINING

VIETNAM ACADEMY
OF SCIENCE AND TECHNOLOGY

GRADUATE UNIVERSITY OF SCIENCE AND TECHNOLOGY

BÙI MINH HUỆ

Major: Atomic and Nuclear Physics

Code: 9440106

STUDY OF ISOMERIC RATIO AND RELATED EFFECTS IN PHOTONUCLEAR AND NEUTRON CAPTURE REACTIONS

ATOMIC AND NUCLEAR PHYSICS DOCTORAL THESIS

SUPERVISORS:

1. Prof. Dr Trần Đức Thiệp
2. Dr. Sergey Mikhailovich Lukyanov

Ha Noi – 2023

Declaration of Authorship

I, Bui Minh Hue, declare that this thesis titled, "STUDY OF ISOMERIC RATIO AND RELATED EFFECTS IN PHOTONUCLEAR AND NEUTRON CAPTURE REACTIONS" and the work presented in it are my own. I confirm that:

- This work was carried out wholly or mainly while in candidature for a research degree at the Graduate University of Science and Technology.
- Where any part of this thesis has previously been submitted for a degree or any other qualification at this Graduate University or any other institution, this has been clearly stated.
- The data in this thesis have not been used in other publications by anyone else.
- Where I have consulted the published work of others, this has always been clearly attributed.
- Where I have quoted from the work of others, the source is always given. With the exception of such quotations, this thesis is entirely my own work.
- I have acknowledged all the main sources of help.

Signed:

Date: 08/03/2023

Abstract

The isomeric ratio (IR) of ^{152m1,m2}Eu, $^{195m,g;197m,g}$Hg, ^{115m,g}Cd, ^{109m,g}Pd, ^{137m,g}Ce and ^{81m,g}Se produced from photonuclear reactions (γ, n) with bremsstrahlung endpoint energies in the Giant Dipole Resonance region and IR of $^{115m,g;117m,g}$Cd, $^{109m,g;111m,g}$Pd, ^{137m,g}Ce and ^{81m,g}Se in thermal-epithermal neutron capture reactions (n, γ) have been experimentally determined using the activation technique and measurement of off-line γ-ray spectroscopy. The bremsstrahlung photons and neutrons were generated using the MT-25 Microtron of the Flerov Laboratory of Nuclear Reaction (FLNR), JINR, Dubna, Russia. Radioisotope activity was determined with a high-resolution γ-ray HPGe detector and dedicated analysis software. This work reports, obtained from reactions (γ, n), the IRs of ^{195m,g}Hg within 14 - 24 MeV, ^{197m,g}Hg within 18 - 24 MeV, and ^{152m1,m2}Eu at 19, 21 and 23 MeV for the first time. Furthermore, the IR results of $^{109m,g;111m,g}$Pd and $^{115m,g;117m,g}$Cd in mixed thermal resonant neutron capture reactions (n, γ), as well as those of ^{111m,g}Pd in the resonance neutron capture reaction (n, γ) have been the first measurements. The impact of the nucleon configuration, spin difference, excitation energy, and reaction channel effects on the experimental IRs was considered. The measured IRs were compared not only with the literature but also with the theoretically calculated IRs for the cases in the photonuclear reaction. The calculated IRs were yielded from calculated cross sections based on TALYS 1.95 code in conjunction with simulated bremsstrahlung based on the GEANT4 toolkit. Six-level density models and eight radiative strength functions were taken into consideration for the theoretical calculations.

Acknowledgements

Honestly, I could not complete this thesis without the support and help of many people. First and foremost, I owe special and great thanks to my supervisors, Prof.Dr.Tran Duc Thiep and Dr.Sergey Mikhailovich Lukyanov, for allowing me to start my Ph.D. and for their guidance, support, and inspiration. I am always thankful for them and consider them not only my supervisor, but also my father. Prof.Dr.Tran Duc Thiep inspired and encouraged me on the abrupt road to science since 2012, when I started as a junior researcher at the Center for Nuclear Physics, Institute of Physics. He was always available to illuminate my questions. I have gained a lot of knowledge and experience from him in research, work, and life.

I would also like to thank Dr.Truong Thi An, Dr.Phan Viet Cuong and Dr.Le Tuan Anh for cooperating on the research projects. I am grateful to the Board of Directors, Mrs.Nguyen Thi Dieu Hong, and the staff of the Institute of Physics, as well as my colleagues at the Center for Nuclear Physics for always helping, encouraging, and giving me convenience.

I had precious time and beautiful memories in Dubna. I always remember the warm hugs and the advice of Prof.Dr.Y.E.Penionzhkevich. I am thankful for the opportunity to exchange ideas and discuss work with my colleagues at the FLNR, JINR, made me feel like part of their group. I express my deepest gratitude to the MT-25 Microtron crew for providing the irradiation beam as well as the chemistry of the transactinides department of the Flerov Laboratory of Nuclear Reaction, JINR for furnishing the experimental apparatus. I am also grateful to Mrs.Trinh Thi Thu My and my Vietnamese friends in Dubna for making my stay very pleasant. I always had you by my side when I took a lunch break or gathered for BBQs on the Volga riverside.

I am also thankful to Dr.S.Nishimura for lending me the equipment when I was at RIKEN.

I am grateful to the Board of Directors and employees of the Graduate University of Science and Technology (GUST) for helping and supporting me throughout the process of doing this thesis. I would like to acknowledge the scientific research support of the GUST for excellent Ph.D. students in 2021. And I offer my gratitude and special thanks to Vingroup JSC and Ph.D. Scholarship Programme of Vingroup Innovation Foundation (VINIF), Institute of Big Data, for funding and supporting my Ph.D. studies within two years under the VINIF.2020.TS.18 and VINIF.2021.TS.081 codes.

Last but not least, from the bottom of my heart, I would like to express my deepest thanks to my family and my parents-in-law who supported and cherished me on this long journey. I am very grateful to my aunt, N.T.Mai, for helping and taking care of me in the stressful period of finalizing this thesis. Especially, I would like to thank my honey husband, Dr.Vi Ho Phong, for helping me a lot with coding. He has always encouraged and given me a happy life. He is the main motivation for me to carry out the present thesis.

Contents

Declaration of Authorship i

Abstract ii

Acknowledgements iii

Contents iv

List of Abbreviations vii

List of Physical Quantities ix

List of Tables xi

List of Figures xiii

Introduction xvii

1 Overview 1

1.1 Formation and classification of isomers . . . 1

1.2 Isomeric ratio and related effects . . . 7

1.2.1 Definition of isomeric ratio . . . 7

1.2.2 Nuclear effects on isomeric ratio . . . 8

1.2.3 Theoretical IR calculation . . . 10

1.3 Photonuclear reaction . . . 17

1.3.1 Formation of photonuclear reaction and photon sources . . . 17

1.3.2 Cross-section of photonuclear reaction . . . 18

Above particle emission threshold up to 30 MeV . . . 19

Below particle emission threshold . . . 21

In the energy range of 30 to 140 MeV . . . 22

1.3.3 (γ, n) reaction . . . 23

1.4 Neutron capture reaction . . . 24

1.4.1 Neutron and neutron sources . . . 24

1.4.2 (n, γ) reaction . . . 25

1.4.3 Neutron capture cross-section . . . 26

1.5 Level density and γ-ray strength function . . . 28

1.5.1 Nuclear level density . . . 28
1.5.2 Gamma-ray strength function . . . 32
1.6 Objectives . . . 36

2 Experimental and theoretical methods **37**
2.1 Experimental method . . . 37
2.1.1 Irradiation sources . . . 37
Microtron MT-25 . . . 38
Bremsstrahlung source . . . 39
Thermal and epithermal neutron source . . . 39
2.1.2 Sample irradiation . . . 41
2.1.3 Gamma spectroscopy . . . 44
2.1.4 Experimental IR determination . . . 46
2.1.5 Spectrum analysis-necessary correction . . . 49
Self-absorption effect . . . 49
Coincidence summing corrections . . . 50
2.2 Theoretical IR calculation in (γ, n) reaction . . . 50
2.2.1 Bremsstrahlung spectra simulation in GEANT4 . . . 50
2.2.2 Cross-section calculation in TALYS . . . 52

3 Results and Discussion **56**
3.1 Isomeric Ratios in (γ, n) reactions . . . 57
3.1.1 ^{152m1,m2}Eu . . . 57
3.1.2 ^{195m,g}Hg and ^{197m,g}Hg . . . 64
3.2 Isomeric Ratios in (n, γ) reactions . . . 70
3.2.1 ^{109m,g}Pd and ^{111m,g}Pd . . . 70
3.2.2 ^{115m,g}Cd and ^{117m,g}Cd . . . 76
3.3 Influence of nuclear channel effect on IRs in (γ, n) and (n, γ) reactions . . . 84
3.3.1 For ^{109m,g}Pd . . . 84
3.3.2 For ^{115m,g}Cd . . . 86
3.4 IRs of ^{137m,g}Ce, ^{115m,g}Cd, ^{109m,g}Pd, and ^{81m,g}Se in inverse reactions . . . 90
3.5 Theoretically calculated IRs in (γ, n) reactions . . . 94
3.5.1 Bremsstrahlung spectra simulation . . . 94
3.5.2 Cross-section calculation . . . 95
3.5.3 IRs in (γ, n) reactions . . . 99

Conclusions and Outlooks **117**

List of Publications used for the Thesis content **120**

References **122**

A Geant4 simulation codes **A1**

A.1 Main program A1

A.2 Geometry declaration A2

A.2.1 Bremsstrahlung irradiation A2

A.2.2 Neutron irradiation A5

A.3 Stepping Actions A11

A.4 Run Actions A12

A.4.1 Bremsstrahlung irradiation A12

A.4.2 Neutron irradiation A15

B Input file of TALYS code **A18**

C CERN ROOT analysis code to calculate IRs using energy flux spectra from GEANT4 and the cross-section outputs from TALYS **A20**

List of Abbreviations

ADC	Analogue to Digital Converter
BCS	Bardeen-Cooper-Schrieffer
BSFG	Back-Shifted Fermi Gas
CTM	Constant Temperature Model
EXFOR	Experimental Nuclear Reaction Data Library
ENSDF	Evaluated Nuclear Structure Data File
FLNR	Flerov Laboratory of Nuclear Reaction
GDR	Giant Dipole Resonance
GEANT	GEometry ANd Tracking
GEDR	Giant Electric Dipole Resonance
GMR	Giant Monopole Resonance
GLO	Generalized Lorentzian Model
GQR	Giant Quadrupole Resonance
GSM	Generalized Superfluid Model
HF	Hauser-Feshbach
HFB	Hartree-Fock-Bogolyubov
HPGe	High Purity Germanium
HVM	Huizenga-Vandebosch Model
IAEA	International Atomic Energy Agency
IC	Internal Conversion
IR	Isomeric Ratio
JINR	Joint Institute for Nuclear Research
LD	Level Density
PDR	Pygmy Dipole Resonance
RIB	Radioactive Ion Beam
RIPL	Reference Input Parameter Library
QD	Quasi-Deuteron
QRPA	Quasiparticle Random Phase Approximation
SLO	Standard Lorentzian
γSF	γ-ray Strength Function

List of Physical Quantities

A	mass number
a	level density parameter
$\tilde{a}$	asymptotic level density parameter
$a(S_n)$	LD parameter at the neutron separation energy
D_0	experimental and theoretical average resonance spacing
J	angular momentum
L	multipolarity
π_i, π_f	parities of the initial and final states
$t_{1/2}$	half-life
λ	decay constant
N	neutron number
Z	atomic number
R	nuclear radius
ϵ_0	electric constant (= 8.8542 x 10^{-12} F/m)
$\hbar$	reduced Planck's constant (= 1.0546 x 10^{-34} J.s)
c	velocity of light (= 3.10^8 m/s)
E_γ	gamma-ray energy
E_u	energy of isomeric state
E_d	energy of ground state
σ_i	cross-section
Y	yield
ϕ	flux
ρ	level density
f_{XL}	gamma strength function
T_{XL}	transmission coefficient
σ	spin cut-off parameter
Γ	decay width
γ	shell damping parameter
Δ	pairing energy
δW	shell correction energy
N_{low}, N_{top}	levels for the matching problem
T	nuclear temperature

$\sigma(S_n)$	spin cut-off parameter at the neutron separation energy
σ_0(M1)	strengths of magnetic dipole resonance peak
σ_0(E1)	strengths of electric dipole resonance peak
E(M1)	centroid energy of magnetic dipole resonance peak
E(E1)	centroid energy of electric dipole resonance peak
Γ(M1)	width of magnetic dipole resonance peak
Γ(E1)	width of electric dipole resonance peak

List of Tables

2.1 Main parameters of MT-25 microtron [116, 118]. 39
2.2 Characteristics of the irradiated samples, electron current and energy, and irradiation time. 43

3.1 γ-rays decay properties of the reaction products of ^{152m1,m2}Eu used in the IR calculation [138]. 58
3.2 A summary of corrections for self-absorption and summing coincidence for given γ-ray energies. 60
3.3 The IR of ^{152m1,m2}Eu in reaction (γ, n). 60
3.4 A summary of error sources considered in the IR calculation of ^{152m1,m2}Eu. 61
3.5 γ-rays decay properties of the reaction products of ^{195m,g}Hg and ^{197m,g}Hg used in the IR calculation [138]. 66
3.6 A summary of corrections for self-absorption and summing coincidence for given γ-ray energies. 67
3.7 Summary of IRs determined for $^{195m,g;197m,g}$Hg isomeric pairs produced in reaction (γ, n) [128]. 68
3.8 Summary of IRs determined for ^{197m,g}Hg and ^{195m,g}Hg isomeric pairs produced in various nuclear reactions. 70
3.9 γ-rays decay properties of reaction products of ^{109m,g}Pd and ^{111m,g}Pd used in the IR calculation [138]. 71
3.10 A summary of corrections for self-absorption and summing coincidence for given γ-ray energies of ^{109m,g}Pd and ^{111m,g}Pd. 72
3.11 A summary of IR results for $^{109m,g;111m,g}$Pd in thermal, resonance, and mixed thermal-resonant neutron-induced reactions and also in a (γ, n) reaction. 73
3.12 A summary of the error sources considered in the IR calculation of ^{109m,g}Pd. 74
3.13 The decay properties of selected γ-rays for IR calculations for ^{115m,g}Cd and ^{117m,g}Cd isomeric pairs [138]. 78

3.14 A summary of self-absorption and summing coincidence correction factors for the γ-rays of interest of $^{115m,g;117m,g}$Cd [130]. 79
3.15 A summary of IR results for ^{115m,g}Cd and ^{117m,g}Cd isomeric pairs produced in different types of nuclear reactions. 80
3.16 A summary of the error sources considered in the IR calculations of $^{115m,g;117m,g}$Cd. 81
3.17 The IRs of ^{109m,g}Pd in thermal, resonance and mixed thermal-resonant neutron capture reactions and in (γ, n) reaction. 86
3.18 The IRs of ^{115m,g}Cd produced in different nuclear reactions. 88
3.19 Selected gamma rays and spectroscopic characteristic data [138]. 93
3.20 The IRs of the studied inverse reactions. 94

List of Figures

1.1 Nuclear chart displaying isomeric states with $T_{1/2} \geq 100$ ns (NUBASE 2020) [13]. 6
1.2 Organization of input-output flows and components of the nuclear model in the TALYS program. Image taken from [56]. 14
1.3 The general total photon absorption cross-section below 30 MeV (taken from the presented slice of N.Tsoneva at ERICE2014). 19
1.4 An schematic illustration of various giant resonance modes of monopole ($\Delta L = 0$), dipole ($\Delta L = 1$) and quadrupoles ($\Delta L = 2$), their magnetic ($\Delta S = 1$) or electric ($\Delta S = 0$), isovector ($\Delta T = 1$) or isoscalar ($\Delta T = 0$) characters [80]. 20
1.5 Total neutron absorption cross-section of ^{nat}Cd, taken from the JEFF-3.3 library. 25
1.6 Neutron capture cross-section of ^{114}Cd, ^{116}Cd, ^{108}Pd and ^{110}Pd, taken from the JEFF-3.3 library. 27
1.7 Nuclear excitation energy regimes [104]. 29

2.1 Schematic drawing and image of the MT-25 Microtron. 38
2.2 The scheme for the production of a bremsstrahlung source. The small figure above is the bremsstrahlung flux simulated by GEANT4. 39
2.3 Schematic illustration of the production method for the source of mixed thermal-epithermal neutron and gamma. 40
2.4 Schematic illustration of the production method for thermal and epithermal neutrons. 40
2.5 The gamma spectrometer diagram. 45
2.6 HPGe detector of the Department of Chemistry of Transactinides, FLNR, JINR, Dubna. 45
2.7 The user interface of the Gamma Vision software. 45
2.8 The efficiency curve for the HPGe detector used in the present work. . 47
2.9 Diagram of the Geant4 user application. 51

2.10 GEANT4 simulation of experimental setups for photonuclear reaction (left) and neutron capture (right). 52
2.11 The bremsstrahlung with end-point energy of 24 MeV simulated by Geant4.10.06 version. 53
2.12 Geant4 simulated neutron energy at a distance of 30 cm from the primary target. 53

3.1 Simplified decay diagram of ^{152m1,m2}Eu [23]. 59
3.2 A typical energy spectrum of the Eu sample irradiated with 17 MeV bremsstrahlung [23]. 59
3.3 IR of ^{152m1}Eu(8^-)/^{152m2}Eu(0^-) versus the bremsstrahlung end-point energies [23]. 61
3.4 Simplified decay schemes of ^{195m}Hg and ^{195g}Hg [128]. 66
3.5 Simplified decay schemes of ^{197m}Hg and ^{197g}Hg [128]. 66
3.6 A typical energy spectrum of the natural Hg sample measured for 2 hours at a distance of 5 cm from the HPGe detector. The sample was irradiated with 20 MeV bremsstrahlung for 1 hour and cooled for 23 hours before measurement [128]. 67
3.7 Measured IRs of $^{195m,g;197m,g}$Hg versus bremsstrahlung endpoint energy. 69
3.8 Simplified decay diagrams of $^{109m,g;111m,g}$Pd [129]. 71
3.9 A typical energy spectrum of Cd-foil-covered natural Pd sample irradiated with energetic neutrons [129]. 72
3.10 ^{115m,g}Cd isomeric pair: a simplified decay scheme [130]. 77
3.11 ^{117m,g}Cd isomeric pair: a simplified decay scheme [130]. 77
3.12 A typical energy spectrum of Cd-foil-covered natural Cd sample irradiated with energetic neutrons [130]. 79
3.13 A typical energy spectrum of Cd-foil-uncovered natural Cd sample irradiated with energetic neutrons [130]. 79
3.14 A γ-ray energy spectrum of the Pd sample irradiated with 24 MeV bremsstrahlung [131]. 85
3.15 A γ-ray energy spectrum of the Cd sample irradiated with 24 MeV bremsstrahlung in 60 minutes, then 275.5 minutes of cooling and 20 minutes of measurements in a 5 cm position from the surface of the HPGe detector [132]. 87
3.16 Simplified scheme of the production of ^{115m,g}Cd from (n,γ), (γ,n), $(n,2n)$, (n,p) and (n,α) reactions [132]. 88

3.17 A typical γ-ray energy spectrum of a Ce sample irradiated with 25 MeV bremsstrahlung in 60 minutes, waited for 60 minutes and then measured for 20 minutes at 5 cm from the surface of the HPGe detector [134]. . . 90
3.18 A γ-rays energy spectrum from the Ce sample. The sample was irradiated with energetic neutrons for 90 minutes, followed by a cooling time of 35 minutes and then measured for 60 minutes at a position of 0 cm from the HPGe detector [134]. 91
3.19 A γ-ray energy spectrum of the Cd sample was measured for 275.5 minutes at a distance of 5 cm from the HPGe detector. The sample was irradiated by 25 MeV bremsstrahlung for 60 minutes, followed by a cooling time of 20 minutes [134]. 91
3.20 A γ-rays energy spectrum of the Se sample measured for 10 minutes on the surface of the HPGe detector. The sample was irradiated with 25 MeV bremsstrahlung for 20 minutes, followed by a cooling time of 60 minutes [134]. 92
3.21 A γ-rays energy spectrum of the Se sample measured for 10 minutes on the surface of the HPGe detector. The sample was irradiated by neutrons for 90 minutes, followed by a cooling time of 25 minutes [134]. 92
3.22 Bremsstrahlung energy spectra calculated by the GEANT4 toolkit with 500 millions primary particles. 95
3.23 (γ, n) reaction cross-section for ^{110}Pd calculated by TALYS 1.95. 96
3.24 (γ, n) cross-section of ^{74,82}Se calculated by TALYS 1.95 and compared with experimental values [195]. 97
3.25 (γ, n) cross-section for ^{138,140}Ce calculated by TALYS 1.95 and compared with experimental values [196]. 97
3.26 (γ, n) reaction cross-section for ^{151,153}Eu calculated by TALYS 1.95 compared to experimental values [197, 198]. 97
3.27 (γ, n) reaction cross-section for ^{195,197}Hg calculated by TALYS 1.95. . . 98
3.28 Calculated cross sections of isomeric and ground state formation in the ^{153}Eu$(\gamma, \mathrm{n})^{152}$Eu reaction. 98
3.29 Theoretically calculated IRs between ^{73g}Se(I=$9/2^+$) and ^{73m}Se(I=$3/2^-$) in comparison with the literature. 100
3.30 Theoretically calculated IRs between ^{81m}Se(I=$7/2^+$) and ^{81g}Se(I=$1/2^-$) in comparison with the literature. 101
3.31 Theoretically calculated IRs between ^{109m}Pd(I=$11/2^-$) and ^{109g}Pd(I=$5/2^+$) in comparison with the literature. 104

3.32 Theoretically calculated IRs between ^{137m}Ce(I=11/2$^-$) and ^{137g}Ce(I=3/2$^+$) in comparison with the literature. 106
3.33 Theoretically calculated IRs between ^{139m}Ce(I=11/2$^-$) and ^{139g}Ce(I=3/2$^+$) in comparison with the literature. 107
3.34 Theoretically calculated IRs between ^{150m}Eu(I=0$^-$) and ^{150g}Eu(I=5$^-$) in comparison with the literature. 108
3.35 Theoretically calculated IRs between ^{152m1}Eu(I=8$^-$) and ^{152g}Eu(I=3$^-$) in comparison with the literature. 110
3.36 Theoretically calculated IRs between ^{152m1}Eu(I=8$^-$) and ^{152m2}Eu(I=0$^-$) in comparison with the literature. 111
3.37 Theoretically calculated IRs between ^{152m2}Eu(I=0$^-$) and ^{152g}Eu(I=3$^-$) in comparison with the literature. 112
3.38 Theoretically calculated IRs between ^{195m}Hg(I=13/2$^+$) and ^{195g}Hg(I=1/2$^-$) in comparison with the literature. 114
3.39 Theoretically calculated IRs between ^{197m}Hg(I=13/2$^+$) and ^{197g}Hg(I=1/2$^-$) in comparison with the literature. 115

Introduction

Understanding the structure and properties of an atomic nucleus via forces between nucleons has always been a major challenge in Nuclear Physics. It can be studied by using natural radioactivity and nuclear reactions. Both processes result in the emission of radiations that carry important information about the characteristics of the nucleus. Detecting, measuring, and analyzing those radiations reveal the nuclear structure and properties. While the number of natural radionuclides is limited to only a few dozen nuclei, nuclear reactions offer a more convenient method for studying all nuclei. The nuclear reaction may occur in various processes such as compound, pre-equilibrium, or direct, depending on the type of projectile and target as well as the incident energy. As a result of nuclear reaction, the residual nucleus can exist in the isomeric or ground states. The isomeric state (isomer) is a metastable excited state of the nucleus that experienced a hindrance in its decay. The half-lives of the isomers range from *nanoseconds* to *years*. In recent decades, there has been rapid growth in radioactive isotope and rare isotope beam (RIB) facilities and cutting-edge nuclear experimental techniques relative to the development of nuclear detectors, digital electronics, analyzers, and computational power, resulting in remarkably theoretical and experimental studies on isomers. Nowadays, an increasing number of isomers are discovered in diverse regions of the nuclear landscape. Isomers play a crucial role in fundamental research in nuclear physics and astrophysics but also can be utilized in many applications such as therapy, medical imaging, γ-ray lasers, nuclear battery, and nuclear clock.

Along with the isomeric investigation, the isomeric ratio (IR), being the probability ratio of the formation of isomeric and ground states, is also a very fascinating issue since it can disclose considerable details about the nuclear structure and features, and the involved reaction mechanism. In addition, the IR correlates strongly with the energy and angular momentum of the projectile, the nuclear level density and spin distribution of the excited nucleus, and many other characteristics. Therefore, IRs can also be precious data for studying not only the nuclear structure, reaction

mechanism, and nuclear applications but also for examining different nuclear reaction models. The experimental IR can be measured with high accuracy, as the isomeric pair is generated simultaneously throughout the nuclear reaction process under the identical experimental setup. To compare the measured IRs with theoretical predictions, several nuclear model codes can be used to calculate IRs. The TALYS code is currently most often employed to simulate nuclear reactions and predict the cross section and the IR. TALYS is a flexible and easy-to-use code that contains the latest nuclear reaction models. The TALYS code can implement reactions between projectiles γ, n, p, d, t, ^3He, and ^4He with energies of 1 keV up to 200 MeV and target nuclei with a mass of 12 to 339 a.m.u. Note that the photon-induced reactions are mainly irradiated by bremsstrahlung photons, due to the lack of a monoenergetic photon source with high intensity. The TALYS code, however, only computes the differential cross-section of reactions with mono-energetic projectiles. Hence, the TALYS code is often combined with the bremsstrahlung simulation code to obtain the integrated cross section, flux-weighted average cross section, and IR in photonuclear reaction irradiated by bremsstrahlung. The GEANT4, a transportation/Monte-Carlo simulation toolkit with a free, open-source software package, can simulate the bremsstrahlung spectra.

This thesis aims to study the experimental IRs in photonuclear reactions (γ, n) with bremsstrahlung endpoint energies in the GDR region on heavy nuclei ^{196,198}Hg and ^{153}Eu as well as IRs in thermal, resonant and mixed thermal-resonant neutron-induced reactions (n, γ) on ^{108,110}Pd and ^{114,116}Cd nuclides. The experiments were conducted using the MT-25 Microtron of FLNR laboratory, JINR, Dubna, Russia. We adopted the activation method in combination with the offline γ-spectrum measurement. The principal reasons for selecting the targets and two kinds of nuclear reactions are insufficient IRs and/or the large discrepancy between the data, and well-known reaction mechanisms. For the photon-induced reaction in the GDR region, the process that occurs is mainly the absorption of an electric dipole γ quantum (E1) by a target nucleus with spin J_0, which constitutes the compound nucleus at excitation states with spins $J_C = J_0, J_0 \pm 1$. Thus, in this case, the theoretical consideration becomes unambiguous. The even-even nuclei ^{196,198}Hg with a spin of 0^+ belong to the nuclear range with Z = 73–81 and A = 182–206. They are located between the strongly deformed nuclear region and the spherical nuclear region in the neighborhood of A = 208. Because of the high angular momentum of the last protons ($1h_{\frac{11}{2}-}$) and neutrons ($1i_{\frac{11}{2}-}$), isomers are expected to populate at the high-spin states through the nuclear reactions. Odd-even

target nucleus ^{153}Eu is strongly deformed and its ground state spin is $\frac{5}{2}^+$ defined by spin of the last proton single-particle state ($\frac{5}{2}^+[413]$). By means of the reaction (γ, n), the residual nucleus ^{152}Eu can be formed and exist in the ground state ^{152g}Eu with a spin of 3^- or in the isomeric states ^{152m1}Eu and ^{152m2}Eu with spins of 8^- and 0^-, respectively. Up till now, there have been missing IR data of isomeric pairs of Hg and Eu isotopes in the photon-irradiated reactions in the GDR region. The numbers of literature data are, moreover, largely scattered. For the thermal and resonant neutron capture reaction, it was presumed that only s-wave neutrons were captured. Thus, this type of reaction presents definite interest due to the striking characteristics: (a) the compound nucleus is excited to the energy level equivalent to its neutron binding energy since the kinetic energies of thermal and resonant neutrons are negligible compared to the binding energy; (b) the incident neutron transferred the angular momentum of $1/2\hbar$ to the target nucleus, resulting in the total angular momentum of the compound nucleus may occupy three values J_0 and $J_0 \pm 1/2$. These features hinder the spin values of excitation levels, leading to the elucidation of the reaction mechanism in a simple and easily understandable way. Accordingly, the study of IR in this type of reaction can provide valuable information on the nuclear level structure and the dependence of the level density on the spin. Up to date, there have been a few works on the measurement of IRs in thermal and resonant neutron capture reactions of ^{108,110}Pd and ^{114,116}Cd nuclei, especially no data for mixed thermal-epithermal neutron capture reactions on all these nuclei and resonant neutron capture on ^{110}Pd nucleus.

In this thesis, we have carried out the following works:

- Determination of the experimental IRs of isomeric pairs $^{195m,g;197m,g}$Hg and ^{152m1,m2}Eu in $^{196,198}Hg(\gamma, n)$ and $^{153}Eu(\gamma, n)$ reactions, respectively, irradiated by bremsstrahlung with endpoint energy within the whole GDR region.

- Measurement of IRs of $^{109m,g;111m,g}$Pd and $^{115m,g;117m,g}$Cd in $^{108,110}Pd(n, \gamma)$ and $^{114,116}Cd(n, \gamma)$ reactions, respectively, induced by thermal, resonant, and mixed thermal-resonant neutrons.

- Consideration of several effects affecting IRs such as spin difference, excitation energy, nucleon configuration, angular momentum transfer, and reaction channel effects in the above-mentioned isomeric pairs formed by various nuclear reactions.

Note that the consideration included the investigated photonuclear and neutron-captured reactions caused by thermal, resonant, and mixed thermal-resonant neutrons, which have not been exposed in the existing literature before.

- Application of the TALYS 1.95 with six nuclear density models and eight γ-ray strength functions in combination with the GEANT4 toolkit to predict the IRs in the photonuclear reactions and compare with our experimental data as well as the literature data.

As is well-known, nuclear data play a vital role in the application of atomic energy and in investigating the nuclear structure and reaction mechanism. Therefore, nuclear data from each type of reaction should be measured by numerous laboratories with various approaches and data analysis methods. In that sense, the IR data with high accuracy presented in this thesis may devote new ones exclusively or contribute additional data to the nuclear data reservoir. Additionally, evaluating the impact of several quantities such as the energy and angular momentum of projectiles transferred to the target nucleus, the spin of the target nucleus, spin of the ground and the excited states of the residual nucleus on the IR values elucidate the role of these quantities and lead to systematic and reliable IRs. Furthermore, studying the IR in photonuclear reactions by TALYS code allows drawing conclusions about the nuclear structure, model parameters, and nuclear reaction mechanism embodying the factors of equilibrium, direct, and pre-equilibrium processes.

This thesis is organized as follows:

Chapter 1 outlines nuclear isomers, the IR and related effects. This chapter also reviews briefly photonuclear and neutron capture reactions. Besides, the calculated programs for nuclear reactions, namely, the TALYS code and the GEANT4 toolkit are also introduced.

Chapter 2 presents and explains the experimental and theoretical methods in detail. The necessary corrections to obtain accurate experimental results are also presented in this chapter.

Chapter 3 demonstrates and discusses the experimental results and theoretically calculated outcomes of this work compared to the literature.

Finally, the conclusion and outlook are drawn.

The thesis includes 22 tables and 58 figures and presents on 119 pages.

Chapter 1

Overview

Nuclear isomers are metastable states of nuclei that undergo a hindrance in their decay. The half-life of isomers ranges from *nanoseconds* to millions of *years*. Currently, nuclear isomers lodge in the center position in the study of nuclear physics, as they can be employed to elucidate the nuclear structure and properties under abnormal conditions and to be applied in numerous applications such as therapy, medical imaging, nuclear clocks, γ -ray lasers, and nuclear batteries. Recent advances in RIB facilities, nuclear detectors, digital electronics and analyzers lead to observing new isomers with very short lifetimes and measuring their detailed properties. One of the research directions relating to isomers is the determination of IR being of great interest. The study of IR can provide invaluable information on the level structure and density, as well as the involved reaction mechanisms. In addition, IRs can be used as precious data for the examination of nuclear reaction models.

This chapter reviews the historical aspects of nuclear isomers and the inhibition mechanisms resulting in their formation and classification. As a central part, the definition and calculation of IR and its related effects in photonuclear and neutron capture reactions by experimental and theoretical methods are presented in section 1.2.

1.1 Formation and classification of isomers

Nuclear isomers have attracted attention since 1917 when Soddy stated *"We can have isotopes with the identity of atomic weight, as well as of chemical character, which is different in their stability and mode of breaking up"* [1]. In 1921, Hahn reported the first experimental measurement about isomers in Uranium salts [2], UZ and UX2, later known as ^{234}Pa and ^{234m}Pa. 15 years later, the first explanation of isomers related to hindered γ -decay was provided by Weizsäcker [3]. It is related to considerable angular momentum variation, especially when combined with low electromagnetic transition

energies leading to the slow transition rate, i.e., the population of isomers with a half-life longer than that of normal excited states. In the early 1950s, the non-spherical shapes of several nuclei were unveiled, which expanded the study of isomeric states in deformed nuclei. Bohr and Mottelson evolved the existence and decay characteristics of isomers of the axially-symmetric deformed nucleus ^{180}Hf [4] as a result of electromagnetic transitions in the rotational band. Although the role of the magnitude of the angular momentum in the formation of isomers had been discussed by Weizsäckers [3], the change in the orientation of the nuclear spin could also be important, as in the case of ^{180}Hf, leading to the population of different types of isomers.

The interpretation of the existence of isomers in terms of hindered gamma transition is based on various physical reasons directly relevant to the selection rules in γ-decay and electromagnetic transition probability. The widely known selection rules in γ-decay arise from the preservation law of parity and angular momentum. The transition from an initial state i to a final state f, having angular momentum $\vec{J_i}$ and $\vec{J_f}$, respectively, can take place as electromagnetic deexcitation by the γ-ray emission carrying away an angular momentum $\vec{L}$. This transition process obeys the angular momentum preservation law: $\vec{J_f} = \vec{J_i} + \vec{L}$ corresponding to the condition:

$$\left|J_i - J_f\right| \leq L \leq J_i + J_f. \tag{1.1}$$

The multipolarity L of the emitted γ-rays is a non-zero positive value since the intrinsic spin of a photon is 1 $\hbar$, and the photon transition $0 \rightarrow 0$ with $L = 0$ is absolutely prohibited. In addition, the conservation law of parity represents $\pi_i\pi_\gamma\pi_f = 1$ and helps to determine the electric or magnetic transition. A L-multipole transition is the electric one when $\pi_i\pi_f = (-1)^L$, and is the magnetic one if $\pi_i\pi_f = (-1)^{L+1}$, here $\pi_{i(f)}$ is the parity of the initial (final) state. In a classical picture, electric γ-ray transition occurs when the radiation field is generated by the displacement of charge distribution, while the magnetic one is due to the change in the current distribution.

Taking its origins from Fermi's golden rule, the electromagnetic transition probability per unit of time denoted as T_{fi} is reduced to the following formula [5]:

$$T_{fi}^{\alpha L} = \frac{2}{\epsilon_0\hbar}\frac{L+1}{L[(2L+1)!!]^2}\left(\frac{E_\gamma}{\hbar c}\right)^{2L+1} B(\alpha L; J_i \rightarrow J_f), \tag{1.2}$$

where $B(\alpha L; J_i \rightarrow J_f)$ is the reduced transition probability, given as:

$$B(\alpha L; J_i \to J_f) = \frac{1}{2J_i+1} \left| < J_f || \widehat{O}_{\alpha L} || J_i > \right|^2, \tag{1.3}$$

with $\alpha = E$ or M indicates the electric or magnetic field, $\widehat{O}_{\alpha L}$ is the operator with regard to the multipole radiation field αL.

The average lifetime and the half-life are given by $t = 1/T_{fi}$, and $t_{1/2} = ln(2)/T_{fi}$, respectively.

Competing with γ-decay is the internal conversion process (IC) to be the deexcitation of the excited nucleus through the energy transfer to kick the electrons off the atomic orbital. This process becomes crucial when low decay energy results in a significant half-life change for low-energy isomeric transition. The IC process is the unique probable decay mode in the $0^+ \to 0^+$ ($E0$) transitions where γ-decay is impossible, as mentioned earlier. The IC process vies with γ-decay quantified by the total internal conversion factor a:

$$a = N_e/N_\gamma, \tag{1.4}$$

where $N_{e(\gamma)}$ is the number of conversion electrons (γ-rays) released from the identical time of an excited nuclide.

When factor a is taken into account, the total transition probability becomes:

$$T_{fi}^{\alpha L} = \frac{2}{\epsilon_0 \hbar} \frac{L+1}{L[(2L+1)!!]^2} \left(\frac{E_\gamma}{\hbar c}\right)^{2L+1} B(\alpha L; J_i \to J_f)(1+a). \tag{1.5}$$

Following the Eqs. (1.2) and (1.3), the electromagnetic decay probability is affected not only by the multipolarity and the γ-decay energy but also by the transition matrix element with respect to the interaction operator and the wave function of the initial and final states carrying the nuclear structure information. It is tricky to calculate the matrix element since it involves the characteristics of the actual wave function.

For the case of the spherical nuclei with radius $R = R_0 A^{1/3} = 1.2A^{1/3}$ fm and the electromagnetic transition of a single nucleon ($J_i = 1/2$ and $J_f = L+1/2$), Weisskopf [6] estimated and represented the reduced transition probability in the approximate expressions:

$$B_W(EL) = \frac{1.2^{2L}}{4\pi} \left(\frac{3}{L+3}\right)^2 A^{\frac{2L}{3}} e^2 f m^{2L}, \tag{1.6}$$

$$B_W(ML) = \frac{10 \times 1.2^{2L-2}}{4\pi} \left(\frac{3}{L+3}\right)^2 A^{\frac{2L-2}{3}} (\mu_N/c)^2 fm^{2L-2}. \tag{1.7}$$

Substituting the Eqs. (1.6) and (1.7) into Eq.(1.2) results in the transition probability (T_W) in Weisskopf unit ($W.U$). Then, the Weisskopf estimate-based lifetime (t_W) of a certain nuclear state can be given by:

$$t_W = \frac{1}{T_W} = \frac{\epsilon_0 \hbar}{2} \frac{L[(2L+1)!!]^2}{L+1} \left(\frac{E_\gamma}{\hbar c}\right)^{-(2L+1)} \frac{1}{B_W(\alpha L)}. \tag{1.8}$$

This estimation is the so-called Weisskopf single-particle estimate, which is particularly beneficial for comparing with the experimental half-life. Although these estimates are not exact theoretical calculations, they can provide reasonable comparative transition rates. If one observes the experimental transition rate of a γ-decay with the order of magnitude much lower than Weisskopf prediction, one can assume a worse fitting of initial and final wave functions while if the measured decay rate is much higher than Weisskopf prediction, there must be the multinucleon transition. Stemming from Weisskopf estimate (1.8), one can deduce two features: (1) Dominant transition modes are with low multipolarities because the increase of one unit in the multipole order leads to the reduction of the transition probability about 10^{-5} times. (2) In medium and heavy nuclides, the electric radiation is more possible than the magnetic one by about two magnitude orders for a given multipole order.

Arising from Eq. (1.2), it is conceivable that the probability of electromagnetic decay depends on three main elements consisting of multipolarity L, the transition matrix element, and the γ -decay energy E_γ. The larger the electromagnetic decay probability the longer the lifetime results in the existence of isomeric states. In other words, isomers can occur because of the electromagnetic transition with high multipolarity, the small matrix element, and/or the small decay energy of the transition. Most of the isomers with large multipole transitions are figured out in spherical nuclei near the magic numbers, so-called spin isomers. Knowledge of the level scheme of the shell model and the magic numbers, together with the selection rules of γ-decay, is adequate to recognize the existence of high-spin isomers close to magic nuclides. For odd-odd or even-even nuclides, the additional rules were revealed by Nordheim [7] and Brennan and Bernstien [8] for allowed and favored spins.

The isomers can exist due to not only the considerable change of the magnitude of the angular momentum vector but also the vector orientation arising in the heavy,

axially-symmetric deformed nuclei. The projection of intrinsic angular momentum on the symmetry axis of the nucleus is characterized by the quantum number K. There are also selection rules for values of K. An absolute selection rule demands the multipolarity of the decay radiation to be at least equal to the change of K value ($L \geq \Delta K$). Nonetheless, in several cases, K-forbidden transitions are inhibited or the K-selection rule is prohibited resulting in $\Delta K > L$ because of possible transitions from symmetry-breaking processes. The forbidden degree ν is determined by $\nu = \Delta K$ - L correlating with the Weisskopf hindrance factor $F_W = t_\gamma / t_W$ and the reduced inhibition factor $f_v = F^{1/\nu} = (t_\gamma / t_W)^{1/\nu}$, in which $t_{\gamma(W)}$ is the experimental partial mean lifetime of γ-ray (Weisskopf estimate) as in Eq. 1.8. The f_ν value depends on the nuclear structure. The expected reduced hindrance is within the range of $f_\nu \sim 30 - 300$ [9]. The isomer that existed due to this physical reason is called the K-isomer.

In another case, the occurrence of isomers might arise from having more than one energy minimum of a nucleus, wherein the primary energy minimum corresponds to the ground state. This reason leads to the existence of the shape isomer or the fission isomer. For instance, it is demonstrated in spontaneous fissile isomers and fission isomers in the actinium region. This type of isomer is characterized by a large quadrupole deformation parameter and great hindrance of γ-ray transitions to the ground state.

In general, based on the inhibition mechanism, the isomers are classified into five main types [10]: (1) spin isomer in the spherical nuclides, (2) seniority isomer in the semi-magic nuclides, (3) K-isomer in the axially-symmetric deformed nuclides, (4) fission isomer in the heavy-fissionable nuclides, and (5) shape isomer in the shape co-existence nuclides. Furthermore, another type of isomer is mentioned, which is an extremely low energy isomer (ELE isomer) as 8 eV isomer in ^{229}Th [5]. It is perceptible that an isomer may also have a mixed origin, as there is more than one physical reason behind its long half-lives.

With the rapid growth of accelerators, RIB facilities, and nuclear experimental techniques, more and more new isomers in various nuclear regions have been discovered to date. The half-life illustration of isomers has also changed to lower limits due to the advanced detector and electronic techniques. The first version of Nubase 1997 defined the isomer as the excited state with a half-life greater than 1 ms; the ENSDF database [11] also defined the same isomeric half-life. Afterward, the Nubase 2003 [12] defined the lower limit of 100 ns. In the Nubase 2020 [13], one still insisted on that limit. However, in the "Atlas of Nuclear Isomers" [14], the limit of isomers is down to

10 ns. These definitions of half-life are not based on certain fundamental reasons, only expedience and measurableness. In the Nubase 2020 version, 1938 excited isomeric states ($T_{1/2} \geq 100ns$) were listed as shown in Fig. 1.1, while the recent "Atlas of Nuclear Isomers" second edition listed 2623 isomers with the lower half-life limit of 10 ns [5]. There are about 866 odd-odd isomers, 445 even-even isomers, 679 even-N odd-Z isomers and 633 odd-N even-Z isomers. There are almost equal numbers of isomers in odd-A nuclei (1312) and even-A nuclei (1311).

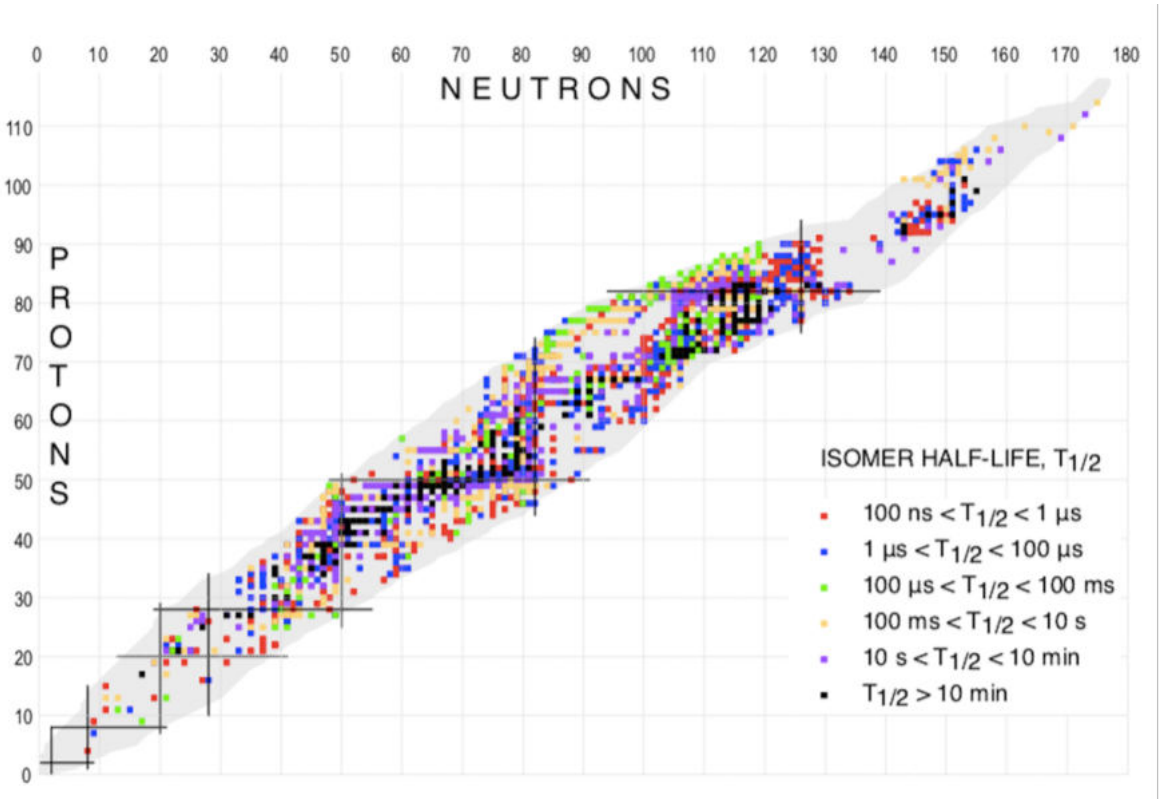

FIGURE 1.1: Nuclear chart displaying isomeric states with $T_{1/2} \geq 100$ ns (NUBASE 2020) [13].

Until now, the entire nuclear landscape has been vastly covered by nuclear isomers, with their characteristics changing from region to region. Apart from isomeric transitions (IT), namely, γ-decay and/or internal conversion, which is the most common decay mode of isomers, isomers can decay following by different modes such as β-decay [15], α-decay [16], spontaneous fission, p-decay [17], $2p$-decay [18], εp-decay [19], β^+p-decay [20], and β^-n-decay [21], etc. These peculiar decay modes of isomers have shed light on the intricate structure of the nuclides and provide a benchmark for probing the wave function, locations of single nucleon orbitals, and characteristics of the nuclear interaction.

In addition to the study of the population and properties of isomers, the investigation

of the isomeric ratio (IR) is particularly interesting. The IR can provide important information on the density and structure of the nuclear-level density and structure and the involved reaction processes. IR values are relevant for various targets and projectiles, excitation energy, spin of target nuclei, and many other nuclear effects. Some of them are demonstrated in the following section.

1.2 Isomeric ratio and related effects

1.2.1 Definition of isomeric ratio

IR is defined as the measured relative population of an isomeric state and an unstable ground state of a nucleus in a nuclear reaction. In the calculation, the IR is expressed as the ratio of the cross sections ($IR = \sigma_m/\sigma_g$) when irradiating the sample with a monoenergetic beam or the ratio of reaction yields ($IR = Y_m/Y_g$) in the case of a continuous energy beam. As the isomeric and ground states differ in spin, the IR is also commonly defined by the ratio of cross-sections or that of yields for forming the high- and low-spin states ($IR = \sigma_h/\sigma_l$ or Y_h/Y_l) [22, 23].

So far, a large number of IRs have been investigated in nuclear reactions bombarded by a variety of projectiles such as photon [24, 25, 26]; neutron [27, 28] tritium [29], alpha [30], deuteron and light ion [28], heavy ion [31] as well as in fission product [32, 33]. Investigation of nuclear reactions irradiated by different projectiles and targets with a broad energy range is crucial for understanding the nuclear structure and processes.

In the case of photonuclear reactions induced by bremsstrahlung, the IR is analytically calculated by the equation below:

$$IR = \frac{Y_m}{Y_g} = \frac{N_0 \int_{E_{th}^m}^{E_\gamma^m} \sigma_m(E)\phi(E)dE}{N_0 \int_{E_{th}^m}^{E_\gamma^g} \sigma_g(E)\phi(E)dE}, \tag{1.9}$$

where E_γ^m, $\phi(E)$, N_0 are the bremsstrahlung endpoint energy, the bremsstrahlung photon flux, and the number of the target nuclei, respectively; $\sigma_{m(g)}(E)$ is the cross sections of the isomeric (ground) state and $E_{th}^{m(g)}$ is the threshold reaction energies for the isomeric (ground) state.

In the case of thermal and resonance neutron capture reactions, the IR is also calculated by the yield ratio since the energy spectrum of thermal neutrons obeys Maxwellian distribution extending to about 0.2 eV, of which the most probable energy

at 20°C is 0.025 eV. The energy spectrum of resonance neutrons ranges from 10 to 300 eV.

The IR connects to various nuclear effects. Some of them are demonstrated in the following subsection.

1.2.2 Nuclear effects on isomeric ratio

Excitation energy

The influence of excitation energy on IR in photonuclear reaction (γ, n) with the bremsstrahlung endpoint energy in the GDR is proved in [34, 35, 36, 37, 38, 39]. The obtained experimental results show that the IR values increase or decrease with increasing end-point energy and reach the maximum (or minimum) value at the end of the GDR and slightly change (or almost unchanged) for higher energies. These depend on the fact that the yield of the isomeric state increases faster or slower than that of the ground state when the bremsstrahlung endpoint energy increases in the GDR region. The pre-equilibrium and direct processes are taken into account for the steady value of IRs at the end and beyond the GDR. The contributions of direct and pre-equilibrium processes can be found in ref. [40]. Furthermore, the contribution of other competitive channels to the IR of an isomeric pair produced in the reaction (γ, n) at the end of the GDR and up to 65 MeV is insignificant, as in the case of ^{85m,g}Sr in ref. [41]. In which the authors estimated the contribution of the reactions $(\gamma, 2n)$ and $(\gamma, 3n)$ to be negligible. In neutron-induced reactions, the IR is also a function of the incident neutron energy. This fact is presented by Nesaraja [42] for ^{69m,g}Zn and ^{71m,g}Zn with the identical spin of the isomeric state and the ground state produced via (n, α), (n, p), and $(n, 2n)$ reactions with the neutron energy range of 6 to 12 MeV. The low-spin isomer is favored at low energies, but with the increasing neutron energy, the population of high-spin isomers increases leading to the increasing trend of the IR. Furthermore, the IR of ^{69m,g}Zn is larger than that of ^{71m,g}Zn revealing the other effect relating to the mass number.

Nucleon configuration

The dependence of IRs on the mass number of isotone nuclei is presented by N. Tsoneva [39]. They measured and observed the large difference of IR values in (γ, n) reactions irradiated by bremsstrahlung for $N = 81$ isotone nuclei (^{137}Ba, ^{139}Ce, ^{141}Nd and ^{143}Sm) under the conditions as the same excitation energy of residual nuclei and the identical spin and parity of isomeric and ground states. In more detail, the IR of

two lighter nuclei equaled approximately twice that of two heavier nuclei, and the IR decreased with increasing atomic number, resulting in the IR depending on the mass number. Similarly, T.D. Thiep studied the IRs in the reaction (γ, n) of $N = 81$ isotones (^{141}Nd and ^{143}Sm) and $_{51}$Sb isotopes [43], $_{56}$Ba isotopes [36] and $_{34}$Se isotopes [35] and concluded that the IR decreased with the growth of neutron/proton number. The dependence of IR on the mass number of isotones and isotopes is called the effect on nucleon configuration.

Reaction channel

The various IR values of an isomeric pair produced via different nuclear reactions have been investigated by Cserpak [44] for ^{60m,g}Co in three neutron induced reactions, by Sudar for ^{58m,g}Co in the neutron, proton, deuterium, and α-induced reactions [27], by Qaim for ^{73m,g}Se and ^{52m,g}Mn in nuclear reactions induced by projectiles of α, ^{3}He, p, d and n [45, 46], by Strohmaier for ^{94m,g}Tc in three nuclear processes [47], by Nesaraja for ^{69m,g}Zn and ^{71m,g}Zn in neutron induced reactions [47], by Tonchev for ^{152m1,m2}Eu in inverse reaction (γ, n) and (n, γ) [34] and by T. D. Thiep and references cited therein studying on Ba, Se, In, Ho, Lu, Ag, Mo and Ce targets in reactions induced by bremsstrahlung and neutrons [34, 43, 48, 36]. The influence of the reaction channel on IRs is considerable. This effect can be explained by the intake impulse of the projectiles. The higher the projectile intake impulse, the higher the IR result. T.D.Thiep reported the IRs of the same isomeric pair in both $(n, 2n)$ and (γ, n) reactions with the identical projectile energy on the Ba, Se, Ce, In, Ag and Lu targets and deduced that the IRs in the former reaction are notable higher than those in the latter because of the larger intake impulse of neutrons.

Intermediate state structure

The IR is, moreover, governed by the level structure of intermediate states. Huber [49] and Carroll [50] evaluated the crucial role of middle state structure on the populating mechanism of the isomeric and ground states in the photonuclear reaction with the bremsstrahlung endpoint energies of 2 – 7 MeV.

Spin and spin difference

Another effect is the spin dependence of the isomeric state. In ref. [36], T.D. Thiep investigated the IRs of the isomeric pairs ^{129m,g}Ba, ^{131m,g}Ba and ^{133m,g}Ba formed in (γ, n) reactions with the same ground-state spin of $1/2^+$ but various isomeric-state spins of $7/2^+$, $9/2^-$ and $11/2^-$, respectively. The results indicated that the IR decreased with the increase in the isomeric state spin. The difference between the spins of the

isomeric and ground states also has an impact on the IR value. In general, the higher the spin difference, the lower the IR [51].

1.2.3 Theoretical IR calculation

In the 1960s, on the basis of the statistical model for compound nuclear reaction, the first theoretical IR calculations were studied and proposed by Huizenga and Vandebosch [52, 53]. Afterward, this IR calculation model is called Huizenga-Vandebosch model (HVM).

Huizenga-Vandebosh model

The HVM is able to apply for calculating the IR in (n, γ) and (γ, n) reactions based on the spin distribution. In the initial interaction between the incident particle and the target nucleus, the compound nucleus formed with the determined spin distribution. After the emission of the particle and γ-ray, the spin distribution was modified and calculated. The IR was determined from the final spin distribution, depending on the spins of the isomeric pair. By fitting the IRs calculated by the HVM with the experimental values, one can obtain information about the dependence of the level density on the spin cutoff and level density parameters. In refs. [48, 51, 54], for the photonuclear reaction, the calculated IRs according to the HVM with a certain spin cutoff were in good agreement with the experimental data at relatively low energies, where the compound process was the main one. Kolev [55] improved the HVM by including a more detailed deexcitation calculation of the charged particle emission process.

In the case of the photoneutron reaction (γ, n), the HVM is represented by the following stages [48, 51]:

1. *Formation of a compound nucleus by absorbing an E1 γ-ray*

   The relative population probability of compound nucleus with spin J_c (positive value) through the absorption of an E1 γ-ray by target nucleus with initial spin J_0 is:

$$P(J_c) \approx 2J_c + 1 \quad , where \quad J_c = J_0, J_0 \pm 1. \tag{1.10}$$

2. *Emission of a neutron from the excited compound nucleus and formation of a residual nucleus*

The relative probability that the compound nucleus emits a neutron with orbital angular momentum l that leads to a residual nucleus with spin J is given by

$$P(J) \approx \rho(J, E^*) \sum_{S=\left|J-\frac{1}{2}\right|}^{\left|J+\frac{1}{2}\right|} \sum_{l=|J_c+S|}^{J_c+S} T_l(E_n), \tag{1.11}$$

where $T_l(E_n)$ - the penetrability (transmission coefficient) of the neutron with angular momentum l and kinetic energy E_n; $\rho(J, E^*)$- the level density of the residual nucleus.

The emitted neutrons are supposed to obey the Maxwell distribution. The evaporation energy E_n is replaced by an average energy $\overline{E_n}$,

$$\overline{E_n} = \frac{1 + \sqrt{1 + 4aU}}{2a}, \tag{1.12}$$

where U – the excitation energy of compound nucleus, $U = at^2 - t$ with t is thermodynamic temperature, a – the level density parameter.

The excitation energy of the residual nucleus E^* is given by:

$$E^* = U - S_n - E_n, \tag{1.13}$$

here S_n and E_n – the separation and kinetic energies of the emitted neutron.

The level density of the residual nucleus is represented by the following formula:

$$\rho(J, E^*) = \rho(E^*)\rho(J) \sim exp\left[2(aE^*)^{1/2}\right](2J+1)exp\left[-\frac{(J+1/2)^2}{2\sigma^2}\right], \tag{1.14}$$

where σ - the spin cut-off parameter, $\sigma^2 = \frac{\theta t}{\hbar^2}$ with θ – the moment of inertia of nucleus.

3. *Emission of γ-ray cascade from the residual nucleus leads to the population of the isomeric and ground states*

The residual nucleus is assumed to deexcite predominantly by E1 γ-ray emission with an average energy for $(i+1)^{th}$ γ-ray:

$$E_{\gamma(i+1)} = 4\left[\frac{E^* - \sum E_{\gamma i}}{a} - \frac{5}{a^2}\right]^{1/2}. \tag{1.15}$$

Here it is supposed that $E_{\gamma 0} = 0$.

The γ-ray transition probability from states with spin J_i to those with spin J_f is assumed to be

$$P(J_f) \sim \sum_{J_i} P(J_i)\rho(J_f). \tag{1.16}$$

The γ-ray cascades continue to occur until the residual energy, i.e. $E = E^* - \sum E_{\gamma i}$ is smaller than the "γ-ray cut-off region" (E_u, E_d). Then, "deciding γ-ray" emits and feeds the state to which the transition has the lowest multipolarity. When the residual γ-ray energy lies within the cutoff region, a subsequent E1 γ-ray and "deciding γ-ray" are partly emitted. In this situation, one must consider the competing channel with the transition probability $P = (E - E_d)/(E_u - E_d)$, which leads to the calculation of IR by the following formula:

$$IR = P\frac{\sum_{J_f=COS}^{J_f=\infty+} P(J_f, E - E_d)}{\sum_{J_f=0}^{J_f=COS} P(J_f, E - E_d)} + (1 - P)\frac{\sum_{J_f=COS}^{J_f=\infty+} P(J_f, E)}{\sum_{J_f=0}^{J_f=COS} P(J_f, E)}, \tag{1.17}$$

where $COS = (S_h + S_l)/2$ is the center of spin with S_h and S_l - spins of high and low spin states. States with spins $> COS$ would feed the isomeric state, while states with spins $< COS$ would feed the ground state, and states with spins $= COS$ feed both states equally.

However, there are several drawbacks to the HVM-based IR calculation. It assumed that the spin cut-off parameter σ was constant, independent of excitation energy. HVM-based IR is sensitive to the supposed spin cutoff parameter σ, which is assumed to be constant and independent of the excitation energy. The IR is also dependent on the assumed multiplicity and multipolarity of the γ-ray cascade after neutron evaporation or neglect of the actual nuclear-level structure in the calculation of final γ-cascades. The HVM has taken into account only the E1 transition in the γ-ray cascade and the application of this model has been limited to nuclear reactions at relatively low energies and spins.

In the case of the (n, γ) reaction induced by thermal and resonant neutrons, it is supposed that only s-wave neutrons with spin of $1/2\hbar$ are captured and governed by the compound mechanism. Therefore, the spin of the excited state in the compound nucleus can be $J_c = J_0, J_0 \pm 1/2$. To calculate IR in this type of reaction, HVM is

also applied as the case of the (γ, n) reaction except for the second stage being absent, and the transitions of primary and intermediate levels of the excited compound nucleus should follow by the formation of the isomeric and ground states.

Until now, to calculate the cross section and IR, several codes have been developed and employed based on the computational scheme for sophisticated nuclear models. Kolev calculated the IR of ^{117m,g}In and ^{120m,g}Sb produced in photonuclear reaction with bremsstrahlung end-point energies of 43 and 18 MeV by means of the code STAPRE and the code COMPLET to interpret the role of angular momentum removal [40]. Currently, similar to EMPIRE, TALYS is a nuclear reaction modeling code employed often for calculating cross sections and the IR.

TALYS code

TALYS is a nuclear reaction program for the analysis and prediction of nuclear reactions created and developed at NRG Petten, the Netherlands, CEA Bruyeres-le-Chatel France, University Libre, Brussels, and at the IAEA, Vienna in recent years. TALYS code can be used to simulate nuclear reactions that involve neutron, gamma, proton, deuteron, triton, helium-3 and α particles in the energy range of 1 keV - 200 MeV on target nuclei of mass 12 and heavier. Unfortunately, the TALYS code has not been resolved completely for the case of thermal and epithermal neutron capture reactions. The code considers different nuclear reaction models, i.e., the optical, compound nucleus, pre-equilibrium, direct reaction, fission models, and the problems connected to level density and γ-ray strength, as illustrated in Fig. 1.2.

The TALYS database of nuclear structure parameters based on the IAEA Reference Input Parameter Library (RIPL) provides validated nuclear model input parameters. The output of this code comprises complete sets of reaction data such as the cross section, energy spectra, and angular distribution of the emitted particles.

There are two main purposes of TALYS, which are strongly connected. First, it is a nuclear physics tool that can be used for the analysis of nuclear reaction experiments. Second, it is a nuclear data tool. Using the available experimental data, TALYS can generate nuclear data for all open reaction channels after fine-tuning the adjustable parameters of the various reaction models. It can interpolate between and extrapolate beyond the experimental data on the user-defined energy and angle grid beyond the resonance region. TALYS offers a complete set of quantitative outputs for a nuclear reaction for all open channels together with associated cross-sections, spectra, and/or

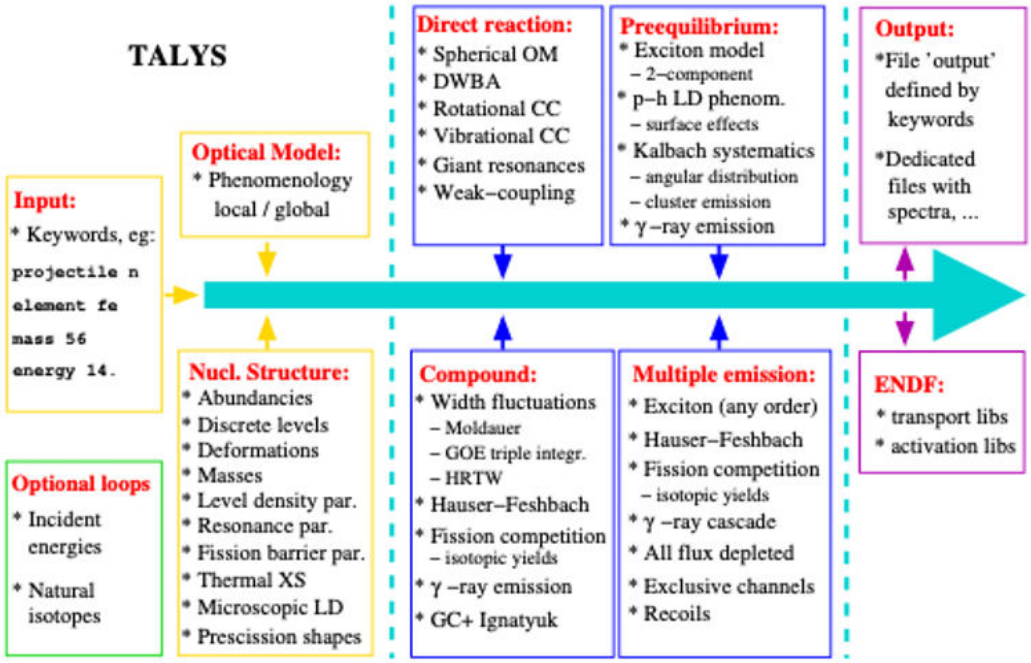

FIGURE 1.2: Organization of input-output flows and components of the nuclear model in the TALYS program. Image taken from [56].

angular distributions. TALYS updates itself depending on the current state of nuclear reaction theory, providing the current capability to model that theory. TALYS output can be generated by more or less sophisticated physical methods or by simpler phenomenological approaches. The latest version of the TALYS code is TALYS 1.96 (release date: December 30, 2021) with approximately 400 keywords that can be changed depending on the user's purposes.

TALYS have been extensively employed to obtain theoretical excitation function and IR in various types of nuclear reactions. Danagulyan [57] using TALYS 1.4 studied IRs in proton and alpha-induced reactions for nuclei in the mass number range of A = 44 – 124. The TALYS-calculated data reveal the dependence of IR on the projectile species, while for several nuclei in high-spin states, the experimental data were not reproduced well by calculation. In another study of Junhua [58, 59], the experimentally measured data for cross sections and IRs in $(n, 2n)$ reactions induced by fast neutrons on Eu, Nb, and Ba targets were compared with calculations using the TALYS 1.8 code with different level density models. The general trend of the experimental and theoretical data was observed in this case.

For one-step photonuclear reactions (γ, n) in the GDR region, there are several recent studies on TALYS code to validate the cross-sections and IRs, such as in refs [60,

61] of Palvanov (for Se and Pd isotopes), Mazur [62] (for Te isotopes) and Danagulyan [63] (for Sn, Te, Hf, and In isotopes). In particular, Makwana et al. [64] have established a new empirical formula for the reaction cross section (γ, n) near the GDR peak for elements with $Z > 60$ and reproduced well by calculations using the Talys 1.6 and EMPIRE – 3.2.2 codes. Danagulyan [63] measured the yields of photonuclear reactions on Sn, Te, and Hf targets, as well as the IRs of ^{117m,g}In, $^{119m,g;121m,g;129m,g}$Te and ^{123m,g}Sn isomeric pairs. The results obtained were considered using TALYS 1.4 and it was indicated that the disagreements between the TALYS-calculated and experimental data may be due to an inaccurate model description of the level density. Rahman [65], Naik [66], and Vodin [67] investigated experimental IRs calculated with TALYS in a few photonuclear reactions on various targets with multiple particle emissions beyond the GDR region. They concluded that the TALYS code was only able to describe definite reactions with definite models.

According to a growing body of recent studies using TALYS code, it is clear that the use of this code to interpret the cross section and IR data has attracted interest. However, since the measured IRs in photonuclear reactions are mainly induced by bremsstrahlung, the TALYS code is often used in combination with the bremsstrahlung spectra obtained from transportation / Monte Carlo simulation codes such as GEANT4 [68], MCNP [69] or FLUKA [70]. Recently, P.V.Cuong et al. [71] have incorporated TALYS-calculated differential cross section data into the GEANT4 toolkit to proceed with a complete simulation of both bremsstrahlung production and photonuclear reaction process, as well as to obtain the IRs. In this work, we employed another method, where only bremsstrahlung spectra obtained from the GEANT4 code were used to couple with TALYS-computed cross sections to analytically calculate the IRs. Although this method seems more schematic than that in [71], it should be free from additional bias from particle transportation involved in the GEANT4 simulation of the photonuclear reaction process.

GEANT4 toolkit

GEANT4 [68] simulation toolkit abbreviation stands for GEometry ANd Tracking, which is a toolkit for Monte Carlo simulations of the passage of particles through matter. This toolkit provides all functionality needed to simulate the detector system, including the interactions of particles, the geometry of the detector system, and the detector response. GEANT4 is a freely available object-oriented software package based on C++, where users build their simulation applications based on existing virtual

classes. With GEANT4, users can add more capabilities as needed, for example, by adding new physical processes or changing the response of some detectors. GEANT4 has been developed for high-energy physics applications, starting from CERN, an international collaboration with participants from more than 10 laboratories in Europe, the USA, Japan, Russia, and Canada. So far, GEANT4 has been employed in various fields such as nuclear and accelerator physics as well as medical and space science.

To utilize GEANT4 for simulation, users have to provide some necessary definitions and the so-called user actions. Users should define the geometry setup, including detectors and other passive materials. This can be done by overriding the methods in the virtual class G4VUserDetectorConstruction. The geometry should be defined together with the materials used in the simulation. The next mandatory user class overrides the virtual class G4VUserPhysicsList, which defines the particles and physical processes. The last user class that needs to be implemented is the G4VUserPrimaryGeneratorAction, in which the methods to create particles to be tracked are defined. To extract useful information from the simulation output, a set of user action classes can be used, namely G4UserRunAction, G4UserEventAction, G4UserStackingAction, G4UserTrackingAction, and G4UserSteppingAction. These virtual classes, which can be overridden by users, allow them to interact with the track of particles in any medium at different levels.

In this work, GEANT4 was used to simulate as closely as possible the experimental condition including the geometry and materials of the setup, the primary electron beam, and all possible interactions and radiations to obtain the flux distribution as a function of bremsstrahlung energies. This distribution was then combined with the theoretical cross-section data calculated by the TALYS code, yielding the theoretical IRs. One of the reasons for choosing GEANT4 as a simulation tool is that it is widely known within the nuclear physics community, with strong support from the community, especially in maintaining an up-to-date experimental cross section database. In addition, unlike MCNP [69], which is also a well-known simulation package, GEANT4 is a free open source software package. And the TALYS code is employed to calculate the cross-section since it has the completeness of reliable nuclear models, flexibility and user-friendliness.

This work aims to study the IRs of several isomeric pairs produced in two types of reactions, namely photonuclear reaction (γ, n) and neutron capture reaction (n, γ). Therefore, the outlines of these reactions are represented in the following section.

1.3 Photonuclear reaction

The study of nuclear reactions induced by photons (photonuclear reaction) plays a crucial role in understanding the interaction mechanism between photons and the nucleus, as well as the nuclear structure. Furthermore, these reactions are widely used for a variety of applications, such as radiation shielding design, radiation transport, absorbed dose calculations for nuclear medicine, the technology of fusion-fission reactors, nuclear transmutation, and waste management [72]. In recent decades, advanced photon sources with strong intensity and high quality combined with state-of-the-art detector technology have paved the way for new scientific discoveries and technological applications [73].

This section focuses on a description of the formation and features of photonuclear reactions below and above the particle-separation threshold, especially in the GDR region.

1.3.1 Formation of photonuclear reaction and photon sources

In 1934, Chadwick and Goldhaber published the first experimental paper on a photonuclear reaction [74]. They observed the emission of a proton and a neutron from the photonuclear reaction on deuterium target induced by 2.6 MeV photons originating from ThC" (^{208}Tl). Three years later, by the use of 440 keV proton beam impinging on ^{7}Li target, Bothe and Gentner [75] observed nuclear transmutation and the emission of 17 MeV γ-rays. These high-energy γ-rays were then employed to carry out several photonuclear reaction studies on various isotopes. In 1947, Baldwin and Klaiber [76] used a continuous γ-ray spectrum (bremsstrahlung) for the first time to study photonuclear reactions. The bremsstrahlung with end-point energy range of 10 to 100 MeV had been generated from a betatron accelerator at the General Electric Laboratory to investigate the excitation function. In August 1959, the first Gordon Research Conference on photonuclear reactions [77] was organized at the Kimball Union Academy. Since then, this topic has developed quickly in scientific findings and applications parallel with the development of high-intensity and fine-quality photon sources and advanced detection techniques.

According to the timelines, there are several photon sources exploited and employed to induce photonuclear reactions [73]:

– 1937: (p, γ) reaction and subsequent photodissociation (Bothe, Gentner)

- 1947: Bremsstrahlung from betatron (Baldwin, Klaiber)
- 1953: Positron annihilation in flight (Colgate, Gilbert)
- 1963: Laser Compton Backscattering (Milburn, Arutyunian, Tumanian)
- 1969: Bremsstrahlung from the Van de Graaff accelerator (Metzger)
- 1983: Tagged photons (Knowles et al.)
- 1980s: High-performance bremsstrahlung (Kneissl, Richter)
- 1990s: High-performance laser Compton backscattering (Litvinenko, Ohgaki, Pietralla)

Currently, popular photon sources used to study photonuclear reactions consist of bremsstrahlung and quasimonoenergetic photon sources. There are three methods to produce the latter including positron annihilation, tagged photons being thin-target bremsstrahlung photons with simultaneous detection of the corresponding decelerated electrons, and Laser Compton Backscattering resulting from the collision of relativistic electrons and laser beam. However, the disadvantage of the first two methods is low intensity and low energy resolution. For the third one, high-intensity quasimonoenergetic and fully-polarized photon beams can be produced in various energy ranges such as keV photons in AIST, MeV photons in ELI-NP, NewSUBARU, HIGS and LLNL, and GeV photons in Spring-8 [78]. This method requires the use of modern, expensive equipment, and sophisticated techniques. Therefore, bremsstrahlung beam is employed as an effective photon source in many studies of photonuclear reaction. Bremsstrahlung is electromagnetic radiation resulting from the deceleration of a charged particle by another charged particle, e.g., an electron by an atomic nucleus. Bremsstrahlung is produced by using particle accelerators such as the Betatron and Microtron to accelerate the electrons, which then impinge on a heavy target. Bremsstrahlung has a continuous spectrum with an end-point energy equal to the energy of accelerated electrons. The energy spectrum of the bremsstrahlung photons is often calculated using Monte Carlo simulation codes such as GEANT4, FLUKA and MCNP.

1.3.2 Cross-section of photonuclear reaction

This subsection describes the cross-section of photonuclear reactions on medium and heavy nuclei with various incident photon energies. The first energy region of interest

is from particle emission threshold up to 30 MeV. The second is incident energy less than the particle emission threshold. The last one is the photon energy range of 30 to 140 MeV. Fig. 1.3 illustrates the general total photon absorption cross section below 30 MeV.

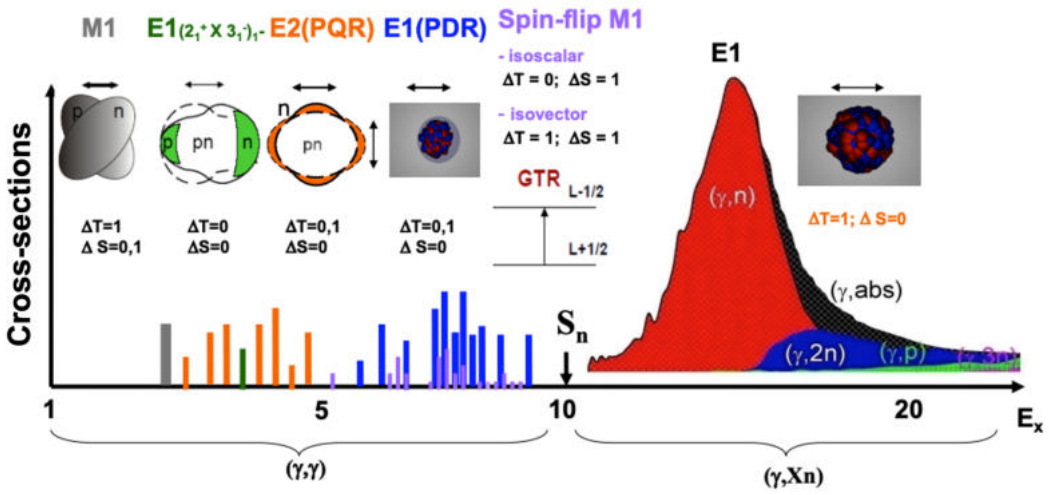

FIGURE 1.3: The general total photon absorption cross-section below 30 MeV (taken from the presented slice of N.Tsoneva at ERICE2014).

Above particle emission threshold up to 30 MeV

If the photon energy is higher than the particle evaporation threshold S_n and up to 30 MeV for most medium and heavy nuclei, the photon wavelength is comparable to the nucleus diameter. The giant resonance, a remarkable feature, may occur due to the collective excitation rapidly broadening the level width and coalescing the levels. In other words, the cross-sections depending on the incident energy, arise a giant peak as in Fig. 1.3.

The various giant resonances observed can be classified according to their multipolarity and character (isoscalar or isovector) [79, 80]. In general, three kinds of giant resonances are observed: (i) Giant Monopole Resonance (GMR), corresponding to the collective motion of the nucleus around a single pole, (ii) Giant Dipole Resonance (GDR), corresponding to two poles oscillating against each other, and (iii) Giant Quadrupole Resonance (GQR), corresponding to the oscillation of four poles in a quadrupole deformed nucleus. Following macroscopic descriptions, the isoscalar character ($\Delta T = 0$) of the giant resonance can be described as the oscillation in a phase of protons and neutrons, while the isovector character ($\Delta T = 1$) corresponds to

neutrons oscillating against the protons. Giant magnetic resonances occur with a spin-flip ($\Delta S = 1$), while electric ones do not. Schematics for the possible giant resonances are shown in Fig. 1.4.

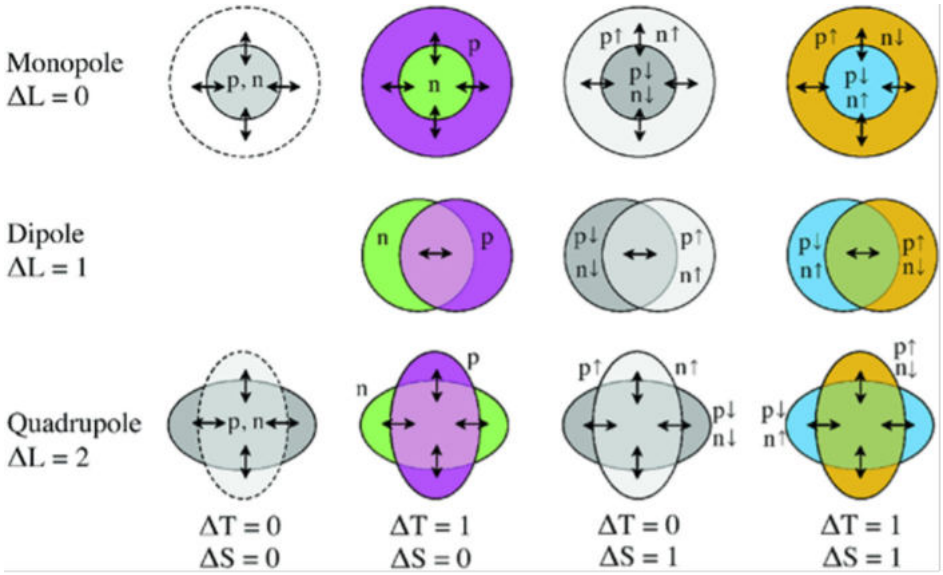

FIGURE 1.4: An schematic illustration of various giant resonance modes of monopole ($\Delta L = 0$), dipole ($\Delta L = 1$) and quadrupoles ($\Delta L = 2$), their magnetic ($\Delta S = 1$) or electric ($\Delta S = 0$), isovector ($\Delta T = 1$) or isoscalar ($\Delta T = 0$) characters [80].

The strongest resonance is the isovector giant electric dipole resonance, first discovered by Bothe and Gentner [75] in a photonuclear reaction and later described by Migdal as an out-of-phase oscillation of the proton fluid against the neutron fluid [81]. Therefore, the region above S_n up to 30 MeV is often called Giant Dipole Resonance (GDR). The energy dependence of the GDR cross-section for the medium and heavy nuclei has often been approximated by a Lorentzian function [73]:

$$\sigma_{GDR}(E_\gamma) = \sum_i \sigma_i \frac{(E_\gamma \Gamma_i)^2}{(E_\gamma^2 - E_i^2)^2 + (E_\gamma \Gamma_i)^2}, \tag{1.18}$$

where σ_i, E_i and Γ_i are the cross-sectional size of the GDR peak, the energy and the decay width, respectively. The index $i = 1$ for spherical nuclei and $i = 1, 2$ for deformed nuclei.

For instance, the GDR peak energy is 13.5 MeV, and the 4 MeV width for the heavy spherical target nucleus ^{208}Pb. With a non-spherical nucleus ^{160}Gd regarding the prolate deformation, the photonuclear cross-section curve has two peaks: one corresponding to a dipole vibration along the axis of deformation and the other perpendicular to that axis. Two Lorentz functions have been fitted giving $E_1 = 12.23$ MeV,

$\Gamma_1 = 2.27$ MeV, and $E_2 = 15.96$ MeV, $\Gamma_2 = 5.28$ MeV. The GDR in light nuclei is often fragmented. The experimental GDR in ^{28}Si has four well-separated peaks. This splitting is probably due to shell effects.

The sum of the photoabsorption cross section is expressed as:

$$\int_0^\infty \sigma_{GDR}(E_\gamma) dE_\gamma = 60 \frac{NZ}{A} \quad (MeV \cdot mb). \tag{1.19}$$

Which depends on the target nucleus mass, neutron and proton numbers (A, N and Z), following the dipole sum rule [82]. The peak width spans between 3 and 10 MeV, where the smallest values are for closed-shell nuclei and the greatest values are for nonspherical nuclei [83]. The peak energy is within the range of 13 and 25 MeV and slowly varies as a function of mass number.

To explain the GDR, Goldhaber and Teller [84] proposed that the giant peak was due to protons and neutrons oscillating against each other in the electromagnetic field of incident photons. Two years later, Steinwedel and Jensen [85] proposed a two-fluid model of the GDR based on a similar idea. They assumed that the nucleus behaved as a nuclear fluid with constant density. In the giant dipole mode, the variation of the neutron and proton density was governed by hydrodynamical equations. The Goldhaber-Teller mechanism or the Steinwedel-Jensen mechanism can obtain the resonance energy function depending on the mass number, $A^{-1/6}$ or $A^{-1/3}$ respectively. However, compared with the experimental results, this dependence can be better described in the combination of two mechanisms. For medium and heavy nuclei, the centroid energy of GDR can be estimated by [73]:

$$E_{GDR} = 31.2 \cdot A^{-1/3} + 20.6 \cdot A^{-1/6}. \tag{1.20}$$

Below particle emission threshold

In the low-energy region below the S_n, the photon wavelength is significantly longer than the nuclear diameter resulting in dominant elastic and inelastic scattering processes, which exhibit a few isolated absorption lines in this region. At the lowest energy, Thomson elastic scattering on the nucleus can occur. The differential cross-section at angle θ is given by [86]:

$$\frac{d\sigma}{d\Omega} = \frac{(Ze)^4}{2(Mc^2)^2}(1 + cos^2\theta). \tag{1.21}$$

This cross section is independent of the photon energy and amounts only to a few nanobarns (nb). Therefore, elastic scattering of photons off nuclei is often considered sub-dominant or even negligible.

Photons with slightly higher energy and below S_n are absorbed by the target nucleus, resulting in "small" resonances. In this case, a resonant absorption process of photons by the nucleus leading to the subsequent reemission of γ radiation has occurred, the so-called resonance photon-scattering reaction or nuclear resonance fluorescence. One conducted the nuclear resonance fluorescence experiments to detect and study "small" resonances such as scissor resonance M1, two-phonon state E1, pygmy quadrupole resonance E2, pygmy dipole resonance E1 and spin-flip M1 (Fig 1.4).

Pygmy resonance

Pygmy dipole resonance (PDR) is found to be a common feature in neutron-rich nuclei (protons) such as the core nucleus and the excess neutrons (protons) vibrating against the core described by Suzuki [87]. The PDR often appears at the top of the low-energy tail of the GDR. The energy centroid of the resonance and its magnitude are smaller than that of the GDR since the restoring force depends on the number of excess neutrons (protons). A review of the pygmy dipole resonance can be found in [88]. Another pygmy resonance predicted theoretically and studied experimentally is the pygmy quadrupole resonance (PQR) in the skin nuclei [89].

Scissors resonance

The scissors resonance is a M1 magnetic dipole resonance, which is located at fairly low energies $\approx$ 3 MeV and is believed to be present only in deformed nuclei [90]. It has been observed in rare-earth nuclei [91], and in actinides [92, 93]. This resonance is generally viewed as the neutrons oscillating against the protons in a scissors-like motion.

Magnetic dipole spin-flip resonance

The magnetic dipole spin-flip resonance results from spin-flip collective excitations [94], where nucleons with spin $\uparrow$ oscillate against those with spin $\downarrow$, acting as an isoscalar mode of excitation. In addition, an isovector excitation mode is possible, where protons with spin $\uparrow$ oscillate against neutrons with spin $\downarrow$ and vice versa.

In the energy range of 30 to 140 MeV

In this region, the photon wavelength is comparable to the size of the intranuclear distance. The neutron-proton pair in the nucleus is likely to absorb the photon and

then be released from the nucleus as quasi-deuteron emission. Besides, two or more nucleons can also be released from the target nucleus by direct reaction, leading to the formation of various reaction products. The QD cross-section, $\sigma_{QD}(E_\gamma)$, is expressed in the model of Chadwick et al. [95] based on a Levinger-type theory [96] as follows:

$$\sigma_{QD}(E_\gamma) = L\frac{NZ}{A}\sigma_d(E_\gamma)f(E_\gamma), \tag{1.22}$$

where L, $\sigma_d(E_\gamma)$ and $f(E_\gamma)$ are the Levinger parameter, experimental deuteron photo-disintegration cross-section and Pauli-blocking function, respectively.

1.3.3 (γ, n) reaction

In the GDR region, the emission probability of a single neutron is highest compared with that of multi-neutrons, a proton, or a charged particle. Since the reaction threshold of (γ, n) reaction is less than that of the reactions $(\gamma, 2n)$ and $(\gamma, 3n)$ reactions, and (γ, n) reaction is not affected by the hindrance of the Coulomb barrier as in the proton-induced reactions, charged particles. Therefore, the (γ, n) cross section dominates in the GDR region. The (γ, n) reaction is a three-step process. In the first step, the target nucleus absorbs incident photons to form a compound nucleus at a high excited state and emits prompt γ radiation. In the second step, after reaching statistical equilibrium, the compound nucleus decays through a specific exit channel (mostly single neutron emission) as an evaporation process to form a residual nucleus. In the final step, this residual nucleus deexcites to the isomeric state or the ground state by direct γ-decay or γ-cascade transitions.

The scope of this work is to study IR in the (γ, n) reaction on heavy spherical or deformed nuclei induced by bremsstrahlung with the end-point energy in the GDR region. This is based on three main reasons. Firstly, in this region, the electromagnetic interaction is well-known, and the absorption of the electric dipole photon E1 is dominant. After absorbing a photon E1, the nucleus with a spin of J_0 is excited to spin J_0, $J_0 \pm 1$, whereby the theoretical consideration is simple. Secondly, although the photonuclear reaction cross-section is very low, the high bremsstrahlung flux and the GDR cross-section result in a high reaction yield enough for the experimental analysis with high accuracy. Finally, the study on the IR in photonuclear reactions reveals considerable interest due to the significant difference from nuclear reactions induced by other projectiles.

1.4 Neutron capture reaction

1.4.1 Neutron and neutron sources

In 1932, Chadwick discovered the existence of neutrons using beryllium to absorb alpha particles originating from a polonium source [97]. Three years later, he won the Nobel Prize in Physics for this discovery. The neutron is a neutral particle with a mass slightly larger than the mass of the proton. A free neutron is unstable and decays with a mean half-life time of about 636 seconds into a proton by β^- emission. Neutrons are arbitrarily classified according to their kinetic energies into various categories as follows [98]:

- Cold Neutrons (0 eV; 0.025 eV).
- Thermal Neutrons. Neutrons in thermal equilibrium with a surrounding medium. The most probable energy at 20°C (68°F) for Maxwellian distribution is 0.025 eV.
- Epithermal Neutrons (0.025 eV; 0.4 eV).
- Cadmium Neutrons (0.4 eV; 0.5 eV). The kinetic energy of this type of neutron is below the cadmium cut-off energy (0.5 eV). The natural cadmium foil absorbs strongly neutrons below 0.5 eV, as shown in Figure 1.5, mainly due to ^{113}Cd isotope (12.23 %).
- Epicadmium Neutrons (0.5 eV; 1 eV). Neutrons of kinetic energy above the cadmium cut-off energy. These neutrons are not absorbed by cadmium.
- Slow Neutrons (1 eV; 10 eV).
- Resonance Neutrons (10 eV; 300 eV).
- Intermediate Neutrons (300 eV; 1 MeV).
- Fast Neutrons (1 MeV; 20 MeV).
- Relativistic Neutrons (>20 MeV)

Neutron sources available in standard laboratories are of three main categories (a) Accelerators-based neutron sources, (b) Radioisotope neutron sources and (c) Nuclear reactor-based neutron sources. The possibilities of using these neutron sources depend on the type of their applications. All available neutron sources emit fast neutrons of various energies and intensities. We can reduce the speed of fast neutrons by collisions

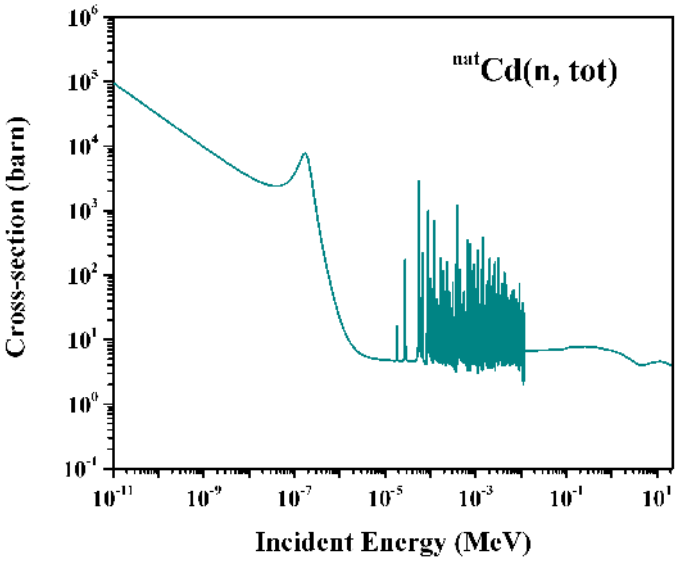

FIGURE 1.5: Total neutron absorption cross-section of ^{nat}Cd, taken from the JEFF-3.3 library.

with atoms of materials (the so-called moderators) such as water, graphite, beryllium, and hydrocarbons. This process of slowing is called moderating the neutrons. The choice of the appropriate neutron source depends on its energy, intensity, cost, size, portability, and shielding requirement.

Depending on the energy, neutrons can induce three main types of interaction with a nucleus such as compound nucleus reaction, scattering, or direct reaction. For fast neutrons, (n,p), (n,α) and (n,2n) reactions are possible. For thermal, epithermal and resonance neutrons, the primary reaction is the capture reaction, in the form of the (n,γ) reaction [99] or other words, the only compound mechanism occurs in this case.

1.4.2 (n, γ) reaction

For the nonfissionable nuclei, the only possible reaction with low-energy neutrons is the absorption reaction or the neutron capture reaction. Neutron capture reaction (n,γ) induced by thermal and epithermal neutrons governed by the compound mechanism. The incident neutrons assumed to be mostly s-wave neutrons with zero angular momentum are completely absorbed to form a compound nucleus in an excited state. After capturing a neutron, the nucleus with a spin of J_0 is excited to spin J_0, $J_0 \pm 1/2$. The excitation energy of the compound nucleus is close to the neutron binding energy due to the negligible kinetic energy of the incident neutrons. Immediately thereafter, the compound nucleus emits the prompt γ radiation with energies up to several MeV.

The compound nucleus continues to decay to the isomeric or ground state of the product nucleus by the direct emission or the cascade transition of γ-rays. In many cases, the product nucleus is a radioactive nucleus, which emits a beta particle to form the nucleus with an increase in atomic number by one.

Studies of neutron capture reactions (n,γ) have contributed to our understanding of neutron separation energies, γ-ray transition probabilities, decay schemes, and the properties of nuclear energy levels. In addition, (n,γ) reaction plays an essential role in the nucleosynthesis of elements heavier than iron created by successive neutron capture reactions and β-decay. Owing to the high Coulomb barrier, these elements can not be produced by charged particle reaction. The nucleosynthesis processes involving neutron capture include the slow neutron capture (s-process) and the rapid neutron capture (r-process), depending on the neutron flux and neutron density. The probability of neutron capture is characterized by the neutron capture cross section.

1.4.3 Neutron capture cross-section

Neutron-induced cross sections play a crucial role not only in fundamental nuclear research but also in applications such as nuclear medicine, fuel, dosimeter, shielding calculation and waste management [100]. The cross-section of neutron capture depends on neutron energy and the target nucleus. Fig. 1.6 shows neutron capture cross sections of ^{114,116} Cd (n,γ) and ^{108,110}Pd (n,γ) corresponding to green, blue, orange and violet lines as a function of the incident neutron energy, taken from the JEFF-3.3 library.

Two regions are distinguished in Fig. 1.6. For the low-energy region, the cross sections obey a dependence of $1/\nu$ with ν being the neutron velocity. Neutrons that interacted in this region are mainly thermal neutrons. For higher incident energies, the cross-sections occur in high peaks superimposed on the $1/\nu$ trend. These peaks are so-called resonance peaks. Most of the neutrons that interact in this region are epithermal and resonance neutrons. For heavy nuclei, high and narrow resonances appear in the eV energy range. The Breit-Wigner formula is used for the single and isolated resonance cross section as follows [99]:

$$\sigma(E) = g\frac{\pi}{k^2}\frac{\Gamma_0\Gamma_f}{(E-E_r)^2+\Gamma^2/4}, \tag{1.23}$$

where $g = (2J+1)/(2J_0+1)$ is the statistical factor or spin factor depending on the total angular momentum of resonance state and initial state (J and J_0); k is the

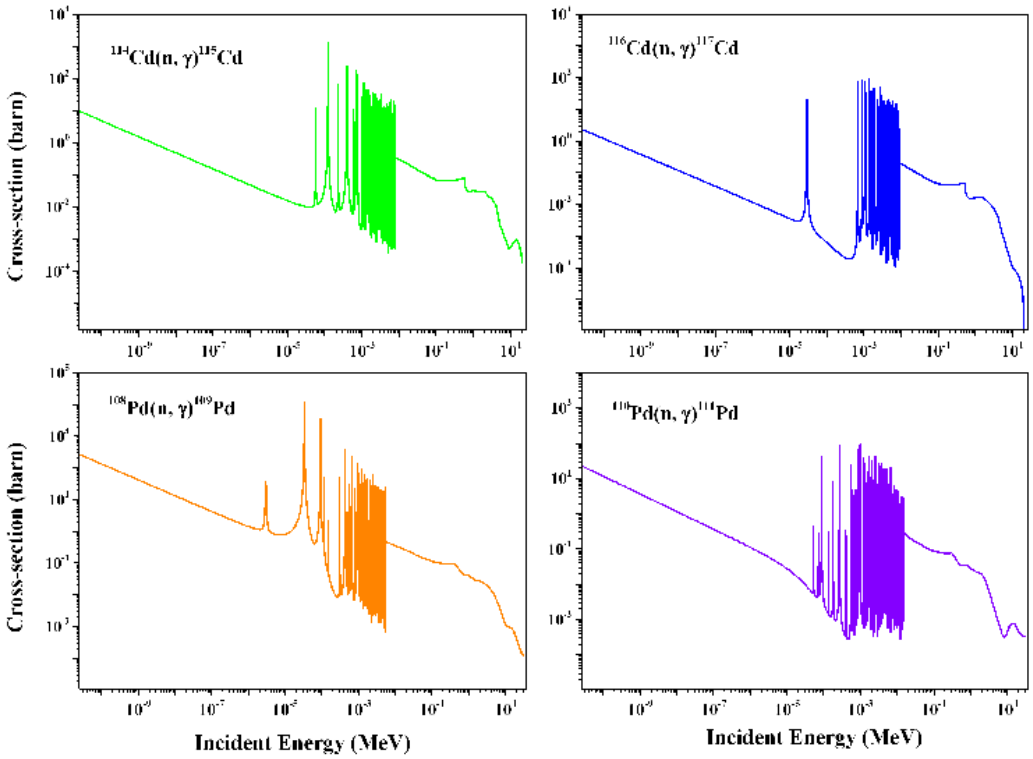

FIGURE 1.6: Neutron capture cross-section of ^{114}Cd, ^{116}Cd, ^{108}Pd and ^{110}Pd, taken from the JEFF-3.3 library.

wavenumber; E_r is the centroid energy; $\Gamma_{0(f)}$ is the partial decay width of the entrance (exit) channel and $\Gamma = \hbar/\tau = \sum \Gamma_i$ is the total decay width.

For incident neutron energies of keV, the number of resonances per energy interval increases, resulting in overlapping resonances and an enhanced continuum. The resonances in this region are complex and difficult to detect individually. Therefore, they can be measured by summing the resonances, i.e. calculating the resonance integral. The thermal-neutron cross section and resonance integral were investigated in refs. [101, 102]. In the fast neutron region, the decrease in the neutron capture probability of the nucleus leads to the rapid reduction of the cross sections.

The Hauser–Feshbach (HF) statistical theory [103] is applied to calculate the cross section of the compound nuclear reaction, which is related to the transmission coefficient. It is difficult to evaluate this coefficient. The level density is employed to estimate the transmission coefficient to form the compound nuclide, and the γ strength function is powerful for describing the γ-ray emission channel. These quantities are presented in the following section.

1.5 Level density and γ-ray strength function

Investigation of the nuclear level density (LD) and γ-ray strength function (γSF) are crucial for interpreting the underlying nuclear structure. LD and γ SF are the key ingredients in nuclear reaction models, used to predict the nuclear reaction rate, cross section and the modeling process in a nuclear reactor and astrophysics. In the following subsections, the theory behind the LD and γSF will be presented, along with the models available in TALYS 1.95.

1.5.1 Nuclear level density

The mean spacing D between individual states can be determined by analyzing the discrete spectrum at low excitation energies. However, it becomes more difficult with increasing energy and nuclear mass. At excitation energies greater than several MeV for medium and heavy nuclei, the spacing D becomes small, and at some points it is impossible to distinguish experimentally between individual states. In this region, the level scheme is often referred to as quasi-continuous. At even higher energies beyond the neutron binding energy, D becomes much narrower than the natural line width Γ of the excited states terminating in overlapping many nuclear resonances. In this case, a continuum of nuclear levels is formed. Therefore, nuclear excitations are frequently classified into three regions, based on a comparison between the mean level spacing D and γ-decay width Γ. Fig. 1.7 [104] illustrates the discrete region, quasi-continuum region, and continuum region. As a result, while counting each level separately is impossible, an average description is employed, that is, the nuclear LD. The LD is inversely proportional to spacing D, and the level density $\rho(E_x, J, \pi)$ is described as the number of nuclear levels per MeV around an excitation energy E_x for a given spin J and parity π.

Several models are available to describe the LD, mainly categorized into semiempirical and microscopic models. The former, so-called phenomenological LD models, have been built similarly to thermodynamics, while the latter solve the Schrodinger equation for many-body.

The most popular LD models are represented in this subsection ranging from phenomenological analytical expressions to tabulated LD of microscopic models [56].

Phenomenological level density model

The Fermi Gas level density

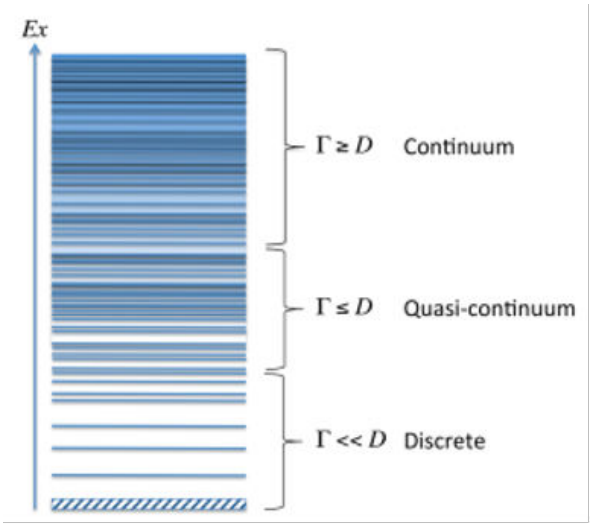

FIGURE 1.7: Nuclear excitation energy regimes [104].

In 1936, H.Bethe introduced the first theoretical calculation of the LD originated from the comparison of the excited nuclear states and the Fermi gas [105], in which it is presumed the non-interactive movement of particles, and the identical space between single-particle states. The initial formula indicates the dependence of LD on the excitation energy E_x as follows:

$$\rho(E_x) = \frac{\sqrt{\pi}}{12} \frac{exp(2\sqrt{aE_x})}{a^{1/4}E_x^{5/4}}. \tag{1.24}$$

Based on Bethe's original expression and data from the literature, Ericson [106] suggested a formula for LD depending on spin, parity, and excitation energy, today the so-called Fermi-gas LD:

$$\rho(E_x, J, \pi) = \frac{1}{2}\frac{2J+1}{2\sqrt{2\pi}\sigma^3} exp\left[-\frac{\left(J+\frac{1}{2}\right)^2}{2\sigma^2}\right] \frac{\sqrt{\pi}}{12}\frac{exp(2\sqrt{aU})}{a^{1/4}U^{5/4}}, \tag{1.25}$$

where J, U, a and σ are the spin of the nucleus, the effective excitation energy, the LD parameter and the spin cutoff parameter, respectively.

The effective excitation energy is given by:

$$U = E_x - \Delta, \tag{1.26}$$

where E_x, Δ are the true excitation energy and the energy shift (an empirical parameter related to the pairing energy).

Summing over all spins yields the total LD given by

$$\rho_F^{tot}(E_x) = \frac{\sqrt{\pi}}{12}\frac{exp(2\sqrt{aU})}{a^{1/4}U^{5/4}}\frac{1}{\sqrt{2\pi}\sigma}. \tag{1.27}$$

The total LD can be calculated from the three parameters: a, σ, and Δ. Currently, various values of a, σ, and Δ are available. Furthermore, these parameters can be extracted independently or depended on the excitation energy. Egidy and Bucurescu [107, 108] assembled the parameter values of a, σ, and Δ for more than 300 nuclides.

The back-shifted Fermi gas model

The back-shifted fermi gas (BSFG) model of Dilg [109], proposed by Gilbert and Cameron in 1965 [110] for the LD is based on the Fermi gas approximation. The expression of LD of the BSFG model is similar in Eqs. 1.25 and 1.27. However, the value of effective excitation energy U is changed by $U = E_x - \Delta^{BFM}$, where the energy shift Δ^{BFM} is given by

$$\Delta^{BFM} = \chi\frac{12}{\sqrt{A}} + \delta, \tag{1.28}$$

with χ = -1, 0 and 1 for odd-odd, odd-even, and even-even nuclei, respectively, and δ - an adjustable parameter to fit experimental data per nucleus.

The constant temperature model

The Constant Temperature Model (CTM) was introduced by Gilbert and Cameron [110]. Within the model, the excitation energy range is divided into a low-energy part from 0 MeV up to a matching energy E_M, and a high-energy part above E_M, where the respective "constant temperature" law and the Fermi gas model apply. There, the total LD is given as

$$\rho^{tot}(E_x) = \begin{cases} \rho_T^{tot}(E_x) & if E_x \leq E_M \\ \rho_F^{tot}(E_x) & if E_x \geq E_M. \end{cases} \tag{1.29}$$

When $E_x \geq E_M$, the total LD is determined by Eq. 1.27.

The effective excitation energy $U = E_x - \Delta^{CTM}$, where the energy shift Δ^{CTM} is given by

$$\Delta^{CTM} = \chi\frac{12}{\sqrt{A}}, \tag{1.30}$$

with χ = 0, 1 and 2 for odd-odd, odd-even and even-even nuclei, respectively.

For low excitation energy $E_x \leq E_M$, the constant temperature part of the total LD reads

$$\rho_T^{tot}(E_x) = \frac{1}{T} exp\left(\frac{E_x - E_0}{T}\right), \tag{1.31}$$

here T is nuclear temperature and E_0 is given by

$$E_0 = E_M - Tln[T\rho_F^{tot}(E_M)], \tag{1.32}$$

$$\frac{1}{T} = \frac{dln\rho_F^{tot}}{dE_x}(E_M). \tag{1.33}$$

Additionally, there is the dependence of T on E_0 resulting from the discrete level region as follows:

$$N_U = N_L + \left(exp\left[\frac{E_U}{T}\right] - exp\left[\frac{E_L}{T}\right]\right) exp\left[\frac{-E_0}{T}\right]. \tag{1.34}$$

The level $N_{L(U)}$ is selected to best describe $\rho_T(E_x)$ of the observed discrete states, reserved in the database. The combination of Eqs. 1.32, 1.33 and 1.34 determines T, E_0 and E_M.

The generalized superfluid model

The Generalized Superfluid Model (GSM) takes superconductive pairing correlations into account according to the Bardeen-Cooper-Schrieffer theory. Similarly, to the CTM, the GSM distinguishes two energy regions corresponding to a phase transition from the superfluid phase to the Fermi gas phase. The separation of these energy regions occurs at the critical energy U_c.

At the effective excitation energy $U^{'} \leq U_c$, a superfluid behavior is expressed through pairing correlations that strongly influence the LD. In this case, the total LD is given by

$$\rho_{GSM}^{tot}(E_x) = \frac{1}{\sqrt{2\pi}\sigma} \frac{e^S}{\sqrt{D}}, \tag{1.35}$$

where S - the entropy, D - the determinant and σ - spin cut-off parameter related to the temperature and excitation energy.

$$U^{'} = E_x + \chi\Delta_0 + \delta, \tag{1.36}$$

where χ= 2, 1 and 0 for odd-odd, odd-even, and even-even nuclei, respectively; $\Delta_0 = \frac{12}{\sqrt{A}}$ and σ is an adjustable shift parameter to obtain the best description of the experimental data per nucleus.

At the effective excitation energy $U \geq U_c$, the LD is described by the Fermi-gas model as in Eqs. 1.25 and 1.27. In this case, the effective excitation energy U is given by $U = E_x - \Delta^{GSM}$.

The parameters are expressed at the critical energy U_c in detail as in [56].

Microscopic level densities

In addition to the aforementioned phenomenological models, there are different options employing microscopic approaches described and implemented in TALYS 1.95 [56]. Goriely has calculated LD on the basis of Hartree-Fock calculations for excitation energies up to 150 MeV and for spin values up to $I = 30$, stored as tables. In another approach, Hilaire and Goriely calculated LD on the basis of the microscopic combinatorial model. This model incorporates detailed microscopic calculations of the intrinsic state density and collective enhancement. Nuclear structure properties determined within the deformed Skyrme-Hartree-Fock-Bogolyubov framework are used in the calculations. The calculations also used tabulated level densities of more than 8500 nuclei for excitation energies up to 200 MeV and for spin values up to $J = 49$. An additional option available in TALYS 1.95 is based on temperature-dependent Hartree-Fock-Bogolyubov calculations using the Gogny force.

1.5.2 Gamma-ray strength function

The γ-ray strength function (γSF) was first introduced by Bartholomew [111] to describe neutron capture data. The γSF representing the distribution of the average probability of the γ transition plays an important role in the description of the gamma transition in a nuclear reaction. The reaction channels (n, γ) and (γ, n) are the best cases to investigate γSF.

The γ-ray strength function $f_{XL}(E_\gamma)$ describes the average transition strength of a gamma ray at an energy Eγ, electromagnetic character X and multipolarity L.

Two types of radiative strength functions can be distinguished [112] as follows:

– The "downward" strength function $\overleftarrow{f_{XL}}$ relates to the average radiative width of gamma decay such as in (n, γ) reaction and is determined for $E_\gamma < S_n$ (neutron separation energy).

– The "upward" strength function $\overrightarrow{f_{XL}}$ relates to the cross section for gamma absorption such as in the reaction (γ, n) and is determined for $E_\gamma > S_n$.

The $\overleftarrow{f_{XL}}$ in the de-excitation process depends on the average width of the states $\langle\Gamma_{XL}\rangle$ and the resonance spacing parameter D_{XL}:

$$\overleftarrow{f_{XL}} = \frac{\langle\Gamma_{XL}\rangle}{E_\gamma^{2L+1} D_{XL}}. \tag{1.37}$$

In the deexcitation process, to calculate the competition between the emission of the γ-ray and other particles, the γ-ray transmission coefficients are used as input to the Hauser-Feshbach calculations. Therefore, γ SF is closely connected to the γ transmission coefficient $T_{XL}(E\gamma)$ given by:

$$\overleftarrow{f_{XL}} = \frac{T_{XL}(E_\gamma)}{2\pi E_\gamma^{2L+1}}. \tag{1.38}$$

The $\overrightarrow{f_{XL}}$ in the excitation process depends on the γ -absorption cross section $\sigma_{XL}(E_\gamma)$ as follows:

$$\overrightarrow{f_{XL}} = \frac{1}{(2L+1)(\pi\hbar c)^2} \frac{\langle\sigma_{XL}\rangle}{E_\gamma^{2L+1}}. \tag{1.39}$$

Eq. 1.39 means that the shape and parameters of the upward γSF are determined by the photoabsorption cross section σ_{XL} summed over all spins and parities.

In the Brink-Axel hypothesis, the upward and downward strengths are approximately equal, given that the same states are populated equally whether it is populated from above or below: $\overleftarrow{f_{XL}}(E_\gamma) = \overrightarrow{f_{XL}}(E_\gamma) = f_{XL}$.

There are different theoretical models that are widely used to interpret γSF for different modes of excitations and multiple types. Eight γSF models including phenomenological and microscopic models are employed in TALYS 1.95 [56].

The Standard Lorentzian model (SLO)

This is the model that implements the Brink-Axel hypothesis and is widely used to describe the giant electric dipole resonance (GEDR) strength. The strength is given by

$$f_{XL}^{SLO} = \frac{1}{(2L+1)(\pi\hbar c)^2} \frac{\sigma_{XL} E_\gamma \Gamma_{XL}^2}{(E_\gamma^2 - E_{XL}^2)^2 + E_\gamma^2 \Gamma_{XL}^2}, \tag{1.40}$$

where σ_{XL}, E_{XL} and Γ_{XL} represent the peak cross section, centroid energy, and width of the GEDR, respectively.

Although the SLO model well describes the GEDR close to the resonance centroid for medium and heavy nuclei, it often predicts the γSF lower than the experimentally observed strength at and below the neutron separation energy S_n.

The generalized Lorentzian model (GLO)

The generalized Lorentzian model (GLO) of Kopecky and Uhl [113] is applied for $E1$ radiation. The GLO has energy- and temperature-dependent widths given by

$$f_{XL}^{GLO}(E_\gamma, T) = \frac{1}{3(\pi\hbar c)^2}\left[\frac{E_\gamma \widetilde{\Gamma}_{E1}(E_\gamma)}{(E_\gamma^2 - E_{E1}^2)^2 + E_\gamma^2 \widetilde{\Gamma}_{E1}(E_\gamma^2)} + \frac{0.7\Gamma_{E1}4\pi^2T^2}{E_{E1}^3}\right]\sigma_{E1}\Gamma_{E1}, \tag{1.41}$$

where the energy-dependent damping width $\widetilde{\Gamma}(E_\gamma)$ is given by

$$\widetilde{\Gamma}(E_\gamma) = \Gamma_{E1}\frac{E_\gamma^2 + 4\pi^2T^2}{E_{E1}^2}. \tag{1.42}$$

And T is the nuclear temperature of the final state related to an LD model. For the Fermi gas model, T is given by

$$T = \sqrt{\frac{E_n + S_n - \Delta - E_\gamma}{a(S_n)}}, \tag{1.43}$$

where E_n, S_n, Δ, and $a(S_n)$ are the incident neutron energy, the neutron binding energy, the pairing correction and the LD parameter, respectively.

The GLO describes well both the low-energy region and the peak region of the GEDR for spherical nuclei but underestimates highly deformed nuclei in the mass range $A \sim 150 - 175$ [114].

In addition, various microscopic γ SF for $E1$ radiation have been stored in tables such as [56]:

- **Hartree-Fock BCS model**: This is a microscopic model for $E1$ radiation. Goriely and Khan calculated the gamma-ray strength functions according to the Hartree-Fock Bardeen-Cooper-Schrieffer (HF-BCS) model with Quasiparticle Random Phase Approximation (QRPA) and stored them as tables.

- **Hartree-Fock-Bogolyubov model**: This is also a microscopic option calculated by Goriely using the Hartree-Fock-Bogolyubov (HFB) model with QRPA.

– **Goriely's hybrid model**: This is a Lorentzian model with energy- and temperature-dependent width, which results in a different type of functional form at low energy than that of Kopecky-Uhl.

– **Goriely T-dependent HFB**: In this model, Goriely extended the temperature dependence of the HFB model with QRPA.

– **T-dependent RMF**: This is the temperature-dependent relativistic mean-field model calculated by Daoutidis and Goriely.

– **Gogny DIM HFB+QRPA**: This is an HFB model with QRPA calculated by Goriely based on the D1M version of the Gogny force.

1.6 Objectives

Taking into account all the points mentioned above, the main goals of this work are as follows:

1. Determine the experimental IR of the deformed and spherical nuclei in the reactions (γ, n) and (n, γ) irradiated by bremsstrahlung and thermal-epithermal neutrons, respectively. The natural Eu, Hg, Cd, Ce, Se, and Pd targets were employed to investigate the IR owing to the scarce data and/or wide discrepancies, various nuclear structure and shapes, as well as their crucial roles in many applications such as medicine, therapy, biology, electronics, material science, and nuclear reactor.

2. Consider several effects that affect the IR value, such as excitation energy, spin difference, angular momentum transfer, nucleon configuration, and reaction channel effects.

3. To compute the theoretical IR in the reaction (γ, n) using the TALYS 1.95 code in combination with the GEANT4 toolkit to compare and validate our experimental data and the others in the existing literature.

4. Contribute experimental results with high accuracy as new data and/or additional ones to the Nuclear Data Bank for fundamental research and applications, and the validity of theoretical nuclear models.

Chapter 2

Experimental and theoretical methods

Experimentally, the measurements were carried out using the activation technique in combination with an off-line γ-ray spectrometer. The activation technique was applied to generate radioisotopes of interest. The principle of this technique is to convert stable isotopes to radioisotopes by using nuclear reactions. It is possible to identify radioisotopes and determine their activity based on the information of typical γ-rays. These are the energy and peak area measured by γ spectroscopy, and the intensity and the half-life originate from the nuclear data. Several advantages of this experimental method are the uncomplicated experimental setup, the reasonably priced experimental apparatus compared to the online measurement system, and the simultaneous determination of various radioisotopes [115].

The irradiation sources, samples, experimental scheme and γ-spectroscopy as well as the experimental IR expression and necessary corrections are outlined in this chapter. In addition, the theoretical IR calculation using the TALYS 1.95 code and the GEANT4 toolkit is also discussed.

2.1 Experimental method

2.1.1 Irradiation sources

The irradiation sources, namely the thermal, epithermal, mixed energy neutrons and the bremsstrahlung, were generated from the Microtron MT-25 electron accelerator at the FLNR, JINR institute, Dubna. The MT-25 accelerator and its characterization will be presented in the following subsection.

Microtron MT-25

The Microtron MT-25 was designed by C. Simane and M. Vognar from Czechoslovakia in the 1970s [116]. It is a small cyclic electron accelerator. The electrons increase in velocity by one radio frequency field (RF) with a constant electric field and uniform magnetic field. The electrons move in circular orbits with the same point of contact in the vacuum chamber. The accelerating cavity excited by the RF field is placed at the point of contact. In other words, electrons are accelerated when they travel across the electric field of the accelerating cavity. After reaching a predefined energy value, accelerated electrons are expelled from the beam extractor [117]. The schematic layout and image of Microtron MT-25 are shown in Fig. 2.1. On the left layout, the numbers from 1 - 9 represent the magnetron, phase shifter, circulator, water load, accelerating cavity, main magnet (vacuum chamber), electron trajectories, adjustable beam extractor, and first deflector, respectively.

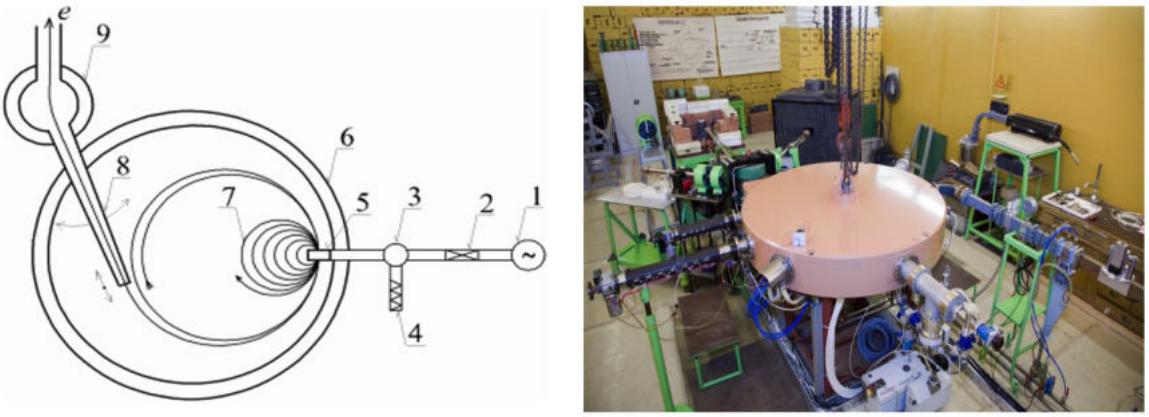

FIGURE 2.1: Schematic drawing and image of the MT-25 Microtron.

The MT-25 is the accessible source for the investigation of nuclear reactions induced by electrons, bremsstrahlung, and neutrons. It is also used to produce artificial radioactive isotopes for various purposes. Additionally, the MT-25 serves as a rather intensive source of both photons and neutrons, which can be used for several different methods and techniques, such as photon activation and thermal-epithermal neutron activation. Table 2.1 presents the main parameters of the MT-25.

The MT-25 accelerator can generate an electron beam with an energy range of 10 to 25 MeV and a step of 1 MeV. The electron beam typically has a small energy spread of about 30–40 keV (up to 600 W of average beam power).

TABLE 2.1: Main parameters of MT-25 microtron [116, 118].

Maximum electron energy	25 MeV
Energy range	10 – 25 MeV
Mean beam current	20 μA
Pulsed current duration	2.2×10^{-6}
Beam spot diameter	5 mm
Monochromatization	50 keV
Power consumption	20 kW
Bremsstrahlung beam	
Bremsstrahlung intensity	10^{14} s^{-1}
Neutron beam	
Thermal neutron flux	10^{9} s^{-1} cm^{-2}
Epithermal neutron flux	5. 10^{7} s^{-1} cm^{-2}
Fast neutron intensity	10^{12} s^{-1}

Bremsstrahlung source

Bremsstrahlung radiations have many applications in material science and technology, activation analysis, and the medical field. In this work, they are employed as projectiles to investigate the photonuclear reactions. Fig. 2.2 shows the production of bremsstrahlung using the accelerated electrons and a proper converter.

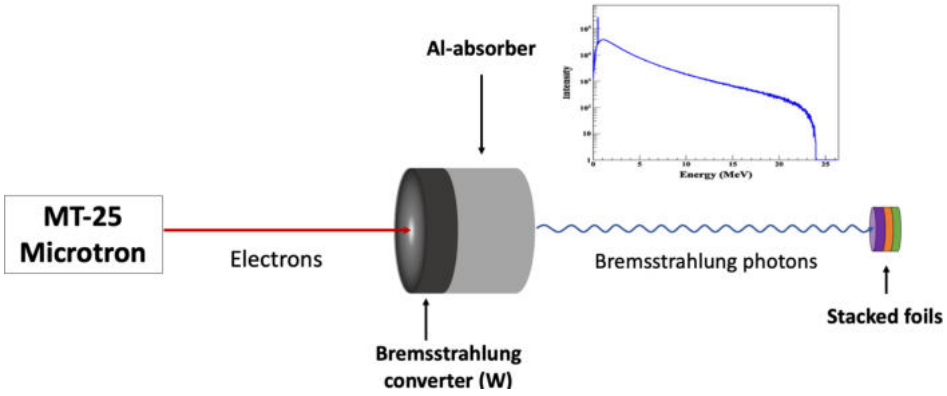

FIGURE 2.2: The scheme for the production of a bremsstrahlung source. The small figure above is the bremsstrahlung flux simulated by GEANT4.

The accelerated electrons impinged on an electron-photon converter made of a 3 mm thickness W disk and cooled by water to generate the bremsstrahlung photons. To absorb low-energy electrons passing through the converter, the 20 mm thick Al absorber was placed behind the converter.

Thermal and epithermal neutron source

To generate electron accelerator-driven thermal and epithermal neutrons, one can employ two installations as shown in Fig. 2.3 and Fig. 2.4.

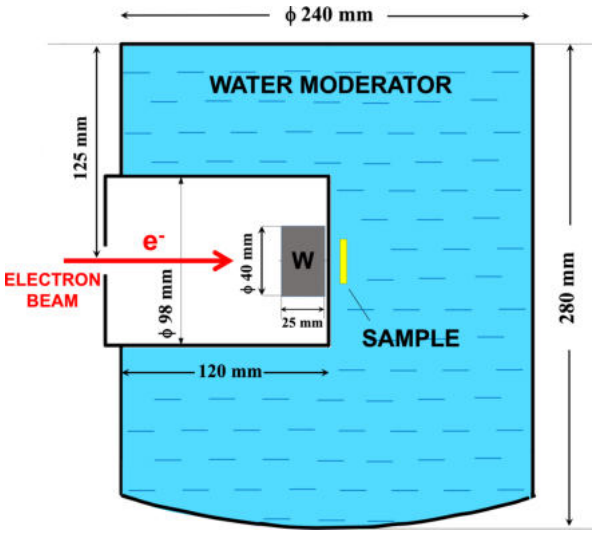

FIGURE 2.3: Schematic illustration of the production method for the source of mixed thermal-epithermal neutron and gamma.

In Fig. 2.3, the W disk of 25 mm thickness and 40 mm diameter enclosed by water was used as a simultaneous electron-γ and γ-neutron converter. By using this scheme, the bremsstrahlung photons are produced via the impingement of an electron beam on the W-disk target. Then, neutrons are generated from the (γ, n) reaction with bremsstrahlung photons on the W-target. The neutrons can be moderated in water to obtain a mixed thermal-epithermal neutron source. At the sample position, it is possible to perform the nuclear reactions with the mixed source of photons and thermal-epithermal neutrons.

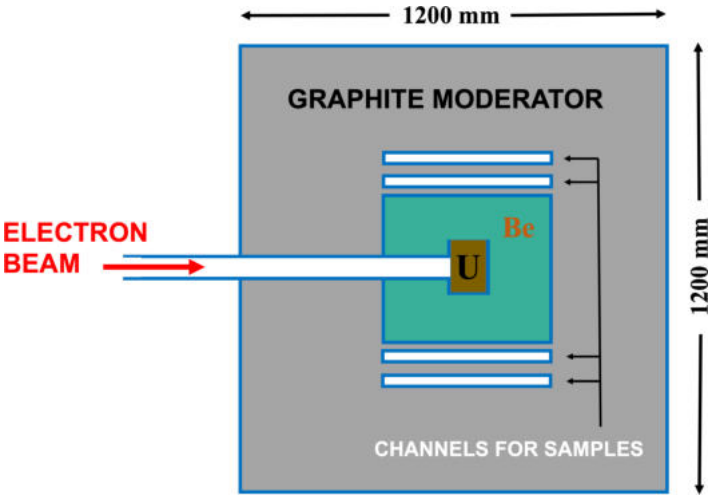

FIGURE 2.4: Schematic illustration of the production method for thermal and epithermal neutrons.

In the second scheme, the bremsstrahlung photons are attained during the electron beam impinging on the U electron-γ converter with a cylinder shape of 10mm diameter and length surrounded by Be. Later, the neutron beam is created by (γ, n) photonuclear

reactions and (γ, f) fission reactions on the U target within the high-energy part and by (γ, n) photonuclear reaction of Be in the low-energy part of the bremsstrahlung photon flux. In addition, Be can generate additional neutrons from its interaction with the scattered photons from the U target. Therefore, the use of U together with Be as a photon-neutron converter could generate neutron flux with higher intensity than a single U converter. This U-Be converter was surrounded by a 120 x 120 x 120 cm^3 graphite cube that served as the principal neutron moderator. The thermal neutron flux at the central position of the graphite cube was 4.10^8 neutron/s.cm^2 at an electron energy of 25 MeV and a current of 20 μA. A detailed construction of this neutron source can be found in Ref. [119].

This work used the second installation to investigate the IRs in thermal and epithermal neutron capture reactions.

2.1.2 Sample irradiation

Before irradiating samples, it is necessary to prepare and determine the mass of the sample, the mean electron current of the electron accelerator, and the irradiation duration to ensure the counting statistics of the characteristic γ-rays. These issues can be solved by preliminary estimation of the reaction yield using the activation method. Additionally, the proper irradiation duration is selected on the basis of the reaction cross section and half-life of the product nuclei. The maximum exposed duration is five times the half-life. After the irradiation, the waiting time is also determined on the basis of the half-life of the product isotopes of interest. To study IRs in the photonuclear and neutron capture reactions, this work used natural samples with the high purity of Se, Pd, Cd, Ce, Eu and Hg elements. The reasons for choosing these samples are the scarce IR data with large discrepancies of isomeric pairs, various nuclear structure and shape, and their prominent roles in numerous applications.

Europium (Eu) is a rare earth element and the softest lanthanide with atomic number Z = 63. Owing to its phosphorescence, Eu is applied in the manufacture of fluorescent glass and color television/computer screens. In astrophysics, the abundance of Eu in stellar spectra can be used to classify stars and give information about the origin of stars [120]. Moreover, Eu is used in nuclear reactor control rods because it is a good neutron absorber [121]. Natural europium consists of two isotopes, ^{151}Eu and ^{153}Eu, with abundances of 47.81 and 52.19%, respectively. Spin and parity $\frac{5}{2}^+$ of ground states of odd-even spherical ^{151}Eu and deformed ^{153}Eu nuclei are defined by

the single-particle state of the $d_{5/2^+}$ proton single-particle state and the $[413]\frac{5}{2}^+$ proton single-particle state, respectively [122].

Mercury (Hg), Z = 80, is a heavy silvery-white element and the only metallic element to be liquid under standard conditions for temperature and pressure. In the past, the use of Hg was widespread in thermometers, sphygmomanometers, fluorescent lamps, cosmetics, and medicine. However, the use of Hg in applications has been significantly reduced today as a result of its toxicity. Natural mercury includes ^{196}Hg, ^{198}Hg, ^{199}Hg, ^{200}Hg, ^{201}Hg, ^{202}Hg and ^{204}Hg isotopes with abundances of 0.15, 9.97, 16.87, 23.1, 13.18, 29.86 and 6.87%, respectively. The nuclei ^{196}Hg and ^{198}Hg belong to the nuclear range with Z = 73-61 and A = 182–206. They lie between strongly deformed nuclei of rare earth elements and the region of spherical nuclei in the vicinity of A = 208. The nuclei ^{198}Hg and ^{196}Hg are spherical even-even nuclei with ground-state spin and parity of 0^+. Their nucleon configuration is well described by the single-particle model. They have two proton holes with respect to the 6th closed shell of protons (Z = 82) or, in other words, the last ten protons are arranged in the subshell $(1h_{11/2})^{10}$. Six neutrons from ^{198}Hg and four neutrons of ^{196}Hg nuclei occupy the outermost orbit $1i_{13/2}$. Hence, high-spin Hg isomers are expected in the nuclear reaction.

Palladium (Pd), Z = 46, is a rare and lustrous silvery-white metal. It is used for a wide range of applications including jewelry, dentistry, blood sugar test strips, aircraft spark plugs, surgical instruments, electrical contacts, and catalytic converters in the automobile industry. Naturally occurring palladium consists of six isotopes ^{102}Pd, ^{104}Pd, ^{105}Pd, ^{106}Pd, ^{108}Pd, and ^{110}Pd with abundances of 1.02, 11.14, 22.33, 27.33, 26.46 and 11.72%, respectively. The nuclei ^{108}Pd and ^{110}Pd are known as vibrational even-even nuclei with ground-state spin and parity of 0^+.

Cadmium (Cd) element, Z = 48, is a soft silvery-white metal. Cadmium is a common component of electric batteries, pigments, coatings, and electroplating and has a significant role in nuclear reactor engineering, being the main compound in the control rod. Natural cadmium is composed of 8 isotopes ^{106}Cd, ^{108}Cd, ^{110}Cd, ^{111}Cd, ^{112}Cd, ^{113}Cd, ^{114}Cd and ^{116}Cd with abundances of 1.25, 0.89, 12.47, 12.8, 24.11, 12.23, 28.75 and 7.51%, respectively. The Cd isotopes have two proton holes with respect to the 5th closed shell (Z = 50). Nuclei ^{114}Cd and ^{116}Cd are vibrational even-even nuclei with ground-state spin and parity of 0^+.

Cerium (Ce) is a rare earth element with Z = 58. It is a soft, ductile, and silvery-white metal that tarnishes when exposed to air. Ce and its compounds are widely used

in glass polish, catalytic converters, white LED light sources, pigments, nanomaterials, nuclear fuel and scintillation detectors ($CeBr_3$, $LaBr_3(Ce)$). Naturally occurring cerium comprises four stable isotopes ^{136}Ce, ^{138}Ce, ^{140}Ce and ^{142}Ce with abundances of 0.186, 0.251, 88.449 and 11.114%, respectively. The nuclei ^{138}Ce and ^{140}Ce are spherical even-even nuclei with ground state spin and parity of 0^+. Following the single-particle model, Ce isotopes have eight protons that fill the subshell $(1g_{7/2})^8$. It is worth noting that ^{138}Ce nucleus has two neutron holes while ^{140}Ce nucleus is a magic one since its neutrons filled up the 6th closed shell (N = 82). This is also the reason why the abundance of ^{140}Ce is much greater than others.

Selenium (Se), Z = 34, is a non-metal and appears in red, black, or gray depending on the temperature change. The use of Se has known for glass production, pigments, electronics, material science, biology, supplements, and the production of therapeutic and medical radioisotopes. Selenium has six natural isotopes including ^{74}Se, ^{76}Se, ^{77}Se, ^{78}Se, ^{80}Se and ^{82}Se with abundances of 0.86, 9.23, 7.6, 23.69, 49.8 and 8.82%, respectively. Nuclei ^{74}Se and ^{82}Se are known as vibrational even-even nuclei with ground-state spin and parity of 0^+.

The characteristics of the irradiated samples, the electron current (I_e), the electron energy (E_e), and the irradiation time (t_{irr}) in the photonuclear and neutron capture reaction experiments are given in Table 2.2.

TABLE 2.2: Characteristics of the irradiated samples, electron current and energy, and irradiation time.

Symbol	Sample	Purity [%]	Weight [g]	Diameter [cm]	I_e [μA]	E_e [MeV]	$t_{irr}(\gamma, n)$ [min.]	$t_{irr}(n, \gamma)$ [min.]
Eu	Eu_2O_3	99.99	0.1	1	15	14 - 23	60 - 90	
Hg	$HgCl_2$	99.99	0.3	1	15	14 - 24	60	
Pd1	PdO	99.99	0.323	1	15	24 - 25	30	
Pd2	PdO	99.99	0.323	1	15	25		90
Cd1	Cd	99.99	0.719	1	15	24 - 25	60	
Cd2	Cd	99.99	0.719	1	15	25		120
Ce1	Ce_2O_3	99.99	0.8	1	12 - 14	25	60	
Ce2	Ce_2O_3	99.99	0.8	1	12 - 14	25		90
Se1	SeO_2	99.99	0.248	1	12	25	20	
Se2	SeO_2	99.99	0.248	1	12	25		90

For the (γ, n) reaction, the samples were exposed to bremsstrahlung (Fig. 2.2) at a distance of 5 cm from the W converter.

For the (n, γ) reaction, the samples were irradiated without and with the 2 mm thick Cd cover and placed at a distance of 40 cm from the center of the graphite cube

(Fig. 2.4), where the Cd ratio is 2.5. The Cd ratio is defined as the ratio of the activity of a bare sample to that of a Cd-covered sample. Au foils were used to monitor the neutron flux in this case.

2.1.3 Gamma spectroscopy

After a definite cooling time, the γ-ray activities of the studied samples were determined by a spectrometer including an HPGe detector with 60.5 mm diameter and 31 mm length attached with the preamplifier, amplifier and ADC and PC-based 8192 channel analyzer (CANBERRA) for data processing, as shown in Fig. 2.6. The HPGe is one type of semiconductor detector most commonly used for γ-ray spectroscopy studies. In a semiconductor detector, electron-hole pairs are created as a result of electrons being excited from the valence band to the conduction band due to thermal excitation and γ-ray interactions. The germanium semiconductors must be maintained at $\sim$ 77 K with liquid nitrogen to reduce thermal noise due to the low energy gap of 1.12 eV between the conduction and valence band. In this way, only γ-ray interactions will contribute to the energy signal by creating electron-hole pairs. Compared to the inorganic scintillation detector NaI(Tl), the performance in terms of the energy resolution of the HPGe is about an order of magnitude better than that of the scintillation detector, whereas, its efficiency is worse than that of the scintillation detector. Therefore, the HPGe detector is the preferred choice for high-energy-resolution studies in nuclear physics. The energy resolution of the used spectrometer is 1.8 keV at the 1332.5 keV γ peak of the ^{60} Co isotope.

Samples were placed at various distances from the end cap of the HPGe detector. The γ-ray counting duration was decided by taking care of activities of the product nuclei, the photopeak areas of the characteristic γ-rays, and the Compton background. Measurements were made with random errors less than 0.5–2% for the γ rays of interest. The product nuclei were identified on the basis of their half-lives and γ-ray energies. The γ-spectrometer used illustrated in Fig. 2.5 consists of the HPGe detector, electronics to collect, amplify, and process the signals produced by the detector, and a computer coupled with processing software to display and analyze the spectrum. The γ-ray spectra were measured and analyzed by employing the Gamma Vision software. This software can determine the count numbers under the photopeaks and the corresponding energy, and its user interface is shown in Fig. 2.7.

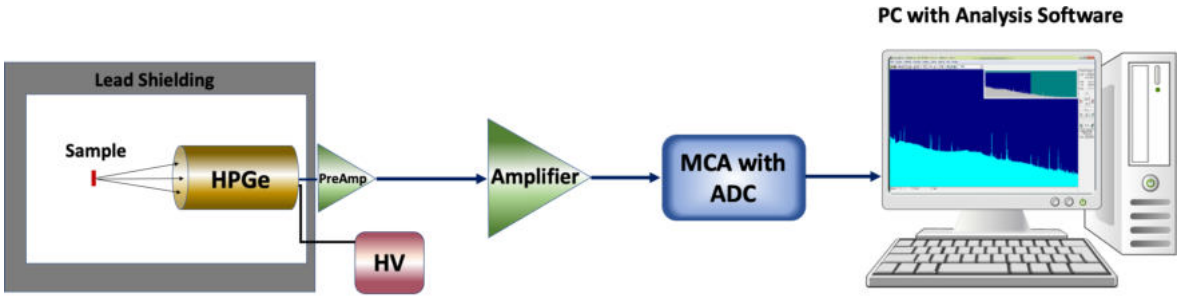

FIGURE 2.5: The gamma spectrometer diagram.

FIGURE 2.6: HPGe detector of the Department of Chemistry of Transactinides, FLNR, JINR, Dubna.

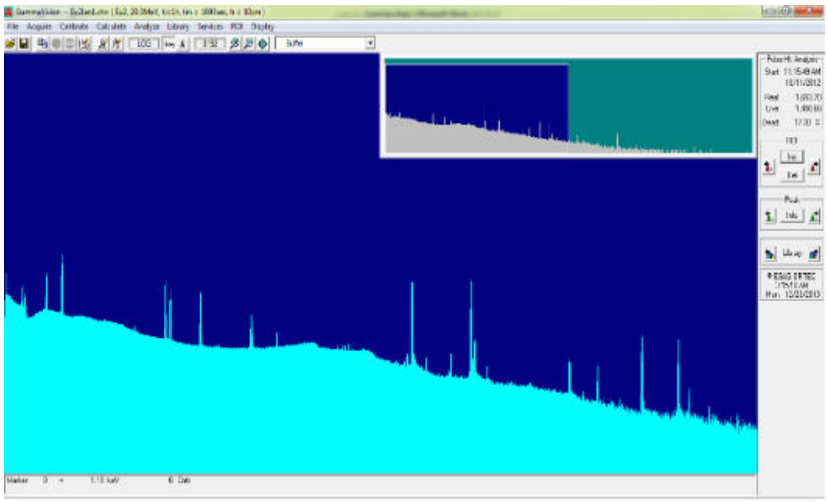

FIGURE 2.7: The user interface of the Gamma Vision software.

Before each measurement, the energy and efficiency calibration was performed using QCY and QCYK mixed nuclide sources with known γ ray energies and radioactivity. These sources contain ^{241}Am, ^{133}Ba, ^{57}Co, ^{60}Co, ^{113}Sn, ^{22}Na, ^{54}Mn, ^{137}Cs, ^{139}Ce, and ^{134}Cs, covering wide range of γ ray energies from 59.54 keV (^{241}Am) to 1365.19 keV (^{134}Cs). Energy calibration used a linear function of energy versus ADC channel number of the corresponding full energy peaks to obtain a set of energy calibration parameters, namely, gain and offset. These parameters were then applied to the offline measurements of the γ-rays of interest.

For the γ-ray spectrometer, the detection efficiency is an important parameter in measurement and data analysis. It contains the full-energy peak efficiency and the total efficiency. The full-energy peak (photopeak) efficiency is the ratio between the number of detected photons at the energy of interest and the number of photons that are emitted from the source. The total efficiency is the ratio of the number of pulses recorded to the total photon emitted from the source. This efficiency is used to correct the coincidence-summing effect. The photopeak efficiency can be calculated using the following formula:

$$\varepsilon(E) = \frac{N}{A \times e^{-\lambda t} \times I_\gamma \times t_m}, \tag{2.1}$$

where N, t_m, A, λ, t and I_γ are the number of counts, measurement time, known activity, decay constant, period from the date of manufacture of the source and γ-ray intensity, respectively.

The photo-peak efficiency ε was calibrated, and was fitted by using the fitting function as follows:

$$\varepsilon(E) = exp(\sum_{i=0}^{5} a_i ln(E)^i), \tag{2.2}$$

where E is the γ ray energy and a_i is the fitting parameters.

The measured efficiency and fitted curves at distances of 5, 10 and 20 cm are shown in Fig. 2.8. The detailed calculation and fitting parameters of the HPGe efficiency curve were represented in [123].

2.1.4 Experimental IR determination

In the activation time t_1, there are two processes that take place simultaneously, namely the formation of an isomeric pair and their decay. The production of isomeric pairs

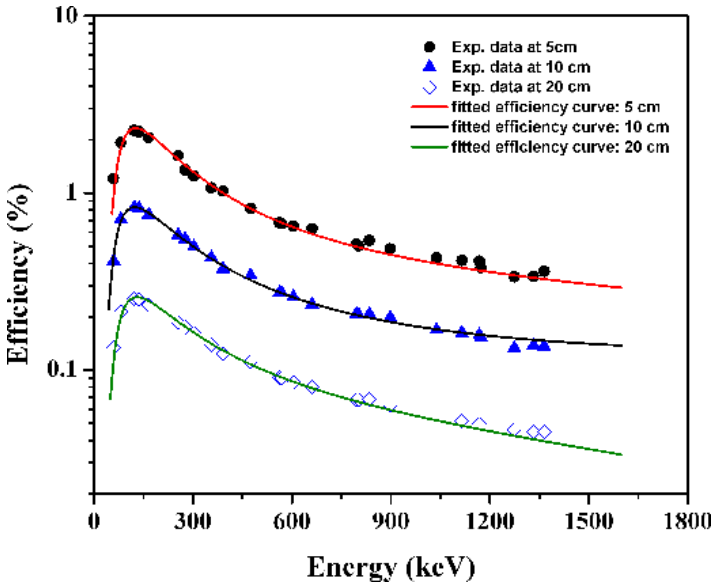

FIGURE 2.8: The efficiency curve for the HPGe detector used in the present work.

over time t_1 can be demonstrated by the following differential equations:

$$\frac{dN_m}{dt} = Y_m - \lambda_m N_m, \tag{2.3}$$

$$\frac{dN_g}{dt} = Y_g - \lambda_g N_g + P_{mg}\lambda_m N_m, \tag{2.4}$$

here m,g - isomeric and ground state; N – number of nuclei; Y – yield; λ - decay constant; P – isomeric transition probability.

The decay equations of the isomeric pair during cooling and measuring time (t_2 and t_3) mimic Eqs. 2.3 and 2.4 but the terms Y_i are absent. The solution of the above equations in three time intervals and the subsequent integration of the reduced activity over t_3 results in

$$\frac{S_m}{\varepsilon_m I_m} = Y_m \Lambda_3^m \Lambda_6^m \Lambda_9^m, \tag{2.5}$$

$$\frac{S_g}{\varepsilon_g I_g} = Y_g \Lambda_2^g \Lambda_5^g \Lambda_8^g + Y_m(\Lambda_1^g \Lambda_5^g \Lambda_8^g + \Lambda_3^g \Lambda_4^g \Lambda_8^g + \Lambda_3^g \Lambda_6^g \Lambda_7^g), \tag{2.6}$$

where S, ε, I – the photo-peak area, absolute photo-peak efficiency, γ-ray intensity, respectively, and Λ_i - time-dependent terms presented as follows:

$$\Lambda_1^g = \frac{P_{m,g}}{\lambda_g}\left[1 - \frac{\lambda_m \lambda_g}{\lambda_m - \lambda_g}\left(\frac{e^{-\lambda_g t_1^g}}{\lambda_g} - \frac{e^{-\lambda_m t_1^g}}{\lambda_m}\right)\right], \tag{2.7}$$

$$\Lambda_2^g = \frac{1}{\lambda_g}(1 - e^{-\lambda_g t_1^g}), \tag{2.8}$$

$$\Lambda_3^g = \frac{1}{\lambda_g}(1 - e^{-\lambda_m t_1^g}), \tag{2.9}$$

$$\Lambda_3^m = \frac{1}{\lambda_m}(1 - e^{-\lambda_m t_1^m}), \tag{2.10}$$

$$\Lambda_4^g = P_{mg}\frac{\lambda_m}{\lambda_m - \lambda_g}(e^{-\lambda_g t_2^g} - e^{-\lambda_m t_2^g}), \tag{2.11}$$

$$\Lambda_5^g = e^{-\lambda_g t_2^g}, \tag{2.12}$$

$$\Lambda_6^g = e^{-\lambda_m t_2^g}, \tag{2.13}$$

$$\Lambda_6^m = e^{-\lambda_m t_2^m}, \tag{2.14}$$

$$\Lambda_7^g = P_{mg}\left[1 - \frac{\lambda_m \lambda_g}{\lambda_m - \lambda_g}\left(\frac{e^{-\lambda_g t_3^g}}{\lambda_g} - \frac{e^{-\lambda_g t_3^g}}{\lambda_m}\right)\right], \tag{2.15}$$

$$\Lambda_8^g = 1 - e^{-\lambda_g t_3^g}, \tag{2.16}$$

$$\Lambda_9^m = 1 - e^{-\lambda_m t_3^m}. \tag{2.17}$$

Under the same irradiation, cooling, and measurement conditions, the equality of the corresponding time of those processes for the isomeric and ground states is assumed, namely $t_1^m = t_1^g = t_1$, $t_2^m = t_2^g = t_2$ and $t_3^m = t_3^g = t_3$.

The IR is obtained from Eqs. 2.5 and 2.6 as follows:

$$\frac{1}{IR} = \frac{\frac{S_g I_m \varepsilon_m}{S_m I_g \varepsilon_g}\Lambda_3^m \Lambda_6^m \Lambda_9^m - \Lambda_1^g \Lambda_5^g \Lambda_8^g - \Lambda_3^g \Lambda_4^g \Lambda_8^g - \Lambda_3^g \Lambda_6^g \Lambda_7^g}{\Lambda_2^g \Lambda_5^g \Lambda_8^g}. \tag{2.18}$$

Based on the photo-peak area, absolute photo-peak efficiency, branching ratio and time-dependent parameters, the IR can be calculated as in the above Eq. 2.18.

Since several γ-ray spectra under different experimental conditions (such as cooling and measurement time intervals) were used to calculate the IRs in this work, the final result was computed by the average value $\overline{IR}$ determined from γ-ray spectra obtained for all experimental conditions. The relative uncertainty was calculated using the following formula:

$$\varepsilon(\overline{IR}) = \frac{\sigma(\overline{IR})}{\overline{IR}} = \frac{\sqrt{\sum_n^{i=1} \sigma_i^2(IR)/n}}{\overline{IR}}, \tag{2.19}$$

where $\sigma_i(IR)$ - the IR uncertainty determined in the experimental condition i^{th} and n - the number of experimental conditions.

To enhance the precision of the measured photopeak areas, the necessary corrections for the accompanying effects must be considered.

2.1.5 Spectrum analysis-necessary correction

The IR determination following Eq. 2.18 depends on many factors, in which S_m and S_g play a significant role. In this work, the criteria for choosing the γ-rays in the data analysis were the following: (a) Their intensities are higher than those of other γ-rays, (b) they are well resolved in the γ-ray energy spectra and (c) they are free of contamination from the products of other nuclear reactions. However, in some cases, the overlapped peaks resulting from the γ-ray interference of other reaction products were used in the data analysis. The counts of these peaks must be corrected using the decay curve method or the peak ratio method. Moreover, the counts can be lost due to self-absorption and coincidence-summing effects.

Self-absorption effect

The error may occur due to the self-absorption effect, especially with low energy γ rays and with a thick sample, when the measurement is performed. For samples with thickness t that is very well known about the composition and concentration of elements, the self-absorption coefficient is given by [124]

$$F_g = \frac{\mu t}{1 - e^{-\mu t}}, \tag{2.20}$$

here μ, t are the linear attenuation factor and the target thickness, respectively. Data μ are taken from [125].

Coincidence summing corrections

The coincidence summing effect takes place when the detector does not distinguish (in time) independent γ-rays or cascade γ-rays. It leads to an increase in the count at the sum peak so-called "summing in" effect or a decrease in the count at cascade peaks called the "summing out" effect. To correct the count loss of the actual γ-peak due to the "summing out" effect, this work used the formula [126] to calculate the correction factor C_c as follows:

$$C_c = \frac{1}{1 - \sum_{i=1}^{i=j} f_i \times \varepsilon_t(i)}, \tag{2.21}$$

where f_i is the fraction of the coincidence photon of energy i in coincidence with the interested γ-ray; $\varepsilon_t(i)$ is the total efficiency of the coincidence photon of energy i.

To correct the effect of "summing in" using the factor C_3 for a sum peak with intensity I_3 and the photopeak efficiency ε_3, one can employ the formula as follows:

$$C_3 = \frac{1}{1 + \frac{I_1}{I_3}\frac{\varepsilon_1\varepsilon_2}{\varepsilon_3}}, \tag{2.22}$$

where I_1 and $\varepsilon_{1(2)}$ are the intensity and the photopeak efficiency of cascade γ-rays.

2.2 Theoretical IR calculation in (γ, n) reaction

As aforementioned, bremsstrahlung has been used to induce photonuclear reactions. Therefore, a convolution of the differential cross section data set calculated by the TALYS 1.95 code and the bremsstrahlung flux simulated by the transportation code GEANT4 is implemented to calculate the yield and the yield IR following Eq. (1.9).

2.2.1 Bremsstrahlung spectra simulation in GEANT4

The Geant4 toolkit has been used to simulate the energy flux of γ-rays in the secondary target. A user application has been written based on an example named "examples/basic/B1" provided in the Geant4 package. Fig. 2.9 shows the diagram of the Geant4 user application in this work.

In this application, the generation of primary particles in a form of an electron beam in the current setup by Monte Carlo sampling has been implemented using the built-in primary generator class G4GeneralParticleSource. This class allows one to run macro-type commands directly before simulation to change the particle species

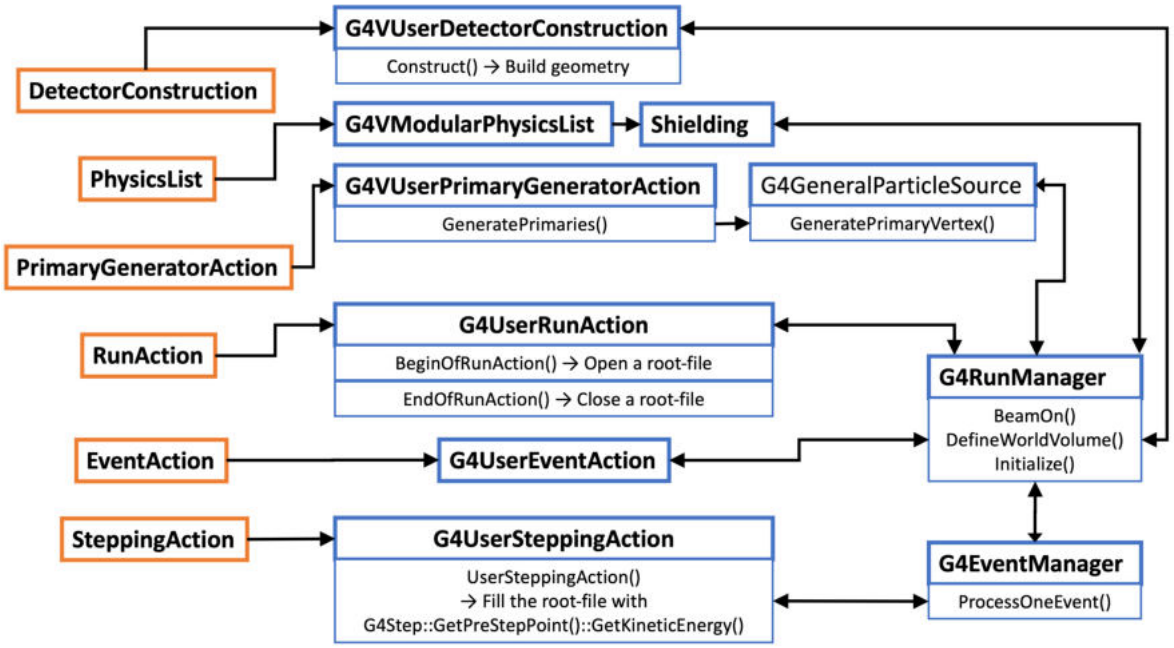

FIGURE 2.9: Diagram of the Geant4 user application.

and their energy spectral, spatial, and angular distribution without changing the user codes. In this work, a beam of electrons was simulated with a circular beam profile and a Gaussian profile of beam energy given by the actual experimental conditions.

To simplify the user codes, the package physics list named "Shielding" was used to describe the physical interactions of particles in matter. It is a convenient and ready-to-use Geant4 physics list, constructed by expert developers at the SLAC facility in the USA. The "shielding" physics list has been primarily designed for simulating a shielding, high-energy or underground detector, where all possible emergent radiations and their interactions need to be considered. This list contains the best-guess selection of electromagnetic and hadronic physics, including the G4EmStandardPhysics for electromagnetic physics, the G4EmExtraPhysics for additional physics related to synchrotron radiation, and gamma nuclear physics. Therefore, this list was considered suitable to simulate the γ-ray energy flux at the secondary target for the current experimental setup.

The geometry of the experimental setup has been modeled as detailed as possible using a user implementation code derived from the virtual G4DetectorConstruction class, as shown in Fig. 2.10 for the photonuclear (left) and neutron capture reactions (right).

The production of bremsstrahlung has been simulated by using a Monte Carlo calculation implemented in the GEANT4 toolkit. GEANT4 tracks the history of individual

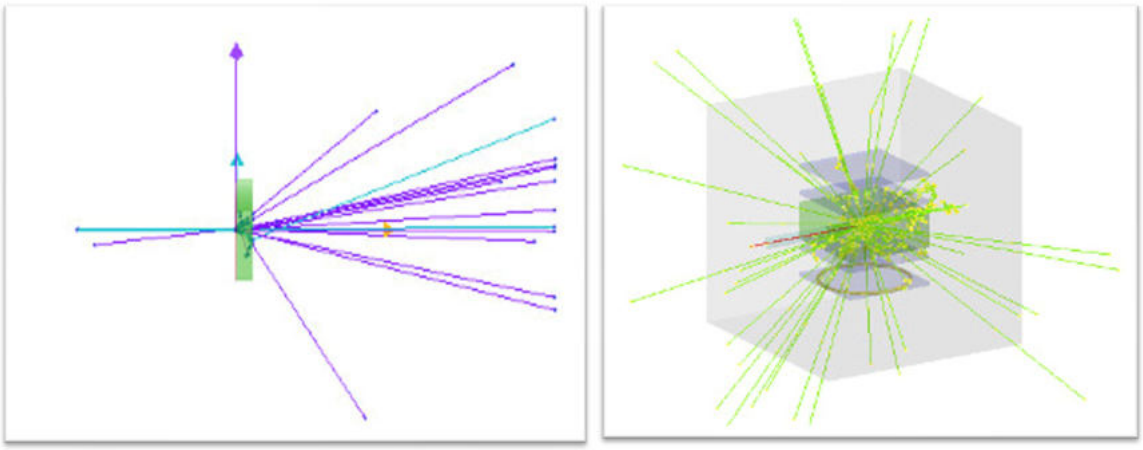

FIGURE 2.10: GEANT4 simulation of experimental setups for photonuclear reaction (left) and neutron capture (right).

particles, while the average behavior is a combination of effects from individual particles. The processes to track photons can be enabled after target modeling and particle source configuration. The so-called "delta" δ information of the tracked photons is extracted and the energy of the photon before interacting with the target was stored as a form of a CERN ROOT [127] NTuples file. Details are implemented in the user-defined "G4UserSteppingAction" class in GEANT4. By analyzing the NTuples file, bremsstrahlung was found to be an energy function of the outgoing photons which is illustrated in Fig. 2.11. Bremsstrahlung radiation was produced when the electron beam with high energy impinges on the primary target (converter). A 3mm W has been used as the converter. The bremsstrahlung spectrum depends on the type of target material and the energy of the incident electron beam. In this work, the bremsstrahlung spectrum for the end-point energies of 10 to 25 MeV with the step of 1 MeV has been simulated separately. The bremsstrahlung spectra have energies in the range from 0 to incident electron beam energy. By analogy, the neutron spectrum shown in Fig. 2.12 is the GEANT4 simulation result following the experimental scheme in Fig. 2.4. This spectrum may be used for further investigation. The simulation codes are given in Appendix A.

2.2.2 Cross-section calculation in TALYS

In the TALYS 1.95 code, the default keywords are projectile, target element, target mass, and projectile energy. There are nearly 340 keywords in TALYS 1.95 that can be implemented depending on the user's purpose. In this work, in addition to default keywords, keywords related to level density models and γSFs were employed to calculate

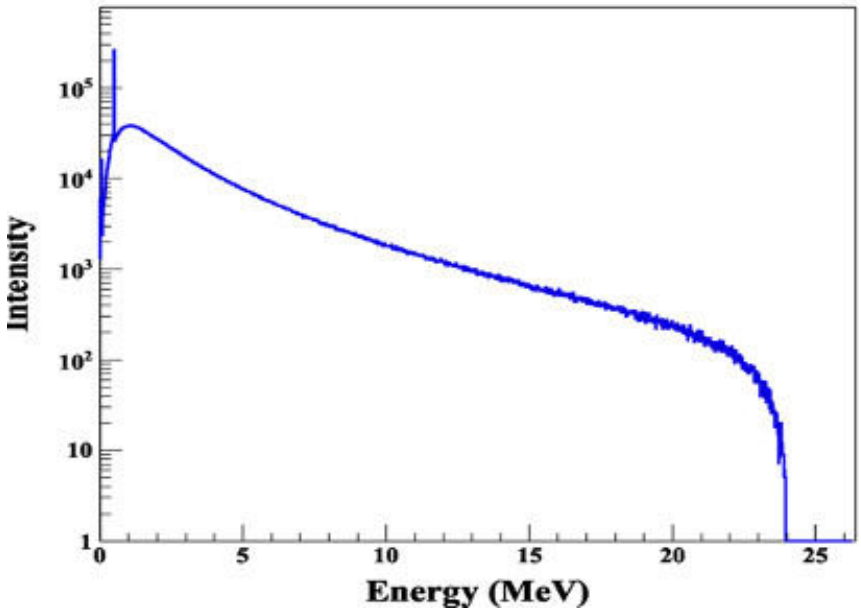

FIGURE 2.11: The bremsstrahlung with end-point energy of 24 MeV simulated by Geant4.10.06 version.

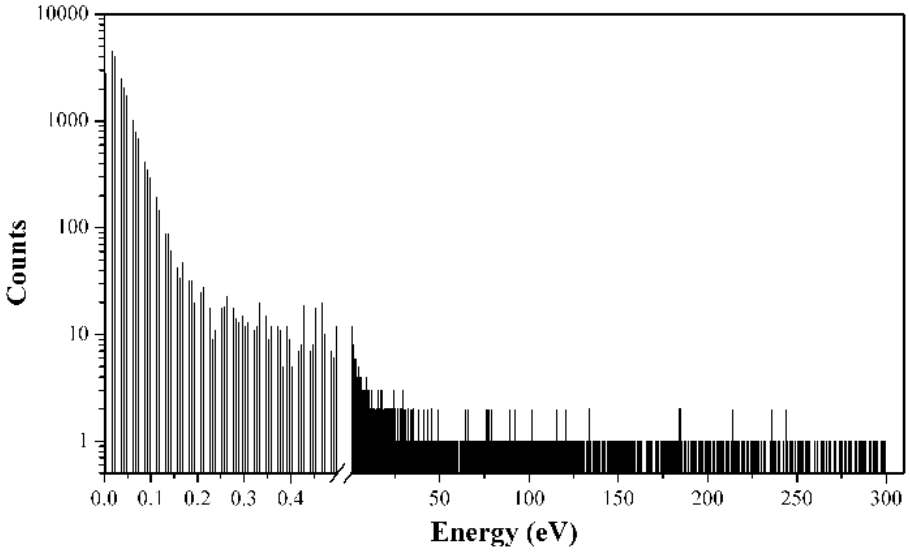

FIGURE 2.12: Geant4 simulated neutron energy at a distance of 30 cm from the primary target.

the cross sections of the photodisintegration reactions interested in the GDR region. The output contains the cross-section files corresponding to the reaction channels. Moreover, when the keyword *outbasic* is set *y* in the input file, all the information on the nuclear structure can be extracted in the output file, comprising all fundamental information required for the reaction calculation as the population of levels, optical-model parameters, transmission coefficients, γ strength functions, discrete levels, level densities, and reaction cross sections.

In detail, this work used the TALYS 1.95 code to compute the reaction cross section (γ, n) in the photon energy range of 10 to 25 MeV on natural Cd, Ce, Se, Pd, Eu, and Hg targets using six-level density models. These include three phenomenological LD models (Ld1-3) and three microscopic LD models (Ld4-6):

- Ld-1: Constant-temperature model + Fermi gas model.
- Ld-2: Back-shifted Fermi gas model.
- Ld-3: Generalized superfluid model.
- Ld-4: Microscopic level densities (Skyrme force) from Goriely's tables.
- Ld-5: Microscopic level densities (Skyrme force) from Hilaire's combinatorial tables.
- Ld-6: Microscopic level densities (temperature-dependent HFB, Gogny force) from Hilaire's combinatorial tables.

In nuclear reactions, in addition to the level density, the γSF representing the distribution of the average γ transition probability is also a crucial ingredient for predicting the reaction cross sections. Thus, for each Ld model, this work used eight γ SFs available in TALYS 1.95 one by one to obtain the differential cross sections of the products, comprising

- S1: Kopecky-Uhl generalized Lorentzian.
- S2: Brink-Axel Lorentzian or standard Lorentzian strength (SLO).
- S3: Hartree-Fock BCS tables.
- S4: Hartree-Fock-Bogolyubov tables.
- S5: Goriely hybrid model.

- S6: Goriely T-dependent HFB.
- S7: T-dependent RMF.
- S8: Gogny D1M HFB+QRPA.

The used keywords are presented in Appendix B.

Chapter 3

Results and Discussion

In this chapter, the experimental IR results obtained from the reactions (γ, n) and (n, γ) are represented in the first four sections. In the last section, the theoretical values calculated using the TALYS code for the reaction (γ, n) are illustrated.

- Section 3.1 presents the IRs of $^{195m,g;197m,g}$Hg and ^{152m1,m2}Eu in the reactions (γ, n) induced by bremsstrahlung with the endpoint energy within the GDR region.
- Section 3.2 shows the IRs in (n, γ) neutron capture reactions induced by thermal and resonance neutrons on ^{108,110}Pd and ^{114,116}Cd.
- Section 3.3 demonstrates the effect of the nuclear channel on the IRs of ^{109m,g}Pd and ^{115m,g}Cd produced from (γ, n) and (n, γ) reactions.
- Section 3.4 presents and discusses IRs in inverse reactions (γ, n) and (n, γ) that produce isomeric pairs ^{137m,g}Ce, ^{115m,g}Cd, ^{109m,g}Pd, and ^{81m,g}Se.
- Finally, section 3.5 summarizes the theoretical IR calculations of the isomeric pairs produced by the reactions (γ, n) on the Se, Pd, Ce, Eu and Hg targets in the GDR region using the TALYS code.

The results of Section 3.1 have been published in Refs. [23, 128]. And our results in Section 3.2 have been revealed in Refs. [129, 130]. The results in Section 3.3 have been printed in Refs. [131, 132]. The results in Section 3.4 have been reported in international conferences [133, 134]. A part of the results in Section 3.5 is published in Ref. [135].

3.1 Isomeric Ratios in (γ, n) reactions

3.1.1 ^{152m1,m2}Eu

One of the goals of this work is to measure the experimental IR of the ^{152m1}Eu$(8^-)/^{152m2}$Eu(0^-) formed in the $^{153}Eu(\gamma, n)^{152}Eu$ reaction within the entire GDR region to explore several internal effects on IR such as the excitation energy, the spin difference of the isomeric and ground states and the channel effect. This is a demand because there are very limited numbers of investigations on the IR of the ^{153}Eu isotope, as well as the discrepancy and incompleteness of the IR data in the GDR region.

Until now, there were only a handful number of IR measurements for ^{152m1}Eu$(8^-)/^{152m2}$Eu(0^-) in various energy regimes. One was carried out by Vishnevsky et al. [136] using the $^{153}Eu(\gamma, n)^{152}Eu$ reaction at 12 MeV bremsstrahlung end-point energy. The authors compared the measured results with the theoretical IR calculated using the TALYS code. In other experimental findings, Kolev [40] reported the IR of ^{152m1,m2}Eu at the maximal bremsstrahlung energy of 43.0 MeV and interpreted the result with the calculation based on the particle evaporation process of the compound nucleus and subsequent γ-ray deexcitation. In this study, it was observed that the statistical model in conjunction with HVM provided a description of the successful reaction mechanism in at least 50% of the reactions investigated. Tonchev et al. [122] measured the IR of ^{152m1}Eu$(8^-)/^{152m2}$Eu(0^-) in both the (γ, n) reaction and the (n, γ) neutron capture reaction to explore the effect of nuclei quadrupole deformation on the IR. It is well-known that photonuclear reactions are distinct from other nuclear reaction types by the low angular momentum transfer and resonant characteristics of the absorption cross section, which provide valuable information on the nuclear reaction mechanism and structure. Interestingly enough, the ^{153}Eu nucleus is deformed and the cross section of the $^{153}Eu(\gamma, n)^{152}Eu$ reaction in the GDR region with an energy range of 8.6 - 22 MeV, there are two maximum peaks corresponding to the oscillation between an oblate and a prolate spheroidal shape [137]. Therefore, the current study is expected to contribute additional data to the current nuclear database, thus providing more robust and complete theoretical interpretations of nuclear reactions.

In the scope of this work, the experimental IR of the pair of ^{152m1}Eu $(8^-)/^{152m2}$Eu

(0^-) has been investigated by means of the reaction (γ, n) in the GDR. The irradiation of the Eu sample is described in subsection 2.1.2 using a bremsstrahlung endpoint energy of 14 to 23 MeV with a step of 1 MeV. The decay characteristics and intense γ-rays of ^{152m1}Eu and ^{152m2}Eu taken from [138] are shown in Table 3.1. Figure 3.1 exhibits the simplified decay schemes of ^{152m1}Eu and ^{152m2}Eu produced in the $^{153}Eu(\gamma, n)^{152m1,m2}Eu$ reaction. The ^{152}Eu excited nucleus in the 8^- state decays to the 3^- ground state by emission of a cascade of γ-ray transitions with energies of 39.7, 18.2 and 89.9 keV and intensities of 0, 1.26 and 70%, respectively. Thus, the isomeric transition coefficient P between ^{152m1}Eu(8^-) and ^{152m2}Eu(0^-) can be considered zero. For the IR calculation, the most intense γ-ray of 89.9 keV was selected. As shown in the bottom part of Fig. 3.1, the ^{152m2}Eu(0^-) state decays by two ways: (1) by β^- 72% to ^{152}Gd following by the emission of 1314.7, 940.4 and 344.3 keV γ-rays, which have relatively low intensities of 0.956, 0.604 and 2.44%, respectively, and (2) by electron capture and β^+ decay with an intensity of 28%, then follow by emission of γ-rays with energies of 547.4, 963.4, 841.6, 562.9 and 121.8 keV and intensities of 0.009, 11.67, 14.20, 0.22 and 7.0%, respectively. For the IR calculation, the most strongly emitted characteristic γ-rays with energies of 121.8, 841.6 and 963.4 keV for ^{152m2}Eu(0^-) have been selected.

TABLE 3.1: γ-rays decay properties of the reaction products of ^{152m1,m2}Eu used in the IR calculation [138].

Nuclear reaction	Reaction product	Spin, Parity $[J^\pi]$	Half-life [h]	Reaction threshold [MeV]	γ-ray energy [keV], (Intensity,%)	Isomeric transition coefficient P[%]
$^{153}Eu(\gamma, n)^{152m1}Eu$	^{152m1}Eu	8^-	1.6	8.7	89.9 (70.0)	0
$^{153}Eu(\gamma, n)^{152m2}Eu$	^{152m2}Eu	0^-	9.274	8.6	121.8 (7.00) 841.6 (14.20) 963.4 (11.67)	

Figure 3.2 shows a typical offline γ-ray spectrum obtained from the $^{153}Eu(\gamma, n)^{152}Eu$ reaction with 17 MeV bremsstrahlung endpoint energy. The irradiation time, cooling time, and measurement time are 90 min, 20 min, and 140 min, respectively. The sample was located at a distance of 5 cm from the detector during the measurement.

With the given irradiation time, due to the long half-life and low formation probability, the decay of ^{150g}Eu and ^{152g}Eu was not observed in the obtained γ-ray spectra. In contrast, characteristic γ rays of the isomeric states ^{150m}Eu(0^-), ^{152m1}Eu(8^-) and ^{152m2}Eu(0^-) can be clearly seen. To improve the precision of IR determination, the

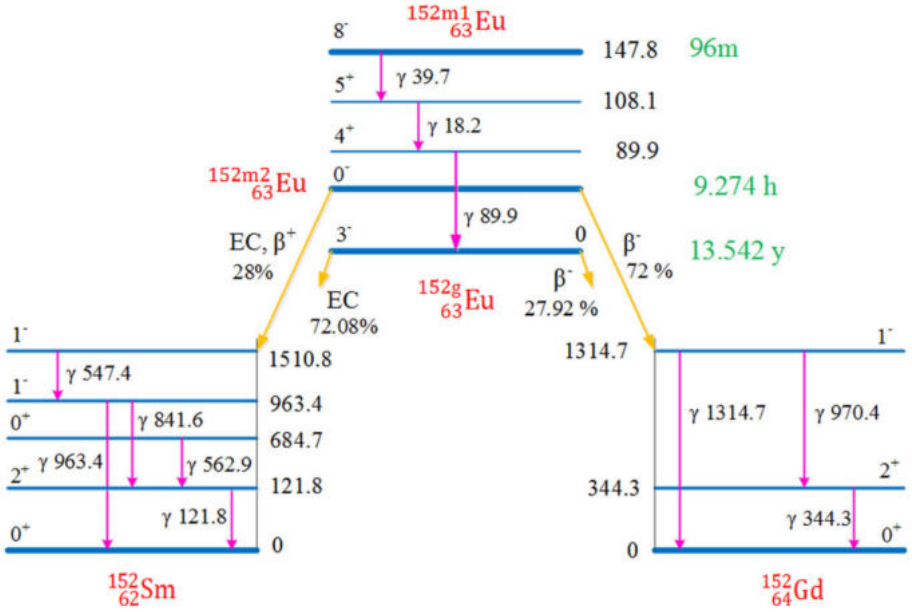

FIGURE 3.1: Simplified decay diagram of ^{152m1,m2}Eu [23].

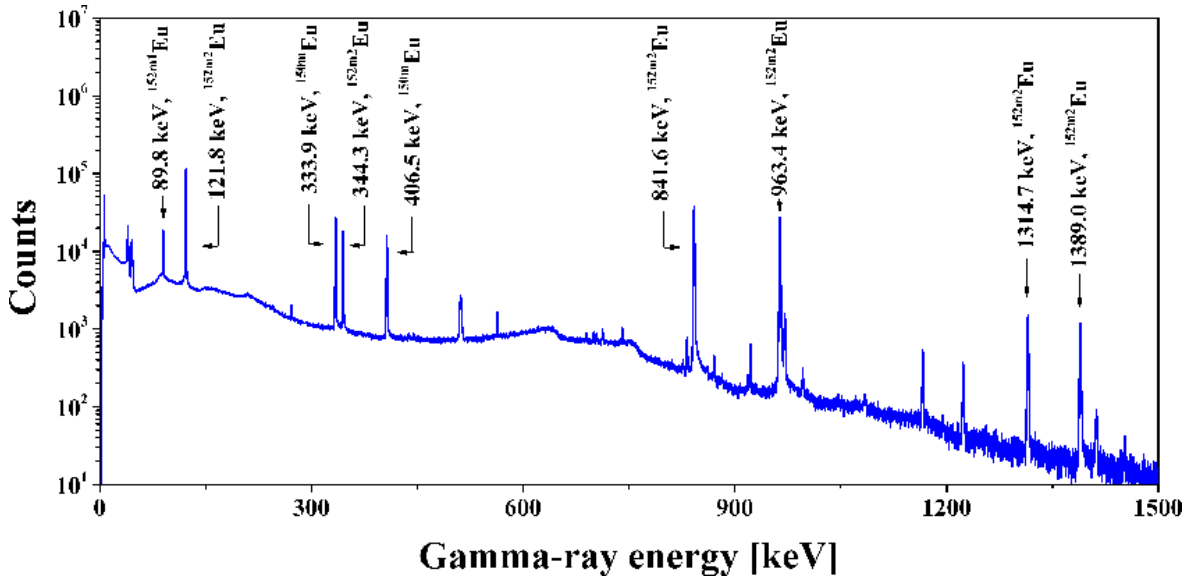

FIGURE 3.2: A typical energy spectrum of the Eu sample irradiated with 17 MeV bremsstrahlung [23].

effects related to coincidence summing and self-absorption have been taken into account and corrected by the factors in Tab. 3.2. The self-absorption factor for γ-rays of 89.8, 121.8, 841.6, and 963.4 keV has been estimated using the formula 2.20. The coincidence summing for the cascade of 121.8 and 841.6 keV has been corrected by the factor as in Eq. 2.21.

TABLE 3.2: A summary of corrections for self-absorption and summing coincidence for given γ-ray energies.

γ-ray energy, keV (Intensity, %)	Self-absorption correction, F_g t = 0.3 g/cm2	Summing coincidence correction, C_c at h = 5 cm
89.8(70.0)	1.19	1
121.8(7.0)	1.09	1.0026
841.6(14.2)	1	1.0006
963.4(11.67)	1	1

As a result, the IR of ^{152m1,m2}Eu has been determined based on Eq. (2.18). Likewise, the IR calculation was applied to other energy spectra of the irradiated Eu targets. The IRs of ^{152m1}Eu$(8^-)/^{152m2}$Eu(0^-) in the ^{153}Eu(γ, n) reaction induced by bremsstrahlung end-point energies of 14 - 23 MeV are demonstrated in Table 3.3 and shown in Figure 3.3. And Table 3.4 details the uncertainties in the isomeric ratio determined of ^{152m1}Eu(8^-) and ^{152m2}Eu(0^-). The total uncertainty of the determined isomeric ratio was estimated to be approximately 7.0%.

TABLE 3.3: The IR of ^{152m1,m2}Eu in reaction (γ, n).

Nuclear reaction	This work		Other works	
	End-point Energy (MeV)	Isomeric ratio $IR = Y_{hs}/Y_{ls}[10^{-2}]$	End-point Energy (MeV)	Isomeric ratio $IR = Y_{hs}/Y_{ls}[10^{-2}]$
$^{153}Eu(\gamma, n)^{152m1,m2}Eu$			12	0.12 ± 0.01 [136]
			12.5	0.14 ± 0.02 [139]
			13	0.22 ± 0.02 [139]
			13.5	0.27 ± 0.02 [139]
	14	0.47 ± 0.03	14	0.35 ± 0.03 [139]
			14.5	0.38 ± 0.03 [139]
	15	0.63 ± 0.04	15	0.47 ± 0.03 [139]
			15.5	0.54 ± 0.04 [139]
	16	0.72 ± 0.05	16	0.61 ± 0.04 [139]
			16.5	0.60 ± 0.04 [139]
	17	0.85 ± 0.06	17	0.62 ± 0.05 [139]
			17.5	0.75 ± 0.04 [139]
			18	0.76 ± 0.05 [139]
			18	1.02 ± 0.10 [41]
	19	1.37 ± 0.09		
	20	1.72 ± 0.12		
	21	1.85 ± 0.13		
	22	1.95 ± 0.13		
	23	1.90 ± 0.13		
			24	1.99 ± 0.20 [41]
			43	1.12 ± 0.20 [40]

TABLE 3.4: A summary of error sources considered in the IR calculation of ^{152m1,m2}Eu.

Random Errors	[%]	Systematic Errors	[%]
Counting statistical	1	Sample-detector distance	1
Detector efficiency	2	γ-ray selection	1
Half-life	1	e-beam variation	1
γ-ray intensity	3	Irradiation time	1.5
		Cooling time	1
Statistical errors	6.5	Systematic errors	2.5
Total error of the measured IR			7

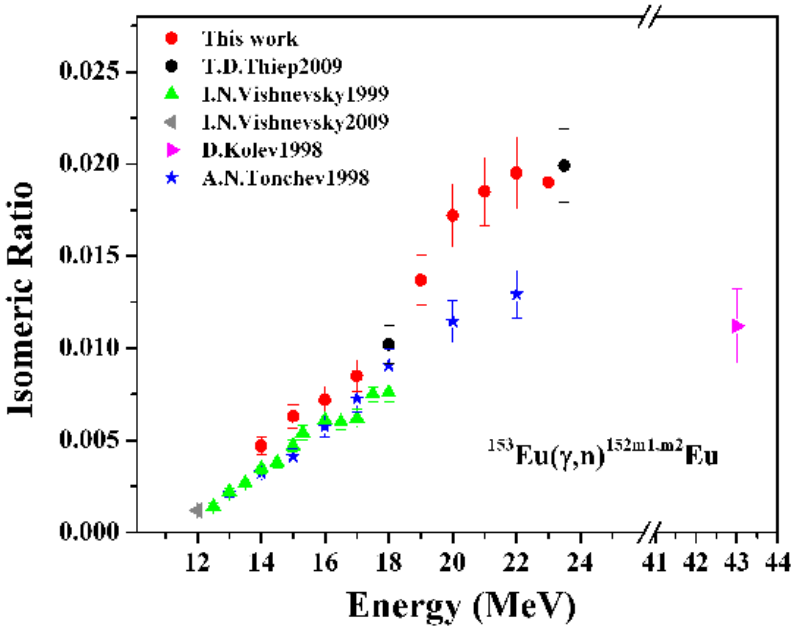

FIGURE 3.3: IR of ^{152m1}Eu$(8^-)/^{152m2}$Eu(0^-) versus the bremsstrahlung end-point energies [23].

In Table 3.3, the measured data from this work are listed together with those of others in the literature. So far, only four measurements of the IR of ^{152m1}Eu$(8^-)/^{152m2}$Eu(0^-) exist in the literature [136, 40, 139, 41]. These complied IRs are shown in Figure 3.3 as a function of the bremsstrahlung endpoint energy within and beyond the GDR region. From Table 3.3 and Figure 3.3, one can see that the IRs from [139] data are lower than those of the present data, while the data from [40] give a low value of the IR at high energy, in contrast with the trend of the IR toward the high energy region. The higher IR values of the present work compared to other works [139, 40] may be due to the fact that the proper correction of the internal conversion phenomena and self-absorption for the 89.8 keV γ ray of ^{152m1}Eu has been carefully taken into account in the present work. The lower IR at the 12 MeV bremsstrahlung end-point energy of [136] can be explained by the fact that the excitation energy is low and the contributions of direct and pre-equilibrium processes are low and do not exceed 5-10%, as pointed out by the author in [136], while these processes can be significant at higher energies. Therefore, data for IR in the GDR region need to be measured, and the present data offer a more complete picture of systematic IR throughout the GDR region. This fact also infers that the IR results in this work could serve as new benchmarks for theoretical calculations that focus on the aforementioned mechanism within the GDR energy region. Furthermore, the IR results for ^{152m1}Eu$(8^-)/^{152m2}$Eu(0^-) isomers produced in the ^{153}Eu(γ, n) reaction are closely related to the quadrupole deformation characteristics of these isomeric states. Indeed, it was also discussed in [122] that the state of nuclear deformation could be altered when the nucleus is produced in an isomeric state, while it may not be the case for the ground state. Therefore, our results on the IRs of ^{152m1}Eu(8^-) and ^{152m2}Eu(0^-) in the GDR region can be considered as a continuation of the work in [122], and also contribute more information to discuss the effect on the changes in nuclear deformation for these isomeric states, particularly when a deformed nucleus is excited with different energies.

It is expected that the IR in the (γ, n) reaction may undergo gradual changes (increase or decrease) in the energy region of the reaction threshold energy toward the end of the GDR region, then becomes stable or increases insignificantly for beyond this energy region. This comes from the definition of the IR in the case of excitation with bremsstrahlung, as presented in [37]. This trend is also observed from the measured IRs in this work, which shows a growth of the IR with increasing excitation energy. Beyond the GDR region, the increase is not significant. This effect can be called the

excitation energy effect on the IR.

Apart from dependence on the excitation energy, it is well-known that the IR also depends strongly on the target spin, the spin of the isomeric and ground states, and the spin difference between states. Examples of such effects can be found in [136, 140, 41, 141, 142, 48, 143], where IRs in mass number regions with Z = 74–82 and A = 183–207 were measured for the reaction (γ, p) of even-odd nuclei and for the reaction (γ, n) of odd-even nuclei. In this nuclear region, the last proton $(h_{11/2})$ of even-odd nuclei and the last neutron $(h_{13/2})$ of odd-even nuclei have large values of angular momentum. This results in a population of high-spin isomers of odd-odd nuclei through (γ, n) and (γ, p) reactions, thus the spin difference between the isomeric and ground states is relatively large. The experimental IRs were compared with those calculated by HVM, and it was shown that for the aforementioned nuclei, the IRs were usually low. In particular, for ^{196m,g}Au the spin difference $\Delta s = 10$, the $IR = 2.94 \times 10^{-4}$ [48] and 3.1×10^{-4} [142] at 18 and 24 MeV; for ^{194m,g}Ir, $\Delta s = 10$, the $IR = 2.9 \times 10^{-4}$ [140] and 10^{-3} [142] at 24 MeV; for ^{182m,g}Ta, $\Delta s = 7$, the $IR = 2.2 \times 10^{-4}$ [142] and $IR = 7.7 \times 10^{-4}$ [143] at 24 and 15 MeV; for ^{190m,g}Ir, $\Delta s = 7$, the $IR = 8.0 \times 10^{-4}$ [141] and $IR = 6.1 \times 10^{-4}$ [136] at 22 and 16 MeV; for ^{206m,g}Tl, $\Delta s = 12$, the $IR = 2.4 \times 10^{-5}$ [142] at 24 MeV. In the current work, during the primary and intermediate level decay process, the isomeric states ^{152m1}Eu (8^-) and ^{152m2}Eu (0^-) are formed with a large spin difference between them $(\Delta s = 8)$. Therefore, the low IR value of ^{152m1,m2}Eu (e.g. IR = 8.5 x 10^{-3} at 17 MeV) seems to be justified. This is called the effect of the spin difference on the IR, where the higher the spin difference, the lower the isomeric ratio.

The average excitation energy used in this study with an electron energy of 23.0 MeV is determined to be 14.5 MeV. This value is calculated using formula (4) from [144]. At the same excitation energy 14.5 MeV, the IR of ^{152m1}Eu$(8^-)/^{152m2}$Eu(0^-) produced in the $^{153}Eu(n, 2n)^{152}Eu$ reaction is 0.270 ± 0.030 [145]. Around this excitation energy regime, similar results are also reported for $^{153}Eu(n, 2n)^{152}Eu$ in Ref. [146]. For the excitation energies of 13.5, 14.1 and 14.8 MeV, the IRs of 0.239 ± 0.038, 0.277 ± 0.042 and 0.315 ± 0.047 were reported. The main difference between these experiments compared to the present work is that the isomeric states are formed in reactions $(n, 2n)$, where the neutron produces a significantly higher angular momentum in the entrance channel compared to the photon in reactions (γ, n). This so-called nuclear channel effect can also be seen in [147, 45, 42, 148].

3.1.2 ^{195m,g}Hg and ^{197m,g}Hg

So far, there is a dearth of data for IRs of isomeric pairs formed by nuclear reactions with Hg isotopes, especially IRs in $^{196}Hg(\gamma,n)^{195m,g}Hg$ and $^{198}Hg(\gamma,n)^{197m,g}Hg$ photonuclear reactions. In an experimental study carried out by Zheltonozhsky et al. [149], the IRs in reactions $^{198}Hg(\gamma,n)$ and $^{197}Au(d,2n)^{197}Hg$ were measured in the energy range of 8-17 MeV and 8-50 MeV, respectively, and the role of the low-lying structure in the IR was discussed. In another study employing reactions (n, 2n), Kasugai et al. [150] measured the independent cross sections for the isomeric and ground states of ^{195m,g}Hg and ^{197m,g}Hg isomeric pairs, where the IRs for each isomeric pair can be inferred from the cross section data. Tilbury and Yaffe [151] studied the IR of ^{195m,g}Hg, ^{197m,g}Hg and ^{196m,g}Au produced in reactions ^{197}Au(p, 3n), ^{197}Au(p, n) and ^{197}Au(p, pn) reactions with proton energies of 8–60 MeV. The obtained data show a dominant role of the compound nucleus mechanism of the nuclear reactions at low excitation energies, as well as a nonnegligible contribution of the direct and pre-equilibrium processes in higher energy regimes. Similar arguments were also drawn in IR measurement with incident particle energies ranging from the threshold value of the $^{197}Au(p,n)^{197m,g}Hg$ reaction up to 20 MeV (Gritsyna et al. [152]). Hansen et al. [153] investigated the excitation functions of the isomeric and ground states of ^{197}Hg using the reaction (p,n) with an incident proton energy of 4 to 13 MeV. The results in the energy range above 7 MeV were can be reasonably explained by the optical model calculation of Bjorklund and Fernbach. Detail exploration for the excitation functions of isomeric pairs of ^{195m,g}Hg and ^{197m,g}Hg was performed by Al-Abyad et al. [154] through the $^{196}Hg(n,2n)$ and $^{198}Hg(n,2n)$ reactions using quasi monoenergetic neutrons from the Julich variable energy compact cyclotron CV-28 with an energy range of 7.6–12.5 MeV. They performed theoretical calculations employing the STAPRE and EMPIRE-2.19 codes. These codes were developed within the framework of the statistical and precompound model formalisms to describe the formation of both the isomeric and ground states. The results of such calculations were compared with the experimental data. It was found that the agreement between the experiment and theory is only approximated. Vandenbosch and Huizenga [52] measured the IR and the excitation functions of ^{197m,g}Hg and ^{195m,g}Hg isomeric pairs produced in the $^{197}Au(p,n)$, $^{197}Au(d,2n)$, $^{196}Hg(n,\gamma)$, $^{196}Hg(d,p)$, $^{198}Hg(n,2n)$, $^{198}Hg(\alpha,\alpha n)$, and $Pt(\alpha,xn)$ reactions. The statistical reaction model revealed the dominant role of the formation of a compound nucleus in these reactions. In addition, relatively small amounts of angular momentum were transferred

in reactions that predominantly proceed by a direct interaction mechanism.

Photonuclear reactions were also used to study the isomeric pairs of ^{195}Hg and ^{197}Hg. Ishkhanov et al. [155, 156] measured the yields of the isomeric and ground states in the reactions $^{196}Hg(\gamma,n)^{195}Hg$ and $^{198}Hg(\gamma,n)^{197}Hg$ at the endpoint energies of the 19.5 and 29.1 MeV bremsstrahlung, where the IRs of the corresponding isomeric pairs can be determined. In the photonuclear reaction, the mechanism of electric dipole absorption of a quantum γ is well known to dominate in the GDR region. In this mechanism, the γ quantum angular momentum $1\hbar$ is transferred to the target nucleus, which is independent of the γ quantum energy. Because of such an effect, the spin range of the excited levels can be restricted, and the interpretation of the reaction mechanism becomes simple. In this sense, the study of photonuclear reactions continues to be an attractive subject [157, 147, 155, 158, 159].

Following the above considerations, a part of this thesis is dedicated to study the IRs of ^{195m,g}Hg and ^{197m,g}Hg. These isomeric pairs were produced in an experiment employing $^{196}Hg(\gamma,n)$ and $^{198}Hg(\gamma,n)$ reactions with excitation energies in the GDR energy region. The obtained IRs are used to discuss the effects of excitation energy, nucleon configuration, and reaction channel effects on the IRs. Furthermore, new data on IRs in the present work are expected to contribute to the Nuclear Database and provide benchmarks for theoretical nuclear reaction models. The natural mercury sample was irradiated by bremsstrahlung with endpoint energies of 14 to 24 MeV with a step of 1 MeV. Detailed nucleon configurations of these nuclei can be found in [160]. Two isomeric pairs of ^{195m,g}Hg and ^{197m,g}Hg were produced in the $^{196}Hg(\gamma,n)$ and $^{198}Hg(\gamma,n)$ reactions. Figs. 3.4 and 3.5 show the simplified decay schemes of these isomeric pairs into Au isotopes. Details of decay characteristics and γ-ray radiation emitted from these decays are presented in Table 3.5 taken from [138]. In this table, γ-rays with high intensities and independent of the contribution of other nuclear reactions were chosen for the IR calculations. Both the isomeric states ^{195m}Hg and ^{197m}Hg have the same spin of $13/2^+$, while the ground states ^{195g}Hg and ^{197g}Hg have the same spin of $1/2^-$.

Fig. 3.6 shows a typical γ -ray spectrum obtained when the natural Hg sample is irradiated with 20 MeV bremsstrahlung endpoint energy for 1 hour and cooled for 2 hours. The measurement time was 1 hour, obtaining sufficient statistics to clearly resolve the characteristic γ rays of isomeric pairs ^{195m,g}Hg and ^{197m,g}Hg.

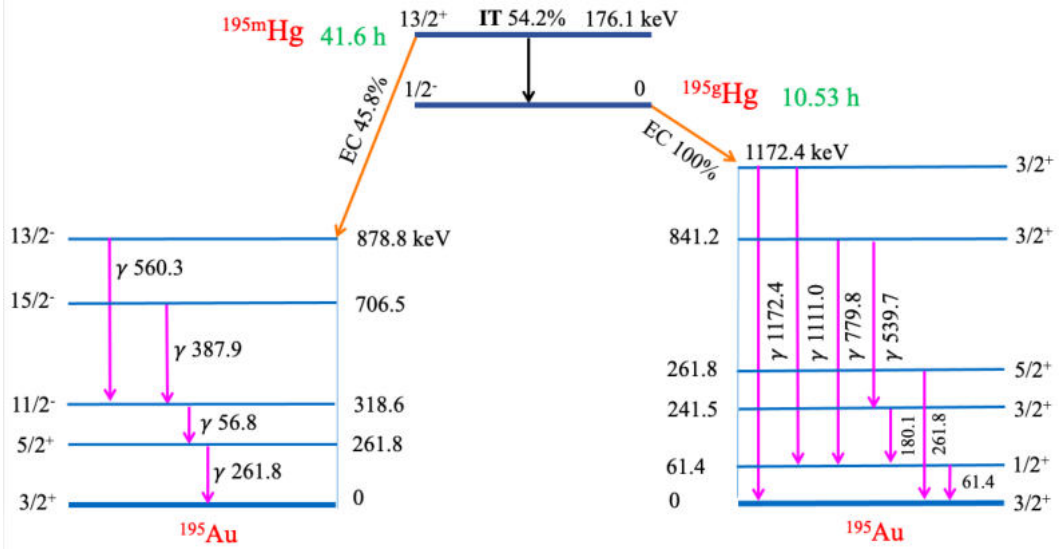

FIGURE 3.4: Simplified decay schemes of ^{195m}Hg and ^{195g}Hg [128].

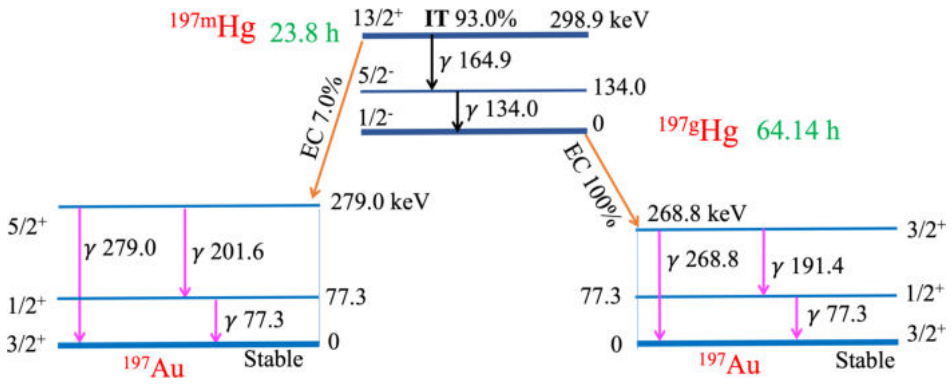

FIGURE 3.5: Simplified decay schemes of ^{197m}Hg and ^{197g}Hg [128].

TABLE 3.5: γ-rays decay properties of the reaction products of ^{195m,g}Hg and ^{197m,g}Hg used in the IR calculation [138].

Nuclear Reaction	Reaction Threshold [MeV]	Nuclear state	Spin Parity [J^π]	Decay Mode [%]	Half-life [h]	γ-ray Energy [keV]	Intensity [%]
$^{196}Hg(\gamma,n)^{195m}Hg$	9.06	^{195m}Hg	13/2+	IT: 54.2 EC: 45.8	41.6	261.7 560.3	30.9 7.0
$^{196}Hg(\gamma,n)^{195g}Hg$	8.88	^{195g}Hg	1/2-	EC: 100	10.53	779.8 1172.4	7.0 1.24
$^{198}Hg(\gamma,n)^{197m}Hg$	8.78	^{197m}Hg	13/2+	IT: 91.4 EC: 8.6	23.8	134.0	33.0
$^{198}Hg(\gamma,n)^{197g}Hg$	8.49	^{197g}Hg	1/2-	EC: 100	64.14	77.3 191.4	18.7 0.632

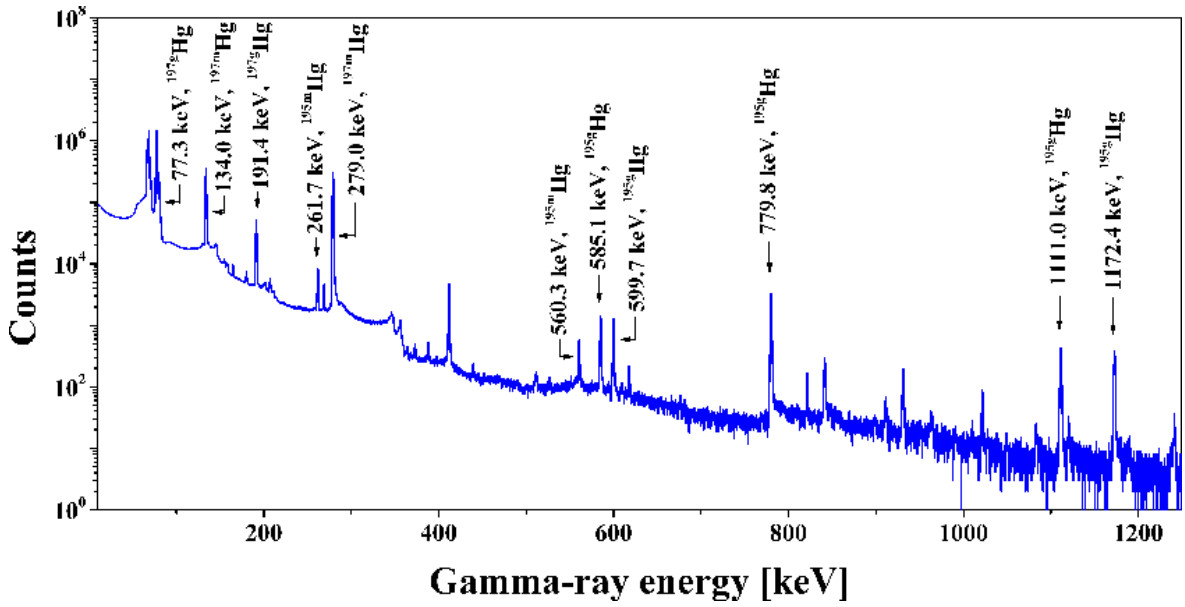

FIGURE 3.6: A typical energy spectrum of the natural Hg sample measured for 2 hours at a distance of 5 cm from the HPGe detector. The sample was irradiated with 20 MeV bremsstrahlung for 1 hour and cooled for 23 hours before measurement [128].

The self-absorption and the summing coincidence effect were estimated and corrected as in Section 2.1.5. Table 3.6 shows the calculated values of the self-absorption and summing correction factors F_g and C_c at different distances h between the sample and the detector.

TABLE 3.6: A summary of corrections for self-absorption and summing coincidence for given γ-ray energies.

γ-ray energy, keV (Intensity, %)	Self-absorption correction, F_g t = 0.3 g/cm2	Summing coincidence correction, C_c	
		at h = 0 cm	at h = 5 cm
261.7(30.9)	1.09	1.013	1.002
560.3(7.0)	1.02	1.08	1.01
779.8(7.0)	1.01	1.019	1.002
1172.4(1.24)	1	1	1
134.0(33.0)	1.37	1	1
77.3(18.7)	1.33	1.001	1
191.4(0.632)	1.13	1.061	1.008

The IRs obtained in the present work are shown in Table 3.7, together with the data from the literature published in only six Refs. [151, 155, 156, 54, 161, 162] concerning the IR of ^{195m,g}Hg and ^{197m,g}Hg.

The systematic errors introduced by the sample to the detector distance, the variation of the electron beam, the irradiation time, and the cooling time were estimated to be 2.5%. The error of the IR calculation was propagated and estimated to be 9.5%. These error sources contribute to the total uncertainty of the IR, which is estimated

TABLE 3.7: Summary of IRs determined for $^{195m,g;197m,g}$Hg isomeric pairs produced in reaction (γ, n) [128].

End-point Energy (MeV)	IR of $^{197m,g}Hg$		IR of $^{195m,g}Hg$	
	This work	Other works	This work	Other work
10		0.003 ± 0.0010 [149]		
11		0.016 ± 0.0014 [149]		
12		0.032 ± 0.0018 [149]		
13		0.052 ± 0.003 [149]		
14	0.082 ± 0.008	0.079 ± 0.006 [149]	0.089 ± 0.009	
15	0.096 ± 0.009	0.093 ± 0.005 [149]	0.102 ± 0.010	
16	0.100 ± 0.010	0.104 ± 0.005 [149]	0.114 ± 0.011	
17	0.108 ± 0.011	0.112 ± 0.006 [149]	0.120 ± 0.012	
18	0.114 ± 0.011		0.124 ± 0.012	
19	0.116 ± 0.012		0.128 ± 0.013	
19.5		0.079 ± 0.022 [155]		0.111 ± 0.039 [155]
20	0.119 ± 0.012		0.131 ± 0.013	
21	0.120 ± 0.012		0.129 ± 0.013	
22	0.117 ± 0.012		0.132 ± 0.013	
23	0.118 ± 0.012		0.129 ± 0.013	
24	0.120 ± 0.012		0.133 ± 0.013	
25		0.11 ± 0.02 [54]		
29.1		0.118 ± 0.035 [155, 156]		0.136 ± 0.038 [155, 156]
30		0.098 [161]		
		0.053 ± 0.010 [162]		

to be approximately 10%.

Fig. 3.7 graphically shows the data from Table 3.7, i.e., the IR values as a function of the bremsstrahlung endpoint energies. These values were taken from this work and from [151, 155, 156, 54, 161, 162] for the isomeric pairs ^{197m,g}Hg and ^{195m,g}Hg within and above the GDR region.

From Table 3.7 and Fig. 3.7, good agreement between our results and the data of Zheltonozhsky et al. [149] can be clearly seen in the energy range from 14 to 17 MeV. Meanwhile, the IRs at 19.5 MeV of Ishkhanov et al. [155] are lower than our result. This discrepancy can be explained by the fact that the IR results in [155] were calculated from the yields of the isomeric and ground states separately, while the IR results of this work were obtained consistently using formula (2.18). Consequently, these IR results are more accurate because the isomeric and ground states were simultaneously measured under the same experimental conditions.

According to the expression (1) in [37], the IR remains unchanged or increases insignificantly for the photonuclear reaction at the end or beyond the GDR region. This implies that the measured results for ^{197m,g}Hg are compatible with the data of Gangrsky [54] and Ishkhanov [155, 156], while the data of Toyoaki [161] and Carver [162] are lower. For ^{195m,g}Hg, the data for IR are scarce with only two experimental results found in the literature [155, 156], both agree well with our results.

It is worth noting that the obtained IRs of $^{195m,g;197m,g}$Hg increase with the increase in end-point bremsstrahlung energy up to the end of the GDR region. Beyond this region, this becomes unchanged or slowly increases, since the pre-equilibrium and direct processes prevail over the compound reaction one.

When comparing the IRs of two isomeric pairs ^{195m,g}Hg and ^{197m,g}Hg in (γ, n) reaction, one finds that the IR of ^{195m,g}Hg is higher, while the mass number of the corresponding reactant ^{196}Hg is smaller than the reactant ^{198}Hg. A similar fact was observed in the photonuclear reaction of the isotopes of Sb [34], Se [35] and Ba[36]. It is understood that due to the effect of the nucleon configuration, the IR in (γ, n) reaction with isotopes of an element generally decreases with increasing isotope mass number.

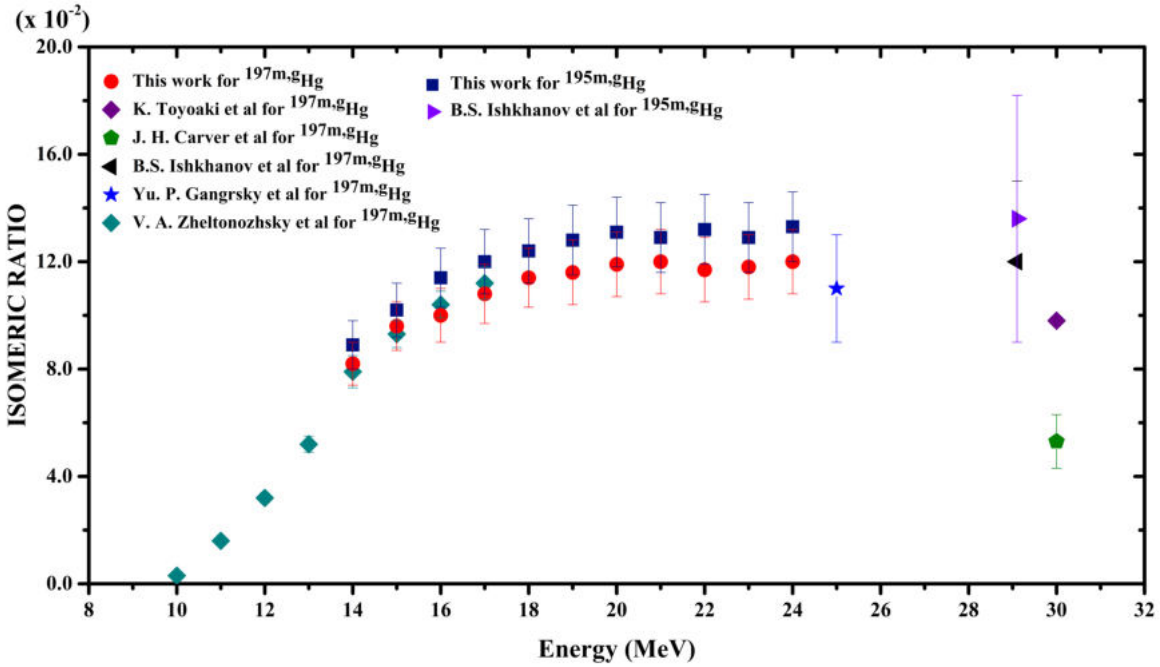

FIGURE 3.7: Measured IRs of $^{195m,g;197m,g}$Hg versus bremsstrahlung endpoint energy.

It is interesting to compare IRs of isomeric pairs produced by different reaction types at similar projectile energy. Table 3.8 shows the IRs of the isomeric pairs ^{197m,g}Hg and ^{195m,g}Hg produced from different nuclear reactions at a projectile energy of 12.5 MeV. Using the formula (4) in Ref. [144], average projectile energy of 12.5 MeV was calculated, equivalent to the endpoint bremsstrahlung energies of 19 and 18 MeV, for $^{198}Hg(\gamma, n)^{197m,g}Hg$ and $^{196}Hg(\gamma, n)^{195m,g}Hg$ photonuclear reactions. The IRs of ^{197m,g}Hg and ^{195m,g}Hg varied from reaction to reaction. This feature is due to the effect of the entrance channel parameters on the IR. Compared to other reactions, the lowest

angular momentum value in the (γ, n) reaction was transferred to the target nucleus, resulting in the lowest measured IR value. For ^{69m,g}Zn and ^{71m,g}Zn [42]; ^{58m,g}Co [42]; ^{87m,g}Y [148]; ^{137m,g}Ce [144], ^{52m,g}Mn [45], ^{135m,g}Xe [38], ^{75m,g}Ge [163] and ^{80m,g}Br [164], we also observed a similar entrance channel effect. For a detailed interpretation of the aforementioned effects, different nuclear reaction models incorporating all reaction mechanisms as statistical, direct, and pre-equilibrium processes need to be employed. Therefore, the results of this work are significant in the sense that they not only provide additional data to the Nuclear Database but can also be used for the test of these models.

TABLE 3.8: Summary of IRs determined for ^{197m,g}Hg and ^{195m,g}Hg isomeric pairs produced in various nuclear reactions.

Projectile Energy (MeV)	$^{198}Hg(\gamma,n)^{197m,g}Hg$	$^{197}Au(p,n)^{197m,g}Hg$	$^{198}Hg(n,2n)^{197m,g}Hg$	$^{197}Au(d,2n)^{197m,g}Hg$
12.5	0.116 ± 0.012 (This work)	0.63 ± 0.11 [151] 1.1 [152]	0.7 ± 0.18 [154]	0.6 ± 0.06 [149] 0.6 ± 0.06 [52]
Projectile Energy (MeV)	$^{196}Hg(\gamma,n)^{195m,g}Hg$		$^{196}Hg(n,2n)^{195m,g}Hg$	
12.5	0.124 ± 0.012 (This work)		1.07 ± 0.28 [154]	

3.2 Isomeric Ratios in (n, γ) reactions

3.2.1 ^{109m,g}Pd and ^{111m,g}Pd

Among the highlight results of the current thesis, IRs in (n, γ) reactions bombarded by thermal, resonance and mixed thermal-resonant neutrons on ^{108,110}Pd nuclei have been measured. The aim of this research is to accumulate more experimental data for IRs in different neutron energies, since there are very limited data for these nuclei existing in the literature and for the theoretical interpretation various new measurements are needed. There are only two works [165, 166] for the target nucleus ^{108}Pd and three works [166, 167, 168] for ^{110}Pd nucleus in (n, γ) reactions. Thus, the results obtained are expected to enrich the Nuclear Data Bank and provide additional data for the interpretation of IRs by different theoretical models.

To study the IRs of isomeric pairs of Pd isotopes in the reaction (n, γ), the Pd sample is prepared and irradiated by the thermal-resonant neutron source created at the MT-25 Microtron as described in Subsection 2.1.2. The experimental setup is detailed in Fig. 2.4. Natural palladium consists of ^{102}Pd, ^{104}Pd, ^{105}Pd, ^{106}Pd, ^{108}Pd and ^{110}Pd. Through the reaction (n, γ) the products ^{103}Pd, ^{107}Pd, ^{109}Pd and ^{111}Pd were formed. Among the reaction products, the γ-rays associated with the β^--decays of ^{103}Pd ($T_{1/2}$ = 16.991 days) have low intensities. Another product ^{107}Pd also decays in the β^-

process, accompanied by 214.9 keV γ-rays. Under current experimental conditions, the γ rays of ^{103}Pd and ^{107}Pd were not observed in the spectrum. The reaction products of interest ^{109}Pd and ^{111}Pd exist in the isomeric and ground states, where the decays of those states would be visible in the γ-ray spectrum.

Figure 3.8 depicts the simplified decay schemes of the produced isomeric pairs ^{109m,g}Pd and ^{111m,g}Pd as well as their decay modes, lifetime, spin, and parity.

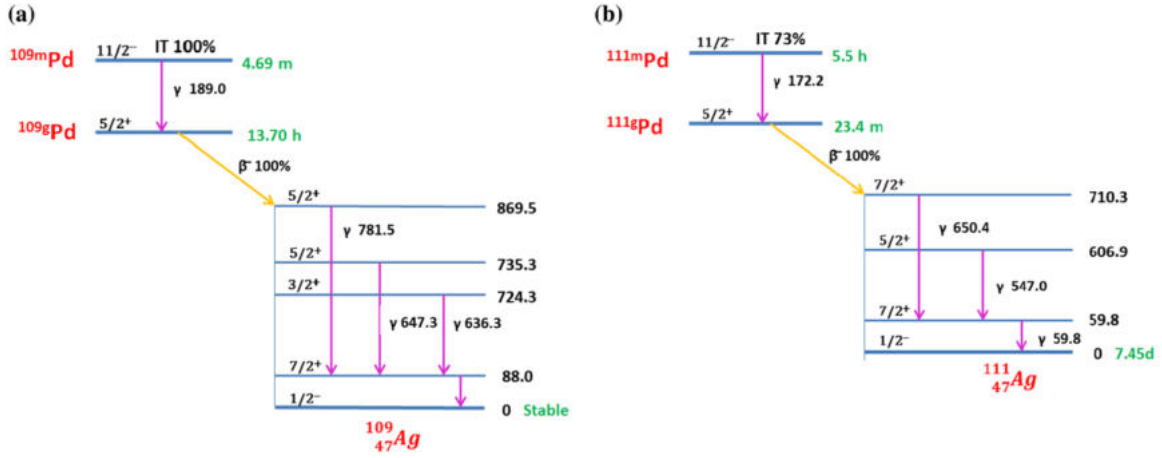

FIGURE 3.8: Simplified decay diagrams of $^{109m,g;111m,g}$Pd [129].

Figure 3.9 presents a typical offline γ-ray spectrum of natural Pd covered with Cd foil. The sample was irradiated for 1.5 h under an electron current of 15 μA, then allowed a cooling time of 11 minutes and measured for 30 minutes at a distance of 0 cm from the HPGe detector. From the obtained γ-ray spectrum, the characteristic γ-rays of the isomeric pairs ^{109m,g}Pd and ^{111m,g}Pd, listed in Table 3.9, are clearly seen.

TABLE 3.9: γ-rays decay properties of reaction products of ^{109m,g}Pd and ^{111m,g}Pd used in the IR calculation [138].

Nuclear Reaction	Target Spin,Parity [J^π]	Nuclear state	Spin, Parity [J^π]	Decay Mode [%]	Half Life	γ-ray Energy [keV]	Intensity [%]
$^{108}Pd(n,\gamma)^{109m}Pd$	0^+	^{109m}Pd	$11/2^-$	IT: 100	4.69 m	189	55.9
$^{108}Pd(n,\gamma)^{109g}Pd$	0^+	^{109g}Pd	$5/2^+$	β^- : 100	13.7 h	88.04	3.6
$^{110}Pd(n,\gamma)^{111m}Pd$	0^+	^{111m}Pd	$11/2^-$	IT: 73 β^- : 27	5.5 h	172.2	34
$^{110}Pd(n,\gamma)^{111g}Pd$	0^+	^{111g}Pd	$5/2^+$	β^- : 100	23.4 m	547 650.4	0.38 0.57

Among the corrections entered in the calculation of the actual γ-ray counts from the decay of isomeric pairs detailed in Chapter 2, the calculated values of the self-absorption and summing correction factors F_g and C_c for the γ-rays used for isomeric pairs ^{109m,g}Pd and ^{111m,g}Pd are listed in Table 3.10.

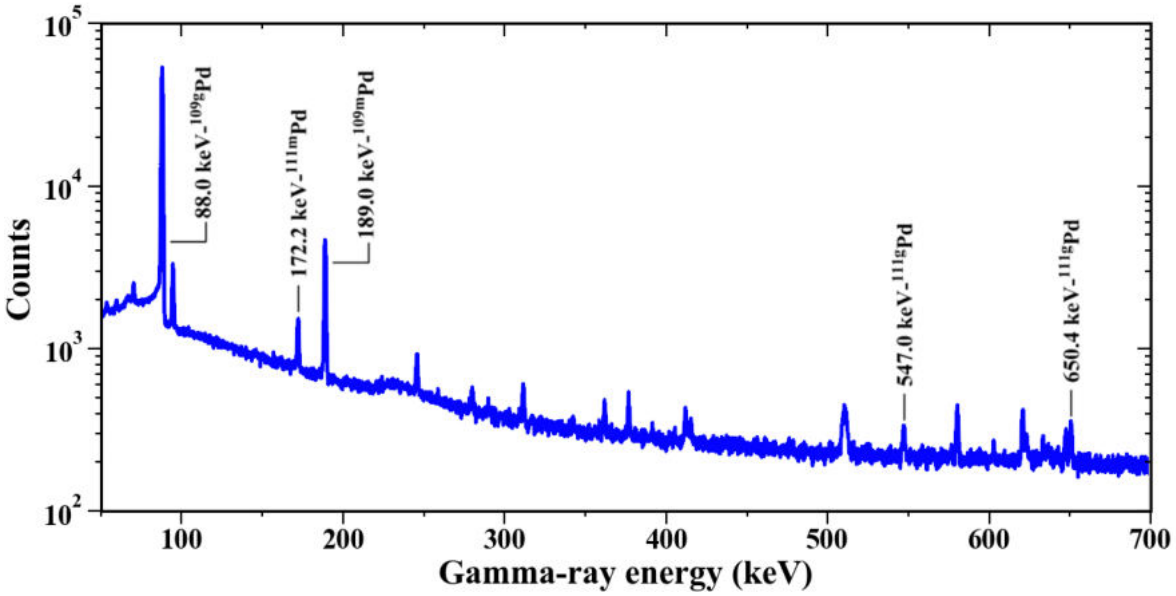

FIGURE 3.9: A typical energy spectrum of Cd-foil-covered natural Pd sample irradiated with energetic neutrons [129].

TABLE 3.10: A summary of corrections for self-absorption and summing coincidence for given γ-ray energies of ^{109m,g}Pd and ^{111m,g}Pd.

γ-ray energy, keV (Intensity, %)	Self-absorption correction, F_g t = 0.323 g/cm2	Summing coincidence correction, C_c	
		at h = 0 cm	at h = 5 cm
88.04 (3.6)	1.24	1	1
172.2(34.0)	1.06	1	1
189.0 (55.9)	1.05	1	1
547.0 (0.38)	1.01	1.01	1
650.4 (0.57)	1	1.01	1

The IR was then calculated using the formula (2.18). Table 3.11 presents the IRs in the capture reactions $^{108}Pd(n,\gamma)^{109m,g}Pd$ and $^{110}Pd(n,\gamma)^{111}Pd$ capture reactions induced by thermal, resonant, and mixed thermal-resonant neutrons obtained in the present work, together with IRs available in the literature [165, 166, 167, 168]. Table 3.11 also lists the IR values in the reactions $^{110}Pd(n,2n)^{109}Pd$, $^{110}Pd(\gamma,n)^{109}Pd$ and $^{114}Cd(n,\alpha)^{111}Pd$, taken from Refs. [61, 169, 170], which produce the same isomeric pairs.

TABLE 3.11: A summary of IR results for $^{109m,g;111m,g}$Pd in thermal, resonance, and mixed thermal-resonant neutron-induced reactions and also in a (γ,n) reaction.

Nuclear reaction	Type of projectile	Product Exc. Energy [MeV]	Isomeric ratio (IR)
$^{108}Pd(n,\gamma)^{109m,g}Pd$	Thermal neutron	6.15	0.023 ± 0.002 [This work]
			0.028 ± 0.005 [165]
			0.018 ± 0.004 [166]
$^{108}Pd(n,\gamma)^{109m,g}Pd$	Resonant neutron	6.15	0.023 ± 0.002 [This work]
			0.028 ± 0.005 [165]
$^{108}Pd(n,\gamma)^{109m,g}Pd$	Mixed Thermal-Resonant neutron	6.15	0.023 ± 0.002 [This work]
$^{110}Pd(\gamma,n)^{109m,g}Pd$	25 MeV Bremstrahlung	6.93	0.065 ± 0.003 [61]
$^{110}Pd(n,2n)^{109m,g}Pd$	14.1 MeV neutron	5.28	0.410 ± 0.039 [61]
			0.41 ± 0.03 [169]
$^{110}Pd(n,\gamma)^{111m,g}Pd$	Thermal neutron	5.75	0.037 ± 0.004 [This work]
			0.263 ± 0.059 [166]
			0.123 ± 0.010 [167]
			0.047 ± 0.001 [168]
$^{110}Pd(n,\gamma)^{111m,g}Pd$	Resonant neutron	5.75	0.037 ± 0.004 [This work]
$^{110}Pd(n,\gamma)^{111m,g}Pd$	Mixed Thermal-Resonant neutron	5.75	0.037 ± 0.004 [This work]
$^{114}Cd(n,\alpha)^{111m,g}Pd$	14.1 MeV neutron	0.96	0.75 ± 0.29 [170]

The associated total uncertainty was estimated to be approximately 10%, shown in Table 3.12, which consists of the statistical errors of the counts of γ-rays, detector efficiency, half-life and intensity of the γ-rays, and systematic errors from the distance from the detector to the sample, the selection of γ rays, the variation of the electron beam, the irradiation and cooling time. All these error sources are propagated to yield the final uncertainty.

In Table 3.11, the product excitation energies of the reactions of interest are also given. For the IR obtained in the current experiment, the product excitation energy is the binding energy of the neutron in the compound nuclei ^{109}Pd and ^{111}Pd, corresponding to the neutron capture reactions on ^{108}Pd and ^{110}Pd with thermal, resonant, and mixed thermal-resonant neutrons. The binding energies were taken from [142]. For the IRs obtained in the $(n,2n)$ reaction, the corresponding product excitation energy $E_{pod.ex}$ is calculated by

TABLE 3.12: A summary of the error sources considered in the IR calculation of ^{109m,g}Pd.

Random Errors	[%]	Systematic Errors	[%]
Counting statistical	1.0 - 2.0	Sample-detector distance	1
Detector efficiency	2	γ-ray selection	1
Half-life	1.5	e-beam variation	1
γ-ray intensity	3	Irradiation time	1.5
		Cooling time	1
Statistical errors	9.6	Systematic errors	2.5
Total error of the measured IR			10.0

$$E_{pod.ex} = E_{ex} - S_{2n}, \tag{3.1}$$

where E_{ex} and S_{2n} are the target excitation energy and the two-neutron separation energy of the compound nucleus, which were taken from [171].

In Table 3.11, the excitation energy of the product in the $^{110}Pd(\gamma, n)^{109m,g}Pd$ photonuclear reaction with the bremsstrahlung energy of the 25 MeV endpoint was calculated as follows:

$$E_{pod.ex} = \overline{E_{ex}} - S_n - \varepsilon_n, \tag{3.2}$$

where S_n - the neutron separation energy, taken from Ref. [171], ε_n - the mean kinetic energy of photoneutrons, taken from Ref. [172], $\overline{E_{ex}}$ - the target excitation energy is equivalent to a mean value of the bremsstrahlung, calculated as follows:

$$\overline{E_{ex}} = \frac{\int_{E_0}^{E_{th}} E\sigma(E)\phi(E, E_0)dE}{\int_{E_0}^{E_{th}} \sigma(E)\phi(E, E_0)dE}, \tag{3.3}$$

where $\sigma(E)$ the excitation function, taken from Ref. [61] and $\phi(E, E_0)$ the Schiff formula for the bremsstrahlung photon flux, described in Ref. [173], E_0 the end-point bremsstrahlung energy and E_{th} the reaction threshold energy, taken from Ref. [171].

For the $^{114}Cd(n, \alpha)^{111m,g}Pd$ reaction, the product excitation energy was calculated as:

$$E_{pod.ex} = E_{ex} - S_\alpha - E_C, \tag{3.4}$$

where E_{ex} the target excitation energy, S_α the separation of the α particle and E_C the Coulomb barrier for a in ^{115}Cd nucleus. S_α and E_C were calculated to be 4.48 and

14.8 MeV, respectively.

From Table 3.11, one finds some discrepancies between our IR results compared to the data from Refs. [166, 167, 168] in neutron capture reactions. In our experiment, the variation of the intensity of the electron beam was 1%, so the neutron flux of the accelerator can be considered constant. In fact, the discrepancies may come from the following sources: (a) In [166, 167, 168], the neutron source was a reactor, while in our experiment the neutron flux was obtained from the accelerator. As a result, the neutron spectra were different, leading to the difference in IR; (b) In this work, the HPGe high resolution semiconductor detector and a more advanced spectra processing program were used for offline γ spectroscopy. Therefore, the gamma spectra and their processing are much better than in previous works, where the authors used scintillation detectors, the end-window beta counter, and radiochemical techniques [166, 167, 168]; (c) the IR in [166, 167, 168] was calculated as the ratio of the values determined separately of the cross sections of the isomeric and ground states, while in our case the IR was obtained directly using formula 2.18 in Chapter 2. Since in our case the isomeric and ground states were measured simultaneously under the same experimental conditions, the IR results are expected to be more accurate.

It is important to note that for the IR of ^{111m,g}Pd from [166], the comparison in Table 3.11 between our IR result and that in [166] is only preliminary. This is because the authors of that article reported only the upper estimate for the cross section, which led to the large difference between the two IR values.

The IRs for the isomeric pairs ^{109m,g}Pd and ^{111m,g}Pd reported in Table 3.11 are the same for thermal, resonant, and mixed thermal-resonant neutron capture reactions, although they have been measured separately. This can be explained by the fact that in both cases, the momentum transfer from the neutrons to the nuclei is the same and equal to $1/2\hbar$ and the excitation energies of the compound nuclei are almost the same because the kinetic energies of the neutrons are insignificant compared to the neutron binding energies.

The IR of the isomeric pair ^{109m,g}Pd obtained in our work for the thermal neutron capture reaction is equal to the average value of the data in Refs. [165] and [166]. For the resonant neutron, the IR value in our experiment is compatible with that of [165]. The IR obtained in the present work for mixed thermal-resonant neutrons is the first measurement, as no data existed in the literature.

For the isomeric pair ^{111m,g}Pd produced in the reaction with thermal neutrons, our

IR value is the lowest compared to the data in Refs. [166, 167, 168], in which the data in Ref. [166, 167] are unexpectedly high. In the case of the resonant and mixed thermal-resonant neutron-induced reaction, there are no data for the isomeric pair ^{111m,g}Pd that exists in the literature, therefore, the IR obtained in the present work can be considered as the first measurement.

Among all reactions that produce isomeric pairs ^{109m,g}Pd, IRs in the $^{108}Pd(n,\gamma)^{109m,g}Pd$ reactions are very small in comparison with that in $^{110}Pd(\gamma,n)^{109m,g}Pd$ and $^{110}Pd(n,2n)^{109m,g}Pd$ reactions, although the product excitation energies in these reactions are insignificantly different. On the other hand, the IR obtained in $^{110}Pd(n,\gamma)^{111m,g}Pd$ is much lower than that in the $^{114}Cd(n,\alpha)^{111m,g}Pd$ reactions, even though the excitation energy of the product in the $^{110}Pd(n,\gamma)^{111m,g}Pd$ reactions is much higher than that of the $^{114}Cd(n,\alpha)^{111m,g}Pd$ reactions. The so-called impulse effect in IR can be an explanation for such phenomena, that is, for nuclear reactions induced by different projectiles leading to the same isomeric pair, and the higher the impulse of the projectile, the higher the IR in the isomeric pair. This effect was also discussed in Refs. [52, 154, 144, 23, 174, 163]

3.2.2 ^{115m,g}Cd and ^{117m,g}Cd

Cadmium element and its isotopes are the subjects of intensive studies due to their important role in nuclear reactor engineering. Despite this importance, current nuclear data of the neutron capture reaction on the Cd isotope are not complete. The available data on the thermal neutron capture cross sections and resonance integrals of Cd isotopes were compiled in [175]. In the present work, IRs have been studied in reactions (n,γ) induced by thermal, resonant, and mixed thermal resonant neutrons on ^{114}Cd and ^{116}Cd. This research aims to accumulate more experimental data, as there is scarce data in general, especially for these nuclei, in the existing literature. Furthermore, many new measurements are needed for theoretical interpretation. Therefore, the results of this work may lead to richer information on the Cadmium element.

Two isomeric pairs ^{115m,g}Cd and ^{117}Cd were produced by low-energy neutron capture reactions on the natural Cd target. The resonance integral and thermal neutron cross sections of ^{114}Cd are 0.34 ± 0.02 and 14.1 ± 0.7 barn, while those of ^{117}Cd are 0.075 ± 0.020 and 1.6 ± 0.3 barn [175]. The simplified schemes of the isomeric pairs ^{115m,g}Cd and ^{117m,g}Cd are shown in Figs. 3.10 and 3.11, which also show the respective γ-rays together with γ cascades deexcited in the daughter nuclei ^{115}In and ^{117}In.

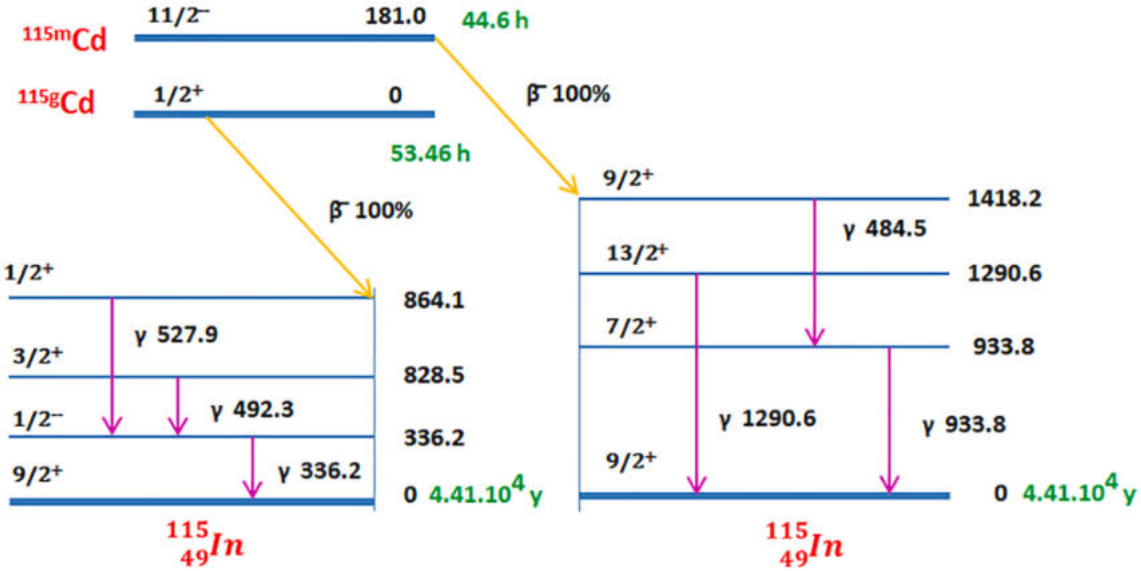

FIGURE 3.10: ^{115m,g}Cd isomeric pair: a simplified decay scheme [130].

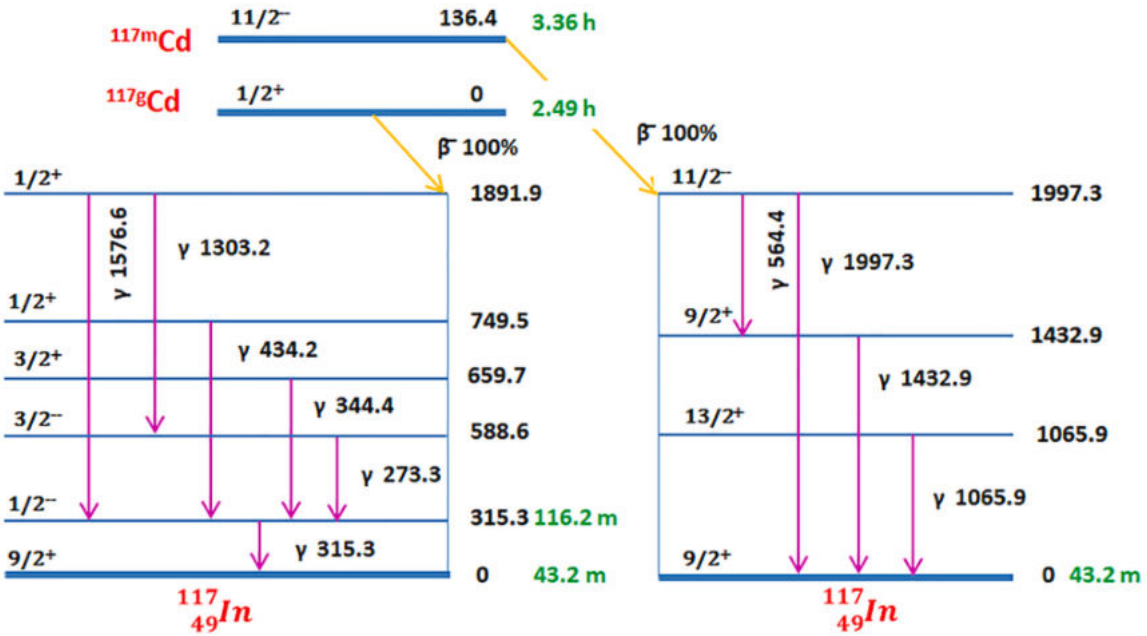

FIGURE 3.11: ^{117m,g}Cd isomeric pair: a simplified decay scheme [130].

Table 3.13 listed the spectroscopic characteristics and selected γ-rays used for the isomeric ratio calculations of isomeric pairs ^{115m,g}Cd and ^{117m,g}Cd.

TABLE 3.13: The decay properties of selected γ-rays for IR calculations for ^{115m,g}Cd and ^{117m,g}Cd isomeric pairs [138].

Nuclear reaction	Target Spin [J^π]	Nuclear state	Spin,Parity [J^π]	Decay Mode [%]	Half-life	γ-ray Energy [keV]	Intensity [%]
$^{114}Cd(n,\gamma)^{115m}Cd$	0^+	^{115m}Cd	$11/2^-$	β^- : 100	44.6 d	933.8	2
$^{114}Cd(n,\gamma)^{115g}Cd$	0^+	^{115g}Cd	$1/2^+$	β^- : 100	2.23 d	336.2	45.9
						492.3	8.03
						527.9	27.45
$^{116}Cd(n,\gamma)^{117m}Cd$	0^+	^{117m}Cd	$11/2^-$	β^- : 100	3.36 h	564.4	14.7
						1065.9	23.1
						1432.9	13.4
$^{116}Cd(n,\gamma)^{117g}Cd$	0^+	^{117g}Cd	$1/2^+$	β^- : 100	2.49 h	273.3	28
						344.4	17.8
						1303.3	

Since the lifetimes of the isomeric pair ^{117m,g}Cd are shorter than those of the isomeric pair ^{115m,g}Cd, the cooling and measurement time intervals were different. To determine the IR of ^{117m,g}Cd, the first batches of γ-ray spectra obtained under shorter measurement and also the cooling time were used. For the IR of ^{115m,g}Cd, the spectra obtained with a longer cooling measurement time were used.

Figure 3.12 presents a γ-ray spectrum of the natural Cd sample covered by Cd foil irradiated in the neutron source for 120 minutes and measured for 30 minutes with a cooling time of 67 minutes at a distance of 0 cm from the detector. The interested γ-rays of ^{117m,g}Cd stand out well in this γ-ray spectrum, but for the ^{115m,g}Cd isomeric pair only the γ-rays 336.2, 492.3, 527.9 keV of interest of the ground state are seen and the γ-ray 933.8 keV of the isomeric state does not emerge. Fig. 3.13 shows the γ-ray spectrum obtained when the neutron source irradiated the sample uncovered by Cd foil for 2 hours, followed by a cooling time of 13.94 days and measured for 12 hours at a distance of 0 cm from the detector surface. One observes an absence of the characteristic γ-rays of ^{117m,g}Cd, while the interested γ-rays of ^{115m,g}Cd are clearly seen. Therefore, the spectra processing is straightforward with reduced error.

In the IR calculation, proper correction of the self-absorption and summing effect is important, as detailed in Chapter 2. These values calculated for the γ-rays of isomeric pairs ^{115m,g}Cd and ^{117m,g}Cd are presented in Table 3.14, where the linear attenuation coefficients were taken from [176].

The IR was calculated using the formula 2.18 in Chapter 2. The results obtained for the IRs of ^{115m,g}Cd and ^{117m,g}Cd are presented in Table 3.15 together with the data available in the literature [177, 178, 179, 180]. In this table, the IR values of

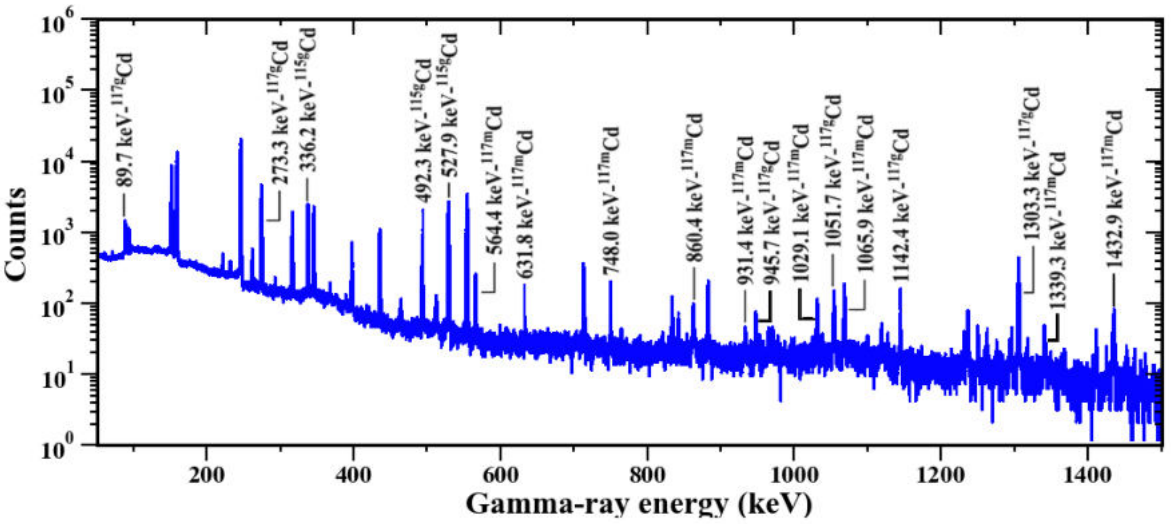

FIGURE 3.12: A typical energy spectrum of Cd-foil-covered natural Cd sample irradiated with energetic neutrons [130].

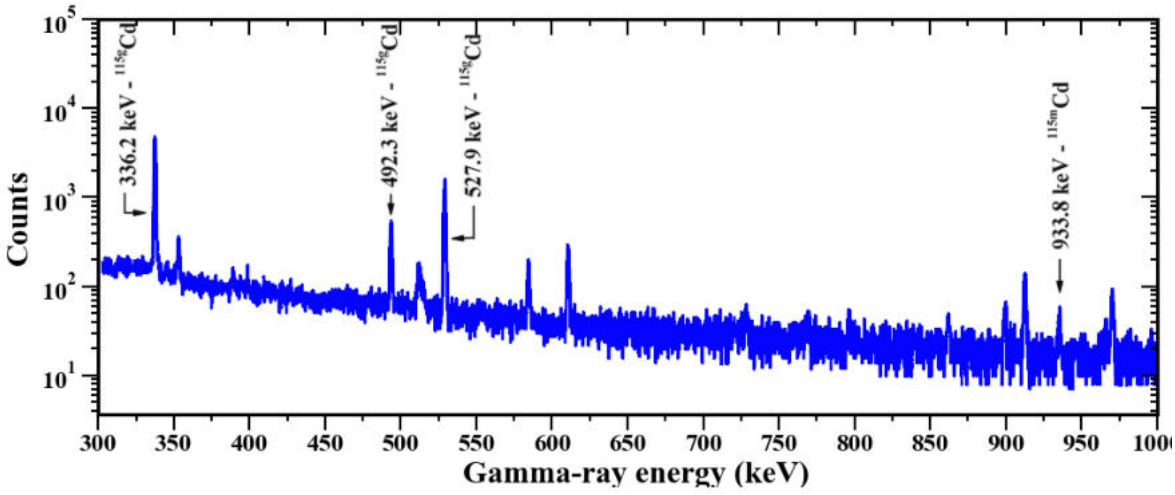

FIGURE 3.13: A typical energy spectrum of Cd-foil-uncovered natural Cd sample irradiated with energetic neutrons [130].

TABLE 3.14: A summary of self-absorption and summing coincidence correction factors for the γ-rays of interest of $^{115m,g;117m,g}$Cd [130].

Nuclear state	γ-ray energy, keV (Intensity, %)	Self-absorption factor F_g	Summing coincidence factor C_c
^{115g}Cd	336.2(45.9)	1.065	1.075
^{115g}Cd	492.3(8.03)	1.05	1.108
^{115g}Cd	527.9(27.45)	1.041	1.11
^{115m}Cd	933.7(2.0)	1.011	1
^{117m}Cd	564.4(14.7)	1.035	1.022
^{117m}Cd	1065.9(23.1)	1	1
^{117m}Cd	1432.9(13.4)	1	1.028
^{117g}Cd	273.3(28.0)	1.083	1.018
^{117g}Cd	344.4(17.8)	1.055	1
^{117g}Cd	1303.3(18.4)	1	1.062

the isomeric pair ^{115m,g}Cd produced in reactions $^{116}Cd(\gamma,n)^{115}Cd$, $^{116}Cd(n,2n)^{115}Cd$, $^{115}In(n,p)^{115m,g}Cd$ and $^{118}Sn(n,\alpha)^{115}Cd$ reactions [41, 181, 182, 183, 170] as well as the isomeric pair ^{117m,g}Cd produced in $^{120}Sn(n,\alpha)^{117}Cd$ reaction [184, 185] are also shown hereby for interpretation.

TABLE 3.15: A summary of IR results for ^{115m,g}Cd and ^{117m,g}Cd isomeric pairs produced in different types of nuclear reactions.

Nuclear Reaction and Product	Target Spin [$\hbar$]	Type of Projectile	Product Ex. Energy, MeV	Isomeric Ratio IR
$^{116}Cd(\gamma,n)^{115m,g}Cd$	0^+	24 MeV Bremsstrahlung	6	0.158 ± 0.016 [41]
$^{114}Cd(n,\gamma)^{115m,g}Cd$	0^+	Thermal neutron	6.1	0.116 ± 0.012 [This work] 0.120 ± 0.083 [180] (cal.) 0.094 ± 0.036 [177] (cal. TC) 0.085 ± 0.038 [177] (cal. GR) 0.088 ± 0.034 [177] (cal. IC) 0.080 ± 0.031 [177] (cal. R)
$^{114}Cd(n,\gamma)^{115m,g}Cd$	0^+	Resonant neutron	6.1	0.137 ± 0.014 [This work] 0.085 ± 0.035 [177] (cal. CL) 0.1 ± 0.051 [177] (cal. R/Cd)
$^{114}Cd(n,\gamma)^{115m,g}Cd$	0^+	Mixed Ther. and Res.	6.1	0.112 ± 0.011 [This work]
$^{116}Cd(n,2n)^{115m,g}Cd$	0^+	14.1 MeV neutron	5.4	0.921 ± 0.130 [181]
		14.4 MeV neutron	5.7	0.694 ± 0.074 [182]
		14.8 MeV neutron	6.1	0.710 ± 0.131 [183]
$^{115}In(n,p)^{115m,g}Cd$	$9/2^+$	14.9 MeV neutron	3.5	0.616 ± 0.118 [170]
$^{118}Sn(n,\alpha)^{115m,g}Cd$	0^+	14.9 MeV neutron	1.4	0.261 ± 0.090 [170]
$^{116}Cd(n,\gamma)^{117m,g}Cd$	0^+	Thermal neutron	5.8	0.209 ± 0.021 [This work] 0.54 ± 0.10 [178] 0.24 ± 0.03 [179] 0.192 ± 0.017 [177] (cal. TC) 0.173 ± 0.026 [177] (cal. GR) 0.223 ± 0.075 [177] (cal. IC) 0.192 ± 0.0177 [177] (cal. R)
$^{116}Cd(n,\gamma)^{117m,g}Cd$	0^+	Resonant neutron	5.8	0.324 ± 0.032 [This work] 0.282 ± 0.044 [177] (cal. CL) 0.288 ± 0.027 [177] (cal. R/Cd)
$^{116}Cd(n,\gamma)^{117m,g}Cd$	0^+	Mixed Ther. and Res.	5.8	0.237 ± 0.024 [This work]
$^{120}Sn(n,\alpha)^{117m,g}Cd$	0^+	14.0 MeV neutron	0.8	0.931 ± 0.137 [184] 1.015 ± 0.141 [185]

Table 3.16 details the sources of uncertainty contributing to the total uncertainty in IR determination, which was estimated to be approximately 10.0%.

Similarly to the previous Section 3.2.1, the excitation energy $E_{prod.ex}$ of the reaction product nuclei can be found as follows:

- For the $^{116}Cd(\gamma,n)^{115m,g}Cd$ reaction, of which IR data were taken from another experiment performed using the Microtron MT-25 accelerator [41], the $E_{prod.ex}$ is calculated using Eqs. 3.2 and 3.3, where the bremsstrahlung photon flux was calculated using the Geant4 [68] simulation performed in this work. Fig. 3.22

TABLE 3.16: A summary of the error sources considered in the IR calculations of $^{115m,g;117m,g}$Cd.

Random Errors	[%]	Systematic Errors	[%]
Counting statistical	0.5 - 2.0	Sample-detector distance	1
Detector efficiency	2	γ-ray selection	1
Half-life	0.4 - 1.5	e-beam variation	1
γ-ray intensity	0.2 - 2.0	Irradiation time	1.5
		Cooling time	1
Statistical errors	9.6	Systematic errors	2.5
Total error of the measured IR			10

shows the bremsstrahlung spectra calculated by Geant4 simulation for various endpoint energies.

- For isomeric pairs ^{115m,g}Cd and ^{117m,g}Cd formed in neutron capture reactions, $E_{prod.ex}$ are the binding energies of the neutron in the compound nuclei ^{115}Cd and ^{117}Cd respectively.

- The excitation energies of reactions $^{116}Cd(n,2n)^{115m,g}Cd$, $^{115}In(n,p)^{115m,g}Cd$ and $^{118}Sn(n,\alpha)^{115m,g}Cd$ and $^{120}Sn(n,\alpha)^{117m,g}Cd$ were calculated by a conventional method, in which the Coulomb potentials of proton and alpha were taken into account.

The available data in the literature related to IRs in Cd isotopes in neutron capture reactions are very limited, with only two publications for $^{114}Cd(n,\gamma)^{115m,g}Cd$ reaction [177, 180] and three works for $^{116}Cd(n,\gamma)^{117m,g}Cd$ reaction [178, 179, 180]. Among these available data in the literature and this work, there are essentially two methods to determine IR: (1) direct method using formula 2.18, (2) as the ratio of cross sections measured separately of the isomeric and ground states. Using the latter method, neutron capture cross sections of stable Cd isotopes have been measured by A. M. Gicking, K. Takahashi, and K. S. Krane [177] using a TRIGA reactor at Oregon State University. In that work, the samples were irradiated in five different facilities under various neutron flux characteristics: thermal column (TC), central core, outer core or G-ring (GR), cadmium-lined in-core irradiation site (IC) and fast pneumatic transfer system, and rabbit (R). Thermal neutron cross sections of the isomeric and ground states of both isomeric pairs ^{115m,g}Cd and ^{117m,g}Cd have been determined by these facilities and also their resonant integrals in the cadmium-lined in-core irradiation tube and rabbit. Using their cross-sectional data, in the present work IRs were

calculated to be of 0.094 ± 0. 036 and 0.192 ± 0.017 for isomeric pairs ^{115m,g}Cd and ^{117m,g}Cd produced in thermal neutron capture reactions, respectively, for irradiation in (TC); 0.085 ± 0.038 and 0.173 ± 0.026, respectively, for irradiation in (GR), 0.088 ± 0.034 and 0.223 ± 0.075, respectively, for irradiation in (IC); and 0.080 ± 0.031 and 0.192 ± 0.0177, respectively, for irradiation in (R). Similarly, the IRs for isomeric pairs ^{115m,g}Cd and ^{117m,g}Cd in the resonant neutron capture reactions have been calculated to be 0.085 ± 0.035 and 0.282 ± 0.044 for the irradiation in (CL); 0.1 ± 0.051 and 0.288 ± 0.027, respectively, for the irradiation in (R/Cd) facilities. It should be noted that in Table 3.15, the mark (cal. X) means the calculated value of IR obtained from the corresponding irradiation facility X (for example, fourth row 0.094 ± 0.036 [177] (cal. TC) means that the calculated IR is 0.094 ± 0.036 measured in the TC irradiation facility).

The thermal neutron capture cross section of ^{114}Cd leading to ^{115}Cd was obtained from the work of S. Pearlstein, R.F. Milligan [180] using gold as a standard in a cavity located in the thermal column of the Brookhaven National Laboratory Medical Reactor. The authors have determined that the cross sections of the isomeric and ground states of this isomeric pair are 0.036 ± 0.007 and 0.300 ± 0.150 barns, respectively. Then we calculated the IR to be 0.120 ± 0.083. In the D. Decat and P. Del Marmol work [178], the authors have measured the IR and independently the capture cross section for the ground state of ^{117}Cd produced in the thermal neutron capture reaction on the ^{116}Cd nucleus using the BR1 reactor at Mol. In that work, the IR was determined by the direct method and the obtained value of 0.54 ± 0.10 for the ^{117m,g}Cd isomeric pair. C. W. Tang, R. L. Eng, and C. D. Coreyell [179] also determined the IR of ^{117m,g}Cd by the direct method, using $^{116}Cd(n,\gamma)^{117}Cd$ reaction induced by thermal neutron at M. I. T reactor resulting in an IR of 0.24 ± 0.03.

The following comments can be made from the results obtained in Table 3.15:

- Compared with the data from A. Gicking et al. [177] and Pearlstein, R.F. Milligan [180] for $^{114}Cd(n,\gamma)^{115m,g}Cd$ reaction, the IR results obtained in this experiment are different. This may be due to the fact that the previous IRs were determined as the ratio of the values obtained separately from the cross sections, while in our case the IR was obtained consistently using formula 2.18. This makes our results more accurate, because the isomeric and ground states were simultaneously measured under identical experimental conditions. However, those authors used the Oregon State University TRIGA and Brookhaven National Laboratory

medical reactors as neutron sources, whereas in this work an accelerator-driven neutron source was used, where the neutron energy spectra are different. The significant difference between our result and the calculated value in Ref [177] for the case of the resonant neutron can be explained for the same reason.

- For the $^{116}Cd(n,\gamma)^{117m,g}Cd$ reaction, in general, a large discrepancy is also observed when comparing our results with the data from Refs. [178, 179], except when our results for the thermal and resonant neutrons are compared with the data from Ref. [177]. In Ref. [177], the Oregon State University TRIGA reactor as neutron source and a p-type GEM HP (Ge) crystal detector were used for the measurement of gamma spectra. In Ref. [178], the sample irradiation was performed at the BR1 reactor at Mol and measured with a 3×3 inches NaI(TI) crystal. The results in [179] were obtained at M. I. T. reactor and the gamma spectra were measured with the NaI(Tl) and small Ge(Li) detectors. Therefore, the discrepancy in the calculated IRs in this work and in Refs. [178, 179] may be explained by the difference in neutron spectra in various sources and also by the lower energy resolution of the γ-ray detector used in those works.

- Our results on IRs in both $^{114}Cd(n,\gamma)^{115}Cd$ and $^{116}Cd(n,\gamma)^{117}Cd$ reactions, induced by mixed thermal and resonant neutrons, can be considered as first measurements, as no existing data are found in the existing literature.

- It can be seen from Table 3.15 that the IRs in the capture reactions with thermal, resonant and mixed thermal-resonant neutrons are lower than those in the reactions $^{116}Cd(\gamma,n)^{115m,g}Cd$, $^{116}Cd(n,2n)^{115m,g}Cd$, $^{115}In(n,p)^{115m,g}Cd$ and $^{118}Sn(n,\alpha)^{115m,g}Cd$ reactions, which produce the same isomeric pair of the ^{115}Cd nucleus. This can be explained by the fact that the intake momentum of the target in the neutron capture reactions is lower than that in the (γ,n) reaction and the (n,p) and (n,α) reactions using 14 MeV neutrons. In detail, the intake momentum is $1/2\hbar$, $1\hbar$ and much higher than $1\hbar$ for the thermal resonant neutron capture reaction, the photonuclear reaction within the GDR region, and the 14 MeV neutron reaction, respectively. This results in a lower IR in the thermal and resonant neutron capture reactions compared with the IR of the two former reactions. It happens even when the excitation energies of the product in the

neutron capture reactions are equal to or higher than those in the other reactions (see 3.15). Similarly, the lower value of IR in $^{116}Cd(n,\gamma)^{117m,g}Cd$ reaction compared to that in $^{120}Sn(n,\alpha)^{117m,g}Cd$ can also be explained.

- The IR obtained in the present work for the neutron capture reaction with a thermal and resonant neutron could serve as a good test ground for further study using the Talys code. Note that this kind of reaction is a simple one-step reaction and is typical of the compound mechanism of nuclear reaction. It is well-known that the more simple processes involved in a reaction, the more definite information can be obtained. However, to verify a nuclear model, more measurements needed to be performed.

3.3 Influence of nuclear channel effect on IRs in (γ, n) and (n, γ) reactions

3.3.1 For ^{109m,g}Pd

Complementing the results in previous Section 3.2.1 for the IR of isomeric pair ^{109m,g}Pd produced in neutron capture reaction, this section presents experimental results on IR of the same isomeric pair produced in photonuclear and neutron capture reactions. Our purpose is to investigate the nuclear channel effect on this isomeric pair and further enrich the Nuclear database of IR for this nucleus.

In this experiment, the high purity PdO target described in Section 3.2.1 was used. This target was irradiated by the bremsstrahlung flux of 24 MeV end-point energy for 30 minutes. To avoid interference from (n,γ) capture reactions, caused by the neutron background from reactions on the accelerating structure or the breaking target itself, the sample was covered with a 2mm thick Cd foil. The sample was irradiated for 90 minutes with an electron beam with an average current of 15 μA. The irradiation time was optimized for γ-rays of interest emitted from ^{109m,g}Pd to ensure good statistics.

The simplified decay scheme of the isomeric pairs ^{109m,g}Pd is depicted in Fig. 3.8, which shows the γ-rays emitted from the deexcitation of the isomeric state, as well as the β-decay process of the ground state. The decay characteristics and γ-rays used for the IR calculation of isomeric pairs ^{109m,g}Pd are detailed in Table 3.9. We chose the γ-rays with the highest intensity, well separated in the γ-ray energy spectrum, and free

from contamination of the other reaction products, thus ensuring good photopeak area processing and counting statistics.

The offline γ-ray spectrum obtained after irradiation of the PdO target with 24 MeV bremsstrahlung is shown in Fig. 3.14. The irradiation time was 20 minutes, the cooling time was 40 minutes and the measurement time was 10 minutes at a distance of 5 cm from the detector. Characteristic γ rays from the isomeric and ground state of ^{109}Pd are clearly observed in the spectra.

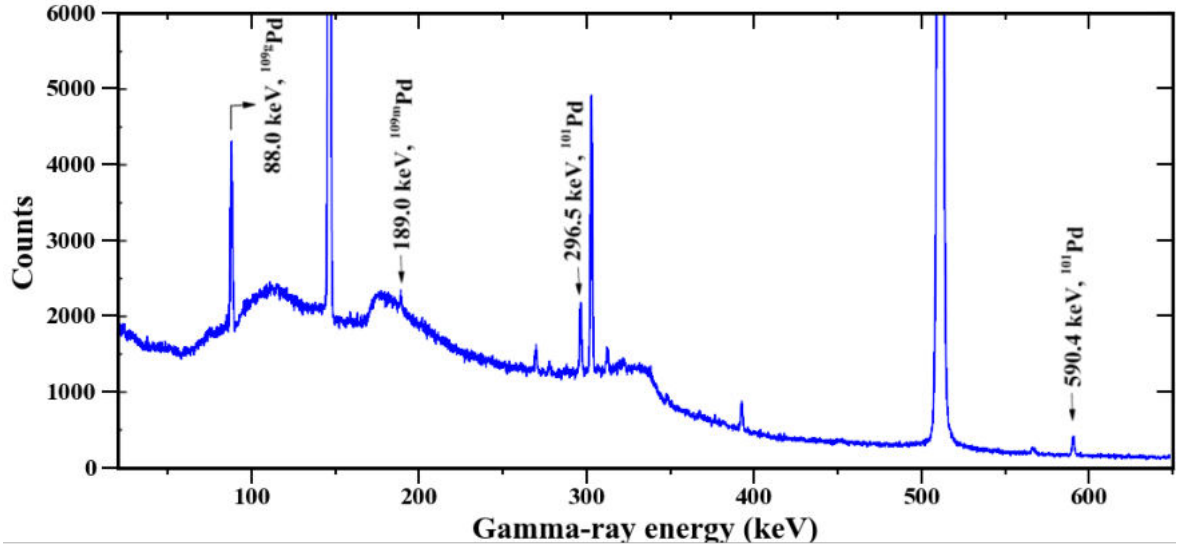

FIGURE 3.14: A γ-ray energy spectrum of the Pd sample irradiated with 24 MeV bremsstrahlung [131].

In the experiment using the photonuclear reaction, the correction factors for coincidence summing F_g were 1.26 and 1.05 for the case of 88.0 and 189.0 keV γ-rays, respectively, at the distance of 0 and 5 cm from the detector.

IRs were determined using the formula 2.18. In Table 3.17, the IRs from the photonuclear reaction $^{110}Pd(\gamma,n)^{109m,g}Pd$ are presented together with those from the neutron capture reaction $^{108}Pd(n,\gamma)^{109m,g}Pd$ taken from the previous Section 3.2.1. The corresponding reaction product excitation energies $E_{prod.ex}$ were also listed, in which $E_{prod.ex}$ for (γ,n) reaction is calculated using the formulas 3.2 and 3.3 described in Section 3.2.1. The IRs of ^{109m,g}Pd available in the literature for the reactions (γ,n), (n,γ) and $(n,2n)$ are also represented in Table 3.17.

The total uncertainty, comprising statistical errors, systematic errors from the distance from the detector to the sample, γ -ray selection, electron beam variation, irradiation time, and cooling time, were estimated to be about 10%.

From the results summarized in Table 3.17, the IR obtained in the present work for ^{110}Pd$(\gamma,$n$)$ is very in good agreement (within 1 σ) with previous work [61]. On

TABLE 3.17: The IRs of ^{109m,g}Pd in thermal, resonance and mixed thermal-resonant neutron capture reactions and in (γ, n) reaction.

Nuclear Reaction and Product	Type of Projectile	Product Ex. Energy, MeV	Isomeric Ratio IR
$^{108}Pd(n,\gamma)^{109m,g}Pd$	Thermal neutron	6.15	0.023 ± 0.002 [This work] 0.028 ± 0.005 [165] 0.018 ± 0.005 [166]
$^{108}Pd(n,\gamma)^{109m,g}Pd$	Resonant neutron	6.15	0.023 ± 0.002 [This work] 0.028 ± 0.005 [165]
$^{108}Pd(n,\gamma)^{109m,g}Pd$	Mixed Ther. and Res.	6.15	0.023 ± 0.002 [This work]
$^{110}Pd(\gamma,n)^{109m,g}Pd$	24 MeV Bremstrahlung	6.5	0.069 ± 0.007 [This work]
	25 MeV Bremsstrahlung	6.93	0.065 ± 0.003 [61]
$^{110}Pd(n,2n)^{109m,g}Pd$	14.1 MeV neutron	5.28	0.410 ± 0.039 [61] 0.41 ± 0.03 [169]

the other hand, the present IR result for the reaction (γ, n) is higher than that for the reaction (n, γ), although the product excitation energies in (γ, n) and (n, γ) are not significantly different. These IR results are also much lower compared to the IR of the same isomeric pair produced by the $(n, 2n)$ reaction with a comparable product excitation energy [61, 169]. This can be explained by the fact that the intake impulse in reaction (γ, n) is higher than in reaction (n, γ), while that in reaction $(n, 2n)$ is the highest among all reactions, causing the IR in reaction $(n, 2n)$ to exceed that in the (γ, n) and (n, γ) reactions. In addition, in the cases of (γ, n) and (n, γ) reactions, the angular momentum transfer to the target nuclei is lower, namely $L = 1$ and $1/2\hbar$, resulting in the compound nuclei with spins $J_c = J_0, J_0 \pm 1$ and $J_0, J_0 \pm 1/2$, respectively. This restricts the spin range of excited levels and makes the IR in those nuclei much lower than that of the other reaction. The intake impulse and angular momentum transfer affecting the IR are a part of the so-called channel effect in a nuclear reaction, where the IRs in different nuclear reactions are different and depend on the projectile type, intake impulse, excitation energy, spins of the isomeric and ground states as well as the nuclear reaction mechanisms.

3.3.2 For ^{115m,g}Cd

This subsection presents the results of the ^{115m,g}Cd in both the photonuclear reaction and the neutron-induced reaction. This investigation can be used to examine the role of the nuclear channel effect and can also provide nuclear data for the theoretical interpretation of nuclear reactions and for nuclear applications.

The isomeric pair ^{115m,g}Cd is formed through the $^{116}Cd(\gamma, n)^{115m,g}Cd$ photonuclear reaction and the $^{116}Cd(n, \gamma)^{115m,g}Cd$ neutron capture reaction, as mentioned in Section

3.2.2. The decay characteristics and the γ-rays emitted from the decay of ^{115m,g}Cd are listed in Table 3.13, in which the γ-rays used in the calculation of the isomeric ratio of the isomeric pair ^{115m,g}Cd are also presented.

In this photonuclear reaction experiment, a target sample made of natural cadmium was also used. The isotopic abundances of cadmium isotopes in this target are mentioned in Section 3.2.2. When irradiated by 24 MeV bremsstrahlung, characteristic γ-rays of the isomeric pair ^{115m,g}Cd as product $^{116}Cd(\gamma,n)^{115m,g}Cd$ photonuclear reaction are very clearly seen in Fig. 3.15. The other γ-rays that appeared in this spectrum come from different products of the interaction between the bremsstrahlung and the other Cd isotopes.

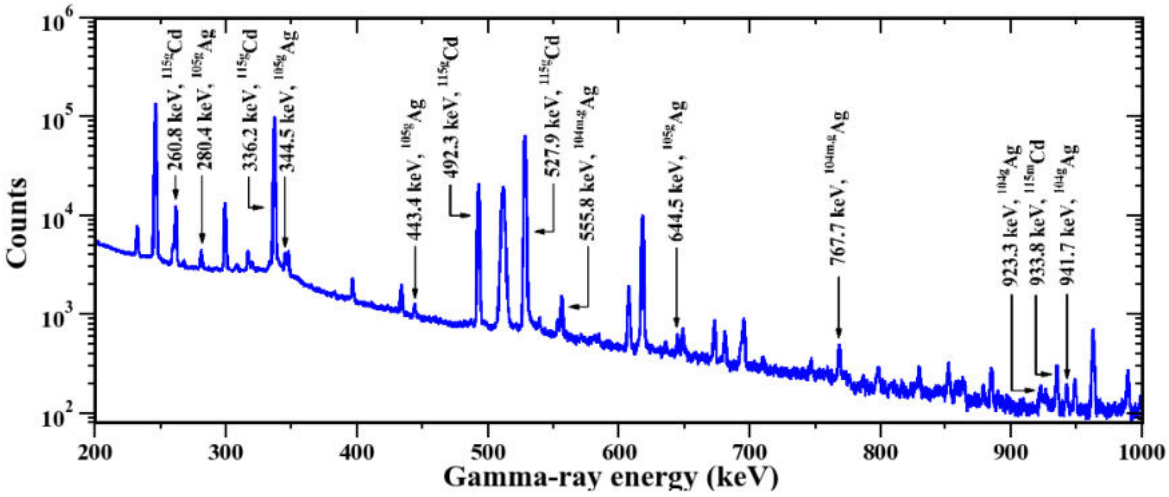

FIGURE 3.15: A γ-ray energy spectrum of the Cd sample irradiated with 24 MeV bremsstrahlung in 60 minutes, then 275.5 minutes of cooling and 20 minutes of measurements in a 5 cm position from the surface of the HPGe detector [132].

Figure 3.16 presents the simplified schemes of production of ^{115m,g}Cd from $^{114}Cd(n,\gamma)$, $^{116}Cd(\gamma,n)$, $^{116}Cd(n,2n)$, $^{115}In(n,p)$ and $^{118}Sn(n,\alpha)$ reactions. These reactions were studied and their corresponding characteristics are summarized in Table 3.18. In the case of the reaction (n,γ) on ^{114}Cd, the excitation energy of the product listed in Table 3.18 was calculated by using the formulas (3.2) and (3.3) mentioned in Section 3.2.1.

The IR value was calculated using the formula (2.18) for the γ-rays of interest from the decay of ^{115m,g}Cd, where the associated uncertainty sources were properly propagated to produce the final uncertainty of the IR. The obtained result for $^{116}Cd(\gamma,n)^{115m,g}Cd$ reaction is in 1σ agreement with the previous work in [41], where the same bremsstrahlung end-point energy was used.

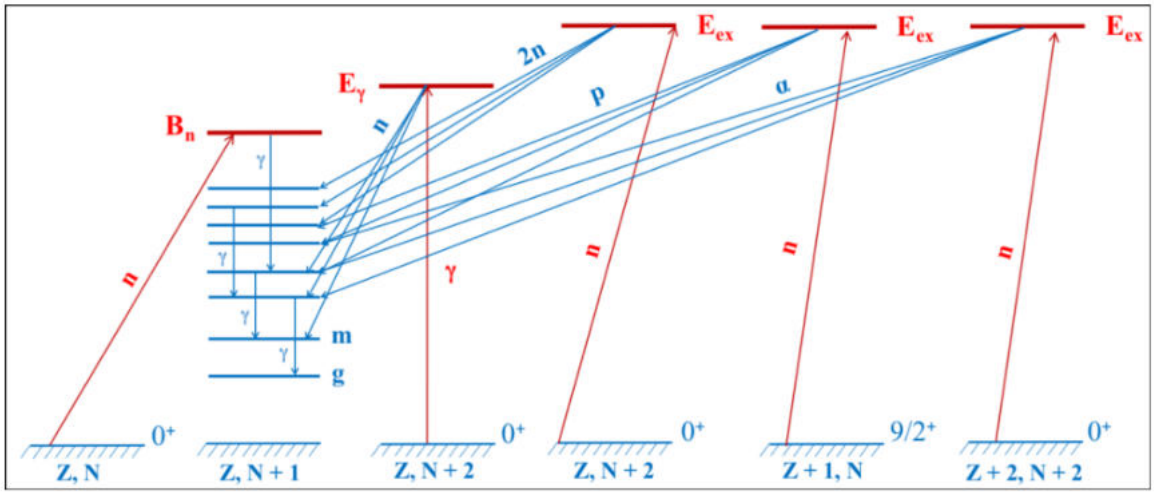

FIGURE 3.16: Simplified scheme of the production of ^{115m,g}Cd from (n,γ), (γ,n), $(n,2n)$, (n,p) and (n,α) reactions [132].

TABLE 3.18: The IRs of ^{115m,g}Cd produced in different nuclear reactions.

Nuclear Reaction and Product	Target Spin [$\hbar$]	Type of Projectile	Product Ex. Energy, MeV	Isomeric Ratio IR
$^{116}Cd(\gamma,n)^{115m,g}Cd$	0^+	24 MeV Bremsstrahlung	6	0.165 ± 0.016 [This work]
				0.158 ± 0.016 [41]
$^{114}Cd(n,\gamma)^{115m,g}Cd$	0^+	Thermal neutron	6.1	0.116 ± 0.012 [This work]
				0.120 ± 0.083 [180]
$^{114}Cd(n,\gamma)^{115m,g}Cd$	0^+	Epither. neutron	6.1	0.137 ± 0.014 [This work]
				0.085 ± 0.035 [177]
				0.1 ± 0.051 [177]
$^{114}Cd(n,\gamma)^{115m,g}Cd$	0^+	Mixed Ther. and Epither.	6.1	0.112 ± 0.011 [This work]
				0.080 ± 0.028 [177]
$^{116}Cd(n,2n)^{115m,g}Cd$	0^+	14.1 MeV neutron	5.4	0.921 ± 0.130 [181]
		14.4 MeV neutron	5.7	0.694 ± 0.074 [182]
		14.8 MeV neutron	6.1	0.710 ± 0.131 [183]
$^{115}In(n,p)^{115m,g}Cd$	$9/2^+$	14.9 MeV neutron	3.5	0.616 ± 0.118 [170]
$^{118}Sn(n,\alpha)^{115m,g}Cd$	0^+	14.9 MeV neutron	1.4	0.261 ± 0.090 [170]

In previous works listed in Table 3.18, the $^{116}Cd(n,2n)^{115m,g}Cd$, $^{115}In(n,p)^{115m,g}Cd$ and $^{118}Sn(n,\alpha)^{115m,g}Cd$ reactions were studied by fast neutrons of nearly the same energy. Therefore, the momentum transferred to the target nuclei is nearly the same. However, the IRs of the isomeric pairs obtained in the three reactions are different, with the highest value in $^{116}Cd(n,2n)^{115m,g}Cd$ and the lowest value in $^{118}Sn(n,\alpha)^{115m,g}Cd$. The difference in the product excitation energies could be an explanation for this interesting feature. According to Table 3.18, the excitation energy of the reaction product is highest in the $^{116}Cd(n,2n)^{115m,g}Cd$ reaction and lower in the reactions $^{115}In(n,p)^{115m,g}Cd$ and $^{118}Sn(n,\alpha)^{115m,g}Cd$ reactions due to the Coulomb barrier of the proton and the α particles. As a result, the probability to excite high-spin states becomes lower, and therefore the IR becomes lower. On the other hand, it is worth noting that in (γ,n), $(n,2n)$, (n,p) and (n,α) reactions, especially for nuclear reactions with the emission of charged particles, direct and pre-equilibrium processes play important roles in suppressing the formation of high-spin states.

In addition to the difference in product excitation energy, the IRs of the isomeric pair ^{115m,g}Cd created in different nuclear reactions are, in principle, different. This effect is called the nuclear channel effect on the IR, which may result in the various IR values of the identical isomeric pair produced from the different reactions. The channeling effect on IR can also be found in the cases of isomeric pairs $^{135m,g}Xe$ populated in reactions $^{134}Xe(n,\gamma)$, $^{136}Xe(\gamma,n)$, $^{136}Xe(n,2n)$ reactions and in the photofission of ^{232}Th, ^{233}U and ^{237}Np [147]; isomeric pair $^{58m,g}Co$ in reactions $^{58}Fe(p,n)$, $^{nat}Fe(d,xn)$, $^{55}Mn(\alpha,n)$ and $^{59}Co(n,2n)$ reactions with projectile energies of the threshold to 14.12 MeV, 12.97 MeV, 25.52 MeV and 13 MeV, respectively [27]; isomeric pair ^{75m,g}Ge through $(n,2n)$, (n,p) and (n,α) reactions measured over 13.73 MeV to 14.77 MeV [163]; isomeric pair ^{87m,g}Y produced from reactions $^{93}Nb(\gamma,\alpha 2n)$ and $^{nat}Zr(\gamma,pxn)$ reactions with the bremsstrahlung end point energy of 45 - 70 MeV [148], and ^{137m,g}Ce produced in the photoneutron reaction $^{138}Ce(\gamma,n)$, neutron capture reaction $^{136}Ce(n,\gamma)$ and two simultaneous reactions in the mixed photon–neutron field [144].

3.4 IRs of ^{137m,g}Ce, ^{115m,g}Cd, ^{109m,g}Pd, and ^{81m,g}Se in inverse reactions

Inverse nuclear reactions, when a projectile from one reaction is the ejectile from another reaction, have been subject to many experimental and theoretical studies since the 1960s [186]. Inverse reactions, including photonuclear and thermal neutron capture reactions, play an important role in astrophysics and the study of nuclear structure and nuclear reaction mechanisms [187, 188].

In this work, the IRs of ^{137m,g}Ce, ^{115m,g}Cd, ^{109m,g}Pd, and ^{81m,g}Se produced in inverse reactions (γ, n) and (n, γ) by the activation method, namely ^{138}Ce$(\gamma, \mathrm{n})^{137m,g}$Ce, ^{136}Ce$(\mathrm{n}, \gamma)^{137m,g}$Ce, ^{116}Cd$(\gamma, \mathrm{n})^{115m,g}$Cd, ^{114}Cd$(\mathrm{n}, \gamma)^{115m,g}$Cd, ^{110}Pd$(\gamma, \mathrm{n})^{109m,g}$Pd , ^{108}Pd$(\mathrm{n}, \gamma)^{109m,g}$Pd, ^{82}Se$(\gamma, \mathrm{n})^{81m,g}$Se and ^{80}Se$(\mathrm{n}, \gamma)^{81m,g}$Se were investigated.

The offline γ-rays spectra following the irradiation of Ce, Cd, Pd and Se targets with 25 MeV bremsstrahlung and thermal neutrons are shown in Figs. 3.17 - 3.21. The characteristic γ-rays from ^{137m,g}Ce, ^{115m,g}Cd, ^{109m,g}Pd, and ^{81m,g}Se are clearly observed in the spectra.

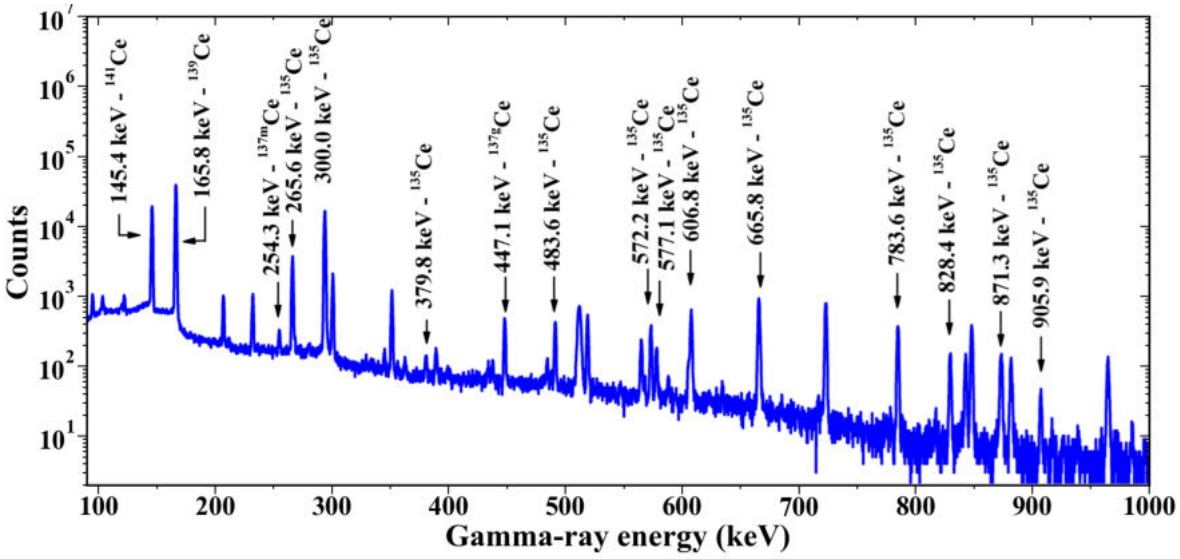

FIGURE 3.17: A typical γ-ray energy spectrum of a Ce sample irradiated with 25 MeV bremsstrahlung in 60 minutes, waited for 60 minutes and then measured for 20 minutes at 5 cm from the surface of the HPGe detector [134].

The selected γ-rays and spectroscopic characteristic data [138] used for the IR calculation were determined and shown in Table 3.19. The losses of the interested γ-ray counts due to the self-absorption and summing coincidence effects, which contributed to the IR determination error, were corrected by Eqs. 2.20 and 2.21.

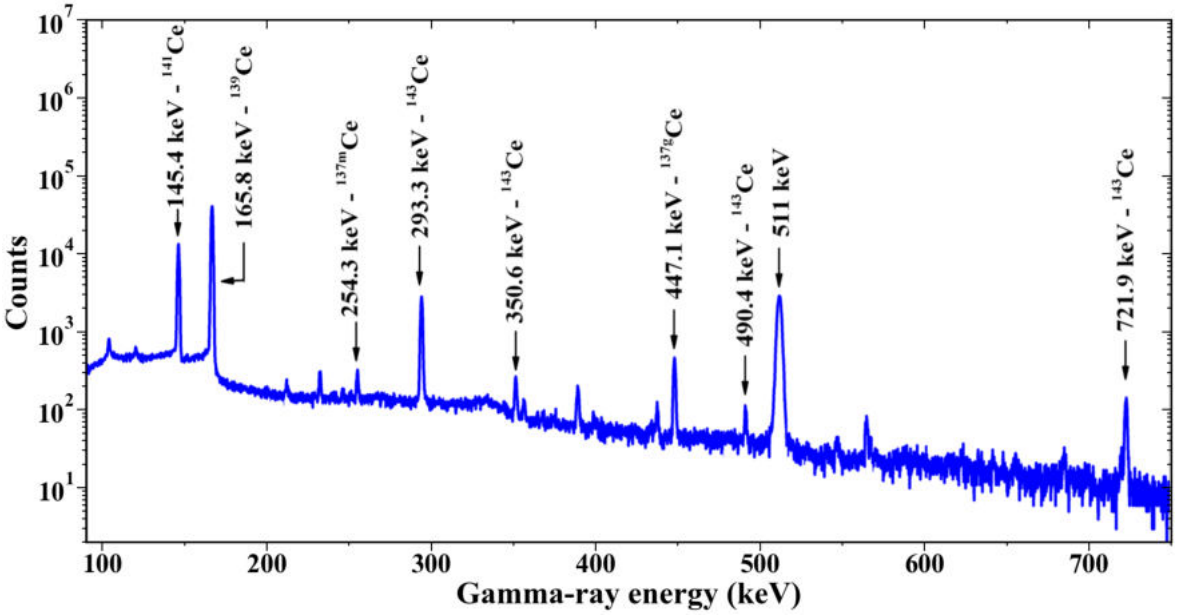

FIGURE 3.18: A γ-rays energy spectrum from the Ce sample. The sample was irradiated with energetic neutrons for 90 minutes, followed by a cooling time of 35 minutes and then measured for 60 minutes at a position of 0 cm from the HPGe detector [134].

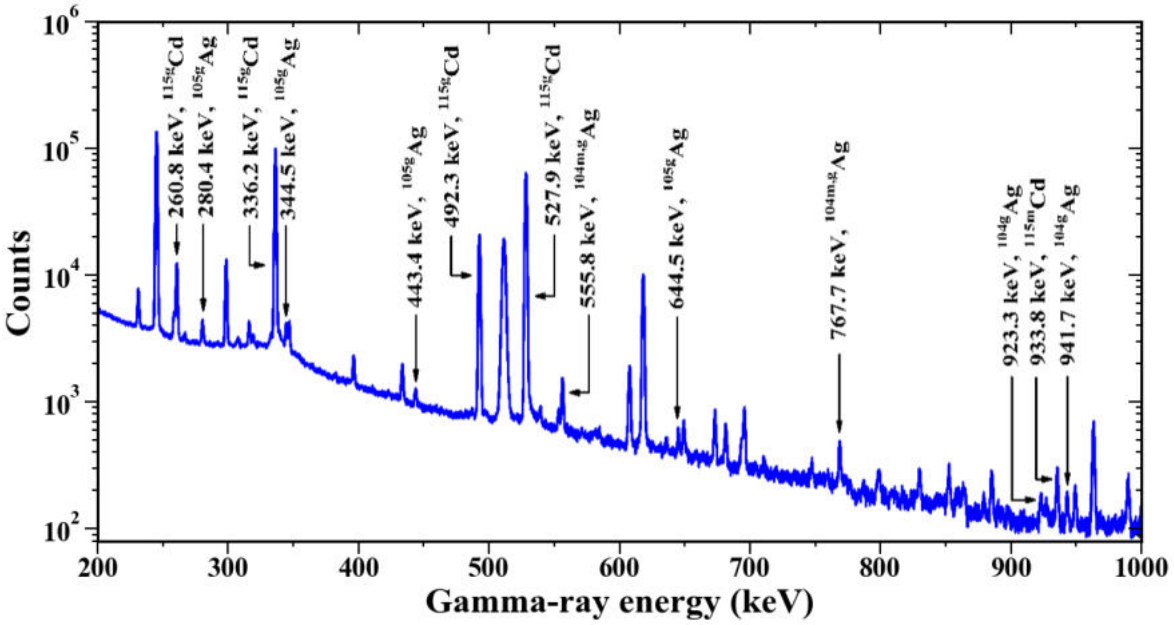

FIGURE 3.19: A γ-ray energy spectrum of the Cd sample was measured for 275.5 minutes at a distance of 5 cm from the HPGe detector. The sample was irradiated by 25 MeV bremsstrahlung for 60 minutes, followed by a cooling time of 20 minutes [134].

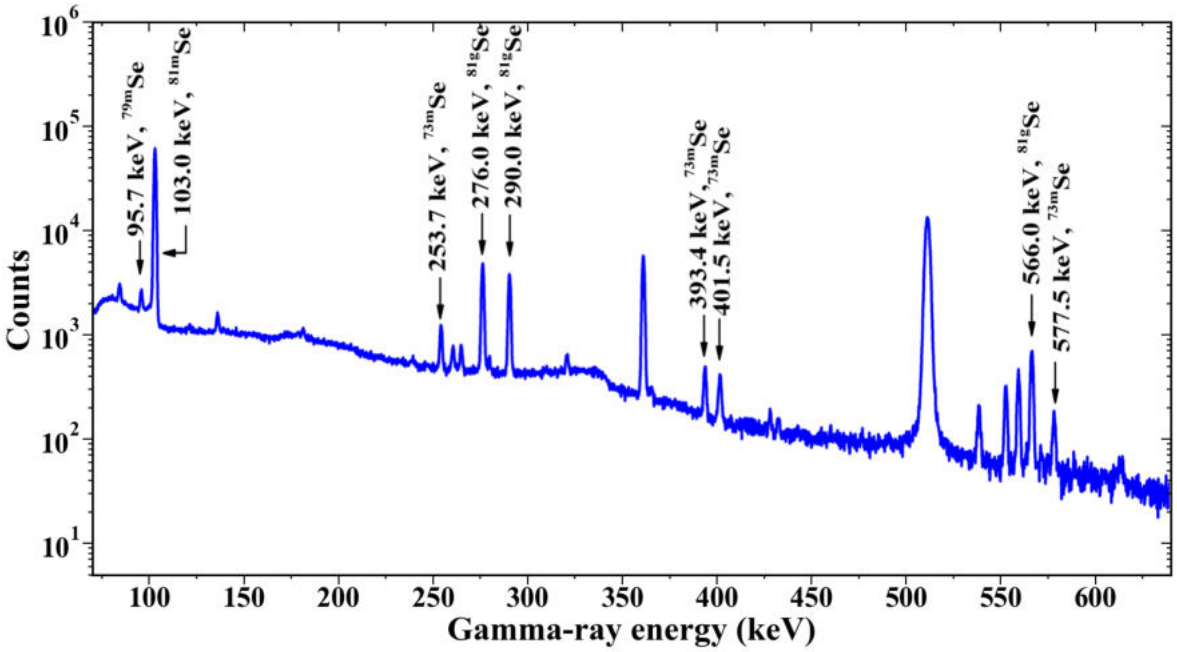

FIGURE 3.20: A γ-rays energy spectrum of the Se sample measured for 10 minutes on the surface of the HPGe detector. The sample was irradiated with 25 MeV bremsstrahlung for 20 minutes, followed by a cooling time of 60 minutes [134].

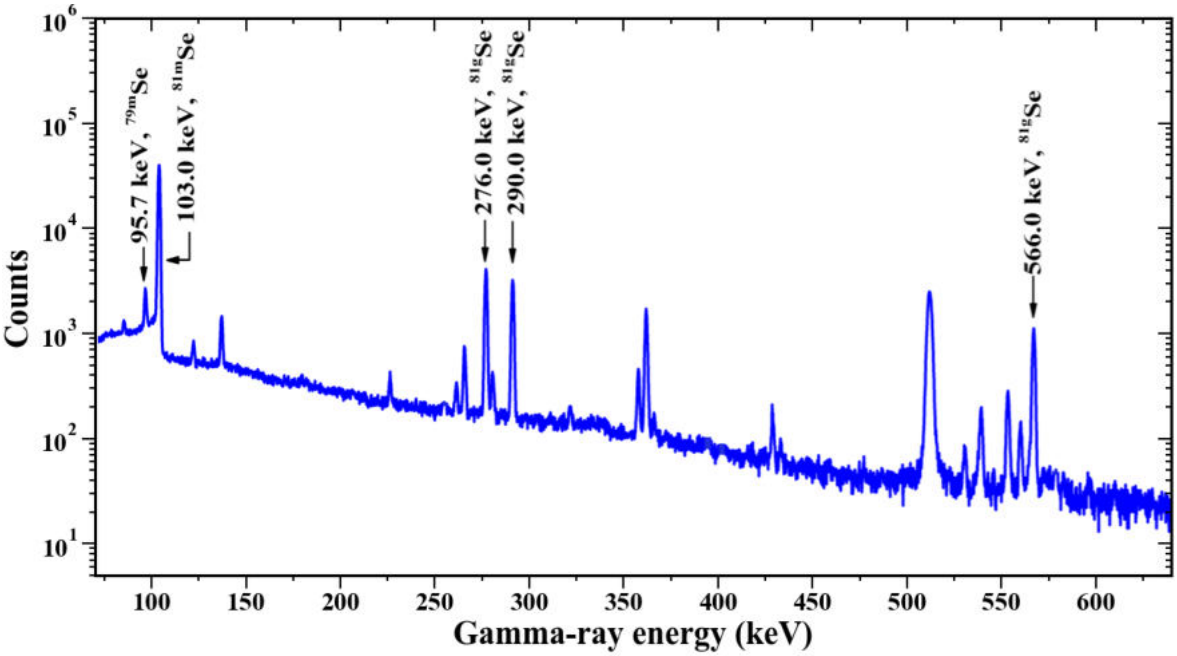

FIGURE 3.21: A γ-rays energy spectrum of the Se sample measured for 10 minutes on the surface of the HPGe detector. The sample was irradiated by neutrons for 90 minutes, followed by a cooling time of 25 minutes [134].

TABLE 3.19: Selected gamma rays and spectroscopic characteristic data [138].

Nuclear Reaction	Target Spin, Parity, [J^{π}]	Nuclear state	Spin Parity [J^{π}]	Decay Mode [%]	Half Life	γ-ray Energy [keV]	Intensity [%]
$^{138}Ce(\gamma,n)^{137}Ce$	0^+	^{137m}Ce	11/2-	IT: 99.2	34.4 h	254.3	99.2
$^{136}Ce(n,\gamma)^{137}Ce$				EC: 0.78			
$^{138}Ce(\gamma,n)^{137}Ce$	0^+	^{137g}Ce	3/2+	EC: 100	9.0 h	447.1	1.8
$^{136}Ce(n,\gamma)^{137}Ce$							
$^{116}Cd(\gamma,n)^{115}Cd$	0^+	^{115m}Cd	11/2-	β^- : 100	44.6 d	933.8	2
$^{114}Cd(n,\gamma)^{115}Cd$							
$^{116}Cd(\gamma,n)^{115}Cd$	0^+	^{115g}Cd	1/2+	β^- : 100	2.23 d	336.2	45.9
$^{114}Cd(n,\gamma)^{115}Cd$						527.9	27.45
$^{110}Pd(\gamma,n)^{109}Pd$	0^+	^{109m}Pd	11/2-	IT: 100	4.69 m	189	55.9
$^{108}Pd(n,\gamma)^{109}Pd$							
$^{110}Pd(\gamma,n)^{109}Pd$	0^+	^{109g}Pd	5/2+	β^- : 100	13.7 h	88.04	3.6
$^{108}Pd(n,\gamma)^{109}Pd$							
$^{82}Se(\gamma,n)^{81}Se$	0^+	^{81m}Se	7/2+	IT: 99.95	57.28 m	103	13
$^{82}Se(n,\gamma)^{81}Se$				β^- : 0.05			
$^{82}Se(\gamma,n)^{81}Se$	0^+	^{81g}Se	1/2-	β^- : 100	18.45 m	276	0.7
$^{80}Se(n,\gamma)^{81}Se$						290	0.55

Table 3.20 presents the experimental results of this work together with the existing data, which were taken from Refs. [165, 144, 61, 54, 191, 192, 193, 177, 166, 189, 190]. The product excitation energies for the reaction (γ, n) were calculated using Eqs. (3.2) and (3.3), while those for the (n, γ) capture reaction induced by the thermal neutron are equal to the binding energy of the neutron in the compound nuclei formed in this reaction. The error of the IRs came from two sources. The first included uncertainties related to the IR calculations using formula (2.18) and the second was associated with systematic uncertainties. The total error in the IR determination was estimated to be approximately 10.0%.

From the experimental results obtained in the present work (summarized in Table 3.20), it can be seen that the IRs in inverse (γ, n) and (n, γ) reactions, which lead to the same isomeric pairs ^{137m,g}Ce, ^{115m,g}Cd, ^{109m,g}Pd, and ^{81m,g}Se are different due to the effect of the reaction channel. The IRs in the reactions (γ, n) are significantly higher than in the reactions (n, γ). This trend can be explained by the intake impulse and angular momentum of the projectiles transferred to the target nuclei; that is, the higher the intake angular momentum and impulse, the higher the IR. For the reactions (γ, n), the IRs of this work and those of [54, 61, 193, 189] within the error limit are in good agreement. Similarly, for the reactions (n, γ), our result and the data from the references agree except for ^{81m,g}Se, which agrees with Refs.[165, 190] and is considerably less than that of Ref. [192].

TABLE 3.20: The IRs of the studied inverse reactions.

Nuclear Reaction and Product	Type of Projectile	Product Ex. Energy [MeV]	Isomeric Ratio IR
$^{138}Ce(\gamma,n)^{137m,g}Ce$	25 MeV Bremsstrahlung	5.5	0.221 ± 0.022 [This work] 0.19 ± 0.02 [54]
$^{136}Ce(n,\gamma)^{137m,g}Ce$	Thermal neutron	7.4	0.112 ± 0.011 [This work] 0.109 ± 0.01 [144] 0.15 ± 0.01 [191] 0.088 ± 0.006 [192]
$^{116}Cd(\gamma,n)^{115m,g}Cd$	25 MeV Bremsstrahlung	5.8	0.165 ± 0.016 [This work] 0.168 ± 0.02 [193]
$^{114}Cd(n,\gamma)^{115m,g}Cd$	Thermal neutron	6.1	0.116 ± 0.012 [This work] 0.099 ± 0.0033 [177]
$^{110}Pd(\gamma,n)^{109m,g}Pd$	25 MeV Bremsstrahlung	6.3	0.069 ± 0.007 [This work] 0.065 ± 0.003 [61]
$^{108}Pd(n,\gamma)^{109m,g}Pd$	Thermal neutron	6.1	0.023 ± 0.002 [This work] 0.018 ± 0.005 [166], 0.028 ± 0.005 [165]
$^{82}Se(\gamma,n)^{81m,g}Se$	25 MeV Bremsstrahlung	6.9	0.556 ± 0.055 [This work] 0.56 ± 0.02 [189]
$^{80}Se(n,\gamma)^{81m,g}Se$	Thermal neutron	6.7	0.114 ± 0.014 [This work] 0.204 ± 0.024 [191] 0.136 ± 0.011 [165] 0.096 ± 0.009 [190]

3.5 Theoretically calculated IRs in (γ, n) reactions

In this work, the IRs of isomeric pairs produced in reactions (γ, n) on Se, Pd, Ce, Eu and Hg targets induced by bremsstrahlung with an endpoint energy range of 10 to 25 MeV were theoretically calculated using the formula (1.9). In which the flux distribution as a function of the endpoint energy of the bremsstrahlung $\phi(E)$ was obtained using the GEANT4 simulation toolkit [68]. This distribution was then combined with the theoretical cross-section data $\sigma_m(E)$ and $\sigma_g(E)$ calculated using the TALYS 1.95 code to obtain the theoretical IRs.

3.5.1 Bremsstrahlung spectra simulation

To simulate the experimental condition as closely as possible, including the geometry and materials of the setup, the primary electron beam, and all possible interactions and radiations were described by using the GEANT4 toolkit leading to a realistic description of the flux distribution. Bremsstrahlung spectra were calculated for endpoint energies of 10 to 25 MeV with a step of 1 MeV using the Geant4.10.06 version as in Fig. 3.22.

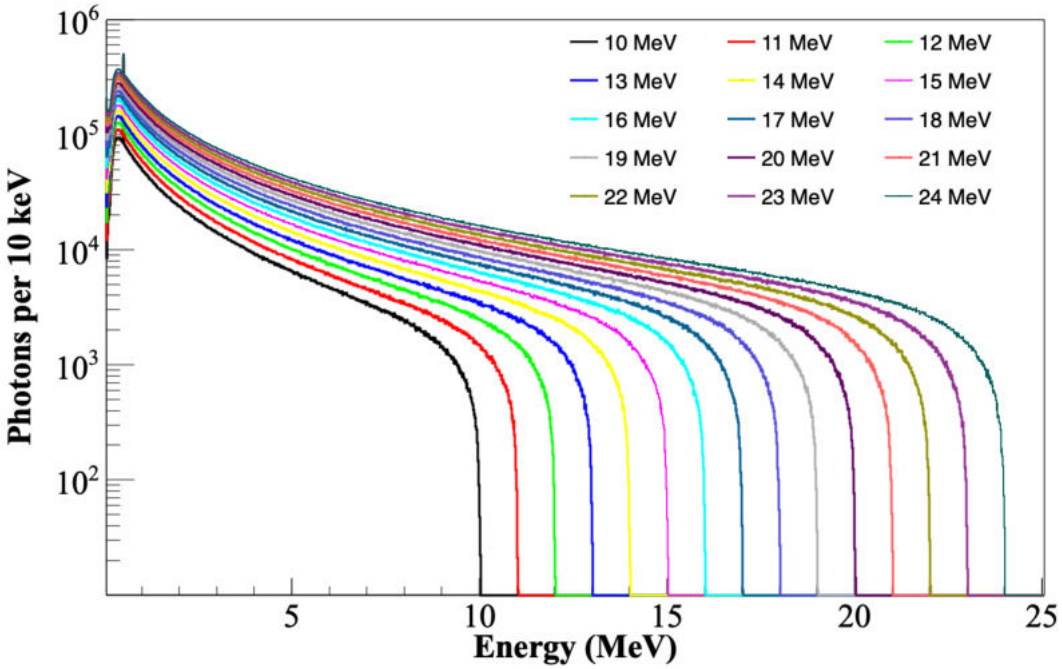

FIGURE 3.22: Bremsstrahlung energy spectra calculated by the GEANT4 toolkit with 500 millions primary particles.

3.5.2 Cross-section calculation

The cross sections of the reaction (γ, n) on Pd, Se, Ce, Eu, and Hg targets irradiated by photons with energies from the reaction threshold to 25 MeV are predicted by the Talys 1.95 code. To investigate the IRs in various level density models, we changed six level density models. For each level density model, we employed eight γSFs one by one to obtain the differential cross sections of isomers. The six-level density models and eight γSF are described in Subsection 2.2.2. A total of 48 computations were performed for each target. All possible reaction channels that lead to the same reaction product are included throughout the calculation. Figs. 3.23 to 3.27 show the total cross sections of the population of ^{109}Pd, ^{73,81}Se, ^{137,139}Ce, ^{150,152}Eu and ^{195,197}Hg from reactions (γ, n) using **ldmodel 1** (Ld1) and **Strength 2** (s2). In these figures, the contribution of the direct, pre-equilibrium, and compound reaction processes is also illustrated. For all calculated reactions, the dominant contribution was due to the compound process, whereas the contribution of pre-equilibrium was insignificant and the direct process did not occur. The compound reactions occurred in the whole energy range from the reaction threshold to 25 MeV, while the pre-equilibrium reactions started taking place from 15, 20.3, 16, 17.3, 16.7, 14.4, 14.9, 15.8 and 15.3 for ^{110}Pd, ^{74}Se, ^{82}Se, ^{138}Ce, ^{140}Ce, ^{151}Eu, ^{153}Eu, ^{196}Hg and ^{198}Hg nuclei, respectively. For ^{110}Pd, the contributions

of the preequilibrium and compound mechanisms are 10.1% and 89.9%, respectively. In the case of ^{74,82}Se, those are 3.59%, 96.4% and 9.89%, 90.1%, respectively. For ^{138,140}Ce, these are 2.41%, 97.6% and 2.88%, 97.1%, respectively. For ^{151,153}Eu, those are 8.81%, 91.2% and 6.5%, 93.5%, respectively. For ^{196,198}Hg, those are 2.0%, 98.0% and 2.45%, 97.5%, respectively.

Figs. 3.24 to 3.26 also exhibit the cross sections of the literature listed in the Experimental Nuclear Reaction Data Library (EXFOR) database [194] for ^{74}Se, ^{140}Ce, ^{151}Eu, and ^{153}Eu, where good agreement is observed between the experimental data evaluated and the calculated results based on TALYS.

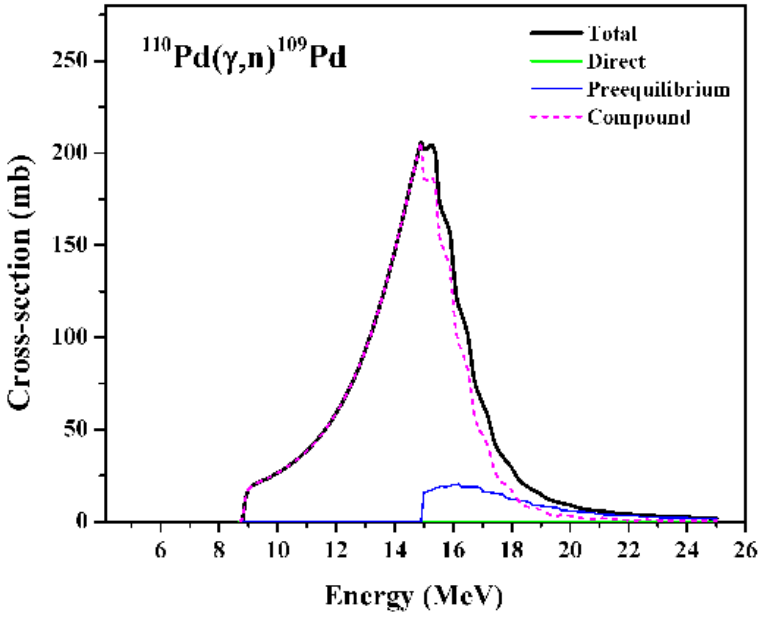

FIGURE 3.23: (γ, n) reaction cross-section for ^{110}Pd calculated by TALYS 1.95.

Furthermore, differential cross sections for the formation of isomeric pairs $^{73m,g;81m,g}$Se, ^{109m,g}Pd, $^{137m,g;139m,g}$Ce, $^{150m,g;152m1,g;152m2,g;152m1,m2}$Eu, and $^{195m,g;197m,g}$Hg were also computed. Figure 3.28 shows the calculated cross sections for the formation of the isomeric and ground states of the ^{152}Eu nucleus. It can be seen that the probability of forming ^{152m1}Eu with high spin (8^-) is much lower than ^{152m2}Eu and ^{152g}Eu with lower spin (0^-) and (3^-), respectively.

In addition to the cross sections, the properties of the target nuclei such as mass, energy levels, spin, parity, and deformation were revealed in the nuclear structure database of the TALYS code, originating from the Reference Input Parameter Library

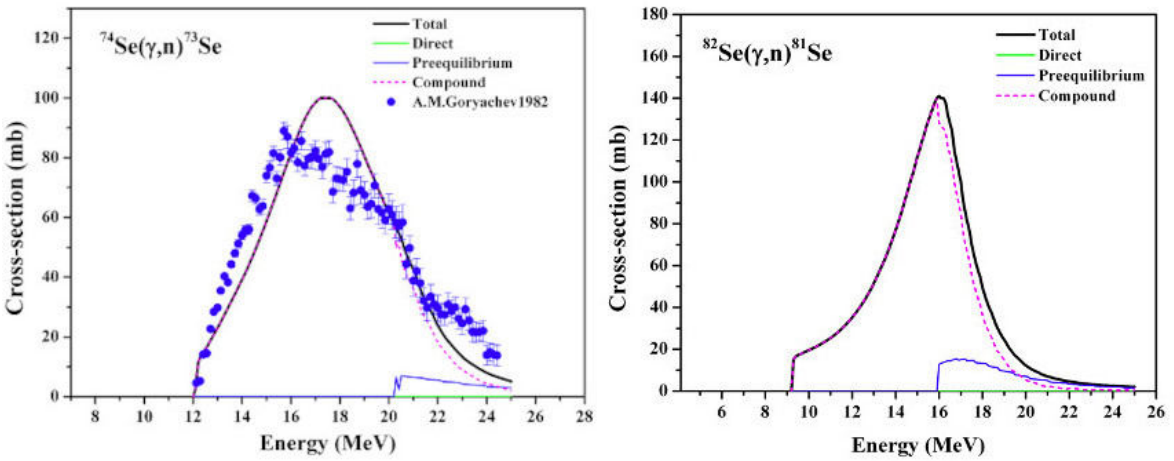

FIGURE 3.24: (γ, n) cross-section of ^{74,82}Se calculated by TALYS 1.95 and compared with experimental values [195].

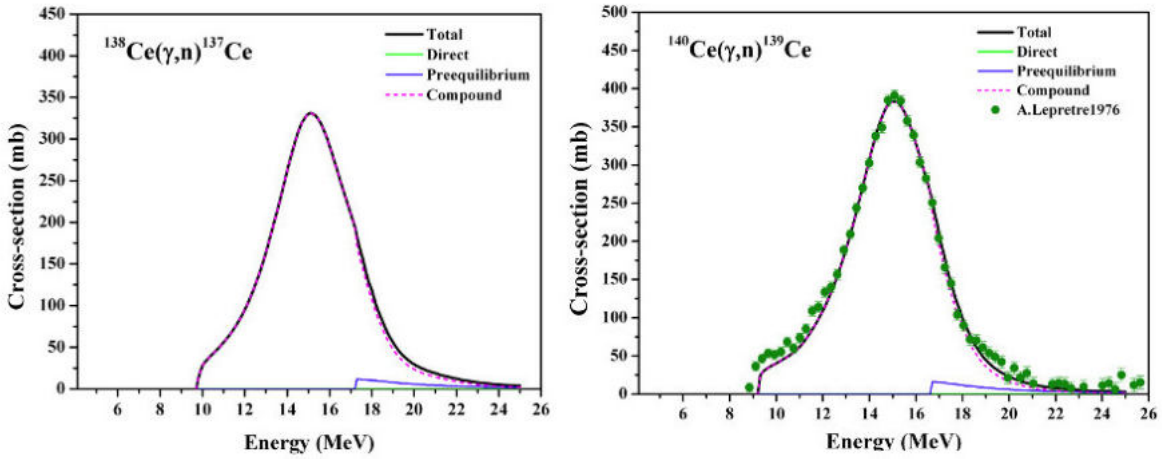

FIGURE 3.25: (γ, n) cross-section for ^{138,140}Ce calculated by TALYS 1.95 and compared with experimental values [196].

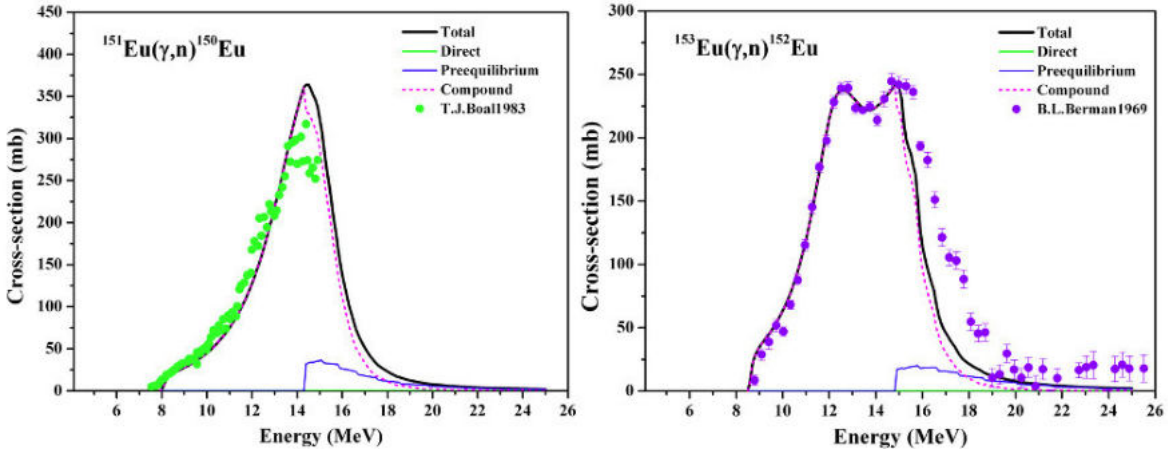

FIGURE 3.26: (γ, n) reaction cross-section for ^{151,153}Eu calculated by TALYS 1.95 compared to experimental values [197, 198].

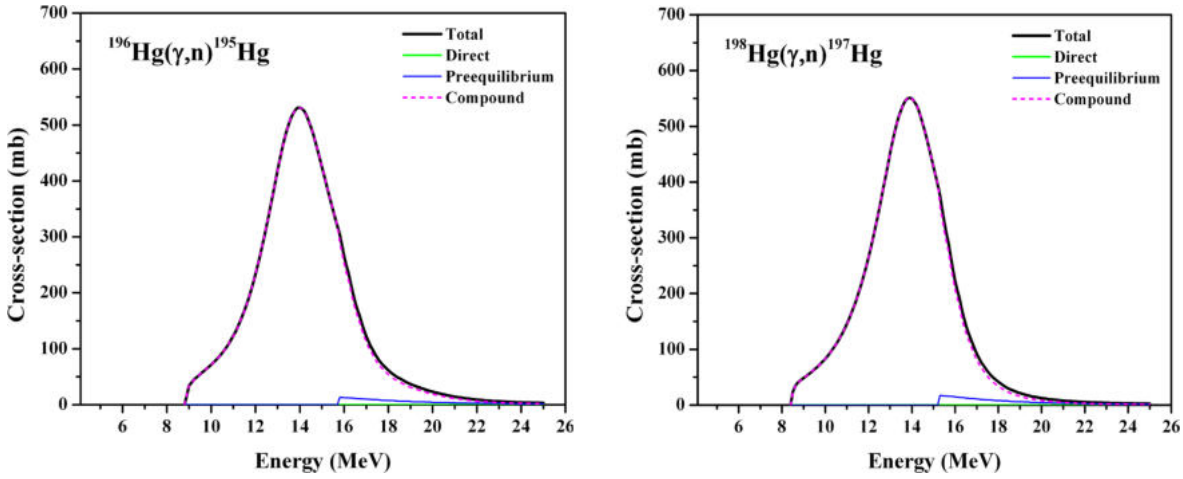

FIGURE 3.27: (γ, n) reaction cross-section for ^{195,197}Hg calculated by TALYS 1.95.

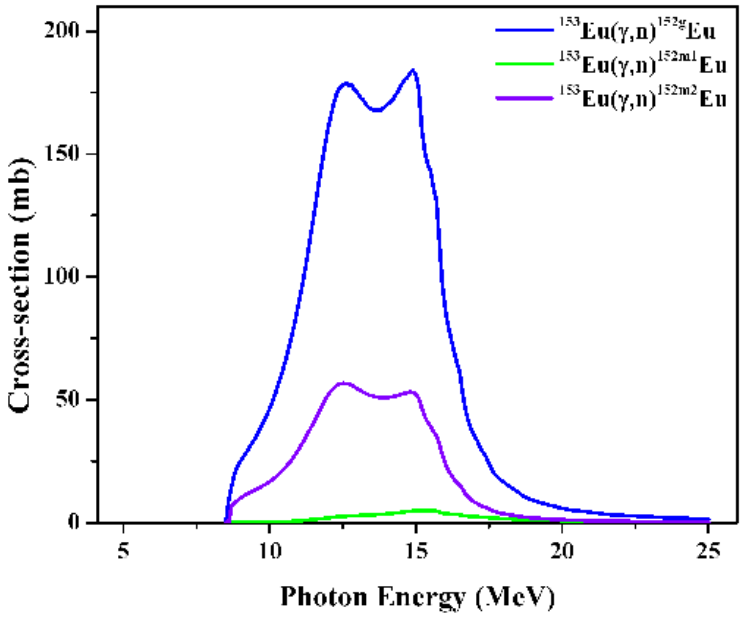

FIGURE 3.28: Calculated cross sections of isomeric and ground state formation in the ^{153}Eu$(\gamma, \mathrm{n})^{152}$Eu reaction.

(RIPL). The database indicated that ^{138,140}Ce and ^{196,198}Hg are the spherical even-even nuclei, and ^{74,82}Se and ^{110}Pd are vibrational even-even nuclei, and ^{151,153}Eu is a rotationally deformed odd-even nucleus characterized by the rotational bands.

3.5.3 IRs in (γ, n) reactions

The IRs following by formula (1.9) resulted from the combination of differential cross sections and bremsstrahlung spectra demonstrated in Fig. 3.22. The calculated results executed with six various level density models in combination with eight different gamma strength functions differed considerably. Through comparison between the experimental outcomes and theoretically calculated data, it can ascertain which model best fits the experimental results. Basic information related to nuclear structure, level populations, optical model parameters, transmission coefficients, reaction cross sections, gamma strength functions, discrete levels, and level densities can be extracted.

The calculated IRs for $^{73m,g;81m,g}$Se, ^{109m,g}Pd, $^{137m,g;139m,g}$Ce, $^{150m,g;152m1,g;152m2,g;152m1,m2}$Eu, and $^{195m,g;197m,g}$Hg are shown in Figs. 3.29 to 3.39. From these results, it is worth making the following remarks:

General trend of the IR dependence on the energy

It is seen that all figures in this subsection have a general trend of the IR dependence on bremsstrahlung end-point energies of 10 to 25 MeV in both theoretical and experimental data. The IRs for $^{73m,g;81m,g}$Se, ^{109m,g}Pd, $^{137m,g;139m,g}$Ce, $^{152m1,g;152m1,m2}$Eu, and $^{195m,g;197m,g}$Hg grow with increasing energy and the IRs for ^{150m,g}Eu and ^{152m2,g}Eu decreases with increasing energy. Note that if the IR of all cases is calculated by the yield ratios of the high-spin state and the low-spin state, the IR will rise along with the energy. In detail, the IRs rapidly increase from the reaction energy threshold to the GDR peak energy, then increase slightly or reach a plateau. This fact is reasonable since in the low-energy region the increase in the angular momentum transferred to the compound nucleus caused the growth of IR along with the excitation energy. This ratio enhances moderately in the higher-energy region possibly because of the contribution of the direct- and pre-equilibrium reaction mechanism.

IRs in (γ, n) reactions on isotopes

a. For Se isotopes

The IRs of ^{73m,g}Se calculated by the TALYS 1.95 code predict well the experimental datum of M. G. Davidov [199] but greatly underestimates that of T. D. Thiep [35] and V. M. Mazur [200]. Meanwhile, for ^{81m,g}Se in Fig. 3.30, the calculated IRs describe

well the experimental data taken from refs. [35, 200] and B. M. Hue [133]. It should be noted that the best agreement between the experimental and theoretically calculated data for ^{81m,g}Se is Ld1-model with s5-γSF (Ld1+s5), Ld2+s6, Ld4+s7, Ld5+s2, and Ld6 with s6-γSFs.

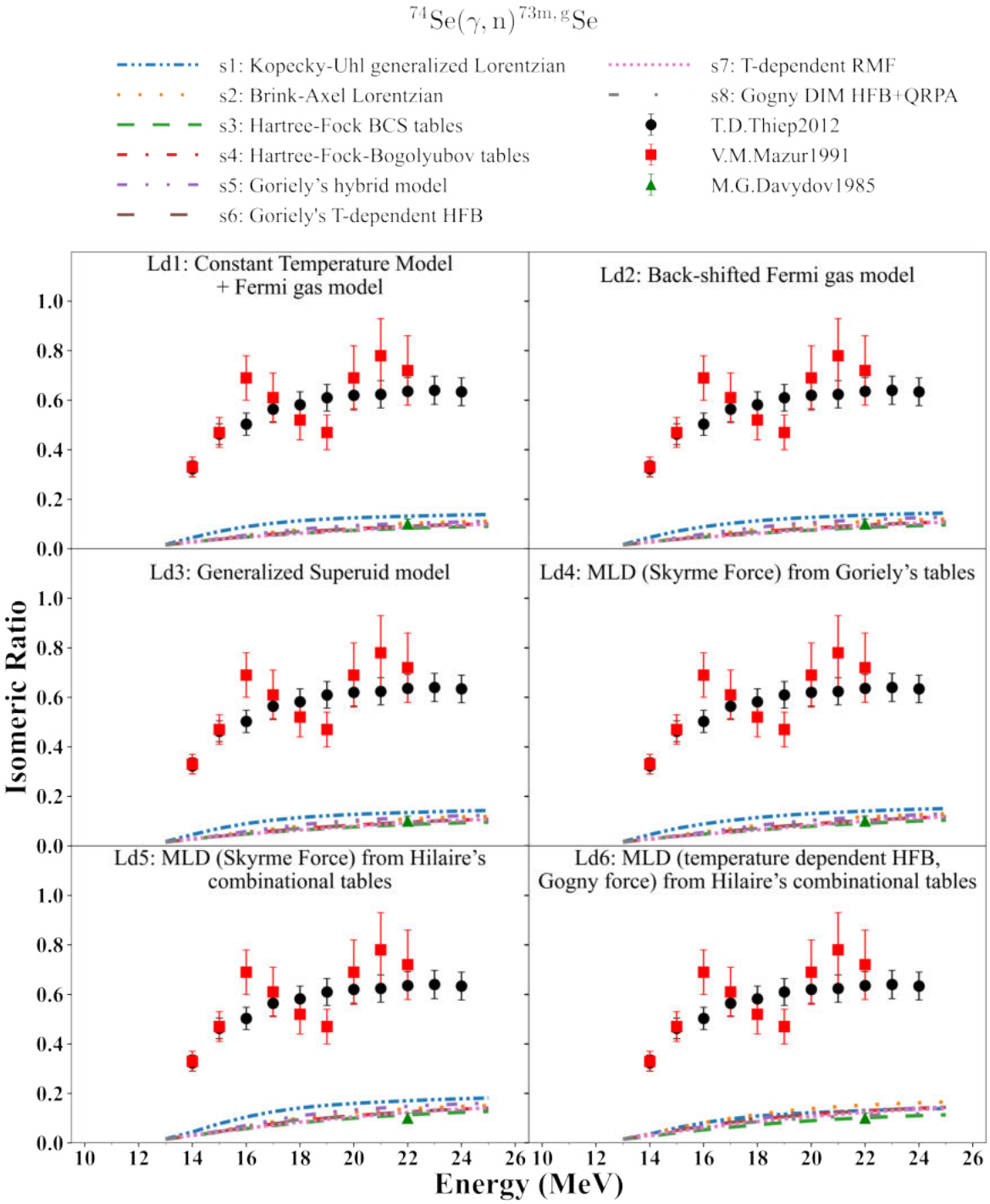

FIGURE 3.29: Theoretically calculated IRs between ^{73g}Se(I=9/2$^+$) and ^{73m}Se(I=3/2$^-$) in comparison with the literature.

From the good agreement between the calculation of Ld1 + s5 (constant temperature and Fermi gas level density model in combination with the hybrid Goriely model γ SF)

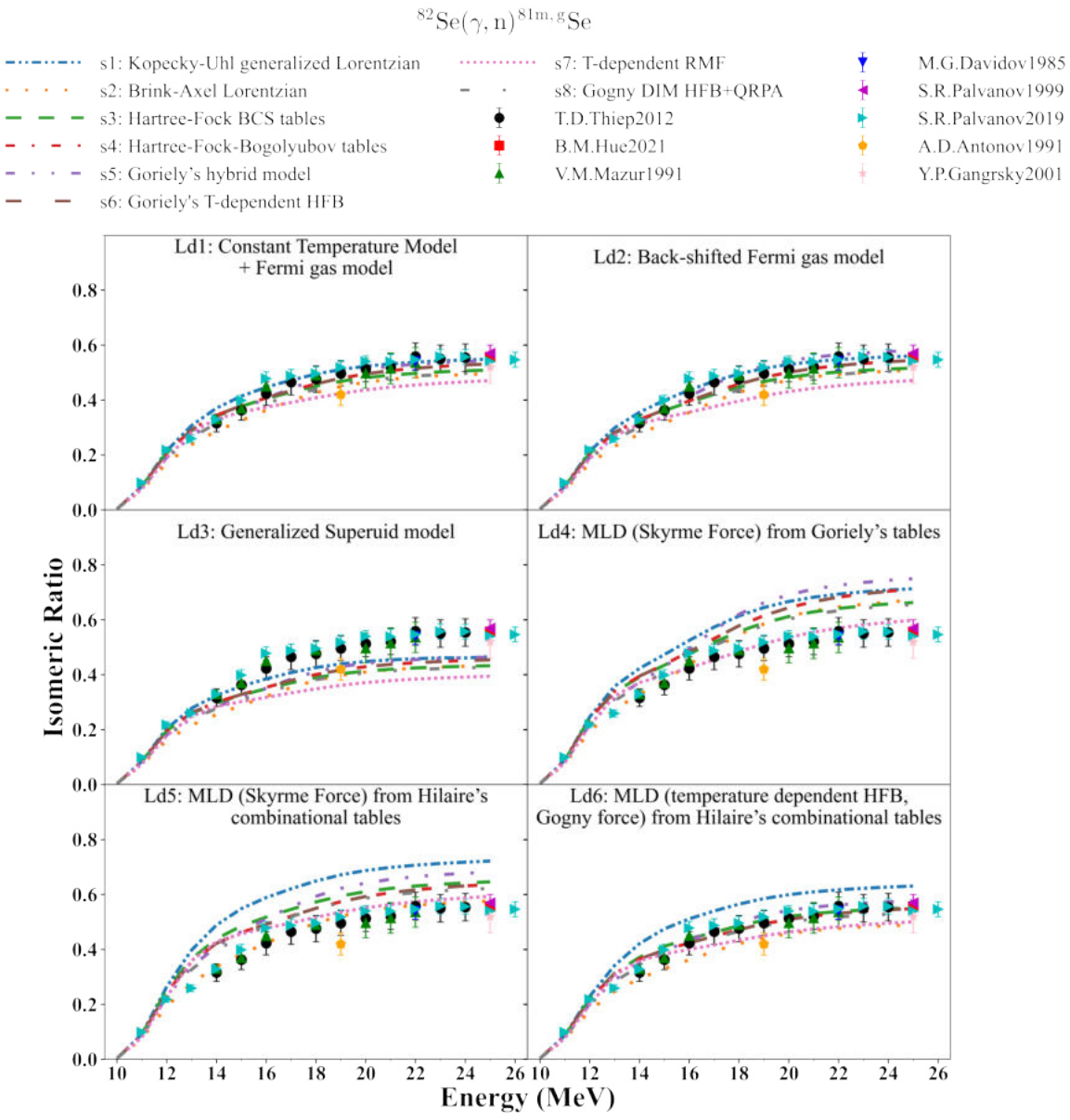

FIGURE 3.30: Theoretically calculated IRs between ^{81m}Se(I=7/2$^+$) and ^{81g}Se(I=1/2$^-$) in comparison with the literature.

and the experimental results, information regarding the nuclear excited state structure and the level density parameters of ^{81}Se nucleus can be completely extracted from the output file.

a(S_n) = 12.76063 MeV^{-1} (LD parameter at neutron separation energy),

D_0 = 2 ± 0.8 keV (experimental and theoretical mean resonance spacing),

$\tilde{a}$ = 11.04827 MeV^{-1} (asymptotic level density parameter),

γ = 0.1001 MeV (shell damping parameter),

Δ = 1.33333 MeV (pairing energy),

δW = 2.00143 MeV (shell correction energy),

E_x = 5.43118 MeV (matching energy),

N_{low} = 7, N_{top} = 19 (levels of the matching problem),

T = 0.73461 MeV (nuclear temperature),

E_0 = -0.19965 MeV (back-shift energy),

σ = 1.64366 (discrete state spin cut-off parameter),

$\sigma(S_n)$ = 3.97335 (spin cut-off parameter in neutron separation energy).

Furthermore, the output file consists of information on the level density parameter a, the spin cut-off parameter, and the level density itself, all as a function of the excitation energy. Herein, the gamma strength function, transmission coefficient, giant resonance parameters, and many other parameters were also presented.

For ^{82}Se nucleus, GDR parameters, gamma strength function f(XL) and transmission coefficient T(XL) are

σ_0(M1) = 1.534, σ_0(E1) = 148;

E(M1) = 9.437 MeV, E(E1) = 16.65 MeV;

Γ(M1) = 4 MeV, Γ(E1) = 5.91 MeV;

f(M1) = 1.7901E^{-10} MeV^{-3}, f(E1) = 8.18775E^{-8} MeV^{-3};

T(M1) = 1.75743E^{-5}, T(E1) = 8.03830E^{-3}.

In [35, 34, 36], it showed the effect of nucleon configuration, which means that the IR in reaction (γ, n) in the GDR region for isotopes of an element decreases with increasing isotope mass number. In the case of Se, the experimental IRs of ^{73m,g}Se are higher than that in ^{81m,g}Se while the theoretical IRs are inverse. Taking into account this fact and the difference in the experimental and calculated results, one can say that the TALYS code may have to make corrections in the level density and the γ SF models.

b. For $^{109m,g}Pd$

The calculated IR results of ^{109m,g}Pd presented in Fig. 3.31 show that six Ld models with the majority of γSFs are almost consistent with the experimental data taken from B. M. Hue [133], S. R. Palvanov [61], H. D. Luc, [201] V. M. Mazur [202], A. G. Belov [203] but not in the entire energy range. There is good agreement between theoretical IRs with Ld5+s1 and experimental ones in energies ranging from 10 to 17 MeV, while theoretical IRs with Ld3+s1/s5 predict exactly experimental ones in the energy range of 18 to 25 MeV.

For the calculation of Ld3 + s5 (generalized superfluid level density model in combination with the Goriely hybrid model γ SF), the model parameters with respect to the nuclear-excited state structure and the level density parameters of the ^{109}Pd nucleus consists of

$a(S_n) = 15.67741$ MeV^{-1},

$D_0 = 182 \pm 33$ eV,

$\tilde{a} = 15.67741$ MeV^{-1},

$\gamma = 0.13581$ MeV,

$\Delta = 1.14939$ MeV,

$\delta W = 3.82721$ MeV,

$E_x = 4.10818$ MeV,

$N_{low} = 8$, $N_{top} = 16$,

$T = 0.65170$ MeV,

$\sigma = 2.81066$,

$\sigma(S_n) = 4.69007$.

For the ^{110}Pd nucleus, GDR parameters, gamma strength function f(XL) and transmission coefficient T(XL) are

$\sigma_0(M1) = 1.08$, $\sigma_0(E1) = 238.746$;

$E(M1) = 8.557$ MeV, $E(E1) = 15.923$ MeV;

$\Gamma(M1) = 4$ MeV, $\Gamma(E1) = 5.138$ MeV;

$f(M1) = 1.19106E^{-10}$ MeV^{-3}, $f(E1) = 9.62216E^{-8}$ MeV^{-3};

$T(M1) = 1.16932E^{-5}$, $T(E1) = 9.44653E^{-3}$.

c. For Ce isotopes

Fig. 3.32 presents theoretically calculated IRs for ^{137m,g}Ce and the experimental data taken from B. M. Hue [133], T. D. Thiep [41, 204], S. R. Palvanov [205] Yu. P. Gangrsky [54]. One can see that there are large deviations between the theoretical

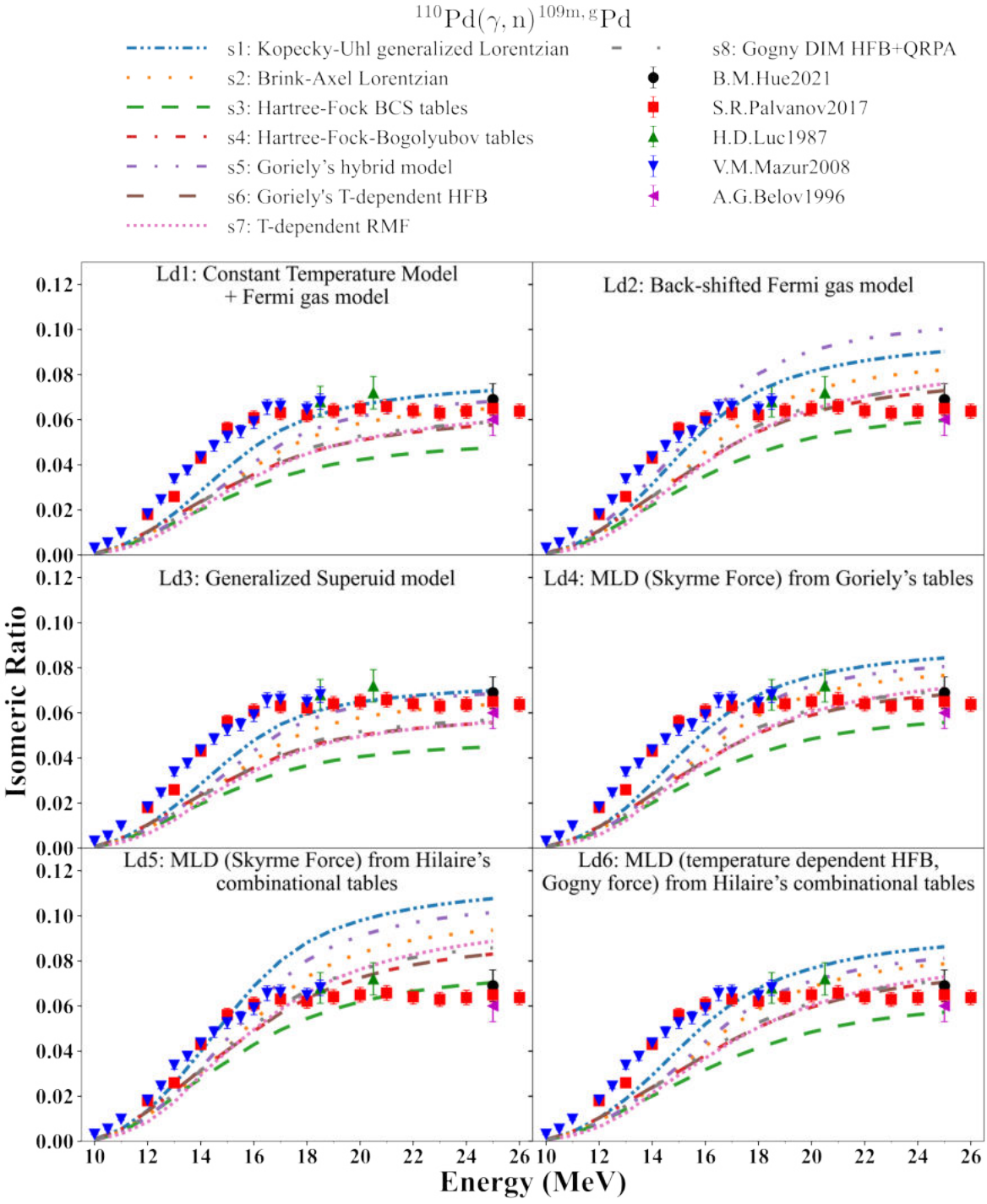

FIGURE 3.31: Theoretically calculated IRs between ^{109m}Pd(I=11/2$^-$) and ^{109g}Pd(I=5/2$^+$) in comparison with the literature.

values and the experimental ones taken from [133, 41, 204, 54]. However, the calculated results of Ld4+s5 and Ld5+s1/s5 are relatively equal to those reported in [205].

Fig. 3.33 shows the calculated IRs of ^{139m,g}Ce and the experimental data taken from S.R. Palvanov [206], V. M. Mazur [207], N. Tsoneva [208], A. G. Belov [209]. The theoretical calculations are in good agreement with the experimental ones, especially Ld4 + s2 / s5, Ld5 + s2 and Ld6 + s5. It is worth noting that ^{140}Ce is a magic nucleus.

The nucleon configuration effect is observed in the experimental results without the TALYS-based obtained ones for Ce isotopes.

For Ld4+s2 (microscopic level densities (Skyrme force) from Goriely's tables in combination with the Brink-Axel Lorentzian γ SF model), the model parameters regarding the nuclear-excited state structure and the level density parameters of the nucleus ^{139}Ce include

$a(S_n) = 15.96688\ \text{MeV}^{-1}$,

$D_0 = 428.26$ eV,

$\tilde{a} = 17.21424\ \text{MeV}^{-1}$,

$\gamma = 0.08361$ MeV,

$\Delta = 1.01783$ MeV,

δW = -1.12045 MeV,

$N_{low} = 4$, $N_{top} = 16$,

$\sigma = 2.14087$,

$\sigma(S_n) = 5.52402$.

For the ^{140}Ce nucleus, GDR parameters, gamma strength function f(XL) and transmission coefficient T(XL) are

σ_0(M1) = 3.073, σ_0(E1) = 383;

E(M1) = 7.896 MeV, E(E1) = 15.04 MeV;

Γ(M1) = 4 MeV, Γ(E1) = 4.410 MeV;

f(M1) = 3.26495E^{-10} MeV^{-3}, f(E1) = 9.43474E^{-8} MeV^{-3};

T(M1) = 3.20536E^{-5}, T(E1) = 9.26254E^{-3}.

d. For Eu isotopes

Fig. 3.34 presents theoretically calculated IRs between ^{150m}Eu(I=0^-) and ^{150g}Eu(I=5^-) in ^{151}Eu(γ, n)^{150m,g}Eu reaction and the experimental data taken from I. N. Vishnevsky [136], A. P. Tonchev [122]. The theoretically calculated values are in good agreement with the experimental data obtained by the authors in [122] but that

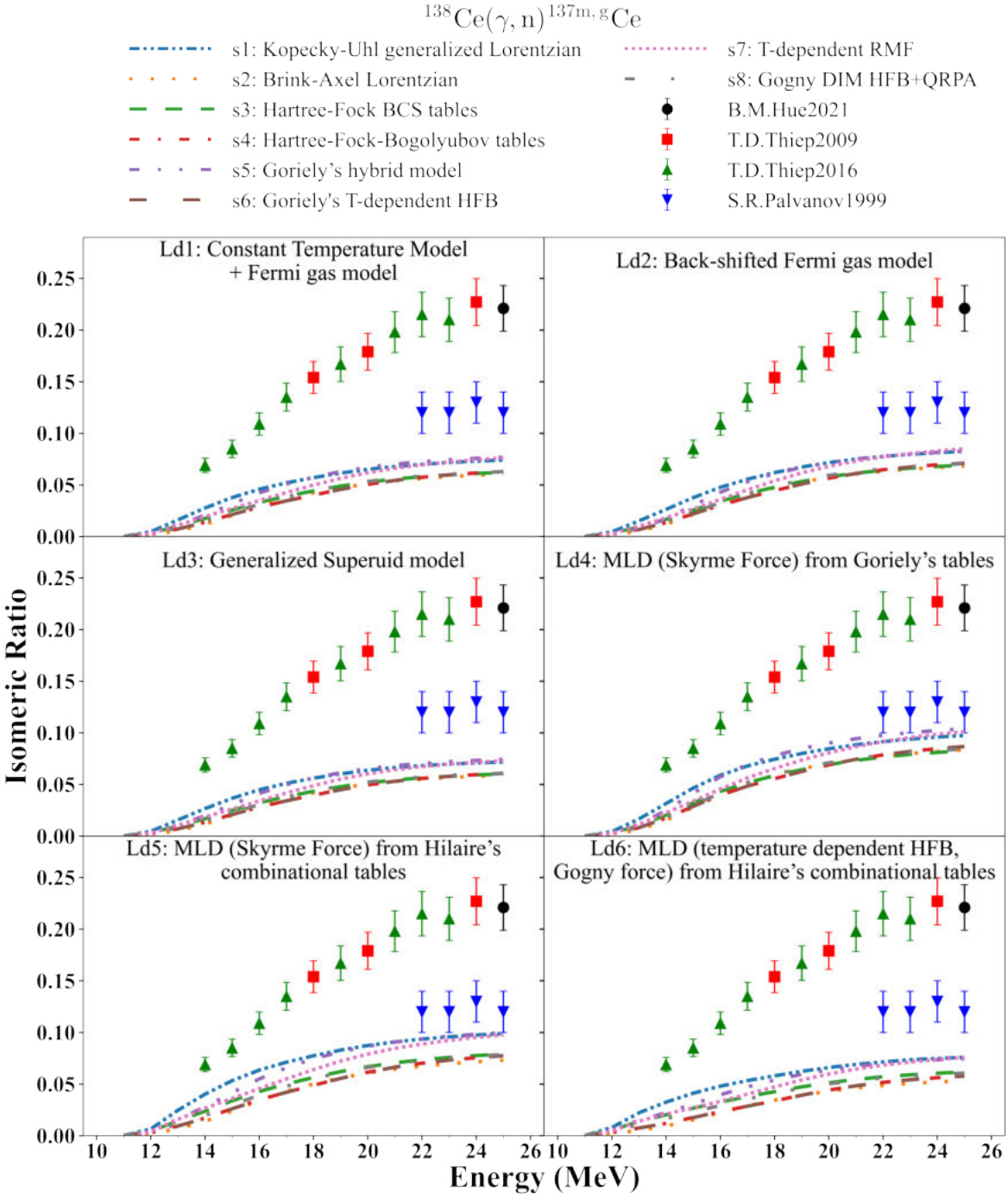

FIGURE 3.32: Theoretically calculated IRs between ^{137m}Ce(I=11/2$^-$) and ^{137g}Ce(I=3/2$^+$) in comparison with the literature.

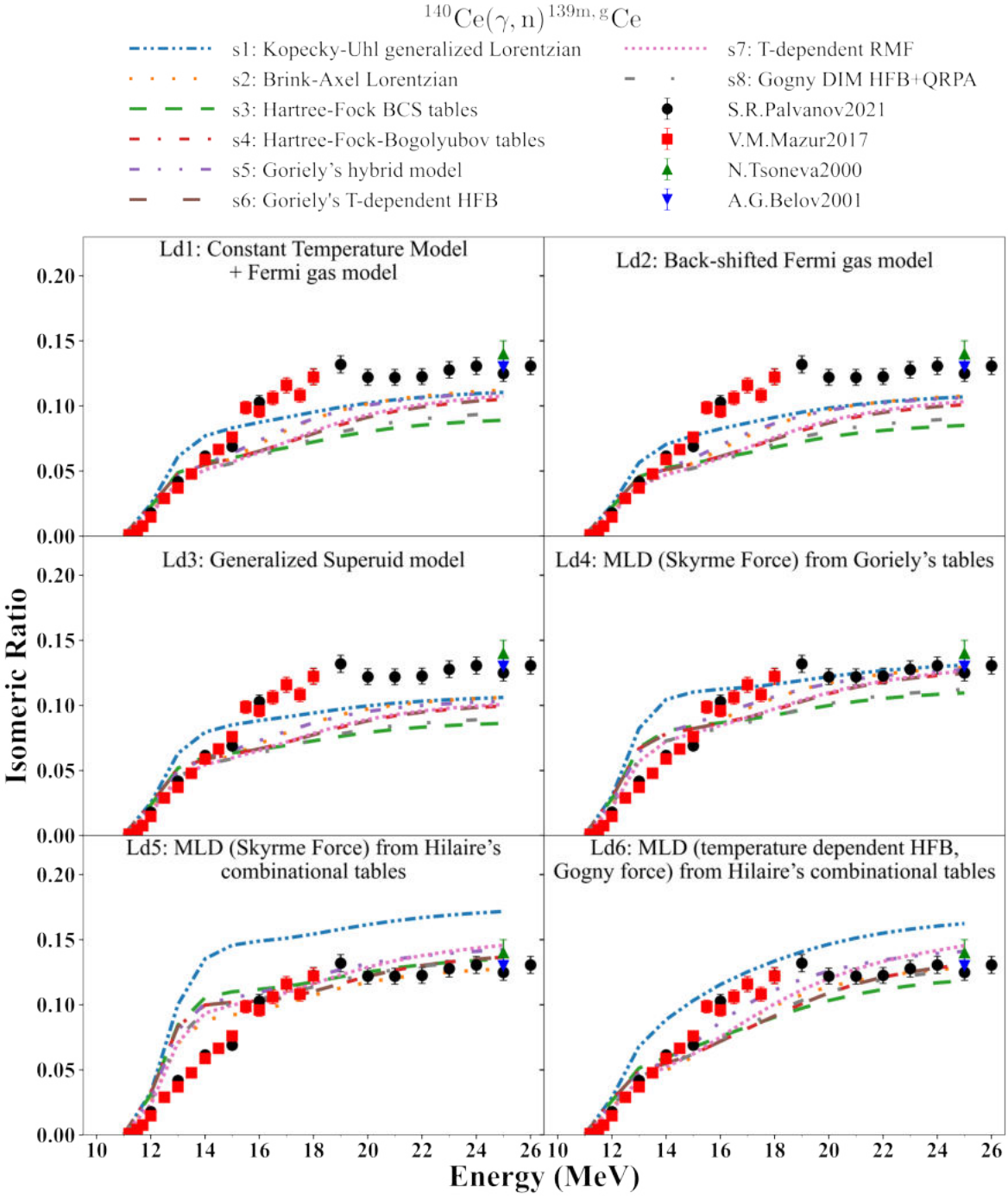

FIGURE 3.33: Theoretically calculated IRs between ^{139m}Ce(I=11/2$^-$) and ^{139g}Ce(I=3/2$^+$) in comparison with the literature.

deviate significantly from the data at 12 MeV taken from Ref. [136]. It is worth noting that ^{150}Eu is a spherical nucleus [160] shown in Fig. 3.26.

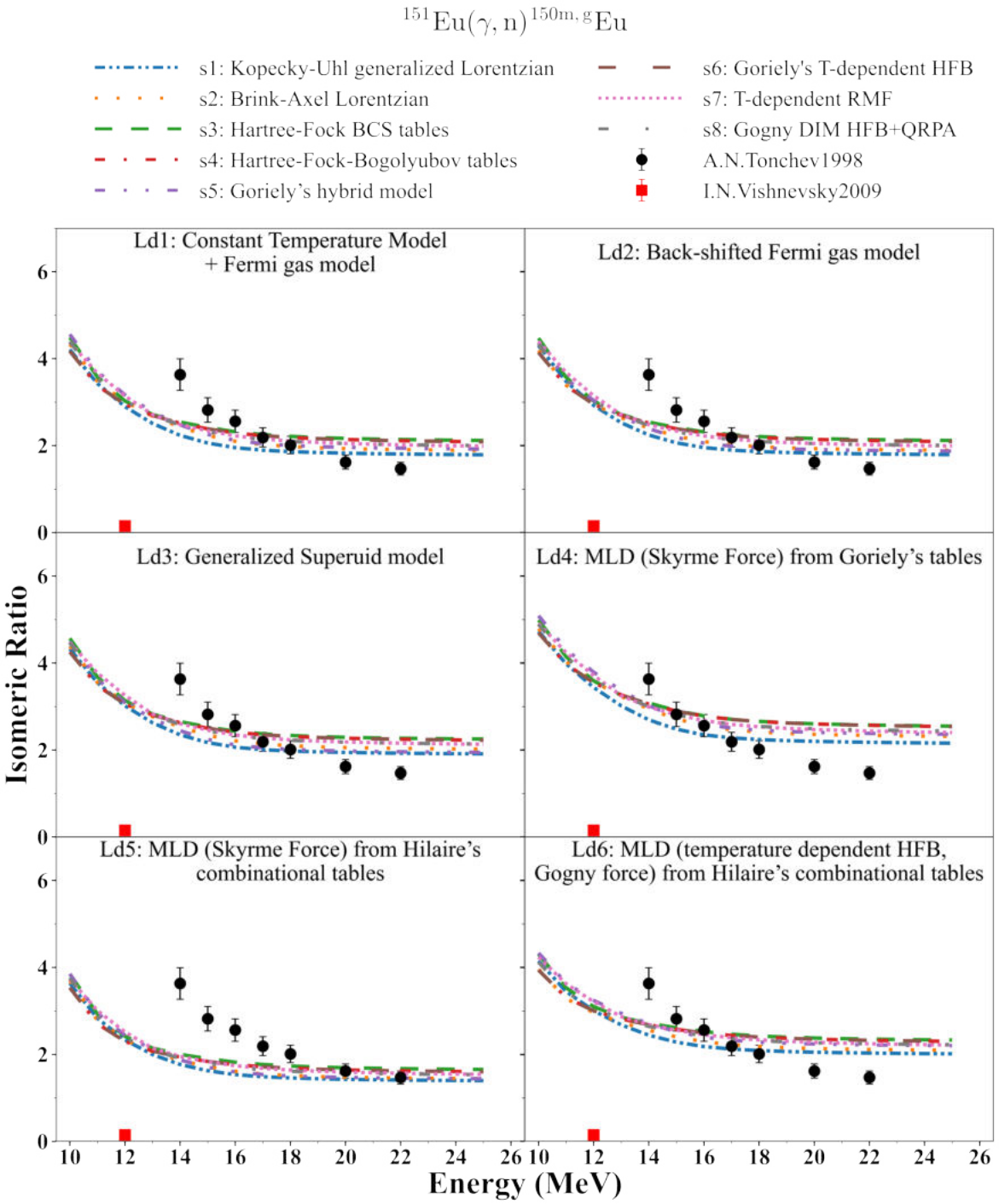

FIGURE 3.34: Theoretically calculated IRs between ^{150m}Eu(I=0$^-$) and ^{150g}Eu(I=5$^-$) in comparison with the literature.

The product of the (γ, n) photonuclear reaction on ^{153}Eu existed in the ground state with a spin of 3$^-$ and two isomeric states with spins of 0$^-$ and 8$^-$ respectively. Fig. 3.35 shows theoretically calculated IRs between ^{152m1}Eu(I=8$^-$) and ^{152g}Eu(I=3$^-$),

and the experimental data taken from A. P. Tonchev [122]. Fig. 3.36 represents theoretically calculated IRs between ^{152m1}Eu(I=8^-) and ^{152m2}Eu(I=0^-), and the experimental data taken from T. D. Thiep [41, 23], A. P. Tonchev [122], I. N. Vishnevsky [136, 139]. Fig. 3.37 shows theoretically calculated IRs between ^{152m2}Eu(I=0^-) and ^{152g}Eu(I=3^-), and the experimental data taken from A. P. Tonchev [122]. It can be seen from these figures that there are significant differences between the experimental data and the theoretical values of the calculations based on TALYS. The calculated IRs considerably overestimate the experimental data for $^{152m1,g;152m1,m2}Eu$, whereas those underestimate the measured values for $^{152m2,g}Eu$. It is worth noting that ^{152}Eu is a strongly deformed nucleus [23] as verified in Fig. 3.26.

For Ld1 + s2 (model of constant temperature and Fermi gas level density in combination with the Brink-Axel Lorentzian model γ SF), the model parameters regarding the nuclear-excited state structure and the level density parameters of the ^{152}Eu nucleus comprise the following.

a(S_n) = 23.96007 MeV^{-1},

D_0 = 0.73 ± 0.07 eV,

$\tilde{a}$ = 18.89487 MeV^{-1},

γ = 0.08115 MeV,

Δ = 0 MeV,

δW = 4.22048 MeV,

E_x = 4.38808 MeV,

N_{low} = 2, N_{top} = 17,

T = 0.51830 MeV,

E_0 = -2.23933 MeV,

σ = 3.20887,

$\sigma(S_n)$ = 6.25665.

For the ^{153}Eu nucleus, The GDR parameters, the gamma strength function f (XL) and the transmission coefficient T (XL) are

σ_0(M1) = 3.241, σ_0(E1) = 155 and 222;

E(M1) = 7.666 MeV, E(E1) = 12.330 MeV and 15.79 MeV;

Γ(M1) = 4 MeV, Γ(E1) = 2.750 MeV and 5.830 MeV;

f(M1) = 3.40147E^{-10} MeV^{-3}, f(E1) = 1.11894E^{-7} MeV^{-3};

T(M1) = 3.33939E^{-5}, T(E1) = 1.09851E^{-2}.

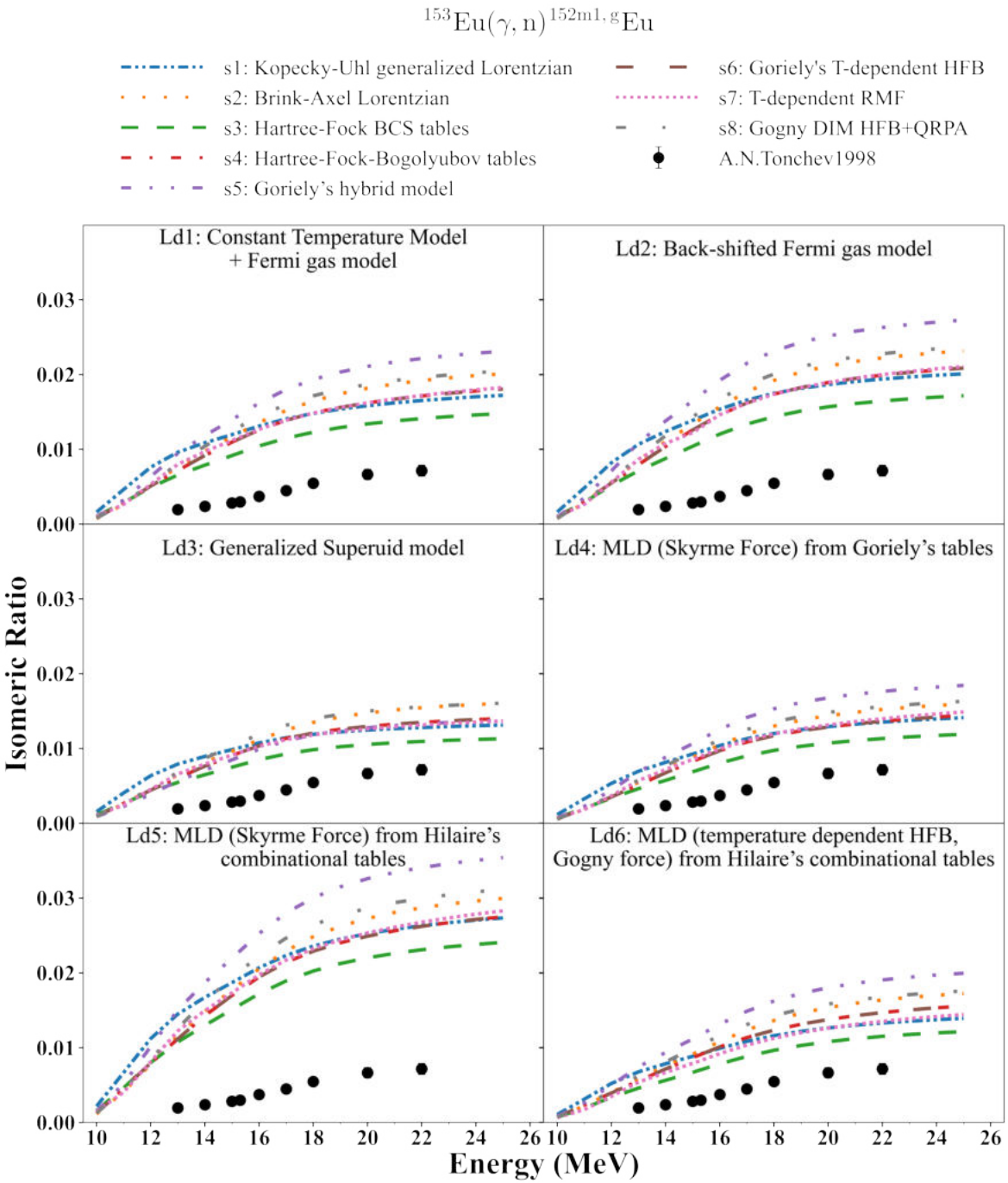

FIGURE 3.35: Theoretically calculated IRs between ^{152m1}Eu(I=8$^-$) and ^{152g}Eu(I=3$^-$) in comparison with the literature.

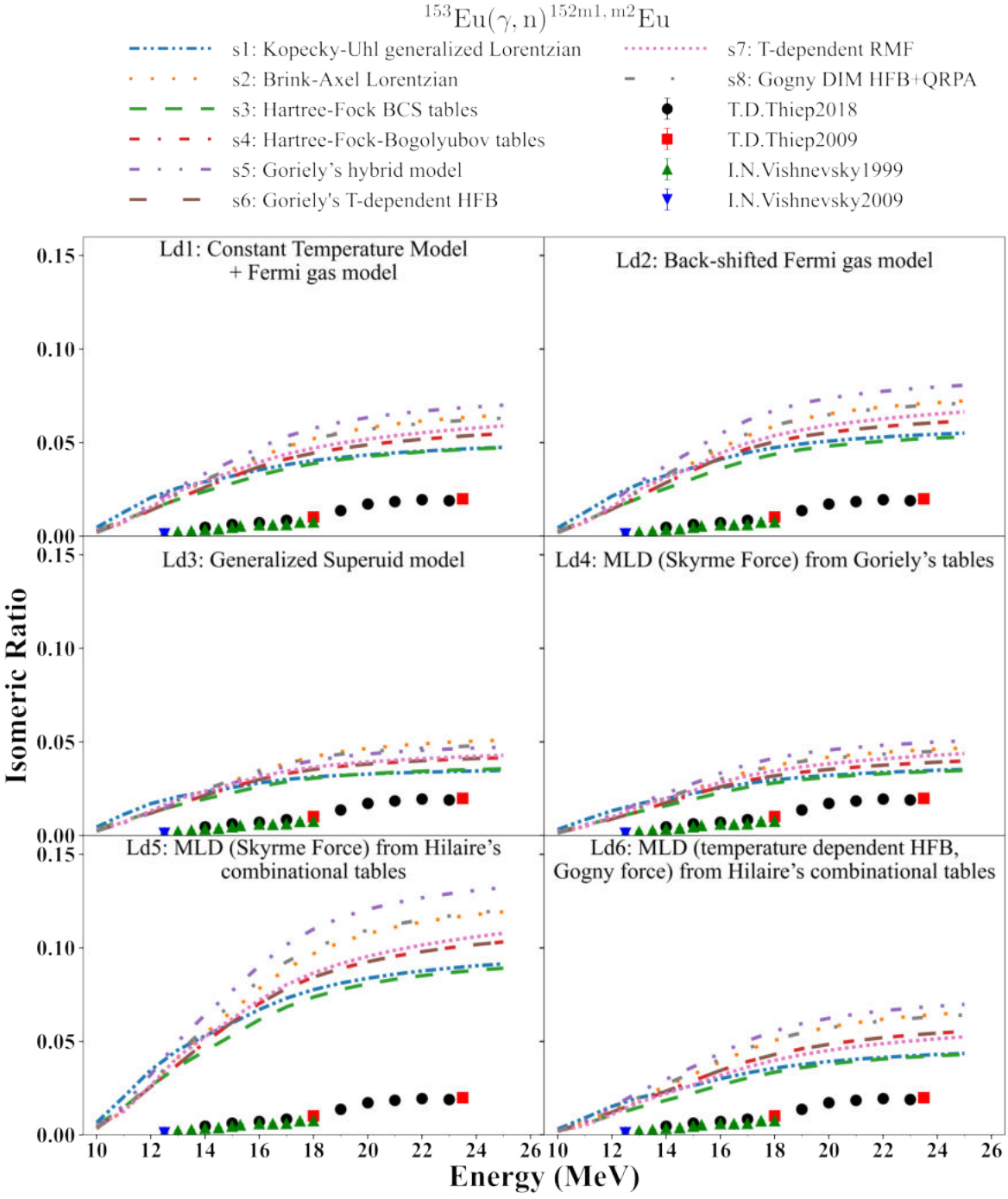

FIGURE 3.36: Theoretically calculated IRs between ^{152m1}Eu(I=8$^-$) and ^{152m2}Eu(I=0$^-$) in comparison with the literature.

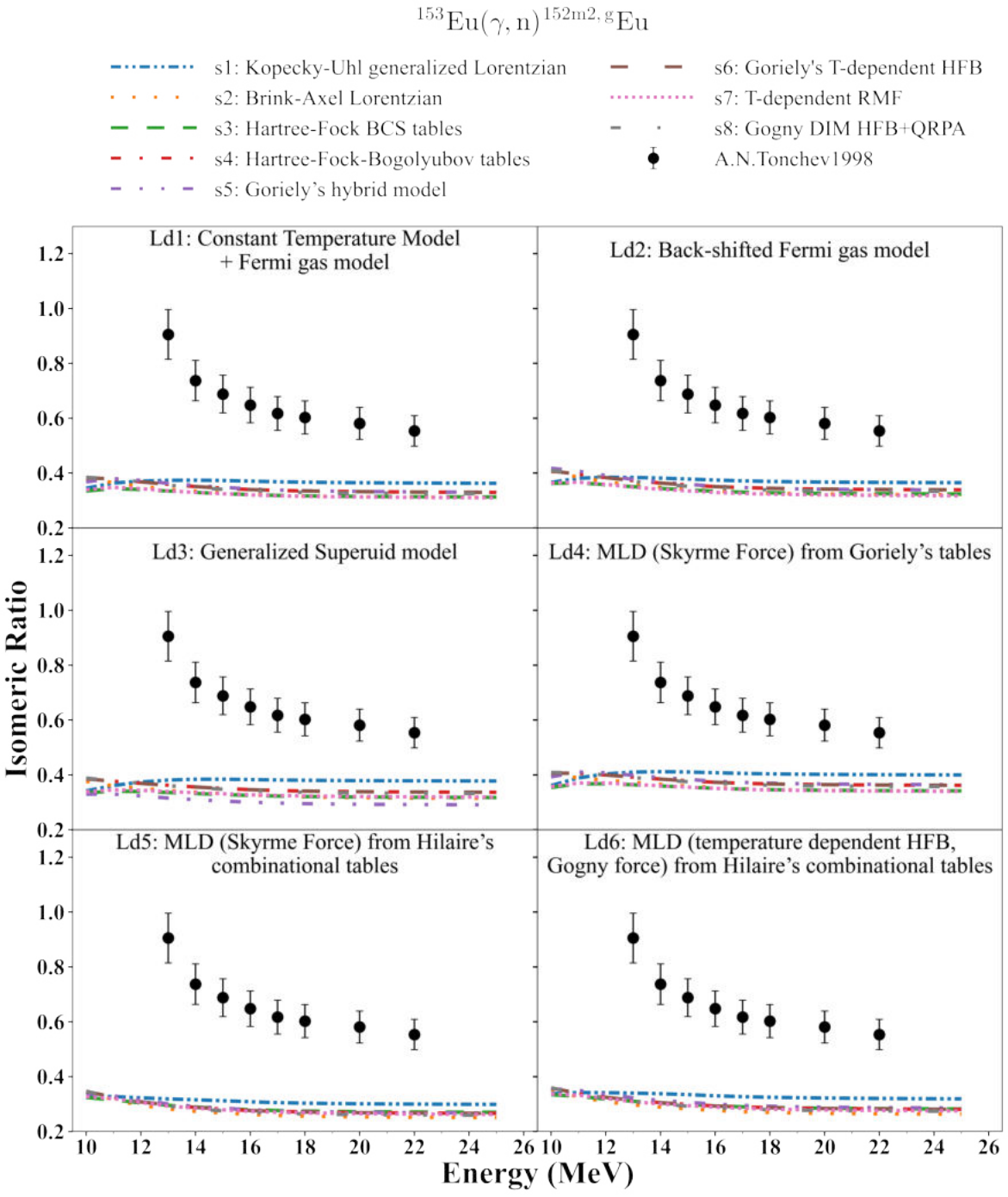

FIGURE 3.37: Theoretically calculated IRs between ^{152m2}Eu(I=0$^-$) and ^{152g}Eu(I=3$^-$) in comparison with the literature.

Instead of being computed by the method in ref. [71], the results obtained with another method in this work are in good agreement with those of [71] calculated by the Talys 1.8 code in the complete simulation process of the GEANT4 toolkit for the bremsstrahlung production and photonuclear reaction process.

e. For Hg isotopes

Fig. 3.38 presents the experimental data taken from T. D. Thiep [128], B. S. Ishkhanov [155] along with the theoretically calculated IRs of ^{195m}Hg(I=13/2$^+$) and ^{195g}Hg(I=1/2$^-$). Fig. 3.39 illustrates the experimental data taken from Yu. P. Gangrsky [54], T. D. Thiep [128], B. S. Ishkhanov [155], V. A. Zheltonozhsky [149] and the theoretically calculated IRs between ^{197m}Hg(I=13/2$^+$) and ^{197g}Hg(I=1/2$^-$).

For ^{195m,g}Hg, six Ld models predict exactly the datum of Ishkhanov et al. [155], while the LD5+s2 model agrees fairly well with our experimental data. For ^{197m,g}Hg, there are large discrepancies between the calculated results and the experimental data originating from [128, 149, 54]. The calculated results significantly underestimate the IRs of T.D.Thiep, V.A.Zheltonozhsky, and Y.P.Gangsky. However, the theoretical predictions of Ld4 + s1 / s2 and Ld5 + s2 are consistent with the IR value of B.S. Ishkhanov [155].

The effect of nucleon configuration is observed in both experimental and theoretical results for Hg isotopes. That is, the IR of ^{195m,g}Hg is higher than that of ^{197m,g}Hg.

For Ld5+s2 (microscopic level density (Skyrme force) from Hilaire's combinatorial tables in combination with Brink-Axel Lorentzian γSF model), the model parameters regarding the nuclear-excited state structure and the level density parameters of the ^{195}Hg nucleus consist of

$a(S_n) = 21.19256\ \text{MeV}^{-1}$,

$D_0 = 19.87$,

$\tilde{a} = 23.01361\ \text{MeV}^{-1}$,

$\gamma = 0.07468$ MeV,

$\Delta = 0.85934$ MeV,

$\delta W = -1.31645$ MeV,

$N_{low} = 8$, $N_{top} = 18$,

$\sigma = 3.57524$,

$\sigma(S_n) = 6.69405$.

For the ^{196}Hg nucleus, GDR parameters, gamma strength function f(XL) and transmission coefficient T(XL) are

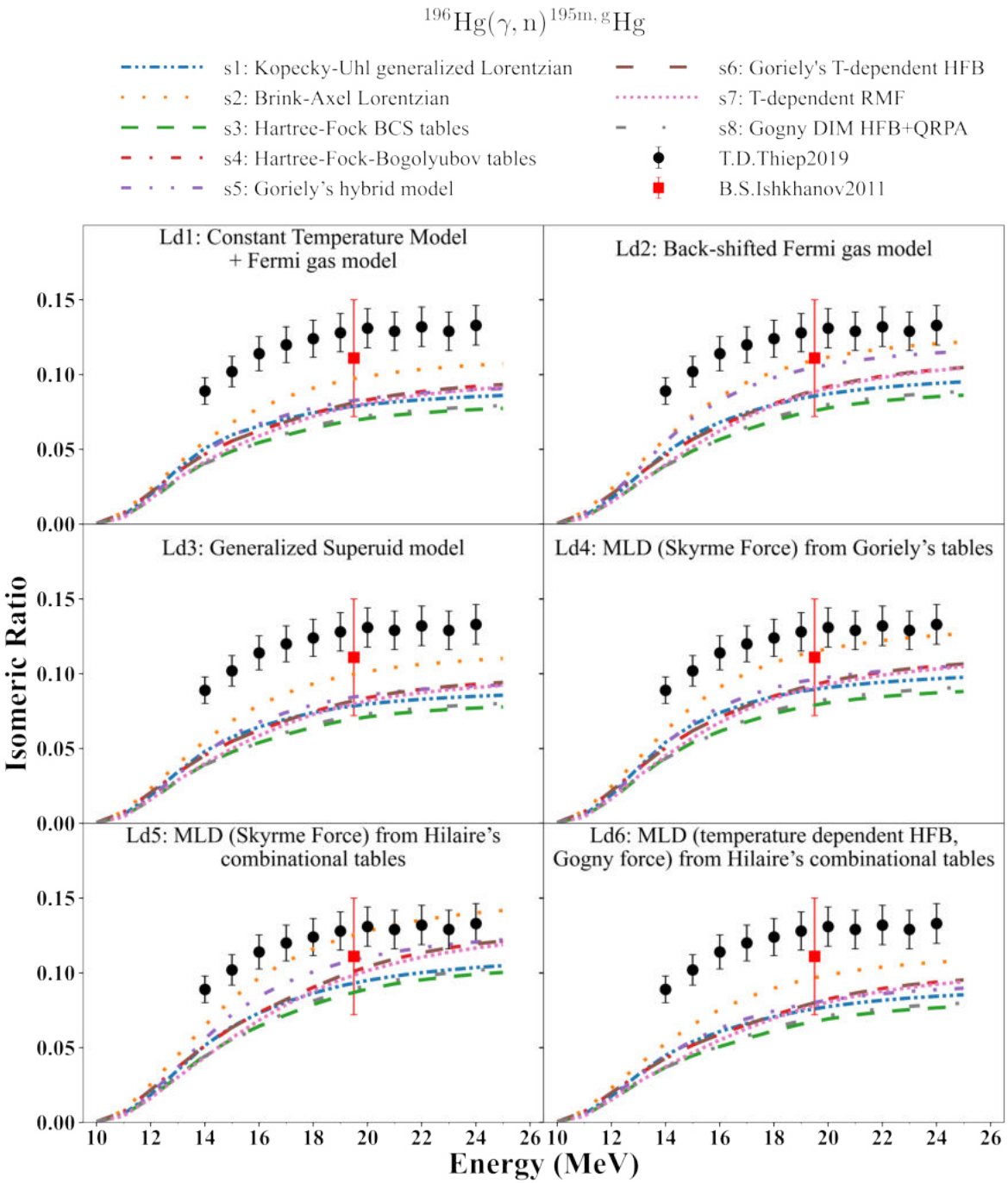

FIGURE 3.38: Theoretically calculated IRs between ^{195m}Hg(I=13/2$^+$) and ^{195g}Hg(I=1/2$^-$) in comparison with the literature.

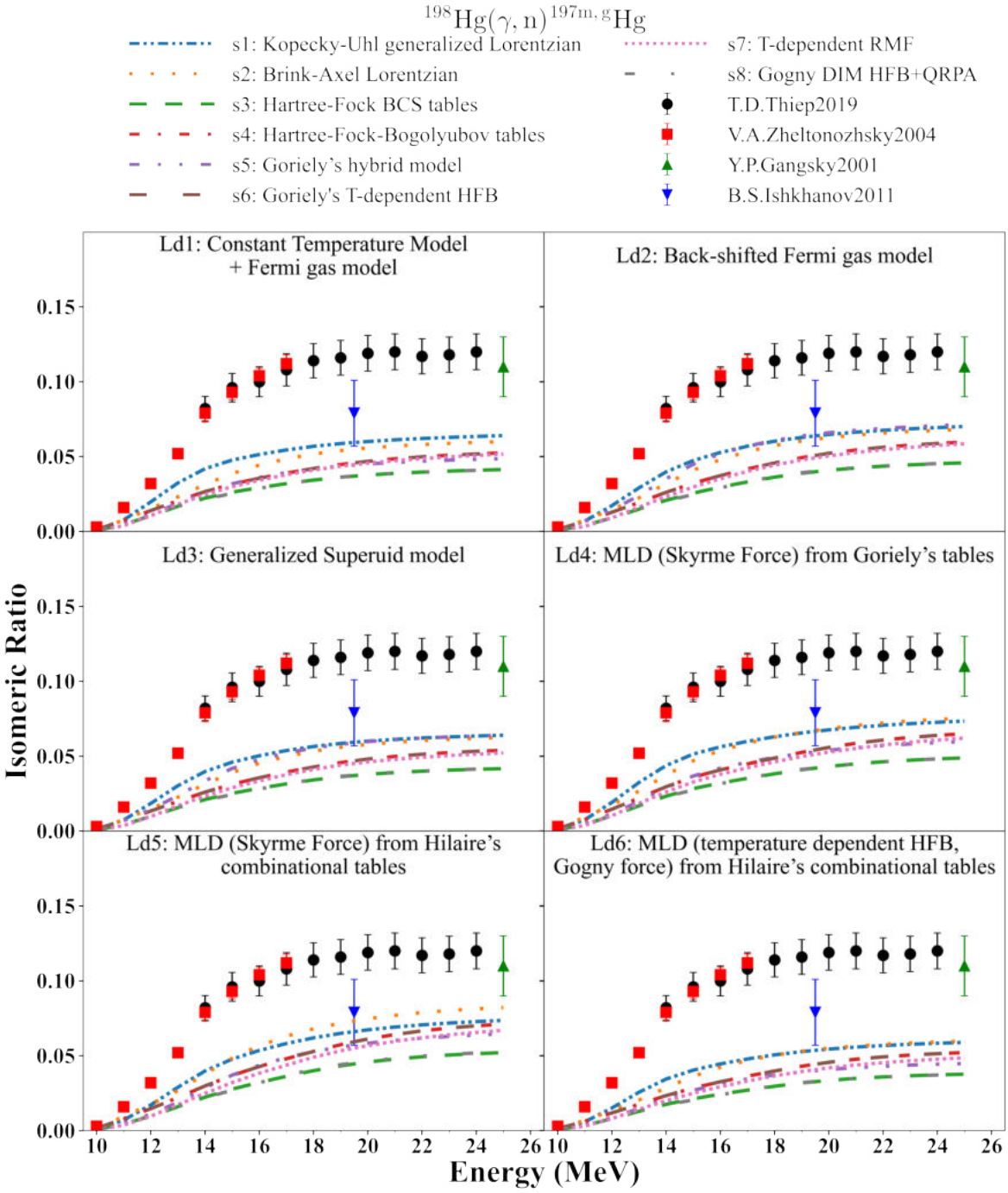

FIGURE 3.39: Theoretically calculated IRs between ^{197m}Hg(I=13/2$^+$) and ^{197g}Hg(I=1/2$^-$) in comparison with the literature.

σ_0(M1) = 3.217, σ_0(E1) = 546.105;

E(M1) = 7.058 MeV, E(E1) = 13.918 MeV;

Γ(M1) = 4 MeV, Γ(E1) = 3.974 MeV;

f(M1) = 3.27509E^{-10} MeV^{-3}, f(E1) = 9.54788E^{-8} MeV^{-3};

T(M1) = 3.21531E^{-5}, T(E1) = 9.37361E^{-3}.

All other information relating to the nuclear model calculation can be extracted in the output file. The shortcomings of the inexactly described nuclear models should be improved and corrected in further study.

Conclusions and Outlooks

In this work, we have studied the IRs of isomeric pairs of Eu, Hg, Cd, Ce, Se and Pd isotopes in the (γ, n) reactions irradiated by bremsstrahlung with end-point energy in the GDR region, as well as the IRs of isomeric pairs of Pd, Cd, Ce and Se isotopes in (n, γ) reactions induced by thermal and epithermal neutrons. In the experiments, the activation method combined with offline γ ray spectroscopy was used. The bremsstrahlung and neutron sources were produced using the MT-25 Microtron, FLNR, JINR, Dubna, Russia. The Eu, Hg, Cd, Ce, Se, and Pd targets were chosen to investigate the isomers and IR because of their various nuclear structures, insufficient IR data, or large discrepancies. They also play a crucial role in many applications, such as medicine, therapy, biology, electronics, materials science, and nuclear reactors. Accordingly, the experimental results obtained with high accuracy in this thesis have expected to contribute to the Nuclear Data Bank for both fundamental science and applications.

Concerning (γ,n) reactions on Hg, Eu, Cd, Ce, Se, and Pd isotopes in the GDR region, we have identified seven isomeric pairs $^{195m,g;197m,g}$Hg, ^{152m1,m2}Eu, ^{115m,g}Cd, ^{137m,g}Ce, ^{81m,g}Se and ^{109m,g}Pd and measured their IRs. In which the data of ^{197m,g}Hg from 18 to 24 MeV, ^{195m,g}Hg from 14 to 24 MeV and ^{152m1,m2}Eu for 19, 21 and 23 MeV have been reported for the first time. For (n,γ) reactions on Pd, Cd, Ce and Se isotopes induced by thermal and resonant neutrons, we have recognized six isomer pairs including $^{109m,g;111m,g}$Pd, $^{115m,g;117m,g}$Cd, ^{137m,g}Ce and ^{81m,g}Se and then determined their IRs. The results of $^{115m,g;117m,g}$Cd and $^{109m,g;111m,g}$Pd irradiated by mixed thermal-resonant neutrons, as well as ^{111m,g}Pd induced by resonant neutrons, are the first measurements. As the most remarkable results of this work, we have devoted the new experimental data of ^{nat}Eu$(\gamma, n)^{152m1,m2}$Eu, ^{nat}Hg$(\gamma, n)^{195m,g;197m,g}$Hg, ^{nat}Pd$(n, \gamma)^{109m,g}$Pd, and ^{nat}Cd$(n, \gamma)^{115m,g;117m,g}$Cd. Until now, the IR data of $^{195m,g;197m,g}$Hg, $^{109m,g;111m,g}$Pd, and $^{115m,g;117m,g}$Cd have been accepted into the EXFOR Library of IAEA. You can access the link (https://www-nds.iaea.org/exfor/) to search for the data.

Our group has been surveying several effects influencing experimental IRs in photonuclear and neutron-induced reactions for many years. As a continuation of our previous research, this work has selected the different incident energies on the nuclei in a wide range of atomic numbers with typical nuclear structure, including spherical even-even nuclei ^{138,140}Ce (Z = 58) and ^{196,198}Hg (Z = 80), vibrational even-even nuclei ^{74,82}Se (Z = 34) and ^{110}Pd (Z = 46), spherical odd-even nucleus ^{151}Eu (Z = 63) and deformed odd-even nucleus ^{153}Eu. The results of this work provide more information to verify and provide unambiguous answers to some effects with respect to IR. The first effect is that of the excitation energy in the reactions (γ, n) in the GDR region, which means that the higher the excitation energy, the higher the IR. This effect is confirmed by the enhancement of the IR as the excitation energy increased in the cases of $^{195m,g;197m,g}$Hg and ^{152m1,m2}Eu, due to the growth of the angular momentum of the compound nucleus. The second effect is the nucleon configuration effect, which is observed by the higher the mass number of Hg isotopes, the lower the IR in (γ, n) reaction. The third effect is the large spin difference that leads to very low IR, illustrated in the case of the isomeric pair ^{152m1}Eu(8^-) and ^{152m2}Eu(0^-). The fourth effect is the reaction channel effect, which causes the IRs of the identical isomeric pair produced in various reactions with the same excitation energy to be different. We gain a deeper understanding of this effect by studying the IRs of the ^{137m,g}Ce, ^{81m,g}Se, ^{115m,g}Cd and ^{109m,g}Pd isomeric pairs in inverse reactions (γ, n) and (n, γ) with the same product excitation energy to elucidate the influence of intake impulses and angular momentum transfer, which is part of the channel effect. This led to the conclusion that the higher the intake impulses and the higher the momentum transfer, the higher the IR values.

To compare the measured IRs of isomeric pairs of Se, Pd, Ce, Eu, and Hg nuclei in (γ, n) reactions, we have computed the IRs in the energy range of 10 to 25 MeV using the TALYS 1.95 statistical nuclear model code and the GEANT4 toolkit. The GEANT4 simulated the bremsstrahlung spectrum while the TALYS code calculated the reaction cross section. We tested the energy-dependent cross section with six-level density models in conjunction with eight γ-strength functions and achieved consistency in the theoretical predictions with the experimental results. The TALYS-based calculations also led to the consequence that the compound mechanism was predominant in the investigated photonuclear reactions. In addition, the deformed shape of the ^{153}Eu nucleus was justified by the display of two resonance peaks in the energy-dependent reaction cross section curve. The IRs calculated using six levels of density models

demonstrated a shape similar to the experimental results. In many cases, the theoretical predictions were in good agreement with the experimental data. Information relative to model calculation such as the discrete level, the level density parameter, spin cut-off, optical model parameters, the gamma strength function, and the transmission coefficient was entirely in the output file. Theoretical results, moreover, showed the effect of the nucleon configuration on Hg isotopes without effect on Se and Ce isotopes. Therefore, one needs to make detailed corrections referring to the level density models, the gamma strength function models, and other parameters.

Overall, this study dedicated the first-ever outcomes exclusively or contributed additional data to the nuclear data reservoir. The consideration of four effects resulted in more systematic and reliable IRs. Additionally, current experimental IRs can be employed as precious data for examining nuclear reaction models. Theoretical IR calculations for photonuclear reactions illuminated by bremsstrahlung were performed using the TALYS 1.95 code in combination with the GEANT4 toolkit. From the comparison of experimental data and calculated results, the best-fitted model could be ascertained, and then valuable information on nuclear level structure, level density, reaction mechanisms, involved effects, and other properties could be extracted. The shortcomings of the incorrectly described nuclear models need to be improved and fixed. More research is needed on this topic.

The scope of this thesis is the study of IR in reaction (γ, n) with the energy of the bremsstrahlung endpoint in the GDR region and reaction (n, γ) induced by thermal and epithermal neutrons. However, it is well-known that the study of isomers and IR is of particular interest in various types of nuclear reactions. At present, there are several individual discrepancies among the experimental data. Thus, more measurements with higher accuracy are indispensable. In order to proceed with this work, we plan to study IR in photonuclear and neutron-induced reactions on a large number of nuclei ranging from light to heavy ones, especially for deformed nuclei with unusual properties and types of isomers. In addition, the bremsstrahlung and neutron spectra arising from electron accelerators and other sources with different kinds and thicknesses of materials will be computed. Furthermore, since the current TALYS version is only applicable for projectiles with energy from 1 keV to 200 MeV, it has not yet solved the reactions irradiated by thermal and resonance neutrons (<300 eV). We will attempt to resolve this issue in future studies.

List of Publications used for the Thesis content

1. **Bui Minh Hue**, Tran Duc Thiep, Truong Thi An, Phan Viet Cuong, S. M. Lukyanov, and S. Mitrofanov . *Isomeric ratios in neutron capture reaction, induced by thermal, resonant and mixed thermal-resonant neutrons on* ^{114}Cd *and* ^{116}Cd *nuclei*. Nuclear Inst. and Methods in Physics Research, B 502, pp. 46-53 (2021).

2. **Bui Minh Hue**, Tran Duc Thiep, Truong Thi An, Phan Viet Cuong, S. M. Lukyanov, A. G. Belov, and S. Mitrofanov. *The isomeric ratios in (n, γ) neutron capture reactions on* ^{108}Pd *and* ^{110}Pd *nuclei*, Journal of Radioanalytical and Nuclear Chemistry 326, no. 1, 503-509 (2020).

3. Tran Duc Thiep, Truong Thi An, Phan Viet Cuong, **Bui Minh Hue**, A. G. Belov, S. Mitrofanov. *Isomeric yield ratios of* $^{195m,g}Hg$ *and* $^{197m,g}Hg$ *in the* $^{196}Hg(\gamma, n)$ *and* $^{198}Hg(\gamma, n)$ *reactions induced by bremsstrahlung energy within giant dipole resonance region*, Nuclear Inst. and Methods in Physics Research, B. 457, 4-9 (2019).

4. Tran Duc Thiep, Truong Thi An, Phan Viet Cuong, Nguyen The vinh, **Bui Minh Hue**, Le Tuan Anh, A. G. Belov. *Isomeric yield ratio of* $^{152m1}Eu(8\text{-})$ *to* $^{152m2}Eu(0\text{-})$ *produced from* ^{153}Eu (γ, n) ^{152}Eu *reaction in the giant dipole resonance region*, J. Radioanal. Nucl. Chem., 317, 1263–1271 (2018).

5. **Bui Minh Hue**, Tran Duc Thiep. *Theoretical consideration of isomeric ratios in some photonuclear reactions induced by bremsstrahlung with endpoint energy in giant dipole resonance region using Talys 1.95 code*, Nuclear Science and Technology, Vol.12, No. 1, pp. 21-31 (2022).

6. Tran Duc Thiep, Truong Thi An, **Bui Minh Hue**, Phan Viet Cuong, Nguyen Hong Ha, A. G. Belov, S. Mitrofanov. *Investigation of the same isomeric pair,*

produced from different nuclear reactions, Nuclear Science and Technology, Vol.10, No. 1, pp. 01-10 (2020).

7. Tran Duc Thiep, Truong Thi An, **Bui Minh Hue**, Phan Viet Cuong, A. G. Belov, S. Mitrofanov. *The nuclear channel effect in the isomeric ratio of the reaction products*, Nuclear Science and Technology, Vol.9, No. 1, pp. 09-20 (2019).

8. **Bui Minh Hue**, Tran Duc Thiep, *Isomeric Ratios in Several Inverse (γ, n) and (n, γ) Reactions*, Proceedings of 28th International Seminar on Interaction of Neutrons with Nuclei, http://isinn.jinr.ru/proceedings/isinn-28/pdf/HueBui.pdf, (2021).

9. **Bui Minh Hue**, Tran Duc Thiep, *Isomeric Ratios in Inverse (γ, n) and (n, γ) Reactions on Ce, Cd, Pd and Se targets*, Proceedings of the 7th Academic Conference on Natural Science for Young Scientist, Master and PhD. Student from ASEAN Countries (CASEAN-7), p388-396 (2021).

Other publication

1. P.V. Cuong, T.D. Thiep, L.T. Anh, T.T. An, **B.M. Hue**, K.T. Thanh, N.H. Tan, N.T. Vinh, T.T. Anh, *Theoretical calculation by Talys code in combination with Geant4 simulation for consideration of (γ, n) reactions of Eu isotopes in the giant dipole resonance region*, Nuclear Inst. and Methods in Physics Research B, 479 (2020) 68-73.

References

[1] Frederick Soddy. "A Chemical Sign of Life. By S. Tashiro. Pp. ix+ 142.(Chicago: University of Chicago Press; Lon-don: Cambridge University Press.) r doJlar, or 4s. net. Manuals of Health. 1., Food. By Dr. A. Hill." (1917).

[2] Otto Hahn. "Über eine neue radioaktive Substanz im Uran". *Berichte der deutschen chemischen Gesellschaft (A and B Series)* 54.6 (1921), pp. 1131–1142.

[3] CF v. Weizsäcker. "Metastabile Zustände der Atomkerne". *Naturwissenschaften* 24.51 (1936), pp. 813–814.

[4] A Bohr and B Mottelson. *Mat. Fys. Medd. Dan. Vid. Selsk.* 1953.

[5] Ashok Kumar Jain, Bhoomika Maheshwari, and Alpana Goel. *Nuclear Isomers: A Primer*. Springer Nature, 2021.

[6] JM Blatt and VF Weisskopf. *Theoretical nuclear physics. New York: John Wiley and Sons*. 1952.

[7] LW Nordheim. "β-decay and the nuclear shell model". *Physical Review* 78.3 (1950), p. 294.

[8] M. H. Brennan and A. M. Bernstein. "jj Coupling Model in Odd-Odd Nuclei". *Phys. Rev.* 120.3 (1960), pp. 927–933.

[9] GD Dracoulis, PM Walker, and FG Kondev. "Review of metastable states in heavy nuclei". *Reports on Progress in Physics* 79.7 (2016), p. 076301.

[10] Philip Walker and George Dracoulis. "Energy traps in atomic nuclei". *Nature* 399.6731 (1999), pp. 35–40.

[11] MR Bhat. "Evaluated nuclear structure data file (ENSDF)". *Nuclear data for science and technology*. Springer. 1992, pp. 817–821.

[12] Georges Audi et al. "The NUBASE evaluation of nuclear and decay properties". *Nuclear physics A* 729.1 (2003), pp. 3–128.

[13] FG Kondev et al. "The NUBASE2020 evaluation of nuclear physics properties". *Chinese Physics C* 45.3 (2021), p. 030001.

[14] Ashok Kumar Jain et al. “Atlas of nuclear isomers”. *Nuclear Data Sheets* 128 (2015), pp. 1–130.

[15] R. Lic ă et al. “Identification of the crossing point at $N = 21$ between normal and intruder configurations”. *Phys. Rev. C* 95.2 (2017), p. 021301.

[16] R. D. Page et al. “Radioactivity of neutron deficient isotopes in the region N>82>Z”. *Phys. Rev. C* 53.2 (Feb. 1996), pp. 660–670.

[17] M Karny et al. “Shell structure beyond the proton drip line studied via proton emission from deformed 141Ho”. *Physics Letters B* 664.1-2 (2008), pp. 52–56.

[18] B. S. Nara Singh et al. “Influence of the *np* interaction on the β decay of ^{94}Pd”. *Phys. Rev. C* 86.4 (Oct. 2012), p. 041301.

[19] I. Mukha et al. “β-delayed proton decay of a high-spin isomer in ^{94}Ag”. *Phys. Rev. C* 70.4 (Oct. 2004), p. 044311.

[20] J. Park et al. “New and comprehensive β- and βp-decay spectroscopy results in the vicinity of ^{100}Sn”. *Phys. Rev. C* 99.3 (Mar. 2019), p. 034313.

[21] A. Lepailleur et al. “Spectroscopy of ^{26}**F** to Probe Proton-Neutron Forces Close to the Drip Line”. *Phys. Rev. Lett.* 110.8 (Feb. 2013), p. 082502.

[22] D Kolev, Duc Thiep Tran, and V Todorov. “Experimental determination of the isomeric yield ratios of 117mg In and 120mg Sb in photonuclear reactions”. *Comptes Rendus de l’Academie Bulgare des Sciences* 47.12 (1994), pp. 49–52.

[23] Tran Duc Thiep et al. “Isomeric yield ratio of 152m1Eu (8-)–152m2Eu (0-) produced in (γ, n) photonuclear reaction in the giant dipole resonance region”. *Journal of Radioanalytical and Nuclear Chemistry* 317.3 (2018), pp. 1263–1271.

[24] SA Karamian et al. “Isomeric to ground state ratio in the 180 Ta m (γ, γ) 180 Ta m, g reaction”. *Physical Review C* 57.4 (1998), p. 1812.

[25] Nguyen Van Do et al. “Measurement of yield ratios for the isomeric pair 137m, gCe in the 141Pr (γ, x) 137m, gCe reactions with bremsstrahlung end-point energies of 50-, 60-, and 70-MeV”. *Radiation Physics and Chemistry* 176 (2020), p. 109016.

[26] Muhammad Nadeem et al. “Measurements of natCd (γ, x) reaction cross sections and isomer ratio of 115m, gCd with the bremsstrahlung end-point energies of 50 and 60 MeV”. *Chinese Physics C* 45.12 (2021), p. 124002.

[27] S Sudar and SM Qaim. "Isomeric cross-section ratio for the formation of Co m, g 58 in neutron, proton, deuteron, and alpha-particle induced reactions in the energy region up to 25 MeV". *Physical Review C* 53.6 (1996), p. 2885.

[28] Alita SERGEY Danagulyan et al. "Investigation of isomeric ratios in high-energy reactions". *Physics of Atomic Nuclei* 76.3 (2013), pp. 349–354.

[29] K Hilgers, S Sudár, and SM Qaim. "Formation of the isomeric pairs Nd 139 m, g and Nd 141 m, g in proton and He 3-particle-induced nuclear reactions". *Physical Review C* 76.6 (2007), p. 064601.

[30] Avinash Agarwal, IA Rizvi, and AK Chaubey. "Excitation function studies of α induced reactions for niobium and preequilibrium effects". *Physical Review C* 65.3 (2002), p. 034605.

[31] Jean-Michel Daugas et al. "Interplay between angular momentum transfer and nuclear structure in the production of isomers at intermediate energies". *Physical Review C* 63.6 (2001), p. 064609.

[32] V. H. Phong et al. "Observation of a μs isomer in $^{134}_{49}\mathrm{In}_{85}$: Proton-neutron coupling "southeast" of $^{132}_{50}\mathrm{Sn}_{82}$". *Phys. Rev. C* 100.1 (July 2019), p. 011302.

[33] Tran Duc Thiep et al. "The isomeric ratio of fragment 135Xe from photofission of 233U induced by 23.5 MeV bremsstrahlung". *Journal of radioanalytical and nuclear chemistry* 285.3 (2010), pp. 511–517.

[34] TD Thiep et al. "Study of isomeric ratios in the photonuclear reactions 121Sb (γ, n) 120m,gSb; 123Sb (γ, n) 122m,gSb and 86Sr (γ, n) 85m,gSr induced by bremsstrahlung in the energy range 15–20 MeV". *Commun. Phys.* 4.3 (1994), pp. 97–102.

[35] Tran Thiep et al. "Study of the isomeric ratios in photonuclear reactions of natural Selenium induced by bremsstrahlungs with end-point energies in the giant dipole resonance region". *Journal of Radioanalytical and Nuclear Chemistry* 292.3 (2012), pp. 1035–1042.

[36] Tran Thiep et al. "The isomeric ratios in photonuclear reactions of natural barium induced by bremsstrahlungs with endpoint energies in the giant dipole resonance region". *Journal of Radioanalytical and Nuclear Chemistry* 292.1 (2012), pp. 89–96.

[37] Tran Duc Thiep et al. “Study of the isomeric ratios in 107 Ag (γ, n) 106m, g Ag reaction of natural silver induced by bremsstrahlungs with endpoint energies in the giant dipole resonance region”. *Journal of Radioanalytical and Nuclear Chemistry* 299.1 (2014), pp. 477–484.

[38] Tran Duc Thiep et al. “On the role of energy separated in fission process, excitation energy and reaction channels effects in the isomeric ratios of fission product 135 Xe in photofission of actinide elements”. *Physics of Particles and Nuclei Letters* 13.4 (2016), pp. 471–479.

[39] N. N. Tsoneva et al. “Population of isomers in the decay of the giant dipole resonance”. *Phys. Rev. C* 61.4 (2000), p. 044303.

[40] Dimitar Kolev. “Studies of some isomeric yield ratios produced with bremsstrahlung”. *Applied radiation and isotopes* 49.8 (1998), pp. 989–995.

[41] TD Thiep et al. “The isomeric ratios in some photonuclear reactions (γ, n),(γ, p),(γ, 2n) and (γ, np) induced by Bremsstrahlung with end-point energies in the giant dipole resonance region”. *Phys Part Nucl Lett* 6.2 (2009), pp. 209–218.

[42] CD Nesaraja, S Sudár, and SM Qaim. “Cross sections for the formation of 69 Zn m, g and 71 Zn m, g in neutron induced reactions near their thresholds: Effect of reaction channel on the isomeric cross-section ratio”. *Physical Review C* 68.2 (2003), p. 024603.

[43] Tran Duc Thiep et al. “Nuclear reactions with 14 MeV neutrons and bremsstrahlungs in giant dipole resonance (GDR) region using small accelerators”. *Nuclear Physics A* 722 (2003), pp. C568–C572.

[44] F Cserpak et al. “Excitation functions and isomeric ratios of the 63Cu (n, α) 60m, gCo, 65Cu (n, α) 60m, gCo and 60Ni (n, p) 60m, gCo processes from 6 to 15 MeV”. *Phys Rev C* 49.3 (1994), pp. 1525–1533.

[45] Syed M Qaim, S Sudar, and A Fessler. “Influence of reaction channel on the isomeric cross-section ratio”. *Radiochimica acta* 93.9-10 (2005), pp. 503–506.

[46] SM Qaim, A Mushtaq, and M Uhl. “Isomeric cross-section ratio for the formation of 73 m, gSe in various nuclear processes”. *Physical Review C* 38.2 (1988), p. 645.

[47] B Strohmaier, M Fassbender, and SM Qaim. “Production cross sections of ground and isomeric states in the reaction systems 93 N b+ 3 He, 92 Mo+ α, and 9 4, 9 5 Mo+ p”. *Physical Review C* 56.5 (1997), p. 2654.

[48] Tran Duc Thiep et al. "Experimental study and theoretical consideration of the isomeric ratio in the photonuclear reaction 197Au (γ, n) 196m,gAu in the giant dipole resonance region". *Physics of Particles and Nuclei Letters* 3.4 (2006), pp. 223–228.

[49] M Huber et al. "Structure of intermediate states in the photoexcitation of the 89Y isomer". *Nuclear Physics A* 559.2 (1993), pp. 253–265.

[50] J. J. Carroll et al. "Intermediate structure in the photoexcitation of $^{77}Se^{m}$, $^{79}Br^{m}$, and $^{137}Ba^{m}$". *Phys. Rev. C* 48.5 (Nov. 1993), pp. 2238–2245.

[51] Tran Duc Thiep et al. "The study of isomeric ratios in photonuclear reactions forming high spin isomers in the giant dipole resonance region". *Communications in Physics* 24.4 (2014), pp. 381–389.

[52] R Vandenbosch and JR Huizenga. "Isomeric Cross-Section Ratios for Reactions Producing the Isomeric Pair Hg197, 197m". *Physical Review* 120.4 (1960), p. 1313.

[53] JR Huizenga and Rt Vandenbosch. "Interpretation of isomeric cross-section ratios for (n, γ) and (γ, n) reactions". *Physical Review* 120.4 (1960), p. 1305.

[54] Yu P Gangrsky et al. "Isomeric Ratios in Crossing (ngamma) and (gamman) Reactions". *Bulletin of the Russian Academy of Sciences: Physics* 65.1 (2001), pp. 121–127.

[55] D Kolev and D Bratovanov. "Interpretation of isomeric ratios obtained in photonuclear reactions". *Comptes Rendus de l'Academie Bulgare des Sciences* 48.7 (1995), pp. 39–42.

[56] AJ Koning, Stephan Hilaire, and M Duijvestijn. "TALYS-1.95 A nuclear reaction program, User manual". *NRG, Netherlands* (2009).

[57] AS Danagulyan et al. "Special features of isomeric ratios in nuclear reactions induced by various projectile particles". *Physics of Atomic Nuclei* 79.3 (2016), pp. 326–334.

[58] Junhua Luo, Suyuan Li, and Li Jiang. "Activation cross section and isomeric cross-section ratio for the 151Eu (n, 2n) 150m, gEu process". *Radiation Physics and Chemistry* 148 (2018), pp. 43–49.

[59] Junhua Luo et al. "Activation cross section and isomeric cross-section ratio for the (n, 2n) reaction on 132,134 Ba". *Radiochimica Acta* 105.10 (2017), pp. 779–787.

[60] Satimbay Palvanov and Turgunali Akhmadzhanov. "Investigation of isomer ratios in the reactions (γ, n) and (n, 2n) on nuclei 76Ge and 82Se". *Bulletin of National University of Uzbekistan: Mathematics and Natural Sciences* 2.4 (2019), pp. 246–256.

[61] SR Palvanov et al. "Excitation of isomeric states in reactions (γ, n) and (n, 2n) on 110Pd nucleus". *World J Res Rev (WJRR)* 5.5 (2017), pp. 28–31.

[62] VM Mazur et al. "Excitation of the 119 Te m, 121 Te m, 123 Te m, 127 Te m, and 129 Te m isomers in (γ, n) reactions from 10 to 22 MeV". *Physical Review C* 87.4 (2013), p. 044604.

[63] AS Danagulyan et al. "Photonuclear reactions on 112,118,124 Sn, natTe, and natHf targets". *Physics of Atomic Nuclei* 77.11 (2014), pp. 1313–1320.

[64] Rajnikant Makwana et al. "New empirical formula for (γ, n) reaction cross section near GDR peak for elements with Z$\leq$60." *Chinese Physics C* 41.4 (2017), p. 044105.

[65] Md Shakilur Rahman et al. "Photonuclear Studies for the Isomeric Yield Ratios in the Production of natFe (γ, xnp) 52m, gMn with 50-, 60-, and 70-MeV Bremsstrahlung". *EPJ Web of Conferences*. Vol. 106. EDP Sciences. 2016, p. 04008.

[66] Haladhara Naik et al. "Measurement of flux-weighted average cross sections for 197Au (γ, xn) reactions and isomeric yield ratios of 196m, gAu with bremsstrahlung". *Nuclear Physics A* 948 (2016), pp. 28–45.

[67] O. M. Vodin et al. "Isomer Ratios in Photonuclear Reactions With Multiple Neutron Emission". *Prob. Atomic Sci. Technol.* 2019.3 (2019), pp. 38–46.

[68] Sea Agostinelli et al. "GEANT4—a simulation toolkit". *Nuclear instruments and methods in physics research section A: Accelerators, Spectrometers, Detectors and Associated Equipment* 506.3 (2003), pp. 250–303.

[69] R.Arthur Forster et al. "MCNP™ Version 5". *Nuclear Instruments and Methods in Physics Research Section B: Beam Interactions with Materials and Atoms* 213 (2004). 5th Topical Meeting on Industrial Radiation and Radioisotope Measurement Applications, pp. 82–86. ISSN: 0168-583X.

[70] Giuseppe Battistoni et al. "Overview of the FLUKA code". *Annals of Nuclear Energy* 82 (2015), pp. 10–18.

[71] Phan Viet Cuong et al. "Theoretical calculation by Talys code in combination with Geant4 simulation for consideration of γ, n reactions of Eu isotopes in the giant dipole resonance region". *Nuclear Instruments and Methods in Physics Research Section B: Beam Interactions with Materials and Atoms* 479 (2020), pp. 68–73.

[72] AR Junghans et al. "Photon data shed new light upon the GDR spreading width in heavy nuclei". *Physics Letters B* 670.3 (2008), pp. 200–204.

[73] A Zilges et al. "Photonuclear reactions—From basic research to applications". *Progress in Particle and Nuclear Physics* 122 (2022), p. 103903.

[74] James Chadwick and Maurice Goldhaber. "A 'Nuclear Photo-effect': Disintegration of the Diplon by γ-Rays". *Nature* 134.3381 (1934), pp. 237–238.

[75] W Bothe and W Gentner. "Atomumwandlungen durchγ-strahlen". *Zeitschrift für Physik* 106.3 (1937), pp. 236–248.

[76] GC Baldwin and GS Klaiber. "Photo-fission in heavy elements". *Physical Review* 71.1 (1947), p. 3.

[77] *Gordon research conference on photonuclear physics*. https://www.grc.org/photonuclear-reactions-conference/1959/. 1959.

[78] Ryoichi Hajima. "Status and perspectives of compton sources". *Physics Procedia* 84 (2016), pp. 35–39.

[79] Josef Speth and Adriaan van der Woude. "Giant resonances in nuclei". *Reports on Progress in Physics* 44.7 (1981), p. 719.

[80] A Van der Woude. "GIANT-RESONANCES". English. *Progress in Particle and Nuclear Physics* 18 (1987), pp. 217–293. ISSN: 0146-6410.

[81] A.B. Migdal. "Quantum collective excitation modes in nuclear physics". *J.Phys. (USSR)* 8 (1994), p. 331.

[82] JS Levinger and HA Bethe. "Dipole transitions in the nuclear photo-effect". *Physical Review* 78.2 (1950), p. 115.

[83] BM Spicer. "The giant dipole resonance". *Advances in nuclear physics*. Springer, 1969, pp. 1–78.

[84] M Goldhaber and E Teller. "On nuclear dipole vibrations". *Physical Review* 74.9 (1948), p. 1046.

[85] Helmut Steinwedel, J Hans D Jensen, and Peter Jensen. "Nuclear dipole vibrations". *Physical Review* 79.6 (1950), p. 1019.

[86] PB Moon. "The hard components of scattered gamma-rays". *Proceedings of the Physical Society. Section A* 63.11 (1950), p. 1189.

[87] Yasuyuki Suzuki, Kiyomi Ikeda, and Hiroshi Sato. "New type of dipole vibration in nuclei". *Progress of Theoretical Physics* 83.2 (1990), pp. 180–184.

[88] S Krewald and J Speth. "Pygmy dipole resonances". *International Journal of Modern Physics E* 18.07 (2009), pp. 1425–1451.

[89] Thomas Aumann. "Low-energy dipole response of exotic nuclei". *The European Physical Journal A* 55.12 (2019), pp. 1–14.

[90] Kris Heyde, Peter von Neumann-Cosel, and Achim Richter. "Magnetic dipole excitations in nuclei: Elementary modes of nucleonic motion". *Reviews of Modern Physics* 82.3 (2010), p. 2365.

[91] D Frekers et al. "Spin excitations in the deformed nuclei 154Sm, 158Gd and 168Er". *Physics Letters B* 244.2 (1990), pp. 178–182.

[92] AS Adekola et al. "Discovery of low-lying E 1 and M 1 strengths in Th 232". *Physical Review C* 83.3 (2011), p. 034615.

[93] M Guttormsen et al. "Scissors resonance in the quasicontinuum of Th, Pa, and U isotopes". *Physical Review C* 89.1 (2014), p. 014302.

[94] Josef Speth. *Electric and magnetic giant resonances in nuclei*. Vol. 7. World Scientific, 1991.

[95] MB Chadwick et al. "Pauli-blocking in the quasideuteron model of photoabsorption". *Physical Review C* 44.2 (1991), p. 814.

[96] David O Hunt, Ari Brynjolfsson, and Raymond D Cooper. *Handbook of photonuclear reactions*. Tech. rep. ARMY NATICK LABS MA NATICK United States, 1963.

[97] James Chadwick. "Possible existence of a neutron". *Nature* 129.3252 (1932), pp. 312–312.

[98] *Neutron energy*. https://www.nuclear-power.com/nuclear-power/reactor-physics/atomic-nuclear-physics/fundamental-particles/neutron/neutron-energy/.

[99] Kenneth S Krane. *Introductory nuclear physics*. John Wiley & Sons, 1991.

[100] JJ Schmidt and A Lorenz. "The IAEA nuclear data programme its role in the nuclear community and its services to developing countries" (1980).

[101] Nguyen Van Do et al. "Thermal neutron cross-section and resonance integral of the 186 W (n, γ) 187 W reaction". *Nuclear Instruments and Methods in Physics Research B* 266.6 (2008), pp. 863–871.

[102] Nguyen Thi Hien et al. "Measurements of the thermal neutron cross-section and resonance integral for the 108Pd (n, γ) 109Pd reaction". *Nuclear Instruments and Methods in Physics Research Section B: Beam Interactions with Materials and Atoms* 424 (2018), pp. 37–42.

[103] Walter Hauser and Herman Feshbach. "The inelastic scattering of neutrons". *Physical review* 87.2 (1952), p. 366.

[104] M. Guttormsen et al. "Experimental level densities of atomic nuclei". *Eur. Phys. J. A* 51.12 (2015), p. 170.

[105] H. A. Bethe. "An Attempt to Calculate the Number of Energy Levels of a Heavy Nucleus". *Phys. Rev.* 50.4 (1936), pp. 332–341.

[106] Torleif Ericson. "The statistical model and nuclear level densities". *Advances in Physics* 9.36 (1960), pp. 425–511.

[107] Till von Egidy and Dorel Bucurescu. "Systematics of nuclear level density parameters". *Phys. Rev. C* 72.4 (2005), p. 044311.

[108] T. von Egidy and D. Bucurescu. "Experimental energy-dependent nuclear spin distributions". *Phys. Rev. C* 80.5 (2009), p. 054310.

[109] W Dilg et al. "Level density parameters for the back-shifted fermi gas model in the mass range 40< A< 250". *Nuclear Physics A* 217.2 (1973), pp. 269–298.

[110] A Gilbert and AGW Cameron. "A composite nuclear-level density formula with shell corrections". *Canadian Journal of Physics* 43.8 (1965), pp. 1446–1496.

[111] G A Bartholomew. "Neutron Capture Gamma Rays". *Annual Review of Nuclear Science* 11.1 (1961), pp. 259–302.

[112] R. Capote et al. “RIPL – Reference Input Parameter Library for Calculation of Nuclear Reactions and Nuclear Data Evaluations”. *Nuclear Data Sheets* 110.12 (2009). Special Issue on Nuclear Reaction Data, pp. 3107–3214. ISSN: 0090-3752.

[113] J. Kopecky and M. Uhl. “Test of gamma-ray strength functions in nuclear reaction model calculations”. *Phys. Rev. C* 41.5 (1990), pp. 1941–1955.

[114] J. Kopecky, M. Uhl, and R. E. Chrien. “Radiative strength in the compound nucleus ^{157}Gd”. *Phys. Rev. C* 47.1 (1993), pp. 312–322.

[115] Nguyen Van Do. “Cac phuong phap phan tich hat nhan”. *Nha xuat ban Dai hoc Quoc gia Hanoi* (2004).

[116] OD Maslov and SN Dmitriev. “Use of MT-25 microtron for scientific and applied investigations” (2003).

[117] Tran Duc Thiep. “May gia toc”. *NXB Khoa hoc va Ky thuat* (2002).

[118] AG Belov et al. “Microtron MT-25 and its Areas of Use”. *Workshop on Application of Microtron in Nuclear Physics* 26.4 (1993), pp. 20–25.

[119] N Sodnom et al. *A project of the laboratory of activation analysis on the basis of microtron of MPR*. Tech. rep. Joint Inst. for Nuclear Research, 1989.

[120] E Biémont et al. “Absolute transition probabilities in the spectra of EU II. III-Astrophysical applications”. *Astronomy and Astrophysics* 107 (1982), pp. 166–171.

[121] EP Klochkov and VD Risovany. “Utilization of europium-containing control rods by development of gamma-europium sources”. *Analysis of Risks Associated with Nuclear Submarine Decommissioning, Dismantling and Disposal*. Springer, 1999, pp. 425–432.

[122] AP Tonchev et al. “Deformation on isomeric excitation of Eu isotopes in (γ, n) and (n, γ) reactions”. *Physical Review C* 58.5 (1998), p. 2851.

[123] Bui Minh Hue. “Master Thesis”. *Hanoi University of Science* (2013).

[124] Klaus Debertin and Richard G Helmer. *Gamma-and X-ray spectrometry with semiconductor detectors*. North Holland, 1988. ISBN: 0444871071.

[125] *NIST: X-Ray Mass Attenuation Coefficients - Table 3*. 2019. URL: http://www.nist.gov/pml/x-ray-mass-attenuation-coefficients.

[126] D Montgomery and G Montgomery. "A method for assessing and correcting coincidence summing effects for germanium detector efficiency calibrations". *Journal of Radioanalytical and Nuclear Chemistry* 193.1 (1995), pp. 71–79.

[127] Rene Brun and Fons Rademakers. "ROOT—An object oriented data analysis framework". *Nuclear instruments and methods in physics research section A: accelerators, spectrometers, detectors and associated equipment* 389.1-2 (1997), pp. 81–86.

[128] Tran Duc Thiep et al. "Isomeric yield ratios of 195m, gHg and 197m, gHg in the 196Hg (γ, n) and 198Hg (γ, n) reactions induced by bremsstrahlung energy within giant dipole resonance region". *Nuclear Instruments and Methods in Physics Research Section B: Beam Interactions with Materials and Atoms* 457 (2019), pp. 4–9.

[129] Bui Minh Hue et al. "The isomeric ratios in (n, γ) neutron capture reactions on 108 Pd and 110 Pd nuclei". *Journal of Radioanalytical and Nuclear Chemistry* 326.1 (2020), pp. 503–509.

[130] Bui Minh Hue et al. "Isomeric ratios in neutron capture reaction, induced by thermal, resonant and mixed thermal-resonant neutrons on 114Cd and 116Cd nuclei". *Nuclear Instruments and Methods in Physics Research Section B: Beam Interactions with Materials and Atoms* 502 (2021), pp. 46–53.

[131] Tran Duc Thiep et al. "Investigation of the same isomeric pair, produced from different nuclear reactions". *Nuclear Science and Technology* 10.1 (2020), pp. 1–10.

[132] Tran Duc Thiep et al. "The nuclear channel effect in the isomeric ratio of the reaction products". *Nuclear Science and Technology* 9.1 (2019), pp. 9–20.

[133] Bui Minh Hue and Tran Duc Thiep. "Isomeric ratios in several inverse (γ, n) and (n, γ) reactions". *Proceedings of the International Seminar on Interaction of Neutrons with Nuclei (ISINN-28)* (2021). URL: http://isinn.jinr.ru/proceedings/isinn-28/pdf/Hue_Bui.pdf.

[134] Bui Minh Hue and Tran Duc Thiep. "Isomeric ratios in inverse (γ, n) and (n, γ) reactions on Ce, Cd, Pd and Se targets". *Proceedings of the 7th Academic Conference on Natural Science for Young Scientist, Master and PhD. Student from ASEAN Countries (CASEAN-7)* 7 (2021), pp. 388–396.

[135] Bui Minh Hue and Tran Duc Thiep. "Theoretical consideration of isomeric ratios in some photonuclear reactions induced by bremsstrahlung with endpoint energy in giant dipole resonance region using Talys 1.95 code". *Nuclear Science and Technology* 12.1 (2022), pp. 21–31.

[136] IN Vishnevsky et al. "Isomeric yield ratios in nuclei Ir 190 and Eu 150, 152". *Physical Review C* 79.1 (2009), p. 014615.

[137] AV Varlamov et al. "Atlas of giant dipole resonances". *Parameters and Graphs of Photonuclear Reaction Cross Sections. INDC (NDS)-394, IAEA NDS, Vienna, Austria* (1999), pp. 1–311.

[138] *NuDat3.0 - National Nuclear Data Center, Brookhaven National Laboratory.* URL: https://www.nndc.bnl.gov/nudat3/.

[139] IN Vishnevsky et al. "Excitation of isomeric states in the (γ, n) reactions on the transition nuclei 152 Eu and 184 Re". *Physics of Atomic Nuclei* 62.5 (1999), pp. 880–885.

[140] Tran Duc Thiep et al. "Study of the isomeric ratios in photonuclear reactions of natural platinum induced by end-point bremsstrahlung energies in the giant dipole resonance region". *Journal of Radioanalytical and Nuclear Chemistry* 303.3 (2015), pp. 1857–1864.

[141] Yu P Gangrsky et al. "Isomeric ratios in reactions induced by gamma rays and fast neutrons in the isotopes of Re, Ir, and Au". *Physics of Atomic Nuclei* 67.7 (2004), pp. 1227–1232.

[142] AG Belov et al. *Excitation of high spin isomers in photonuclear reactions.* Tech. rep. Joint Institute for Nuclear Research, 2004.

[143] Tran Duc Thiep et al. "Study on the isomeric ratios in (γ, p)-photonuclear reactions from targets Zr and W in the giant dipole resonance region". *Communications in Physics* 16.3 (2006), pp. 163–169.

[144] Tran Duc Thiep et al. "Channel effect in isomeric ratio of 137m, g Ce produced in different nuclear reactions". *Journal of Radioanalytical and Nuclear Chemistry* 314.3 (2017), pp. 1777–1784.

[145] SM Qaim et al. *Handbook of spectroscopy.* CRC, Boca Raton, 1981.

[146] Junhua Luo, Li Jiang, and Suyuan Li. "Activation cross section and isomeric cross section ratios for the (n, 2n) reaction on Eu153". *Physical Review C* 96.4 (2017), p. 044617.

[147] Tran Thiep et al. "Study of the isomeric ratio of fission product Xe produced in the photo-fission of Th and U induced by end-point bremsstrahlung energy of 13.5 MeV." *Journal of Radioanalytical and Nuclear Chemistry* 303.1 (2015).

[148] H Naik et al. "Isomeric yield ratios of 87m, g Y from different nuclear reactions". *The European Physical Journal A* 50.7 (2014), pp. 1–13.

[149] VA Zheltonozhsky, VM Mazur, and ZM Bigan. "Investigation of the excitation of metastable states of 197 Pt and 197 Hg in (γ, n) and (d, 2 n) reactions". *Physics of Atomic Nuclei* 67.5 (2004), pp. 875–881.

[150] Yoshimi Kasugai et al. "Measurement of activation cross sections for mercury isotopes in the neutron energy range between 13.4 and 14.9 MeV". *Journal of nuclear science and technology* 38.12 (2001), pp. 1048–1056.

[151] RS Tilbury and L Yaffe. "Nuclear isomers Hg197m, g, Hg195m, g and Au196m, g formed by bombardment of gold with protons of energies from 8 to 60 MeV". *Canadian Journal of Chemistry* 41.10 (1963), pp. 2634–2641.

[152] VT Gritsyna et al. "Ratio of the cross sections for the production of the isomer and ground states of nuclei in the (p, n) reaction at the energies from the threshold to 20 MeV". *Sov. Phys. JETP* 17 (1963), pp. 1186–1189.

[153] LF Hansen et al. "Ta181 (p, n) W181 and Au197 (p, n) Hg197 excitation functions between 4 and 13 MeV". *Nuclear Physics* 30 (1962), pp. 389–398.

[154] M Al-Abyad et al. "Cross sections and isomeric cross-section ratios in the interactions of fast neutrons with isotopes of mercury". *Physical Review C* 73.6 (2006), p. 064608.

[155] BS Ishkhanov, VN Orlin, and S Yu Troschiev. "Photonuclear reactions on mercury isotopes in the region of the giant-dipole-resonance energy". *Physics of Atomic Nuclei* 74.5 (2011), pp. 706–713.

[156] BS Ishkhanov and S Yu Troshchiev. "Yields of photonuclear reactions on Hg isotopes under a bremsstrahlung beam with a maximum energy of 29.1 MeV". *Bulletin of the Russian Academy of Sciences: Physics* 75.4 (2011), pp. 566–568.

[157] D De Frenne et al. “Independent isomeric yield ratios and primary angular momenta in the photofission of U 2 3 5, 2 3 8 with 12-30-MeV bremsstrahlung”. *Physical Review C* 29.5 (1984), p. 1777.

[158] Nguyen Van Do et al. “Isomeric yield ratios for the natSb (γ, xn) 120m, g, 122m, gSb reactions measured at 40-, 45-, 50-, 55-, and 60-MeV bremsstrahlung energies”. *Nuclear Instruments and Methods in Physics Research Section B: Beam Interactions with Materials and Atoms* 283 (2012), pp. 40–45.

[159] Md Shakilur Rahman et al. “Measurement of flux-weighted average cross-sections and isomeric yield ratios for 103 Rh (g, xn) reactions in the bremsstrahlung end-point energies of 55 and 60 MeV”. *The European Physical Journal A* 52.7 (2016), pp. 1–12.

[160] Pierre Marmier and Eric Sheldon. *Physics of Nuclei and Particles: Volume II*. Vol. 2. Academic Press, 2013.

[161] Toyoaki Kato and Yoshinaga Oka. “Yields of photonuclear reactions for photon-activation analysis with high-energy bremsstrahlung”. *Talanta* 19.4 (1972), pp. 515–525.

[162] JH Carver, GE Coote, and TR Sherwood. “Isomeric (γ, n) cross section ratios and the spin dependence of the nuclear level density”. *Nuclear Physics* 37 (1962), pp. 449–456.

[163] FMD Attar et al. “Cross-sections for the formation of isomeric pair 75Gem, g through (n, 2n),(n, p) and (n, α) reactions measured over 13.73 MeV to 14.77 MeV and calculated from near threshold to 20 MeV neutron energies”. *Nuclear Physics A* 828.3-4 (2009), pp. 253–266.

[164] R Debuyst and A Vander Stricht. “Excitation functions and yield ratios for the isomeric pair 80Br 80mBr formed in (d, 2n),(α, np),(α, p) and (p, n) reactions on selenium”. *Journal of Inorganic and Nuclear Chemistry* 30.3 (1968), pp. 691–698.

[165] CT Bishop, HK Vonach, and JR Huizenga. “Isomer ratios for some (n, γ) reactions”. *Nuclear Physics* 60.2 (1964), pp. 241–249.

[166] ML Sehgal, HS Hans, and PS Gill. “Thermal neutron cross-sections for producing some isomers”. *Nuclear Physics* 12.3 (1959), pp. 261–268.

[167] SK Mangal and PS Gill. “Thermal neutron activation cross-sections for isomer production”. *Nuclear Physics* 36 (1962), pp. 542–548.

[168] MN Namboodiri et al. "Isomeric cross-section ratios in the (n, γ) reactions on 130Te and 110Pd". *Journal of Inorganic and Nuclear Chemistry* 28.1 (1966), pp. 1–4.

[169] Dac Luc Hoang et al. "Isomeric yield ratios in the productions of Sm 143m, g, Nd 141m, g, Zr 89m, g and Pd 109m, g by 14 MeV neutrons and 15-20.5 MeV bremsstrahlung". *Bulgarian Journal of Physics* 14.2 (1987), pp. 152–156.

[170] D Brune and JJ Schmidt. *Handbook on Nuclear Activation Cross-sections: Neutron, Photon and Charged-particle Nuclear Reaction Cross-section Data*. Vol. 156. International Atomic Energy Agency, 1974.

[171] Richard B Firestone and VS Shirley. *Table of isotopes, 8th edn, CD ROM edition, Version 1.0*. 1996.

[172] AM Goriachev and GL Zalesnyi. "Determination of parameters of the back-shift Fermi gas model from measurement of the average energy in photo-neutron spectra". *Bull USSR Acad Sci* 54.11 (1990), pp. 2240–2243.

[173] LI Schiff. "Energy-angle distribution of thin target bremsstrahlung". *Physical review* 83.2 (1951), p. 252.

[174] S Sudár and SM Qaim. "Cross sections for the formation of Hg 195 m, g, Hg 197 m, g, and Au 196 m, g in α and He 3-particle induced reactions on Pt: Effect of level density parameters on the calculated isomeric cross-section ratio". *Physical Review C* 73.3 (2006), p. 034613.

[175] SF Mughabghab. "Thermal neutron capture cross sections resonance integrals and g-factors". *INDC(NDS)* (2003), p. 440.

[176] *X-Ray Mass Attenuation Coefficients*. https://physics.nist.gov/PhysRefData/XrayMassCoef/tab3.html. 2021.

[177] AM Gicking, K Takahashi, and KS Krane. "Neutron capture cross sections of stable Cd isotopes". *The European Physical Journal A* 55.4 (2019), pp. 1–10.

[178] D Decat and P Del Marmol. "Thermal Neutron Activation Cross Section of 116Cd for the Production of the 117Cd Isomers". *Radiochimica Acta* 6.1 (1966), pp. 29–31.

[179] CW Tang, RL Eng, and CD Coryell. *Isomeric-yield ratios of sup117 Cd in the (n, gamma) and (d, p) reactions*. Tech. rep. Massachusetts Inst. of Tech., Cambridge, 1973.

[180] S Pearlstein and RF Milligan. "Thermal cross section and resonance integrals of cadmium-114". *Nuclear Science and Engineering* 26.2 (1966), pp. 281–282.

[181] R Jo Prestwood and BP Bayhurst. "(n, 2 n) Excitation Functions of Several Nuclei from 12.0 to 19.8 Mev". *Physical Review* 121.5 (1961), p. 1438.

[182] Wen-deh Lu, N Ranakumar, and RW Fink. "Activation Cross Sections for (n, 2 n) Reactions at 14.4 MeV in the Region Z= 40- 60: Precision Measurements and Systematics". *Physical Review C* 1.1 (1970), p. 350.

[183] CS Khurana and HS Hans. "Cross-sections for (n, 2n) reactions at 14.8 MeV". *Nuclear Physics* 28.4 (1961), pp. 560–569.

[184] Emil Beták et al. "Activation cross sections for reactions induced by 14 MeV neutrons on natural tin and enriched 112Sn targets with reference to 111In production via radioisotope generator 112Sn (n, 2n) 111Sn→ 111In". *Radiochimica Acta* 93.6 (2005), pp. 311–326.

[185] Michael Fleming, Jiri Kopecky, and Jean-Christophe Sublet. *Integro-Differential Verification and Validation, FISPACT-II & TENDL-2014 nuclear data libraries.* Culham Centre for Fusion Energy, 2015.

[186] SG Cohen, PS Fisher, and EK Warburton. "Inverse Photonuclear Reactions N 14 (p, γ) O 15 and N 15 (p, γ) O 16 in the Region of the Giant Resonance". *Physical Review* 121.3 (1961), p. 858.

[187] HG Wahsweiler and Walter Greiner. "Angular Distributions for the Inverse Photonuclear Process in Si 28 IN the Eigenchannel Reaction Theory". *Physical Review Letters* 19.3 (1967), p. 131.

[188] M Beard et al. "Photonuclear and radiative-capture reaction rates for nuclear astrophysics and transmutation: 92–100 Mo, 88 Sr, 90 Zr, and 139 La". *Physical Review C* 85.6 (2012), p. 065808.

[189] SR Palvanov. "Cross Section of Excitation of Isomer States 81m,gSe in the Reaction (γ, n) and (n, 2n)". *Journal of Scientific and Engineering Research* (2018), pp. 41–45.

[190] Shoji Nakamura et al. "Thermal-Neutron Capture Cross Sections and Resonance Integrals of the 80Se (n, γ) 81m, 81gSe Reactions". *Journal of nuclear science and technology* 45.2 (2008), pp. 116–122.

[191] Bernard Keisch. "Yield ratios of isomers produced by neutron activation". *Physical Review* 129.2 (1963), p. 769.

[192] S Torrel and KS Krane. "Neutron capture cross sections of 136, 138, 140, 142 Ce and the decays of 137 Ce". *Physical Review C* 86.3 (2012), p. 034340.

[193] A.V Kyryjenko et al. "Investigation of the cadmium nuclei isomers state excitation in the photonuclear reactions". *Uzhgorod University Scientific Herald, Series Physics* 19 (2006), pp. 85–89.

[194] VV Zerkin and B Pritychenko. "The experimental nuclear reaction data (EXFOR): Extended computer database and Web retrieval system". *Nuclear Instruments and Methods in Physics Research Section A: Accelerators, Spectrometers, Detectors and Associated Equipment* 888 (2018), pp. 31–43.

[195] AM Goryachev. "The studying of the photoneutron reactions cross sections in the region of the giant dipole resonance in zinc, germanium, selenium, and strontium isotopes". *Voprosy Teoreticheskoy i Yadernoy Fiziki* 8 (1982), p. 121.

[196] A Leprêtre et al. "A study of the giant dipole resonance in doubly even tellurium and cerium isotopes". *Nuclear Physics A* 258.2 (1976), pp. 350–364.

[197] TJ Boal, EG Muirhead, and DJS Findlay. "The photoneutron cross section of 151Eu, 153Eu and 156Gd in the giant resonance region". *Nuclear Physics A* 406.2 (1983), pp. 257–268.

[198] BL Berman et al. "Giant resonance in deformed nuclei: Photoneutron cross sections for Eu 153, Gd 160, Ho 165, and W 186". *Physical Review* 185.4 (1969), p. 1576.

[199] MG Davydov et al. "Isomeric ratios of photonuclear reaction yields for gamma activation analysis". *Atomnaya Ehnergiya* 58.1 (1985), pp. 47–50.

[200] VM Mazur, IV Sokolyuk, and ZM Bigan. "Transversal cross sections of (. gamma., n) sup m reaction for sup 78, 80'82 Se in region of giant E1-resonance. Poperechnye secheniya reaktsii (gamma, n) sup m dlya yader sup 78'80'82 Se v oblati gigantskogo E1-rezonansa". *Yadernaya Fizika;(USSR)* 54.4 (1991).

[201] Hoang Dac Luc et al. "Isomeric Yield Ratios In The Productions of Sm143m, g Sm143m, g Sm143m, g Sm143m, g by 14 MeV Neutrons and 15-20.5 MeV Bremstrahlungs, Bulg". *J. Phys* 14.2 (1987), pp. 152–156.

[202] VM Mazur, ZM Bigan, and DM Symochko. "Excitation of 109Pd and 112In nuclear isomers in (γ, n) reactions". *Physics of Particles and Nuclei Letters* 5.4 (2008), pp. 374–378.

[203] AG Belov et al. "Excitation of isomeric 1h11/2 states in the reactions (γ, n)". *Physics of Atomic Nuclei* 59.4 (1996), pp. 553–559.

[204] Tran Duc Thiep et al. "Isomeric ratio of 137mCe to 137gCe produced in 138Ce (γ, n) 137m, gCe photonuclear reaction induced by end-point bremsstrahlung energies from 14 to 17, 21 to 23 and at 19 MeV". *Journal of Radioanalytical and Nuclear Chemistry* 311.1 (2017), pp. 887–892.

[205] SR Palvanov and O Razhabov. "Isomer yield ratios of photonuclear reactions at E γmax 25 and 30 MeV". *Atomic Energy* 87.1 (1999), pp. 533–536.

[206] SR Palvanov, FR Egamova, and MI Mamayusupova. "Study Of Isomer Ratio in (n; 2n) and (γ, n) Reactions on the 140Ce Nucleus". *Acta Physica Polonica B, Proceedings Supplement* 14.4 (2021), pp. 827–833.

[207] VM Mazur, ZM Bigan, and PS Derechkej. "Study of the excitation of 11/2- isomeric state of the nucleus 139 Ce in reaction (gamma, n) m in the giant E1-resonance region". *Yaderna Fyizika ta Energetika* 18.2 (2017), pp. 146–150.

[208] N Tsoneva et al. "Isomeric ratios in odd N= 81 isotones". *AIP Conference Proceedings*. Vol. 529. 1. American Institute of Physics. 2000, pp. 753–756.

[209] AG Belov et al. "Excitation of isomeric 1h 11/2 states in nuclear reactions induced by γ rays and neutrons and in beta decay". *Physics of Atomic Nuclei* 64.11 (2001), pp. 1901–1908.

Appendix A

Geant4 simulation codes

Geant4 simulation code written in C++ programming language to mimic the experimental setup and simulate the bremsstrahlung and neutron energy flux is given in this Appendix

A.1 Main program

```
#include "B1DetectorConstruction.hh"
#include "B1ActionInitialization.hh"
#include "Shielding.hh"
#ifdef G4MULTITHREADED
#include "G4MTRunManager.hh"
#else
#include "G4RunManager.hh"
#endif
#include "G4UImanager.hh"
#include "B3PhysicsList.hh"
#include "G4VisExecutive.hh"
#include "G4UIExecutive.hh"
#include "Randomize.hh"
#include "Shielding.hh"
int main(int argc,char** argv)
{
#ifdef G4MULTITHREADED
  G4MTRunManager* runManager = new G4MTRunManager;
  runManager->SetNumberOfThreads(16);
#else
```

```
  G4RunManager* runManager = new G4RunManager;
#endif
  runManager->SetUserInitialization(new B1DetectorConstruction
     ());
  runManager->SetUserInitialization(new Shielding);
  runManager->SetUserInitialization(new B1ActionInitialization
     ());
  runManager->Initialize();
  G4VisManager* visManager = new G4VisExecutive;
  G4UImanager* UImanager = G4UImanager::GetUIpointer();
  if (argc!=1)
    {
      G4String command = "/control/execute ";
      G4String fileName = argv[1];
      UImanager->ApplyCommand(command+fileName);
    }
  else {
G4UIExecutive* ui = 0;
      if ( argc == 1 ) {
        ui = new G4UIExecutive(argc, argv);
      }
        UImanager->ApplyCommand("/control/execute init_vis.mac
           ");
        ui->SessionStart();
        delete ui;
  }
  delete visManager;
  delete runManager;
}
```

A.2 Geometry declaration

A.2.1 Bremsstrahlung irradiation

```
#include "B1DetectorConstruction.hh"
#include "G4RunManager.hh"
#include "G4NistManager.hh"
#include "G4Box.hh"
#include "G4Tubs.hh"
#include "G4LogicalVolume.hh"
#include "G4PVPlacement.hh"
#include "G4RotationMatrix.hh"
#include "G4Transform3D.hh"
#include "G4SDManager.hh"
#include "G4MultiFunctionalDetector.hh"
#include "G4VPrimitiveScorer.hh"
#include "G4PSEnergyDeposit.hh"
#include "G4VisAttributes.hh"
#include "G4PhysicalConstants.hh"
#include "G4SystemOfUnits.hh"
#include "G4SubtractionSolid.hh"
#include "G4GeometryManager.hh"
#include "G4PhysicalVolumeStore.hh"
#include "G4LogicalVolumeStore.hh"
#include "G4SolidStore.hh"
#include "G4UnionSolid.hh"
#define N_CHAMBER 4
#define N_SAMPLE 121*3
#define N_SAMPLE_ONE 121

B1DetectorConstruction::B1DetectorConstruction()
: G4VUserDetectorConstruction(),
  fScoringVolume(0) { }
B1DetectorConstruction::~B1DetectorConstruction() { }
G4VPhysicalVolume* B1DetectorConstruction::Construct()
{
    G4NistManager* nist = G4NistManager::Instance();
```

```
G4bool checkOverlaps = true;
G4double world_sizeXY = 40.*cm;
G4double world_sizeZ  = 80.*cm;
G4Material* world_mat = nist->FindOrBuildMaterial("
   G4_Galactic");
G4Box* solidWorld =
        new G4Box("World",
                  0.5*world_sizeXY, 0.5*world_sizeXY, 0.5*
                     world_sizeZ);
G4LogicalVolume* logicWorld =
        new G4LogicalVolume(solidWorld,
                            world_mat,
                            "World");
G4VPhysicalVolume* physWorld =
        new G4PVPlacement(0, G4ThreeVector(), logicWorld,
           "World", 0, false, 0, checkOverlaps);
G4double primTar_sizeR = 25.*mm;
G4double primTar_sizeZ  = 2.*mm;
G4Tubs* primTar =
        new G4Tubs("PrimaryTarget",0, primTar_sizeR,
           primTar_sizeZ/2,0,twopi);
G4Material* primTar_mat = nist->FindOrBuildMaterial("G4_W
   ");
G4LogicalVolume* logicPrimTar =
        new G4LogicalVolume(primTar, primTar_mat, "
           PrimaryTarget");
G4double primTarZpos=0*mm;
new G4PVPlacement(0, G4ThreeVector(0,0,primTarZpos),
   logicPrimTar, "PrimaryTarget", logicWorld, false, 0,
   checkOverlaps);
G4double nhom_sizeR = 25.*mm;
G4double nhom_sizeZ  = 20.*mm;
G4Tubs* nhom =
```

```
            new G4Tubs("Nhom", 0, nhom_sizeR,nhom_sizeZ/2,0,
                twopi);
    G4Material* nhom_mat = nist->FindOrBuildMaterial("G4_Al");
    G4LogicalVolume* logicNhom =
            new G4LogicalVolume(nhom, nhom_mat, "Nhom");
    G4double nhomZpos=nhom_sizeZ/2. + primTar_sizeZ/2.;
    new G4PVPlacement(0, G4ThreeVector(0,0,nhomZpos),
        logicNhom, "Nhom", logicWorld, false, 0, checkOverlaps)
        ;
    G4double secTar_sizeR = 5.*mm;
    G4double secTar_sizeZ  = 0.05*mm;
    G4Tubs* secTar =
            new G4Tubs("SecondaryTarget", 0, secTar_sizeR,
                secTar_sizeZ/2, 0, twopi);
    G4Material* secTar_mat = nist->FindOrBuildMaterial("G4_Eu
        ");
    G4LogicalVolume* logicSecTar =
            new G4LogicalVolume(secTar, secTar_mat, "
                SecondaryTarget");
    G4double distanceSecTar=3.*cm;
    G4double secTarZpos = primTar_sizeZ/2+nhom_sizeZ+
        distanceSecTar+secTar_sizeZ/2.;
    new G4PVPlacement(0, G4ThreeVector(0,0,secTarZpos),
        logicSecTar, "SecondaryTarget", logicWorld, false, 0,
        checkOverlaps);
    fScoringVolume = logicSecTar;
    return physWorld;
}
```

A.2.2 Neutron irradiation

```
#include "B1DetectorConstruction.hh"
#include "G4RunManager.hh"
#include "G4NistManager.hh"
```

```
#include "G4Box.hh"
#include "G4Tubs.hh"
#include "G4LogicalVolume.hh"
#include "G4PVPlacement.hh"
#include "G4RotationMatrix.hh"
#include "G4Transform3D.hh"
#include "G4SDManager.hh"
#include "G4MultiFunctionalDetector.hh"
#include "G4VPrimitiveScorer.hh"
#include "G4PSEnergyDeposit.hh"
#include "G4VisAttributes.hh"
#include "G4PhysicalConstants.hh"
#include "G4SystemOfUnits.hh"
#include "G4SubtractionSolid.hh"
#include "G4GeometryManager.hh"
#include "G4PhysicalVolumeStore.hh"
#include "G4LogicalVolumeStore.hh"
#include "G4SolidStore.hh"
#include "G4UnionSolid.hh"
#define N_CHAMBER 4
#define N_SAMPLE 121*3
#define N_SAMPLE_ONE 121

B1DetectorConstruction::B1DetectorConstruction()
: G4VUserDetectorConstruction(),
  fScoringVolume(0) { }
B1DetectorConstruction::~B1DetectorConstruction() { }
G4VPhysicalVolume* B1DetectorConstruction::Construct()
{
     G4GeometryManager::GetInstance()->OpenGeometry();
     G4PhysicalVolumeStore::GetInstance()->Clean();
     G4LogicalVolumeStore::GetInstance()->Clean();
     G4SolidStore::GetInstance()->Clean();
  G4NistManager* nist = G4NistManager::Instance();
```

```
G4bool checkOverlaps = true;
G4double world_sizeXY = 200.*cm;
G4double world_sizeZ  = 200.*cm;
G4Material* world_mat = nist->FindOrBuildMaterial("
    G4_Galactic");
G4Box* solidWorld =
  new G4Box("World",0.5*world_sizeXY, 0.5*world_sizeXY, 0.5*
      world_sizeZ);
G4LogicalVolume* logicWorld =
  new G4LogicalVolume(solidWorld, world_mat, "World");
G4VPhysicalVolume* physWorld =
  new G4PVPlacement(0, G4ThreeVector(), logicWorld, "World",
       0, false, 0, checkOverlaps);
G4double GM_sizeXY = 120.*cm;
G4double GM_sizeZ  = 120.*cm;
G4Material* GM_mat = nist->FindOrBuildMaterial("G4_GRAPHITE
    ");
G4Box* solidGM =
  new G4Box("GraphiteModerator", 0.5*GM_sizeXY, 0.5*
      GM_sizeXY, 0.5*GM_sizeZ);
G4LogicalVolume* logicGM =
  new G4LogicalVolume(solidGM, GM_mat, "GraphiteModerator");
G4VPhysicalVolume* physGM=new G4PVPlacement(0, G4ThreeVector
    (0,0,0),"GraphiteModeratorPV", logicGM, physWorld, false,
     0, checkOverlaps);
G4double BP_sizeR = 3.*cm;
G4double BP_sizeZ  = 60*cm-0.5*cm;
G4Material* BP_mat = nist->FindOrBuildMaterial("G4_Galactic
    ");
G4Tubs* solidBP =
  new G4Tubs("BeamPipe", 0, BP_sizeR,BP_sizeZ/2,0,twopi);
G4LogicalVolume* logicBP =
        new G4LogicalVolume(solidBP, BP_mat, "
            BeriliumChamber");
```

```
G4double BP_posZ = GM_sizeZ/2 - BP_sizeZ/2;
new G4PVPlacement(0, G4ThreeVector(0,0,BP_posZ), "
    BeriliumChamberPV", logicBP, physGM, false, 0,
    checkOverlaps);
G4double BeC_sizeY = 20.*cm;
G4double BeC_sizeXZ  = 50.*cm;
G4Material* BeC_mat = nist->FindOrBuildMaterial("G4_Be");
G4Box* solidBeC =
          new G4Box("BeriliumChamber",                0.5*
              BeC_sizeXZ, 0.5*BeC_sizeY, 0.5*BeC_sizeXZ);
G4Tubs* solidBP_4sub =
   new G4Tubs("BeamPipe_4sub", 0, BP_sizeR,BP_sizeZ/2,0,twopi
       );
G4VSolid* solidBeC_sub  = new G4SubtractionSolid("
    BeriliumChamber-BeamPipe", solidBeC, solidBP_4sub, 0,
    G4ThreeVector(0.,0.,BP_posZ));
G4LogicalVolume* logicBeC =
          new G4LogicalVolume(solidBeC_sub, BeC_mat, "
              BeriliumChamber");
G4PVPlacement* physBeC = new G4PVPlacement(0, G4ThreeVector
    (0,0,0), "BeriliumChamberPV", logicBeC, physGM, false, 0,
     checkOverlaps);
G4double UTar_sizeR = 1*cm;
G4double UTar_sizeZ  = 1.*cm;
//G4Material* UTar_mat = nist->FindOrBuildMaterial("G4_U");
G4Material* UTar_mat = nist->FindOrBuildMaterial("G4_U");
G4double* isoi=UTar_mat->GetElement(0)->
    GetRelativeAbundanceVector();
size_t niso=UTar_mat->GetElement(0)->GetNumberOfIsotopes();
G4cout<<"NIST NATURAL URANIUM"<<G4endl;
for (G4int i=0;i<niso;i++)
{G4cout<<UTar_mat->GetElement(0)->GetIsotope(i)->GetName()
    <<" - fraction = "<<isoi[i]<<G4endl;}
G4Tubs* solidUTar =
```

```
  new G4Tubs("UraniumTarget", 0, UTar_sizeR,UTar_sizeZ/2,0,
      twopi);
G4LogicalVolume* logicUTar =
        new G4LogicalVolume(solidUTar, UTar_mat, "
            UraniumTarget");
new G4PVPlacement(0, G4ThreeVector(0,0,0), "UraniumTargetPV
    ", logicUTar, physBeC, false, 0, checkOverlaps);
G4double SC_sizeY = 2.*cm;
G4double SC_sizeXZ  = 50.*cm;
G4Material* SC_mat = nist->FindOrBuildMaterial("G4_AIR");
G4Box* solidSC[N_CHAMBER];
G4LogicalVolume* logicSC[N_CHAMBER];
G4VPhysicalVolume* physSC[N_CHAMBER];
G4double SC_posY[]={-30*cm,-15*cm,15*cm,30*cm};
G4double Sample_R_out = 1.*cm;
G4double Sample_R_in = 0.*cm;
G4double Sample_Z = 1.5*cm;
G4Tubs* solidSample[N_SAMPLE];
G4LogicalVolume* logicSample[N_SAMPLE];
G4double Sample_posXpos[]={-24*cm,-19*cm,-14*cm, -9*cm, -4*
    cm,0*cm, 4*cm, 9*cm,14*cm,19*cm, 24*cm};
G4double Sample_posZpos[]={-24*cm,-19*cm,-14*cm, -9*cm, -4*
    cm,0*cm, 4*cm, 9*cm,14*cm,19*cm, 24*cm};
G4Material* Sample_mat = nist->FindOrBuildMaterial("G4_Cd");
for (G4int i=0;i<N_CHAMBER;i++){
    char tmp[50];
    sprintf(tmp,"_%d",i);
    G4String tmpid=(G4String) tmp;
    solidSC[i] =
            new G4Box("SampleChamber"+tmpid, 0.5*SC_sizeXZ,
                0.5*SC_sizeY, 0.5*SC_sizeXZ);
    logicSC[i] =
            new G4LogicalVolume(solidSC[i], SC_mat, "
                SSSSampleChamber"+tmpid);
```

```
    physSC[i] = new G4PVPlacement(0, G4ThreeVector(0,SC_posY
        [i],0), "SampleChamberPV"+tmpid, logicSC[i], physGM,
        false, 0, checkOverlaps);
}
G4int nn = N_SAMPLE_ONE;
G4int n = (G4int) sqrt(N_SAMPLE_ONE);
G4int nchamberwsample = 3;
G4int chamberids[] ={0,2,3};
for (G4int i=0;i<nchamberwsample;i++){
    for (G4int k=0;k<nn;k++){
        G4int j = i*N_SAMPLE_ONE+k;
        G4int xx = k/n;
        G4int zz = k%n;
        char tmp[50];
        sprintf(tmp,"_%d",j);
        G4String tmpid=(G4String) tmp;
        solidSample[j] =
                new G4Tubs("SampleSolid"+tmpid, Sample_R_in,
                    Sample_R_out,Sample_Z/2,0,twopi);
        logicSample[j] =
                new G4LogicalVolume(solidSample[j],
                    Sample_mat, "Sample"+tmpid);
        G4RotationMatrix* rotM = new G4RotationMatrix;
        rotM->rotateX(90.*deg);
        new G4PVPlacement(rotM, G4ThreeVector(Sample_posXpos
            [xx],0,-Sample_posZpos[zz]), "SamplePV"+tmpid,
            logicSample[j], physSC[chamberids[i]], false, 0,
            checkOverlaps);
    }
}
fScoringVolume = logicSC[0];
  for (G4int i=0;i<N_SAMPLE;i++){
        logicSample[i]->SetVisAttributes(Yellow);
  }
```

```
  return physWorld;
}
```

A.3 Stepping Actions

```
#include "B1SteppingAction.hh"
#include "B1EventAction.hh"
#include "B1DetectorConstruction.hh"
#include "G4Step.hh"
#include "G4Event.hh"
#include "G4RunManager.hh"
#include "G4LogicalVolume.hh"
#include "G4SystemOfUnits.hh"
#include "g4root.hh"

B1SteppingAction::B1SteppingAction(B1EventAction* eventAction)
: G4UserSteppingAction(),
  fEventAction(eventAction),
  fScoringVolume(0)
{}
B1SteppingAction::~B1SteppingAction()
{}
void B1SteppingAction::UserSteppingAction(const G4Step* step)
{
  if (!fScoringVolume) {
    const B1DetectorConstruction* detectorConstruction
      = static_cast<const B1DetectorConstruction*>
        (G4RunManager::GetRunManager()->
           GetUserDetectorConstruction());
    fScoringVolume = detectorConstruction->GetScoringVolume();
  }
  G4LogicalVolume* volume
    = step->GetPreStepPoint()->GetTouchableHandle()
```

```
        ->GetVolume()->GetLogicalVolume();//prestep on Primary
            target
    if (volume != fScoringVolume) return;
    G4double preE=step->GetPreStepPoint()->GetKineticEnergy();
    if (step->GetPreStepPoint()->GetStepStatus()==fGeomBoundary
       &&step->GetTrack()->GetDefinition()->GetParticleName()=="
       gamma"&&preE>0){
         //G4cout<<"eeee"<<preE<<G4endl;
         G4AnalysisManager* analysisManager = G4AnalysisManager::
            Instance();
         analysisManager->FillNtupleDColumn(0,0);
         analysisManager->FillNtupleDColumn(1,preE);
         analysisManager->AddNtupleRow();
    }
    G4double edepStep = step->GetTotalEnergyDeposit();
    fEventAction->AddEdep(edepStep);
}
```

A.4 Run Actions

A.4.1 Bremsstrahlung irradiation

```
    #include "B1RunAction.hh"
#include "PrimaryGeneratorAction.hh"
#include "B1DetectorConstruction.hh"
// #include "B1Run.hh"
#include "G4RunManager.hh"
#include "G4Run.hh"
#include "G4AccumulableManager.hh"
#include "G4LogicalVolumeStore.hh"
#include "G4LogicalVolume.hh"
#include "G4UnitsTable.hh"
#include "G4SystemOfUnits.hh"
#include "G4GeneralParticleSource.hh"
```

```
class G4GeneralParticleSource;
B1RunAction::B1RunAction()
: G4UserRunAction(),
  fEdep(0.),
  fEdep2(0.)
{
  // Register accumulable to the accumulable manager
  G4AccumulableManager* accumulableManager =
      G4AccumulableManager::Instance();
  accumulableManager->RegisterAccumulable(fEdep);
  accumulableManager->RegisterAccumulable(fEdep2);
  G4AnalysisManager* analysisManager=G4AnalysisManager::
      Instance();
  analysisManager->CreateNtuple("BremSpec","step Inform");
  analysisManager->CreateNtupleDColumn("id");
  analysisManager->CreateNtupleDColumn("E");
  analysisManager->FinishNtuple();
}
B1RunAction::~B1RunAction()
{}
void B1RunAction::BeginOfRunAction(const G4Run*)
{
  G4RunManager::GetRunManager()->SetRandomNumberStore(false);
  G4AccumulableManager* accumulableManager =
      G4AccumulableManager::Instance();
  accumulableManager->Reset();
  G4AnalysisManager* analysisManager = G4AnalysisManager::
      Instance();
  G4String fileName = "result";
  analysisManager->OpenFile(fileName);
}
void B1RunAction::EndOfRunAction(const G4Run* run)
{
```

```
G4int nofEvents = run->GetNumberOfEvent();
if (nofEvents == 0) return;
G4AccumulableManager* accumulableManager =
   G4AccumulableManager::Instance();
accumulableManager->Merge();
G4double edep  = fEdep.GetValue();
G4double edep2 = fEdep2.GetValue();
G4double rms = edep2 - edep*edep/nofEvents;
if (rms > 0.) rms = std::sqrt(rms); else rms = 0.;
const B1DetectorConstruction* detectorConstruction
 = static_cast<const B1DetectorConstruction*>
   (G4RunManager::GetRunManager()->
      GetUserDetectorConstruction());
G4double mass = detectorConstruction->GetScoringVolume()->
   GetMass();
G4double dose = edep/mass;
G4double rmsDose = rms/mass;
const PrimaryGeneratorAction* generatorAction
 = static_cast<const PrimaryGeneratorAction*>
   (G4RunManager::GetRunManager()->
      GetUserPrimaryGeneratorAction());
G4String runCondition;
if (generatorAction)
{
  const G4GeneralParticleSource* particleGun =
     generatorAction->GetParticleGun();
  runCondition += particleGun->GetParticleDefinition()->
     GetParticleName();
  runCondition += " of ";
  G4double particleEnergy = particleGun->GetParticleEnergy()
     ;
  runCondition += G4BestUnit(particleEnergy,"Energy");
}
```

```
  G4AnalysisManager* analysisManager = G4AnalysisManager::
      Instance();
  analysisManager->Write();
  analysisManager->CloseFile();
  if (IsMaster()) {
    G4cout
     << G4endl
     << "--------------------End of Global Run
         ------------------------------";
  }
  else {
    G4cout
     << G4endl
     << "--------------------End of Local Run
         ------------------------------";
  }
}
void B1RunAction::AddEdep(G4double edep)
{
  fEdep  += edep;
  fEdep2 += edep*edep;
}
```

A.4.2 Neutron irradiation

```
#include "B1SteppingAction.hh"
#include "B1EventAction.hh"
#include "B1DetectorConstruction.hh"
#include "G4Step.hh"
#include "G4Event.hh"
#include "G4RunManager.hh"
#include "G4LogicalVolume.hh"
#include "G4SystemOfUnits.hh"
#include "g4root.hh"
```

```
B1SteppingAction::B1SteppingAction(B1EventAction* eventAction)
: G4UserSteppingAction(),
  fEventAction(eventAction),
  fScoringVolume(0) {}
B1SteppingAction::~B1SteppingAction() {}
void B1SteppingAction::UserSteppingAction(const G4Step* step)
{
  if (!fScoringVolume) {
    const B1DetectorConstruction* detectorConstruction
      = static_cast<const B1DetectorConstruction*>
        (G4RunManager::GetRunManager()->
           GetUserDetectorConstruction());
    fScoringVolume = detectorConstruction->GetScoringVolume();
  }
  // get volume of the current step
  G4LogicalVolume* volume
    = step->GetPreStepPoint()->GetTouchableHandle()
      ->GetVolume()->GetLogicalVolume();//prestep on Primary
         target
  G4String volumeName= volume->GetName();
  if (volumeName.substr(0,6) != "Sample") return;
  G4int volumenum=atoi((volumeName.substr(7,volumeName.length
     ()-6)).c_str());
  G4double preE=step->GetPreStepPoint()->GetKineticEnergy()/
     keV;
  if (step->GetTrack()->GetDefinition()->GetParticleName()=="
     neutron"
          &&preE>0){
       //G4cout<<"vol. "<<volumenum<<"- E = "<<preE<<G4endl;
       G4AnalysisManager* analysisManager = G4AnalysisManager::
          Instance();
       analysisManager->FillNtupleDColumn(0,volumenum);
       analysisManager->FillNtupleDColumn(1,preE);
       analysisManager->AddNtupleRow();
```

```
    }
    if (volume != fScoringVolume) return;
    G4double preE=step->GetPreStepPoint()->GetKineticEnergy();
    if (step->GetPreStepPoint()->GetStepStatus()==fGeomBoundary
       &&step->GetTrack()->GetDefinition()->GetParticleName()=="
       gamma"&&preE>0){
         G4AnalysisManager* analysisManager = G4AnalysisManager::
             Instance();
         analysisManager->FillNtupleDColumn(0,0,preE);
         analysisManager->AddNtupleRow(0);
    }
    // collect energy deposited in this step
    G4double edepStep = step->GetTotalEnergyDeposit();
    fEventAction->AddEdep(edepStep);
}
```

Appendix B

Input file of TALYS code

This work has used not only default parameters but also adjusted parameters in TALYS 1.95 code. To calculate the differential cross-section of isotopes of interest, the parameters relating to the level density models and gamma strength functions have also been taken into account. One typical input file consists of the following parameters:

Input keywords for TALYS calculations

\# **General**

projectile g

element Eu

mass 0

energy 8.0 25. 0.1

channels y

\# **Compound nucleus**

compound y

widthmode 1

resonance y

\# **Pre-equilibrium**

preeqmode 2

mpreeqmode 2

preeqspin 1

\# **Gamma emission**

gammax 6

strength 1

strengthM1 2

\# **Level densities**

ldmodel 1

shellmodel 1

spincutmodel 1

Output

outbasic y

fileresidual y

components y

Appendix C

CERN ROOT analysis code to calculate IRs using energy flux spectra from GEANT4 and the cross-section outputs from TALYS

```
#include "TF1.h"
#include "TTree.h"
#include "TFile.h"
#include "TH1.h"
#include "TGraph.h"
TGraph* grc_Ce137g;
TGraph* grc_Ce137m;
TGraph* grflux;

Double_t grc_Ce137g_tf1_f(Double_t *x, Double_t *) { return
   grc_Ce137g->Eval(x[0]);}
Double_t grc_Ce137m_tf1_f(Double_t *x, Double_t *) { return
   grc_Ce137m->Eval(x[0]);}
Double_t grflux_tf1_f(Double_t *x, Double_t *) {
    if (x[0]>25000000) return 0;
    else
        return grflux->Eval(x[0]);}
Double_t grProd_Ce137g_tf1_f(Double_t *x, Double_t *) {
    if (x[0]>25000000) {
```

```
        return 0;
    }else{
        return grc_Ce137g->Eval(x[0])*grflux->Eval(x[0]);
    }
}
Double_t grProd_Ce137m_tf1_f(Double_t *x, Double_t *) {
    if (x[0]>25000000) {
        return 0;
    }else{
        return grc_Ce137m->Eval(x[0])*grflux->Eval(x[0]);
    }
}
void cal()
{
    grc_Ce137g=new TGraph("talyscross_Ce137mg.txt","%lg %lg %*
       lg");
    grc_Ce137m=new TGraph("talyscross_Ce137mg.txt","%lg %*lg %
       lg");
//     grc_Ce137g->Draw("APL");
//     grc_Ce137m->SetLineColor(2);
//     grc_Ce137m->Draw("PLSAME");
    TF1* grc_Ce137g_tf1=new TF1("grc_Ce137g_tf1",
       grc_Ce137g_tf1_f,9000000,30000000);
    TF1* grc_Ce137m_tf1=new TF1("grc_Ce137m_tf1",
       grc_Ce137m_tf1_f,9000000,30000000);
    grc_Ce137g_tf1->SetNpx(2000);
    grc_Ce137m_tf1->SetNpx(2000);
    TFile* f=TFile::Open("hflux_12MeV.root");
    TH1F* hflux = (TH1F*)f->Get("hflux");
    //hflux->Draw();
    Int_t nbins = hflux->GetNbinsX();
    Double_t xx[500];
    Double_t yy[500];
    for (Int_t i=0;i<nbins;i++){
```

```
        xx[i] = hflux->GetBinCenter(i+1);
        yy[i] = hflux->GetBinContent(i+1)/hflux->GetBinWidth
            (1);
    }
    grflux = new TGraph(nbins,xx,yy);
    TF1* grflux_tf1=new TF1("grflux_tf1",grflux_tf1_f
        ,9000000,30000000);
    TF1* grProd_Ce137g_tf1=new TF1("grProd_Ce137g_tf1",
        grProd_Ce137g_tf1_f,9000000,30000000);
    TF1* grProd_Ce137m_tf1=new TF1("grProd_Ce137m_tf1",
        grProd_Ce137m_tf1_f,9000000,30000000);
    //grc_Ce137g_tf1->Draw();
    //grc_Ce137m_tf1->Draw("same");
    grflux_tf1->Draw();
    grProd_Ce137g_tf1->Draw("same");
    grProd_Ce137m_tf1->Draw("same");
    cout<<grProd_Ce137g_tf1->Integral
        (10000000,25000000,0.0001)<<endl;
    cout<<grProd_Ce137m_tf1->Integral
        (10000000,25000000,0.0001)<<endl;
    cout<<grProd_Ce137m_tf1->Integral
        (10000000,25000000,0.0001)/grProd_Ce137g_tf1->Integral
        (10000000,25000000,0.0001)<<endl;
    for (Int_t i=0;i<grc_Ce137g->GetN();i++){
        cout<<grc_Ce137g->GetX()[i]<<"\t"<<grflux_tf1->Eval(
            grc_Ce137g->GetX()[i])<<endl;
    }
}
```

VIỆN HÀN LÂM
KHOA HỌC VÀ CÔNG NGHỆ VN
HỌC VIỆN KHOA HỌC VÀ CÔNG NGHỆ

CỘNG HÒA XÃ HỘI CHỦ NGHĨA VIỆT NAM
Độc lập - Tự do - Hạnh phúc

Số: 2304 /QĐ-HVKHCN

Hà Nội, ngày 29 tháng 12 năm 2022

QUYẾT ĐỊNH
Về việc thành lập Hội đồng đánh giá luận án tiến sĩ cấp Học viện

GIÁM ĐỐC
HỌC VIỆN KHOA HỌC VÀ CÔNG NGHỆ

Căn cứ Quyết định số 2051/QĐ-VHL ngày 29/12/2014 của Chủ tịch Viện Hàn lâm Khoa học và Công nghệ Việt Nam về việc ban hành Quy chế tổ chức và hoạt động của Học viện Khoa học và Công nghệ;

Căn cứ Thông tư số 08/2017/TT-BGDĐT ngày 04/04/2017 của Bộ trưởng Bộ Giáo dục và Đào tạo ban hành Quy chế tuyển sinh và đào tạo trình độ tiến sĩ;

Căn cứ Quyết định số 1948/QĐ-HVKHCN ngày 28/12/2018 của Giám đốc Học viện Khoa học và Công nghệ về việc ban hành Quy định đào tạo trình độ tiến sĩ tại Học viện Khoa học và Công nghệ;

Căn cứ Quyết định số 508/QĐ-HVKHCN ngày 25/6/2018 của Giám đốc Học viện Khoa học và Công nghệ về việc công nhận nghiên cứu sinh;

Căn cứ Quyết định số 2224/QĐ-HVKHCN ngày 23/12/2022 của Giám đốc Học viện Khoa học và Công nghệ về việc gia hạn lần 2 thời gian học tập cho nghiên cứu sinh Bùi Minh Huệ.

Xét đề nghị của Trưởng phòng Đào tạo.

QUYẾT ĐỊNH:

Điều 1. Thành lập Hội đồng đánh giá luận án tiến sĩ cấp Học viện cho nghiên cứu sinh Bùi Minh Huệ, Khoa Vật lý,

Tên đề tài tiếng Việt **Nghiên cứu tỷ số đồng phân và các hiệu ứng liên quan trong phản ứng quang hạt nhân và phản ứng bắt neutron**

Tên đề tài tiếng Anh: **Study of isomeric ratio and related effects in photonuclear and neutron capture reactions**

Chuyên ngành: Vật lý nguyên tử và hạt nhân. Mã số: 9 44 01 06.

Danh sách thành viên Hội đồng đánh giá luận án kèm theo Quyết định này.

Điều 2. Hội đồng có trách nhiệm đánh giá luận án tiến sĩ theo đúng quy chế hiện hành của Bộ Giáo dục và Đào tạo, của Học viện Khoa học và Công nghệ.

Hội đồng tự giải thể sau khi hoàn thành nhiệm vụ.

Điều 3. Trưởng phòng Tổ chức - Hành chính và Truyền thông, Trưởng phòng Đào tạo, Trưởng phòng Kế toán, các thành viên có tên trong danh sách Hội đồng và nghiên cứu sinh có tên tại Điều 1 chịu trách nhiệm thi hành Quyết định này./.

***Nơi nhận*:**
- Như Điều 3;
- Lưu hồ sơ NCS;
- Lưu: VT, ĐT.HK16.

GIÁM ĐỐC

VIỆN HÀN LÂM KHOA HỌC VÀ CÔNG NGHỆ VIỆT NAM
HỌC VIỆN KHOA HỌC VÀ CÔNG NGHỆ

GS. TS. Vũ Đình Lãm

DANH SÁCH HỘI ĐỒNG ĐÁNH GIÁ LUẬN ÁN TIẾN SĨ CẤP HỌC VIỆN

(Kèm theo quyết định số 2304 /QĐ-HVKHCN ngày 29 / 12 /2022 của Giám đốc Học viện Khoa học và Công nghệ)

Cho luận án của nghiên cứu sinh: Bùi Minh Huệ

Tên đề tài tiếng Việt: **"Nghiên cứu tỷ số đồng phân và các hiệu ứng liên quan trong phản ứng quang hạt nhân và phản ứng bắt neutron".**

Tên đề tài tiếng Anh: **"Study of isomeric ratio and related effects in photonuclear and neutron capture reactions".**

Chuyên ngành: Vật lý nguyên tử và hạt nhân. Mã số: 9 44 01 06.

Người hướng dẫn 1: GS.TS. Trần Đức Thiệp,
Viện Vật lý, Viện Hàn lâm KHCNVN.

Người hướng dẫn 2: TS. Sergey Mikhailovich Lukyanov,
Viện Liên hiệp Nghiên cứu Hạt nhân, Dubna, LB Nga

TT	Họ và tên, học hàm, học vị	Chuyên ngành	Cơ quan công tác	Trách nhiệm trong Hội đồng
1	GS.TS. Nguyễn Văn Đỗ	Vật lý nguyên tử và hạt nhân	Trường Đại học Duy Tân, Bộ Giáo dục và Đào tạo	Chủ tịch
2	PGS.TS. Nguyễn Trung Tính	Vật lý nguyên tử và hạt nhân	Cục An toàn Bức xạ Hạt nhân, Bộ Khoa học và Công nghệ	Phản biện 1
3	PGS.TS. Nguyễn Quang Miên	Vật lý nguyên tử và hạt nhân	Viện Khảo cổ học, Viện Hàn lâm KHXHVN	Phản biện 2
4	TS. Lê Xuân Chung	Vật lý nguyên tử và hạt nhân	Viện KH và Kỹ thuật hạt nhân, Viện NL nguyên tử Việt Nam	Phản biện 3
5	TS. Ngô Hải Tân	Vật lý nguyên tử và hạt nhân	Trường Đại học Phenikaa, Bộ Giáo dục và Đào tạo	Ủy viên - Thư ký
6	GS.TS. Lê Hồng Khiêm	Vật lý nguyên tử và hạt nhân	Viện Vật lý, Viện Hàn lâm KHCNVN	Ủy viên
7	PGS.TS. Bùi Văn Loát	Vật lý nguyên tử và hạt nhân	Trường ĐH Khoa học Tự nhiên, Đại học Quốc gia Hà Nội	Ủy viên

(Hội đồng gồm 07 thành viên)./.

(Mẫu 21-HV-BB của HĐ cấp Học viện)

VIỆN HÀN LÂM
KHOA HỌC VÀ CÔNG NGHỆ VN
HỌC VIỆN KHOA HỌC VÀ CÔNG NGHỆ

CỘNG HÒA XÃ HỘI CHỦ NGHĨA VIỆT NAM
Độc lập - Tự do - Hạnh phúc

Hà Nội, ngày 22 tháng 02 năm 2023

BIÊN BẢN CỦA
HỘI ĐỒNG ĐÁNH GIÁ LUẬN ÁN TIẾN SĨ CẤP HỌC VIỆN

Họ và tên NCS: **Bùi Minh Huệ**

Tên đề tài luận án: *"Nghiên cứu tỷ số đồng phân và các hiệu ứng liên quan trong phản ứng quang hạt nhân và phản ứng bắt neutron"*

Chuyên ngành: Vật lý Nguyên tử và Hạt nhân

Mã số: 9440106

Người hướng dẫn: GS. TS. Trần Đức Thiệp, TS. Sergey Mikhailovich Lukyanov

Đại biểu tham dự:

- Phó Giám đốc Học Viện Khoa Học và Công Nghệ, Viện HLKH&CN Việt Nam,
- Đại diện cơ quan của NCS (Trung tâm Vật lý hạt nhân, Viện Vật lý) và các bạn Đồng nghiệp.

Phần I:

1. Đại diện cơ sở đào tạo tuyên bố lý do, đọc quyết định của Giám đốc Học viện Khoa học và Công nghệ về việc thành lập Hội đồng đánh giá luận án tiến sĩ cấp Học viện và đề nghị Chủ tịch Hội đồng điều khiển phiên họp
2. Chủ tịch Hội đồng công bố danh sách thành viên có mặt, thông qua chương trình buổi bảo vệ, đề nghị Thư ký thông báo các điều kiện chuẩn bị cho buổi bảo vệ và đọc lý lịch khoa học của NCS

- Hội đồng đánh giá luận án tiến sĩ cấp học viện cho NCS Bùi Minh Huệ theo Quyết định của Giám đốc Học viện gồm 07 thành viên, các thành viên hội đồng đều có mặt đầy đủ.

3. Thư ký thông báo các điều kiện cho buổi bảo vệ
4. Các thành viên hội đồng và những người tham dự nêu câu hỏi hoặc ý kiến thắc mắc (nếu có) về lý lịch khoa học và quá trình đào tạo của nghiên cứu sinh

- Các thành viên hội đồng và các đại biểu tham dự không có ý kiến thắc mắc nào khác về lý lịch khoa học và quá trình đào tạo của nghiên cứu sinh.

5. Nghiên cứu sinh trình bày nội dung luận án trong thời gian 30 phút.

6. Các phản biện đọc nhận xét và đặt câu hỏi:

Phản biện 1: PGS.TS. Nguyễn Trung Tính- Cục an toàn và bức xạ Hạt nhân, Bộ Khoa học và Công nghệ:

- Đọc bản nhận xét (có Bản nhận xét kèm theo),

- Đặt câu hỏi:

1) Trong tính toán lý thuyết thấy có sự phù hợp với thực nghiệm trong trường hợp của hạt nhân cầu ^{150}Eu nhưng kết quả tính toán lại cao hơn so với thực nghiệm đối với hạt nhân biến dạng ^{152}Eu. Lý do tại sao? Tương tự như vậy đối với hạt nhân ^{195}Hg, ^{197}Hg, tại sao lại chỉ có sự phù hợp đối với hạt nhân ^{195}Hg và dự đoán lý thuyết là thấp hơn so với thực nghiệm đối với hạt nhân ^{197}Hg?

2) Trong phản ứng đối ngẫu, NCS giải thích vì sao tỷ số đồng phân trong phản ứng (γ,n) luôn cao hơn so với trong phản ứng (n, γ)?

3) Trong vùng năng lượng 10-25 MeV mà NCS nghiên cứu, khi tính toán lý thuyết cho hạt nhân ^{109}Pd lại thấy sự phù hợp giữa phần năng lượng thấp nhưng lại khác xa lý thuyết ở phần năng lượng cao hơn, NCS có lý giải gì?

Phản biện 2: PGS.TS. Nguyễn Quang Miên– Viện Khảo cổ học, Viện Hàn lâm Khoa học và Xã hội Việt Nam:

- Đọc bản nhận xét (có Bản nhận xét kèm theo),

- Đặt câu hỏi:

1) Tác giả phát hiện trạng thái đồng phân và xác định được những tỷ số đồng phân mới, lý giải vì sao nhóm tác giả cũ không đo được?

2) Thời gian tồn tại của trạng thái đồng phân có được thảo luận chưa?

Phản biện 3: TS. Lê Xuân Chung Viện Khoa học và kỹ thuật Hạt nhân, Viện năng lượng nguyên tử Việt Nam.

- Đọc bản nhận xét (có Bản nhận xét kèm theo),

- Đặt câu hỏi:

1) Trong luận án, NCS có viết hạt nhân rung chẵn chẵn nhưng tại sao lại nói là do chuyển động của các nucleon hoá trị?

NCS trả lời các câu hỏi của 03 Phản biện

Sau khi nghe 03 Phản biện đọc Bản nhận xét, nêu ý kiến góp ý và đặt câu hỏi, NCS đã trả lời thỏa đáng các câu hỏi (có Bản trả lời các câu hỏi của NCS kèm theo).

7. Các thành viên khác trong Hội đồng đưa ra ý kiến nhận xét và đặt câu hỏi

GS. TS. Nguyễn Văn Đỗ, chủ tịch Hội đồng:

- Đọc Bản nhận xét (có Bản nhận xét kèm theo),

- Đặt câu hỏi:

1) NCS hiểu thế nào là cộng hưởng lưỡng cực khổng lồ?

2) NCS trình bày thế nào là summing out và thế nào là summing in trong coincidence summing?

PGS. TS. Bùi Văn Loát, Ủy viên Hội đồng:

- Đọc Bản nhận xét (có Bản nhận xét kèm theo),

- Đặt câu hỏi:

1) NCS đã có những hiệu chỉnh gì để tăng độ chính xác của kết quả đo?

2) Tỷ số đồng phân có phụ thuộc điều kiện thực nghiệm không?

GS. TS. Lê Hồng Khiêm, Ủy viên Hội đồng:

- Đọc Bản nhận xét (có Bản nhận xét kèm theo),

- Đặt câu hỏi:

1) NCS cho biết vai trò của cân mẫu là gì?

2) Mẫu mà NCS sử dụng có độ tinh khiết là bao nhiêu và nếu nó không tinh khiết 100% thì ảnh hưởng gì đến số liệu?

3) NCS có tính đến hiệu ứng tự che chắn neutron không và nó ảnh hưởng thế nào tới kết quả đo?

TS. Ngô Hải Tân, Thư ký Hội đồng:

- Đọc Bản nhận xét (có Bản nhận xét kèm theo),

- Đặt câu hỏi:

1) Cần chỉnh sửa phần nào cho TALYS và GEANT4 khi muốn mô tả tốt hơn cho hạt nhân không cầu?

NCS trả lời câu hỏi của các thành viên khác trong Hội đồng

Sau khi nghe thành viên khác trong Hội dồng đọc Bản nhận xét, nêu ý kiến góp ý và đặt câu hỏi, NCS đã trả lời thỏa đáng các câu hỏi (có Bản trả lời các câu hỏi của NCS kèm theo).

8. Sau khi NCS trả lời, các ủy viên Hội đồng và những người tham dự không đặt thêm câu hỏi. Phần trả lời của NCS kết thúc.

9. Đại diện tập thể hướng dẫn phát biểu ý kiến bằng văn bản.
   - GS.TS. Trần Đức Thiệp, người hướng dẫn 1 đã phát biểu ý kiến nhận xét, đánh giá tích cực về tinh thần học tập, nghiên cứu và kết quả thu được của NCS (có Văn bản kèm theo).

Phần II: Hội đồng họp riêng để bầu ban kiểm phiếu, bỏ phiếu kín và thảo luận thông qua quyết nghị của Hội đồng

1. Hội đồng đã bầu Ban kiểm phiếu gồm 3 người (1 trưởng ban và 2 ủy viên). Chủ tịch Hội đồng không tham gia ban kiểm phiếu

   Trưởng ban kiểm phiếu: GS. TS. Lê Hồng Khiêm

   Ủy viên ban kiểm phiếu: PGS. TS. Nguyễn Quang Miên

   Ủy viên ban kiểm phiếu: PGS. TS. Bùi Văn Loát.

2. Hội đồng đã thảo luân, đánh giá luận án và bỏ phiếu kín tán thành luận án.

3. Quyết nghị của Hội đồng: Hội đồng đã nhất trí đánh giá:
   1) Các kết quả nghiên cứu thuộc luận án có ý nghĩa khoa học. Các số liệu về tỷ số đồng phân đã thu dược trình bày trong luận án có giá trị ứng dụng thực tiễn.
   2) Phương pháp nghiên cứu và kỹ thuật thực nghiệm sử dụng trong nghiên cứu phù hợp. Trong quá trình nghiên cứu đã thực hiện những hiệu chỉnh cần thiết nhằm nâng cao có độ tin cậy của kết quả.
   3) Đã kết hợp giữa nghiên cứu thực nghiệm với tính toán lý thuyết sử dụng chương trình tính TALYS để so sánh kết quả.
   4) Đã thu được nhiều số liệu về tỷ số đồng phân, trong đó có những số liệu mới (lần đầu tiên được công bố), đóng góp cho thư viện số liệu hạt nhân Quốc tế.
   5) Nội dung và hình thức của luận án đáp ứng yêu cầu của một **luận án Tiến sĩ Vật lý, chuyên ngành Vật lý nguyên tử và Hạt nhân** theo quy định hiện hành của Bộ giáo dục và đào tạo về đào tạo tiến sĩ.

6) Hội đồng yêu cầu NCS chỉnh sửa một số thiếu sót về nội dung và hình thức của luận án như đã được Hội đồng nêu ra trong buổi bảo vệ.

4. **Kiến nghị của Hội đồng**: Căn cứ kết quả bỏ phiếu đánh giá luận án của Hội đồng: 05 phiếu xuất sắc, và 02 phiếu tán thành, Hội đồng Kiến nghị Học viện Khoa học và Công nghệ, Viện Hàn lâm Khoa học và Công nghệ Việt Nam công nhận và cấp bằng tiến sĩ cho NCS: Bùi Minh Huệ sau khi hoàn thiện luận án theo các góp ý của Hội đồng và hoàn tất các thủ tục khác theo quy định.

Nghị quyết của Hội đồng đã được tất cả các thành viên Hội đồng nhất trí thông qua bằng biểu quyết công khai với số phiếu tán thành là 07/07.

Phần III:

1. Trưởng ban kiểm phiếu công bố kết quả đánh giá luận án

   Số phiếu phát ra: 07 phiếu.

   Số phiếu thu về: 07 phiếu.

   Số phiếu hợp lệ: 07 phiếu

   Số phiếu không hợp lệ: 0 phiếu

   Số phiếu tán thành: 07 phiếu

   Số phiếu không tán thành: 0 phiếu

   Số phiếu đánh giá luận án đạt loại xuất sắc: 05 phiếu

2. Chủ tịch Hội đồng đọc quyết nghị của Hội đồng

3. Chủ tịch Hội đồng tuyên bố Hội đồng đã hoàn thành nhiệm vụ và trao lại quyền điều khiển cho Cơ sở đào tạo.

THƯ KÝ	CHỦ TỊCH
TS. Ngô Hải Tân	GS.TS. Nguyễn Văn Đỗ

XÁC NHẬN CỦA CƠ SỞ ĐÀO TẠO

KT. GIÁM ĐỐC
PHÓ GIÁM ĐỐC

HỌC VIỆN KHOA HỌC VÀ CÔNG NGHỆ

Nguyễn Thị Trung

(Mẫu 22-HV-Quyết nghị)

VIỆN HÀN LÂM
KHOA HỌC VÀ CÔNG NGHỆ VN
HỌC VIỆN KHOA HỌC VÀ CÔNG NGHỆ

CỘNG HÒA XÃ HỘI CHỦ NGHĨA VIỆT NAM
Độc lập - Tự do - Hạnh phúc

Hà Nội, ngày 22 tháng 02 năm 2023

QUYẾT NGHỊ CỦA
HỘI ĐỒNG ĐÁNH GIÁ LUẬN ÁN TIẾN SĨ CẤP HỌC VIỆN

Họ và tên NCS: **Bùi Minh Huệ**

Tên đề tài luận án: *"Nghiên cứu tỷ số đồng phân và các hiệu ứng liên quan trong phản ứng quang hạt nhân và phản ứng bắt neutron"*

Chuyên ngành: Vật lý Nguyên tử và Hạt nhân

Mã số: 9440106

Người hướng dẫn: GS. TS. Trần Đức Thiệp, TS. Sergey Mikhailovich Lukyanov

Quyết nghị của Hội đồng

5. Kết quả bỏ phiếu đánh giá luận án của Hội đồng

   Số phiếu hợp lệ: 07 phiếu.

   Số phiếu không hợp lệ: 0 phiếu.

   Số phiếu tán thành: 07 phiếu

   Số phiếu không tán thành: 0 phiếu

   Số phiếu đánh giá luận án đạt loại xuất sắc: 05 phiếu.

6. Ý kiến đánh giá của Hội đồng:

   Sau khi thảo luận và bỏ phiếu kín tán thành luận án, Hội đồng đã nhất trí đánh giá:

   a. Các kết quả nghiên cứu thuộc luận án có ý nghĩa khoa học. Các số liệu về tỷ số đồng phân đã thu được trình bày trong luận án có giá trị ứng dụng thực tiễn.

   b. Phương pháp nghiên cứu và kỹ thuật thực nghiệm sử dụng trong nghiên cứu phù hợp. Trong quá trình nghiên cứu đã thực hiện những hiệu chỉnh cần thiết nhằm nâng cao độ tin cậy của kết quả.

c. Đã kết hợp giữa nghiên cứu thực nghiệm với tính toán lý thuyết sử dụng chương trình tính TALYS để so sánh kết quả.

d. Đã thu được nhiều số liệu về tỷ số đồng phân, trong đó có những số liệu mới (lần đầu tiên được công bố), đóng góp cho thư viện số liệu hạt nhân Quốc tế.

e. Nội dung và hình thức của luận án đáp ứng yêu cầu của một **luận án Tiến sĩ Vật lý, chuyên ngành Vật lý nguyên tử và Hạt nhân** theo quy định hiện hành của Bộ giáo dục và đào tạo về đào tạo tiến sĩ.

f. NCS cần tiếp thu và hoàn thiện luận án theo các ý kiến đóng góp của các thành viên trong Hội đồng trước khi nộp luận án cho Học viện và cho Thư viện Quốc gia Việt Nam.

7. **Hội đồng kiến nghị** Học viện Khoa học và Công nghệ, Viện Hàn lâm Khoa học và Công nghệ Việt Nam công nhận trình độ và cấp bằng tiến sĩ cho NCS Bùi Minh Huệ sau khi hoàn thiện luận án theo các góp ý của Hội đồng và hoàn tất các thủ tục khác theo quy định.
8. Các thành viên trong Hội đồng đã biểu quyết công khai thông qua nghị quyết của Hội đồng với kết quả thông qua là 07/07 thành viên.

THƯ KÝ	CHỦ TỊCH
TS. Ngô Hải Tân	GS.TS. Nguyễn Văn Đỗ

XÁC NHẬN CỦA CƠ SỞ ĐÀO TẠO

KT. GIÁM ĐỐC
PHÓ GIÁM ĐỐC

VIỆN HÀN LÂM KHOA HỌC VÀ CÔNG NGHỆ VIỆT NAM
HỌC VIỆN KHOA HỌC VÀ CÔNG NGHỆ

Nguyễn Thị Trung

(Mẫu 7-HV-Mẫu nhận xét luận án)

BẢN NHẬN XÉT/ PHẢN BIỆN LUẬN ÁN TIẾN SĨ CẤP HỌC VIỆN

Tên đề tài luận án: Study of isomeric ratio and related effects in photonuclear and neutron capture reactions (Nghiên cứu tỷ số đồng phân và các hiệu ứng liên quan trong phản ứng quang hạt nhân và phản ứng bắt neutron).

Chuyên ngành: Vật lý Nguyên tử và Hạt nhân

Mã số: 9440106

Nghiên cứu sinh: Bùi Minh Huệ

Người hướng dẫn: 1. GS.TS. Trần Đức Thiệp

2. TS. Sergey Mikhailovich Lukyanov

Người phản biện: 1. PGS.TS. Nguyễn Trung Tính

2. PGS.TS. Nguyễn Quang Miên

3. TS. Lê Xuân Chung

Người nhận xét: GS.TS. Nguyễn Văn Đỗ

Cơ quan công tác: Trường Đại học Duy Tân.

Nội dung nhận xét:

Luận án được viết bằng tiếng Anh, gồm 04 trang mở đầu và 118 trang nội dung, 22 trang phụ lục bao gồm Phụ lục A (17 trang), Phụ lục B (2 trang) và Phụ lục C (3 trang). NCS sử dụng 09 công bố của tác giả và cộng sự làm nội dung luận án và trích dẫn 209 tài liệu tham khảo, Tóm tắt luận án gồm hai bản, một bản tiếng Anh và một bản tiếng Việt, dài 24 trang.

1. *Tính cần thiết, thời sự, ý nghĩa khoa học và thực tiễn của đề tài luận án.*
   Đề tài luận án có ý nghĩa khoa học trong nghiên cứu vật lý hạt nhân cơ bản. Nghiên cứu tỷ số đồng phân cung cấp những thông tin có giá trị về cấu trúc hạt nhân và về cơ chế của phản ứng hạt nhân. Nhiều hạt nhân đồng phân có giá trị ứng dụng, đặc biệt là trong lĩnh vực y học phóng xạ. Vì vậy, hướng nghiên cứu này đã và đang được quan tâm nghiên cứu cả ở trong và ngoài nước.

2. *Sự không trùng lặp của đề tài nghiên cứu so với các công trình, luận án đã công bố ở trong và ngoài nước; tính trung thực, rõ ràng và đầy đủ trong trích dẫn tài liệu tham khảo.*

Theo những thông tin mà người viết nhận xét có được thì luận án này không trùng lặp với các công trình, luận án đã công bố ở trong và ngoài nước; trích dẫn tài liệu tham khảo trung thực, rõ ràng và đầy đủ.

3. *Sự phù hợp giữa tên đề tài với nội dung, giữa nội dung với chuyên ngành và mã số chuyên ngành.*

Tên đề tài và nội dung phù nhợp với nhau; nội dung phù hợp với chuyên ngành và mã số chuyên ngành.

4. *Độ tin cậy và tính hiện đại của phương pháp đã sử dụng để nghiên cứu.*

Đã tiến hành nghiên cứu thực nghiệm, sử dụng phương pháp kích hoạt phóng xạ kết hợp với đo phổ gamma trễ để xác định hoạt độ của các sản phẩm phản ứng là những đồng vị phóng xạ. Đây là phương pháp đã và đang được sử dụng phổ biến trong nghiên cứu phản ứng hạt nhân thực nghiệm.

Cùng với nghiên cứu thực nghiệm cũng đã tiến hành tính lý thuyết. Việc kết hợp giữa nghiên cứu thực nghiệm với lý thuyết phù hợp với xu thế và yêu cầu nghiên cứu hiện nay, nó không những giúp kiểm tra chéo các kết quả thu được mà còn giúp kiểm định sự phù hợp của các mô hình lý thuyết đã được tiên đoán.

5. *Kết quả nghiên cứu mới của tác giả.*

Luận án thu được nhiều số liệu về tỷ số đồng phân của các cặp hạt nhân đồng phân là sản phẩm của các phản ứng hạt nhân (gamma,n) và (n,gamma) và ghi nhận được một số hiệu ứng liên quan tới tỷ số đồng phân. Trong số những kết quả thu được có một số được đo lần đầu tiên.

6. *Ưu điểm và nhược điểm về nội dung, kết cấu và hình thức của luận án.*

Luận án trình bày rõ ràng, hợp lý những nội dung nghiên cứu đã thực hiện và các kết quả đã thu được. Bố cục của luận án hợp lý và hình thức trình bày đẹp.

Luận án và Tóm tắt luận án cần bổ sung và chỉnh sửa một vài chi tiết sau đây:

6.1. Trong mục 2.1.5 của luận án có trình bày về Hiệu chính trùng phùng tổng (Coincidence summing corections) và phương pháp hiệu chính. Về nội dung này cần trình bày rõ cả hai trường hợp: (1) suming out và (2) summing in cũng như phương pháp hiệu chính cho từng trường hợp.

6.2. Khi trình bày về đo hoạt độ của mỗi đồng vị phóng xạ cần nói cụ thể (những) tia gamma đã được sử dụng.

6.3. Trong bản Tóm tắt luận án tiếng Việt: cần chuyển tất cả các ghi chú bằng bằng tiếng Anh cho các biểu, bảng và hình vẽ sang tiếng Việt.

7. *Nội dung luận án đã được công bố trên tạp chí, kỷ yếu hội nghị khoa học nào và giá trị khoa học của các công trình đã công bố.*

Nội dung luận án đã được công bố:

- 04 bài trên Tạp chí Quốc tế ISI (trong đó 02 trên Tạp chí Nuclear Instruments and Methods in Physics reseach B, 02 trên tạp chí Journal of Radioanalytical and Nuclear Chemistry),

- 03 bài trên Tạp chí trong nước (Nuclear Science and Technology),

- 02 báo cáo đăng trên biên bản Hội nghị (Proceedings).

8. *Kết luận chung cần khẳng định mức độ đáp ứng các yêu cầu đối với một luận án tiến sĩ chuyên ngành. Bản tóm tắt luận án phản ảnh trung thành nội dung cơ bản của luận án hay không; luận án có thể đưa ra bảo vệ cấp Học viện để nhận học vị tiến sĩ được hay không.*

Bản luận án đáp ứng với yêu cầu của một luận án Tiến sĩ chuyên ngành Vật lý Nguyên tử và Hạt nhân, Mã số 9440106. Tóm tắt luận án phù hợp với nội dung luận án. Luận án có thể đưa ra bảo vệ cấp Học viện để nhận học vị Tiến sĩ.

Hà Nội, ngày 27 tháng 01 năm 2023

Xác nhận của cơ quan công tác

BỘ GIÁO DỤC VÀ ĐÀO TẠO
VIỆN NGHIÊN CỨU LÝ THUYẾT VÀ ỨNG DỤNG
TRƯỜNG ĐẠI HỌC DUY TÂN

Vũ Thị Kim Lưu

Người nhận xét

GS.TS. Nguyễn Văn Đỗ
Trường Đại học Duy Tân

BẢN NHẬN XÉT/ PHẢN BIỆN LUẬN ÁN TIẾN SĨ CẤP HỌC VIỆN

Tên đề tài luận án: ***Nghiên cứu tỷ số đồng phân và các hiệu ứng liên quan trong phản ứng quang hạt nhân và phản ứng bắt neutron.***

Chuyên ngành: Vật lý nguyên tử và hạt nhân.

Mã số: 9440106

Nghiên cứu sinh: Bùi Minh Huệ

Người hướng dẫn: GS. TS. Trần Đức Thiệp
TS Sergey Mikhailovich Lukyanov

Người nhận xét: Ngô Hải Tân
Cơ quan công tác: Khoa Khoa học cơ bản, Trường Đại học Phenikaa

Nội dung nhận xét:

- Tính cần thiết, thời sự, ý nghĩa khoa học và thực tiễn của đề tài luận án: Kiến thức về trạng thái isomer là phần quan trọng của vật lý hạt nhân và thiên văn cũng như được sử dụng trong y học hạt nhân, công nghệ pin, laze. Đặc biệt nghiên cứu về các trạng thái isomer của các cặp đồng phân Hg và Eu trong phản ứng quang hạt nhân ở vùng cộng hưởng khổng lồ được trình bày trong luận án này đóng góp thông tin có giá trị về cấu trúc mức hạt nhân và sự phụ thuộc của mật độ mức vào spin đồng thời thêm dữ liệu vào miền dữ liệu hạt nhân còn thiếu và rải rác trong miền năng lượng này.
- Đề tài không có sự trùng lặp với các công trình, luận án đã công bố ở trong và ngoài nước, các tài liệu tham khảo được trích dẫn đầy đủ, rõ ràng, trung thực.
- Tên luận án phù hợp với nội dung được trình bày và phù hợp với chuyên ngành Vật lý Nguyên tử và Hạt nhân.
- Độ tin cậy và tính hiện đại của phương pháp đã sử dụng để nghiên cứu: Đề tài sử dụng số liệu thu được trong thí nghiệm tiến hành bằng máy gia tốc MT-25 Microtron tại phòng thí nghiệm FLNR, JINR, Dubna, Nga, sử dụng phương pháp tính toán với phần mềm TALYS, GEANT4 là những chương trình tính toán hữu dụng, hiện đại, tin cậy của cộng đồng nghiên cứu vật lý hạt nhân.
- Kết quả nghiên cứu mới của tác giả: đóng góp số liệu hạt nhân mới cho cơ sở dữ liệu hạt nhân của thế giới, làm rõ thêm cơ chế phản ứng quang hạt nhân qua sự xuất hiện của trạng thái isomer.
- Ưu điểm và nhược điểm về nội dung, kết cấu và hình thức của luận án: Luận án được trình bày đẹp, rõ ràng. Phần tổng quan khá dài và chi tiết, có thể phân bổ lại để sử dụng một phần làm nội dung cho phần 2.

- Nội dung luận án đã được công bố trên các tạp chí Nuclear Inst. and Methods in Physics Research B, Journal of Radioanalytical and Nuclear Chemistry là các tạp chí uy tín thế giới, đặc biệt tạp chí Nuclear Inst. and Methods in Physics Research B là tạp chí hàng đầu thế giới về khoa học kỹ thuật và công nghệ hạt nhân. Luận án cũng có công bố tại kỷ yếu hội nghị uy tín quốc gia về Công nghệ hạt nhân "Nuclear Science and Technology".
- Kết luận chung: Luận án đáp ứng các yêu cầu đối với một luận án tiến sĩ chuyên ngành; Bản tóm tắt luận án phản ánh được các nội dung cơ bản của luận án; Đề nghị luận án được đưa ra bảo vệ cấp Học viện để nhận học vị tiến sĩ.

Hà Nội, ngày tháng 01 năm 2023

Xác nhận của cơ quan công tác

KT. TRƯỞNG PHÒNG TỔ CHỨC - NHÂN SỰ

TRƯỜNG ĐẠI HỌC PHENIKAA

Phạm Thị Thu Hoài

Người nhận xét

Ngô Hải Tân

CỘNG HÒA XÃ HỘI CHỦ NGHĨA VIỆT NAM
Độc lập- Tự do – Hạnh phúc

BẢN NHẬN XÉT ĐÁNH GIÁ LUẬN ÁN TIẾN SĨ

Của Nghiên cứu sinh: BÙI MINH HUỆ

Với đề tài: **Study of isomeric ratio and related effects in photonuclear and neutron capture reactions**

Ngành: Vật lý nguyên tử và hạt nhân - 9440106

Họ và tên người nhận xét: Nguyễn Trung Tính

Học vị: Tiến sĩ Học hàm: Phó Giáo sư

Chuyên môn: Vật lý hạt nhân

Trách nhiệm trong Hội đồng: Phản biện 1

Ý KIẾN NHẬN XÉT

1. Tính cần thiết, thời sự, ý nghĩa khoa học và thực tiễn của đề tài

Tỷ số đồng phân hạt nhân đã được nghiên cứu từ rất lâu, vì nó có ý nghĩa cả về khoa học và thực tiễn. Về mặt khoa học, từ tỷ số đồng phần cho chúng ta biết thông tin về cấu trúc hạt nhân, cơ chế của phản ứng hạt nhân, lĩnh vực vẫn đang là thách thức với các nhà vật lý hạt nhân. Ngoài ra, tỷ số đồng phân còn có tương quan mật thiết với năng lượng, động lượng góc của hạt; mật độ mức hạt nhân, spin,...Thời gian sống của trạng thái đồng phân trải rộng từ vài nano giây đến nhiều năm. Số lượng hạt nhân đồng phân càng ngày càng được phát hiện nhiều. Luận án nghiên cứu tính toán thực nghiệm tỷ số đồng phân của các phản ứng quang hạt nhân (γ,n) với chùm gamma phát ra từ bức xạ hãm có năng lượng cực đại trong vùng GDR trên các hạt nhân nặng Hg196,198 và Eu152 và phản ứng (n, γ) trên hạt nhân Pd108,110 và Cd114,116 trong vùng năng lượng nhiệt, cộng hưởng và hỗn hợp nhiệt-cộng hưởng; đây là các vấn đề đang được quan tâm.

Bên cạnh đó, về mặt thực tiễn, các hạt nhân đồng phân đang được ứng rộng rộng rãi trong nền kinh tế quốc dân, chẳng hạn trong y tế, chăm sóc sức khỏe cộng đồng; chẳng hạn như trong y học hạt nhân để điều trị hoặc chẩn đoán (Tc99m). Do vậy việc nghiên cứu của đề tài Luận án là cần thiết, khoa học và có tính thời sự.

2. Đề tài Luận án không trùng lặp với các đề tài luận án, các nghiên cứu khoa học khác đã được công bố trong và ngoài nước. Các trích dẫn tài liệu tham khảo trong luận án là đầy đủ, trung thực và rõ ràng.

3. Sự phù hợp giữa tên đề tài với nội dung. Giữa nội dung với chuyên ngành đào tạo

Nội dung của luận án phù hợp với tên đề tài luận án và phù hợp với chuyên ngành đào tạo Vật lý nguyên tử và hạt nhân.

4. Độ tin cậy và tính hiện đại của phương pháp đã sử dụng để nghiên cứu.

Thực hiện đề tài Luận án, tác giả đã sử dụng cách tiếp cận hiện đại trong tính toán tỷ số đồng phân. Thiết bị sử dụng là thiết bị của các phòng thí nghiệm tại cơ sở nghiên cứu hiện đại của nước ngoài, do vậy có độ tin cậy cao.

5. Kết quả nghiên cứu của Luận án:

Thực hiện luận án của mình, tác giả đã tiến hành tính toán tỷ số đồng phân trong phản ứng (γ, n) gây bởi bức xạ hãm với năng lượng từ 10 - 25 MeV trên bia Se, Pd, Ce, Eu và Hg theo các mô hình lý thuyết sử dụng code TALYS 1.95 và công cụ mô phỏng GEANT4 để so sánh với các kết quả thực nghiệm. Từ mẫu mô tả tốt nhất kết quả thực nghiệm có thể rút ra được các thông tin quan trọng liên quan tới cơ chế, cấu trúc mức kích thích, mật độ mức, phân bố spin và một số các thông số khác liên quan tới quá trình tính toán mẫu và cấu trúc hạt nhân.

Ngoài ra, Luận án cũng đã khảo sát một số hiệu ứng ảnh hưởng tới tỷ số đồng phân như: năng lượng kích thích, cấu hình nucleon, sự sai khác về spin và hiệu ứng kênh.

6. Kết quả nghiên cứu mới của Luận án:

Thực hiện Luận án, tác giả đã thu được một số kết quả mới, các kết quả này góp phần làm phong phú kho số liệu hạt nhân của thế giới, cụ thể:

1) Số liệu tỷ số đồng phân thực nghiệm của phản ứng (γ,n) đối với các cặp195m,gHg với bức xạ gamma năng lượng 14 - 24 MeV, cặp197m,gHg với bức xạ gamma năng lượng 18 - 24 MeV, cặp 152m1,m2Eu tại năng lượng gamma 19, 21 và 23 MeV; Đây là các số liệu mới được công bố.
2) Số liệu tỷ số đồng phân thực nghiệm của phản ứng (n,γ), đối với các cặp 115m,g;117m,gCd và 109m,g;111m,gPd gây bởi nơtron hỗn hợp nhiệt và cộng hưởng và tỷ số đồng phân của 111m,gPd gây bởi nơtron cộng hưởng được công bố lần đầu tiên. Những kết quả cho các cặp 195m,g;197m,gHg và 109m,g;111m,gPd, 115m,g;117m,gCd đã được đưa vào thư viện số liệu phản ứng hạt nhân thực nghiệm (EXFOR) của Cơ quan Năng lượng Nguyên tử Quốc tế (IAEA).

7. Ưu điểm, nhược điểm về nội dung, kết cấu và hình thức của luận án, tóm tắt luận án:

a) Ưu điểm của Luận án

Luận án đã tìm hiểu tương đối kỹ về tỷ số đồng phân; các phản ứng quang hạt nhân và phản ứng bắt notron cũng như code Talys.

Luận án đã thực hiện khá nhiều thực nghiệm để xác tỷ số đồng phân với các phản ứng ứng (γ,n) trong vùng năng lượng gamma từ 18-24 MeV, cũng như đối với các phản ứng hạt nhân (n,γ) trong vùng năng lượng nhiệt và Cộng hưởng.

Các kết quả thu được của luận án là các kết quả mới, góp phần làm phong phú kho số liệu hạt nhân thế giới.

Kết cấu của Luận án tương đối khoa học; Tóm tắt Luận án thể hiện đúng tinh thần và nội dung cốt yếu của Luận án.

b) Nhược điểm của luận án

Một số câu văn chưa rõ nghĩa và vẫn còn lỗi chính tả

8. Các công trình khoa học đã công bố của NCS:

- NCS đã sử dụng 09 công trình nghiên cứu khoa học được công bố trong thời gian thực hiện Luận án để hoàn thành Luận án của mình. Các bài báo hoặc báo cáo khoa học tại hội nghị đã thể hiện được nội dung luận án.

- Nội dung của từng bài báo, báo cáo khoa học đều có những tri thức mới biểu thị theo một trong các tiêu chí là: số liệu mới; phương pháp mới; biện luận mới. Các bài báo đều có chất lượng tốt.
- Các tạp chí đăng bài báo của tác giả thể hiện nội dung luận án là các tạp chí có uy tín trong và ngoài nước. Cụ thể:

1. Bui Minh Hue, Tran Duc Thiep, Truong Thi An, Phan Viet Cuong, S. M. Lukyanov, and S. Mitrofanov . Isomeric ratios in neutron capture reaction, induced by thermal, resonant and mixed thermal-resonant neutrons on 114Cd and 116Cd nuclei. Nuclear Inst. and Methods in Physics Research, B 502, pp. 46-53 (2021).

2. Bui Minh Hue, Tran Duc Thiep, Truong Thi An, Phan Viet Cuong, S. M. Lukyanov, A. G. Belov, and S. Mitrofanov. The isomeric ratios in (n, γ) neutron capture reactions on 108P d and 110P d nuclei, Journal of Radioanalytical and Nuclear Chemistry 326, no. 1, 503-509 (2020).

3. Tran Duc Thiep, Truong Thi An, Phan Viet Cuong, Bui Minh Hue, A. G. Belov, S. Mitrofanov. Isomeric yield ratios of 195m,gHg and 197m,gHg in the 196Hg(γ, n) and 198Hg(γ, n) reactions induced by bremsstrahlung energy within giant dipole resonance region, Nuclear Inst. and Methods in Physics Research, B. 457, 4-9 (2019).

4. Tran Duc Thiep, Truong Thi An, Phan Viet Cuong, Nguyen The vinh, Bui Minh Hue, Le Tuan Anh, A. G. Belov. Isomeric yield ratio of 152m1Eu(8-) to 152m2Eu(0-) produced from 153Eu (γ, n) 152Eu reaction in the giant dipole resonance region, J. Radioanal. Nucl. Chem., 317, 1263–1271 (2018).

5. Bui Minh Hue, Tran Duc Thiep. Theoretical consideration of isomeric ratios in some photonuclear reactions induced by bremsstrahlung with endpoint energy in giant dipole resonance region using Talys 1.95 code, Nuclear Science and Technology, Vol.12, No. 1, pp. 21-31 (2022).

6. Tran Duc Thiep, Truong Thi An, Bui Minh Hue, Phan Viet Cuong, Nguyen Hong Ha, A. G. Belov, S. Mitrofanov. Investigation of the same isomeric pair, 120 produced from different nuclear reactions, Nuclear Science and Technology, Vol.10, No. 1, pp. 01-10 (2020).

7. Tran Duc Thiep, Truong Thi An, Bui Minh Hue, Phan Viet Cuong, A. G. Belov, S. Mitrofanov. The nuclear channel effect in the isomeric ratio of the reaction products, Nuclear Science and Technology, Vol.9, No. 1, pp. 09-20 (2019).

8. Bui Minh Hue, Tran Duc Thiep, Isomeric Ratios in Several Inverse (γ, n) and (n, γ) Reactions, Proceedings of 28th International Seminar on Interaction of Neutrons with Nuclei, http://isinn.jinr.ru/proceedings/isinn-28/pdf/HueBui.pdf, (2021).

9. Bui Minh Hue, Tran Duc Thiep, Isomeric Ratios in Inverse (γ, n) and (n, γ) Reactions on Ce, Cd, Pd and Se targets, Proceedings of the 7th Academic Conference on Natural Science for Young Scientist, Master and PhD. Student from ASEAN Countries (CASEAN-7), p388-396 (2021).

8.Kết luận

* Luận án đạt yêu cầu: X *Không đạt yêu cầu:
* Bản tóm tắt Luận án đã phản ánh nội dung cơ bản của Luận án
* Nghiên cứu sinh xứng đáng được công nhận học vị và cấp bằng tiến sĩ.

Xác nhận của cơ quan công tác

BỘ KHOA HỌC VÀ CÔNG NGHỆ
VĂN PHÒNG
CỤC AN TOÀN BỨC XẠ VÀ HẠT NHÂN

Lê Minh Tuấn

Hà Nội, Ngày 25/01/2023

Người nhận xét

Nguyễn Trung Tính

BẢN PHẢN BIỆN LUẬN ÁN TIẾN SĨ CẤP HỌC VIỆN

Tên đề tài luận án: NGHIÊN CỨU TỶ SỐ ĐỒNG PHÂN VÀ CÁC HIỆU ỨNG LIÊN QUAN TRONG PHẢN ỨNG QUANG HẠT NHÂN VÀ PHẢN ỨNG BẮT NEUTRON

Chuyên ngành: **Vật lý Nguyên tử và Hạt nhân**

Mã số: **944 01 06**

Nghiên cứu sinh: **Bùi Minh Huệ**

Người hướng dẫn khoa học 1: GS. TS. Trần Đức Thiệp

Người hướng dẫn khoa học 2: TS. Sergey Mikhailovich Lukyanov

Người phản biện: PGS.TS. Nguyễn Quang Miên

Cơ quan công tác: Viện Hàn lâm Khoa học xã hội Việt Nam, Viện Khảo cổ học

A. Nội dung phản biện:

1. Tính cần thiết, thời sự, ý nghĩa khoa học và thực tiễn của đề tài luận án:

Đồng phân hạt nhân là một hiện tượng vật lý quan trọng của nguyên tử và hạt nhân, nghiên cứu các đặc tính đồng phân hạt nhân sẽ cho chúng ta có những hiểu biết sâu sắc và toàn diện hơn về trạng thái và cấu trúc của hạt nhân nguyên tử, từ đó không những góp phần nâng cao nhận thức chung về cấu tạo thế giới vật chất mà còn trực tiếp góp phần thúc đẩy khoa học công nghệ phát triển và nâng cao đời sống kinh tế xã hội. Trong khoảng vài chục năm gần đây, nhờ những tiến bộ vượt bậc về công nghệ ghi nhận và xử lý số liệu bức xạ hạt nhân, nhiều cơ sở sản xuất chùm đồng vị phóng xạ đã được hình thành với những thành tựu đáng kể về đồng phân hạt nhân, đặc biệt là trong tìm hiểu cấu trúc và tính chất của các hạt nhân lạ nằm xa đường bền, cũng như trong những ứng dụng thực tế về sinh học hạt nhân, y học hạt nhân, nhiên liệu hạt nhân, thời gian hạt nhân... Trong nghiên cứu đồng phân hạt nhân thì tỷ số xác xuất hình thành trạng thái đồng phân và trạng thái cơ bản không bền hay còn gọi là tỷ số đồng phân luôn cung cấp những thông tin giá trị về cấu trúc và cơ chế hạt nhân liên quan. Tỷ số đồng phân liên quan trực tiếp tới cấu trúc và mật độ mức của hạt nhân kích thích, cơ chế phản ứng và nhiều đặc tính khác. Đó luôn là những dữ liệu quý giá để kiểm định các mẫu phản ứng hạt nhân khác nhau. Luận án với 4 mục tiêu chính là:

- Xác định tỷ số đồng phân thực nghiệm của một số hạt nhân trung bình và nặng hình dạng cầu hoặc biến dạng trong phản ứng (γ, n) và (n, γ) tương ứng gây bởi bức xạ hãm và nơtron nhiệt-trên nhiệt.

- Xem xét một số yếu tố ảnh hưởng tới tỷ số đồng phân như năng lượng kích thích, sự sai khác spin, mô men xung lượng, cấu hình nucleon và hiệu ứng kênh.

- Tính toán tỷ số đồng phân theo lý thuyết trong phản ứng (γ, n) bằng việc sử dụng mã TALYS 1.95 và công cụ GEANT4 để so sánh với các kết quả thực nghiệm của luận án và của tác giả khác

- Đóng góp các kết quả thực nghiệm với độ chính xác cao vào ngân hàng dữ liệu hạt nhân để sử dụng cho các nghiên cứu cơ bản và ứng dụng hạt nhân.

Những điều này cho thấy, đề tài luận án của nghiên cứu sinh có ý nghĩa khoa học và thực tiễn, đáp ứng nhu cầu nghiên cứu phát triển ngành Vật lý Nguyên tử và Hạt nhân hiện nay.

2. Sự không trùng lặp của đề tài nghiên cứu so với các công trình, luận án đã công bố ở trong và ngoài nước; tính trung thực, rõ ràng và đầy đủ trong trích dẫn tài liệu tham khảo.

Tác giả luận án đã thực hiện nghiên cứu tỷ số đồng phân (IR) và một số hiệu ứng liên quan trong các phản ứng quang hạt nhân (γ,n) với bức xạ hãm có năng lượng cực đại trong vùng cộng hưởng khổng lồ trên các bia Eu, Hg, Cd, Ce, Se, và Pd và nghiên cứu IR trong phản ứng bắt nơtron nhiệt và trên nhiệt (n,γ) trên các bia Pd, Cd, Ce và Se. Các thí nghiệm đã được thực hiện với nguồn photon hãm và nơtron, tạo ra từ máy gia tốc MT-25 của phòng thí nghiệm Flerow, Dubna (CHLB Nga). Ngoài ra, để đánh giá kết quả thực nghiệm quang hạt nhân (γ,n), các tác giả cũng đã so sánh với những tính toán tỷ số IR theo các mẫu lý thuyết dựa trên mã TALYS 1.95 và công cụ mô phỏng GEANT4. Theo đó, có thể thấy đối tượng và nội dung nghiên cứu của luận án không trùng lặp với các công trình khác đã công bố. Luận án có 209 tài liệu tham khảo và đã được trích dẫn nghiêm túc, trung thực và rõ ràng.

3. Sự phù hợp giữa tên đề tài và nội dung.

Nội dung nghiên cứu của luận án phù hợp tên đề tài luận án và phù hợp với chuyên ngành Vật lý nguyên tử và hạt nhân, mã số 9440106.

4. Độ tin cậy và tính hiện đại của phương pháp đã sử dụng để nghiên cứu:

Luận án đã nghiên cứu các phản ứng quang hạt nhân và phản ứng bắt nơtron bằng phương pháp kích hoạt hạt nhân và đo phổ gamma off-line. Nguồn photon hãm và nơtron được tạo ra từ việc sử dụng máy gia tốc điện tử MT-25 của phòng thí nghiệm phản ứng hạt nhân Flerov (FLNR), JINR thuộc viện nghiên cứu hạt nhân Dubna (CHLB Nga). Đây là phòng thí nghiệm hiện đại có bề dày nghiên cứu lâu năm và có uy tín quốc tế.

Luận án cũng đã những nghiên cứu so sánh đánh giá kết quả thực nghiệm với những tính toán về tỷ số IR theo các mẫu lý thuyết dựa trên mã TALYS 1.95 và công cụ mô phỏng GEANT4, chứng tỏ tác giả luận án luôn có sự tìm hiểu và liên hệ chặt chẽ giữa thực nghiệm và lý thuyết.

Luận án cũng có số lượng đáng kể những tài liệu tham khảo mới công bố trong các năm gần đây. Kết quả nghiên cứu của luận án đã được các tác giả công bố qua 10 bài báo khoa học trên các tạp chí và hội nghị khoa học chuyên ngành có uy tín trong nước và quốc tế.

Theo đó, có thể xác định phương pháp nghiên cứu của luận án là hiện đại và tin cậy, các kết quả công bố trong luận án có giá trị khoa học và thực tiễn.

5. Kết quả nghiên cứu mới của tác giả:

5.1. Thông qua nghiên cứu thực nghiệm về sự phụ thuộc vào năng lượng của tỷ số đồng phân trong phản ứng (γ, n) trong vùng năng lượng cộng hưởng khổng lồ trên các đồng vị Hg, Eu, Cd, Ce, Se và Pd. Luận án đã nhận diện được 7 cặp đồng phân và tính toán tỷ số đồng phân của $^{195m,g;197m,g}$**Hg**, ^{152m1,m2}**Eu**, ^{115m,g}**Cd**, ^{137m,g}**Ce**, ^{81m,g}**Se** và ^{109m,g}**Pd**. Trong đó, các dữ liệu về tỷ số đồng phân thực nghiệm của ^{195m,g}**Hg** từ 14 - 24 MeV, ^{197m,g}**Hg** từ 18 - 24 Mev và ^{152m1,m2}**Eu** tại 19, 21 và 23 Mev lần đầu được công bố.

5.2. Đối với phản ứng (n,γ) trên các đồng vị của **Pd**, **Cd**, **Ce** và **Se** gây bởi nơtron nhiệt và cộng hưởng, luận án đã nhận diện được sáu cặp đồng phân và tính tỷ số đồng phân bao gồm $^{109m,g;111m,g}$**Pd**, $^{115m,g;117m,g}$**Cd**, ^{137m,g}**Ce** và ^{81m,g}**Se**. Trong đó, các dữ liệu về tỷ số đồng phân của $^{115m,g;117m,g}$Cd và $^{109m,g;111m,g}$Pd gây bởi nơtron hỗn hợp nhiệt và cộng hưởng và tỷ số đồng phân của ^{111m,g}Pd gây bởi nơtron cộng hưởng lần đầu được công bố. Đặc biệt nổi bật là các dữ liệu thực nghiệm mới về trạng thái đồng phân của ^{nat}**Eu**(γ, n), ^{152m1,m2}**Eu**, ^{nat}**Hg**(γ, n), $^{195m,g;197m,g}$**Hg**, ^{nat}**Pd**(n, γ), ^{109m,g}**Pd**, and ^{nat}**Cd**(n, γ), $^{115m,g;117m,g}$**Cd**. Trong đó, các kết quả về **Hg**, $^{109m,g;111m,g}$**Pd** đã được Cơ quan Năng lượng Nguyên tử Quốc tế (IAEA) chấp nhận đưa vào thư viện dữ liệu phản ứng hạt nhân thực nghiệm (EXFOR). Người phản biện đánh giá đây là đóng góp mới có ý nghĩa cao của luận án.

5.3. Luận án cũng đã có nghiên cứu một số yếu tố ảnh hưởng tới tỷ số đồng phân hạt nhân, bao gồm năng lượng kích thích, cấu hình nucleon, sự sai khác về spin và hiệu ứng kênh phản ứng, phản ứng đối ngẫu (γ, n) và (n, γ) tạo ra các cặp đồng phân với cùng năng lượng kích thích sản phẩm để thấy được ảnh hưởng của xung và mômen xung lượng như là một phần của hiệu ứng kênh.

5.4. Luận án đã sử dụng công cụ GEANT4 để mô phỏng bức xạ hãm phát ra từ gia tốc điện tử MT-25 và mô hình lý thuyết sử dụng mã TALYS 1.95 để tính toán tỷ số IR trong phản ứng (γ, n) trên bia **Se**, **Pd**, **Ce**, **Eu** và **Hg** với năng lượng bức xạ hãm từ 10 - 25 MeV. Luận án cũng đã khảo sát hàm kích thích với sáu mẫu mật độ mức và tám hàm lực gamma. Từ đó, đã xác định được xu hướng phụ thuộc vào năng lượng của các kết quả tính toán lý thuyết là tương tự đối với kết quả thực nghiệm. Ngoài ra, hiệu ứng cấu hình nucleon cũng được xác nhận trong trường hợp của Hg.

6. Ưu điểm và nhược điểm về nội dung, kết cấu và hình thức của luận án:

Luận án được viết bằng tiếng Anh, bối cục hợp lý, các hình ảnh và biểu bảng rõ ràng, trích dẫn đầy đủ đúng theo quy định. Nội dung nghiên cứu phong phú, thể hiện kết hợp chặt chẽ giữa nghiên cứu thực nghiệm và lý thuyết, cũng như nghiên cứu so sánh với các nghiên cứu của các tác giả khác. Các kết quả thu được đều được lý giải, bình luận và đánh giá khách quan.

Một số góp ý để hoàn thiện hơn. Luận án còn có một số lỗi vi tính, lỗi chế bản nên cần được rà soát và chỉnh sửa. Trong Bảng 3.3 (trang 59) nên cấu trúc lại để có thể thấy rõ ràng hơn những kết quả đóng góp mới của luận. Trong bản tóm tắt tiếng Việt, một số câu văn nên được viết cho rõ nghĩa hơn.

7. Nội dung luận án đã được công bố trên tạp chí, kỷ yếu hội nghị khoa học nào và giá trị khoa học của các công trình đã công bố:

Tập thể tác giả luận án đã có 10 bài báo được công bố trong các tạp chí khoa học chuyên ngành hay kỷ yếu hội thảo khoa học có phản biện đánh giá. Trong đó, có 4 công trình đăng trên tạp chí thuộc hệ thống ISI có chỉ số IF cao, 3 công trình đăng trên tạp chí chuyên ngành uy tín và 2 báo cáo tại 2 Hội nghị khoa học chuyên ngành. Nội dung các bài báo đã phản ánh những kết quả nghiên cứu chính của Luận án và nghiên cứu sinh cũng là người đứng đầu hoặc là tác giả chính của 5 công trình trên.

Kết luận chung: Luận án có nội dung nghiên cứu phong phú, chất lượng tốt, đáp ứng các yêu cầu đối với một luận án tiến sĩ chuyên ngành Vật lý Nguyên tử và Hạt nhân, mã số 9440106. Bản tóm tắt luận án phản ánh trung thành cơ bản nội dung của luận án. Luận án có thể đưa ra bảo vệ cấp Học viện để nhận học vị tiến sĩ.

Hà Nội, ngày tháng 01 năm 2023

Xác nhận của cơ quan công tác

VIỆN KHẢO CỔ HỌC

PHÓ VIỆN TRƯỞNG

Hà Văn Cẩn

Người nhận xét

PGS.TS. Nguyễn Quang Miên

(Mẫu 7-HV-Mẫu nhận xét luận án)

BẢN NHẬN XÉT PHẢN BIỆN LUẬN ÁN TIẾN SĨ CẤP HỌC VIỆN

Tên đề tài luận án: Nghiên cứu tỷ số đồng phân và các hiệu ứng liên quan trong phản ứng quang hạt nhân và phản ứng bắt neutron

Chuyên ngành: Vật lý Nguyên tử và Hạt nhân

Mã số: 9440106

Nghiên cứu sinh: Bùi Minh Huệ

Người hướng dẫn: 1. GS. TS. Trần Đức Thiệp

2. TS. Sergey Mikhailovich Lukyanov

Người phản biện: TS. Lê Xuân Chung

Cơ quan công tác: Viện Khoa học và Kỹ thuật hạt nhân

Nội dung nhận xét:

- *Tính cần thiết, thời sự, ý nghĩa khoa học và thực tiễn của đề tài luận án.*

Nghiên cứu cấu trúc hạt nhân là hướng nghiên cứu quan trọng và cơ bản nhất của Vật lý hạt nhân, trong đó bao gồm nghiên cứu lý thuyết thông qua các mô hình và thực nghiệm thông qua việc đo đạc số liệu hạt nhân. Hai phương pháp nghiên cứu này có vai trò tương hỗ và luôn cần được tiến hành song song. Nếu như các mô hình cho ta khả năng dự đoán cấu trúc hạt nhân thì số liệu hạt nhân là cơ sở để chuẩn hoá và kiểm chứng tính đúng đắn của các mô hình. Thông tin về cấu trúc hạt nhân có thể thu được thông qua việc đo đạc các đặc trưng của phản ứng hạt nhân hoặc của phân rã phóng xạ hạt nhân.

Đề tài trình bày các nghiên cứu thực nghiệm đo đạc số liệu tỉ số đồng phân của cặp: (i) $^{195m,g;\ 197m,g}$Hg và ^{152m1,m2}Eu hình thành từ phản ứng (γ, n) gây bởi bức xạ hãm có năng lượng cự đại trong vùng cộng hưởng lưỡng cực khổng lồ (GDR); (ii) $^{109m,g;\ 111m,g}$Pd và $^{115m,g;117mg}$Cd hình thành từ phản ứng (n, γ) gây bởi chùm nơtron nhiệt, cộng hưởng và nhiệt-cộng hưởng. Trong đó, tỷ số đồng phân thực nghiệm của ^{195m,g}Hg từ 14 - 24 MeV, ^{197m,g}Hg từ 18 - 24 MeV, ^{152m1,m2}Eu tại 19, 21 và 23 MeV; của $^{115m,g;117m,g}$Cd và $^{109m,g;111m,g}$Pd gây bởi nơtron hỗn hợp nhiệt và cộng hưởng và ^{111m,g}Pd gây bởi nơtron cộng hưởng lần đầu được công bố. Những số liệu khác cũng là nguồn bổ sung quan trọng vào kho số liệu hạt nhân quốc tế.

Chính vì vậy đề tài luận án có tính cần thiết, thời sự, ý nghĩa khoa học và thực tiễn cao.

- *Sự không trùng lặp của đề tài nghiên cứu so với các công trình, luận án đã công bố ở trong và ngoài nước; tính trung thực, rõ ràng và đầy đủ trong trích dẫn tài liệu tham khảo.*

Như được nhắc đến ở trên, nội dung luận án bao gồm nhiều số liệu tỉ số đồng phân lần đầu tiên được công bố. Các số liệu khác có vai trò bổ sung, kiểm chứng chéo với các số liệu khác, luôn là vấn đề cần thiết trong nghiên cứu thực nghiệm. Do vậy, có thể nói rằng đề tài nghiên cứu không bị trùng lặp với các công trình, luận án đã công bố ở trong và ngoài nước. Việc trích dẫn tài liệu tham khảo mang tính trung thực, rõ ràng và đầy đủ.

- *Sự phù hợp giữa tên đề tài với nội dung, giữa nội dung với chuyên ngành và mã số chuyên ngành.*

Có sự phù hợp

- *Độ tin cậy và tính hiện đại của phương pháp đã sử dụng để nghiên cứu.*

Phương pháp nghiên cứu trong luận án là phương pháp kích hoạt mẫu bằng chùm bức xạ hãm và nơtron phát ra sau khi chiếu chùm electon từ máy gia tốc MT25 (tại Viện Nghiên cứu Liên hợp hạt nhân Dubna, Liên bang Nga) vào các bia thích hợp. Các hạt nhân phóng xạ sau phản ứng sẽ phát tia gamma. Bằng cách đo lượng các tia gamma đặc trưng phát ra từ các trạng thái spin thấp và cao, tỷ số đồng phân của các hạt nhân được xác định.

Tia gamma phát ra bởi các hạt nhân trong mẫu kích hoạt được đo bởi detector Germani siêu tinh khiết HPGe có độ phân giải năng lượng cao. Các sản phẩm của phản ứng được nhận diện dựa vào chu kỳ bán rã và năng lượng tia gamma phát ra. Kết quả thu được từ thực nghiệm được so sánh với giá trị tính toán theo chương trình Talys và các giá trị thực nghiệm công bố trước đó. Đối với trường hợp sử dụng bức xạ hãm, phổ năng của chùm được mô phỏng bằng chương trình GEANT4.

Từ đó có thể thấy, phương pháp nghiên cứu là hợp lý và có độ tin cậy cao.

- *Kết quả nghiên cứu mới của tác giả.*

Đối với phản ứng (γ, n), các tác giả đã xác định tỷ số đồng phân của bảy cặp bao gồm $^{195m,g;197m,g}$Hg với năng lượng bức xạ hãm cực đại từ 14 - 24 MeV (bước 1 MeV), ^{152m1,m2}Eu với năng lượng bức xạ hãm cực đại từ 14 - 23 MeV (bước 1 MeV), ^{115m,g}Cd với năng lượng bức xạ hãm cực đại 24 và 25 MeV, các cặp ^{137m,g}Ce, ^{81m,g}Se và ^{109m,g}Pd với năng lượng bức xạ hãm cực đại 25 MeV.

Đối với phản ứng (n,γ), các tác giả đã xác định tỷ số đồng phân của sáu cặp bao gồm $^{109m,g;111m,g}$Pd, $^{115m,g;117m,g}$Cd, ^{137m,g}Ce và ^{81m,g}Se gây bởi nơtron nhiệt và cộng hưởng.

- *Ưu điểm và nhược điểm về nội dung, kết cấu và hình thức của luận án.*

<u>Ưu điểm:</u> Kết quả thực nghiệm phong phú về tỉ số đồng phân của các cặp thu được từ phản ứng gây bởi chùm gamma và nơtron như được nhắc đến ở trên. Bên cạnh đó, mô phỏng thu phổ bức xạ hãm từ chương trình GEANT4 và các tính toán lý thuyết sử dụng

chương trình Talys cũng được thực hiện để so sánh với kết quả đo. Từ đó có thể thấy rằng, phương pháp nghiên cứu là hiện đại và logic, kết quả thu được trong luận án là đáng tin cậy. Luận án cũng bao gồm phần tóm lược các vấn đề vật lý chính liên quan đến chủ đề đang được đề cập, cho thấy một vấn đề khoa học hoàn chỉnh và chặt chẽ.

Nhược điểm: Vẫn còn một số thiếu sót về mặt trình bày, cụ thể như sau:

+ Cần giải thích các đại lượng khi thảo luận (VD: E_u và E_d trong trang 12)

+ Mục 1.3 và 1.3.3 có tên trùng nhau

+ Một số ký hiệu nên được điều chỉnh phù hợp (VD: L nên chuyển thành ΔL trong nhãn của hình 1.4).

+ Nên trình bày tốt hơn ở một số chỗ (VD: trang 27 chỉ có 1 hình 1.6, hay còn nhiều khoảng trống tại các trang 53,58,60,72,78,79, 92).

+ Phần hình nhỏ (inset) trên hình 2.2 nên được giải thích

+ Còn lỗi chính tả (VD: trang 44,46,49,52,68,76,81,93, và 99)

+ Nên chỉnh nhãn của hình 2.7 từ "Gamma Vision Software" thành "The user interface of Gamma Vision Software"

+ Có thể đổi đánh thứ tự 2.5 và 2.6 để phù hợp với thứ tự thảo luận trong luận án.

+ Nên thống nhất cách trích dẫn đến công thức là cho trong ngoặc (VD: công thức (2.20))

+ Nên thống nhất cách kí hiệu các đồng vị để đứng (VD: không nghiêng $^{115m,g}Cd$)

+ Phụ lục A không được nhắc đến trong luận án, nên trích dẫn trong phần 2.2.1

+ Cách diễn đạt câu có chỗ chưa rõ ràng, không đúng bản chất vật lý (VD: trang 56 "Sherical and deformed shapes of $^{151, 153}$Eu are characterized by one peak and two peaks, respectively of the total photoneutron cross sections in Fig. 3.26")

+ Trang 98, Vibrational motion là một biến dạng do dao động tập thể. Nên cần kiểm tra lại khái niệm neutron velence trong câu "…, and ^{74,82}Se and ^{110}Pd are vibrational even-even nuclei owing to the residual interaction among the valence nucleons resulting in the vibrational motion in nuclei, …"

+ Từ trang 99-115 chỉ nên trình bày một số đặc trưng cơ bản của trạng thái hạt nhân như chẵn-lẻ, năng lượng kích thích (E_x) và mật độ mức $\rho(E_x, J^\pi)$. Không nên liệt kê các tham số trong file output để người đọc tự hiểu.

Cần phải nói thêm rằng những thiếu sót chỉ ra ở trên không làm ảnh hưởng đến chất lượng của luận án mà chỉ góp phần hoàn thiện thêm luận án.

- *Nội dung luận án đã được công bố trên tạp chí, kỷ yếu hội nghị khoa học nào và giá trị khoa học của các công trình đã công bố.*

Kết quả thu được từ Luận án được công bố trên các tạp chí là:

+ 05 công bố quốc tế

- 02 bài trên tạp chí Journal of Radioanalytical and Nuclear Chemistry, có chỉ số IF=1.754 năm 2021

- 03 bài trên tạp chí Nuclear Instrument in Physics Research B, có chỉ số IF=1.377 năm 2023

+ 03 công bố quốc gia: trên tạp chí Communications in Physics

+ 02 Báo cáo tại Hội nghị quốc tế

-01 tại Hội nghị "^{28}th International Seminar on Interaction of Neutrons with Nuclei" (2021)

-01 tại Hội nghị "The 7th Academic Conference on Natural Science for Young Scientist, Master and PhD. Student from ASEAN Countries (CASEAN-7)" (2021)

Những tạp chí được nhắc đến ở trên là những tạp chí chuyên ngành có quá trình phản biện chặt chẽ, có uy tín ở trong và ngoài nước. Từ đó có thể thấy rằng các kết quả thu được có độ tin cậy và tính khoa học cao.

- *Kết luận chung cần khẳng định mức độ đáp ứng các yêu cầu đối với một luận án tiến sĩ chuyên ngành. Bản tóm tắt luận án phản ảnh trung thành nội dung cơ bản của luận án hay không; luận án có thể đưa ra bảo vệ cấp Học viện để nhận học vị tiến sĩ được hay không.*

Kết quả trình bày trong luận án là rất phong phú, có độ tin cậy cao, được công bố trên 05 tạp chí quốc tế và 03 tạp chí trong nước như đã nhắc đến ở trên. Chính vì vậy, luận án đáp ứng các yêu cầu đối với một luận án tiến sĩ chuyên ngành.

Bản tóm tắt luận án phản ánh trung thành nội dung cơ bản của luận án.

Luận án có thể được đưa ra bảo vệ cấp Học viện để nhận học vị tiến sĩ.

Hà Nội, ngày 27 tháng 01 năm 2023

Xác nhận của cơ quan công tác

KT. VIỆN TRƯỞNG
TRƯỞNG PHÒNG HÀNH CHÍNH TỔ CHỨ

BỘ KHOA HỌC VÀ CÔNG NGHỆ
VIỆN KHOA HỌC VÀ KỸ THUẬT HẠT NHÂN
VIỆN NĂNG LƯỢNG NGUYÊN TỬ VIỆT NAM

Lưu Trung Hiếu

Người nhận xét

Lê Xuân Chung

(Mẫu 7-HV-Mẫu nhận xét luận án)

BẢN NHẬN XÉT/ PHẢN BIỆN LUẬN ÁN TIẾN SĨ CẤP HỌC VIỆN

Tên đề tài luận án: Nghiên cứu tỷ số đồng phân và các hiệu ứng liên quan trong phản ứng quang hạt nhân và phản ứng bắt neutron.

Chuyên ngành: Vật lý nguyên tử và hạt nhân

Mã số: 9440106

Nghiên cứu sinh: Bì Minh Huệ

Người hướng dẫn: GS.TS. Trần Đức Thiệp

TS. Sergey Mikhailovich Lukyanov

Người nhận xét/ Người phản biện: GS.TS. Lê Hồng Khiêm

Cơ quan công tác:Viện Vật lý

Nội dung nhận xét:

- Tính cần thiết, thời sự, ý nghĩa khoa học và thực tiễn của đề tài luận án.

  Các thông tin về tỷ số đồng phân và các hiệu ứng liên quan là cần thiết cho việc nghiên cứu cấu trúc của hạt nhân. Luận án của NCS đo tỷ số đồng phân của một số đồng vị sử dụng phản ứng hạt nhân gây bởi chùm bức xạ hãm và neutron với năng lượng khác nhau là có ý nghĩa khoa học và có ý nghĩa thực tiễn trong việc cung cấp số liệu để kiểm chứng và hoàn thiện các mô hình về cấu trúc hạt nhân.
- Sự không trùng lặp của đề tài nghiên cứu so với các công trình, luận án đã công bố ở trong và ngoài nước; tính trung thực, rõ ràng và đầy đủ trong trích dẫn tài liệu tham khảo.

  - Đề tài nghiên cứu của luận án không trùng lặp với các công trình, luận án đã công bố ở trong và ngoài nước.

  - Việc trích dẫn tài liệu tham khảo là trung thực, rõ ràng và đầy đủ.
- Sự phù hợp giữa tên đề tài với nội dung, giữa nội dung với chuyên ngành và mã số chuyên ngành.
- Độ tin cậy và tính hiện đại của phương pháp đã sử dụng để nghiên cứu.
- Kết quả nghiên cứu mới của tác giả.

- Ưu điểm và nhược điểm về nội dung, kết cấu và hình thức của luận án.
  - Luận án có nội dung tốt.
  - Kết cấu của luận án hợp lý.
  - Hình thức của luận án tốt.
- Nội dung luận án đã được công bố trong 07 bài báo khoa học trong các tạp chí quốc tế và trong nước và 02 báo cáo trong các hội nghị khoa học được liệt kê dưới đây:

[1]. Bui Minh Hue, Tran Duc Thiep, Truong Thi An, Phan Viet Cuong, S. M. Lukyanov, and S. Mitrofanov . Isomeric ratios in neutron capture reaction, induced by thermal, resonant and mixed thermal-resonant neutrons on 114Cd and 116Cd nuclei. Nuclear Inst. and Methods in Physics Research, B 502, pp. 46-53 (2021).

[2]. Bui Minh Hue, Tran Duc Thiep, Truong Thi An, Phan Viet Cuong, S. M. Lukyanov, A. G. Belov, and S. Mitrofanov. The isomeric ratios in (n, γ) neutron capture reactions on 108Pd and 110Pd nuclei, Journal of Radioanalytical and Nuclear Chemistry 326, no. 1, 503-509 (2020).

[3]. Tran Duc Thiep, Truong Thi An, Phan Viet Cuong, Bui Minh Hue, A. G. Belov, S. Mitrofanov. Isomeric yield ratios of 195m,gHg and 197m,gHg in the 196Hg(γ, n) and 198Hg(γ, n) reactions induced by bremsstrahlung energy within giant dipole resonance region, Nuclear Inst. and Methods in Physics Research, B. 457, 4-9 (2019).

[4]. Tran Duc Thiep, Truong Thi An, Phan Viet Cuong, Nguyen The vinh, Bui Minh Hue, Le Tuan Anh, A. G. Belov. Isomeric yield ratio of 152m1Eu(8-) to 152m2Eu(0-) produced from 153Eu (γ,n) 152Eu reaction in the giant dipole resonance region, J. Radioanal. Nucl. Chem., 317, 1263–1271 (2018).

[5]. Bui Minh Hue, Tran Duc Thiep. Theoretical consideration of isomeric ratios in some photonuclear reactions induced by bremsstrahlung with endpoint energy in giant dipole resonance region using Talys 1.95 code, Nuclear Science and Technology, Vol.12, No. 1, pp. 21-31 (2022).

[6]. Tran Duc Thiep, Truong Thi An, Bui Minh Hue, Phan Viet Cuong, Nguyen Hong Ha, A. G. Belov, S. Mitrofanov. Investigation of the same isomeric pair, produced from different nuclear reactions, Nuclear Science and Technology, Vol.10, No. 1, pp. 01-10 (2020).

[7]. Tran Duc Thiep, Truong Thi An, Bui Minh Hue, Phan Viet Cuong, A. G. Belov, S. Mitrofanov. The nuclear channel effect in the isomeric ratio of the reaction products, Nuclear Science and Technology, Vol.9, No. 1, pp. 09-20 (2019).

[8]. Bui Minh Hue, Tran Duc Thiep, Isomeric Ratios in Several Inverse (γ, n) and (n, γ) Reactions, Proceedings of 28th International Seminar on Interaction of Neutrons with Nuclei (2021).

[9]. Bui Minh Hue, Tran Duc Thiep, Isomeric Ratios in Inverse (γ. n) and (n. γ) Reactions on Ce, Cd, Pd and Se targets, Proceedings of the 7th Academic Conference on Natural Science for Young Scientist, Master and PhD. Student from ASEAN Countries (CASEAN-7), p388-396 (2021).

Các bài báo từ [1] đến [4] được công bố trong các tạp chí thuộc danh mục SCIE. Đây là các tạp chí quốc tế chuyên ngành có uy tín. Điều này khẳng định chất lượng cao của các công bố.

Các bài báo từ [5], [6] và [7] được công bố trong tạp chí Nuclear Science and Technology do Viện Năng lượng Nguyên tử Việt Nam xuất bản. Các bài báo công bố trong tạp chí này được Hội đồng Giáo sư chuyên ngành vật lý cho 1.0 điểm nên có thể xem các bài báo này có chất lượng tốt.

Nội dung của các công bố phản ánh nội dung của luận án.

- Kết luận chung:
  - Luận án đã đáp ứng các yêu cầu đối với một luận án tiến sĩ chuyên ngành.
  - Bản tóm tắt luận án phản ánh trung thành nội dung cơ bản của luận án.
  - Luận án có thể đưa ra bảo vệ cấp Học viện để nhận học vị tiến sĩ.

Xác nhận của cơ quan công tác

TRƯỞNG PHÒNG QUẢN LÝ TỔNG HỢP

VIỆN HÀN LÂM KHOA HỌC VÀ CÔNG NGHỆ VIỆT NAM
VIỆN VẬT LÝ

Võ Thị Xuân Yến

Người nhận xét

Lê Hồng Khiêm

BẢN NHẬN XÉT LUẬN ÁN TIẾN SĨ CẤP HỌC VIỆN

Tên đề tài luận án: **NGHIÊN CỨU TỶ SỐ ĐỒNG PHÂN VÀ CÁC HIỆU ỨNG LIÊN QUAN TRONG PHẢN ỨNG QUANG HẠT NHÂN VÀ PHẢN ỨNG BẮT NEUTRON**

Nghiên cứu sinh: **Bùi Minh Huệ**

Chuyên ngành: **Vật lý Nguyên tử và Hạt nhân**

Mã số: **9440106**

Người hướng dẫn khoa học 1: GS. TS. Trần Đức Thiệp

Người hướng dẫn khoa học 2: TS. Sergey Mikhailovich Lukyanov

Người nhận xét: PGS.TS. Bùi Văn Loát

Cơ quan công tác: Khoa Vật lý, Trường Đại học Khoa học Tự nhiên, ĐHQGHN

A. Nội dung nhận xét:

I. **Tính cần thiết, thời sự, ý nghĩa khoa học và thực tiễn của đề tài luận án:**

Trong những năm gần đây, với sự phát triển nhanh chóng của các cơ sở sản xuất chùm đồng vị phóng xạ cùng với những kỹ thuật và hệ thiết bị ghi nhận thực nghiệm hiện đại, tiên tiến dẫn tới hướng nghiên cứu về đồng phân hạt nhân càng phát triển. Đồng phân hạt nhân có thể được sử dụng trong nghiên cứu cơ bản và ứng dụng, đặc biệt là nghiên cứu các cấu trúc và tính chất của các hạt nhân lạ nằm xa đường bền hoặc sử dụng trong nhiều ứng dụng thiết yếu như y học hạt nhân, pin hạt nhân, đồng hồ hạt nhân,,. Trong nghiên cứu về đồng phân thì tỷ số đồng phân cung cấp những thông tin giá trị về cấu trúc và cơ chế phản ứng hạt nhân liên quan. Tỷ số đồng phân liên quan trực tiếp tới cấu trúc và mật độ mức của hạt nhân kích thích, cơ chế phản ứng và nhiều đặc tính khác. Tỷ số đồng phân có thể là những dữ liệu quý giá để kiểm định các mẫu phản ứng hạt nhân khác nhau. Mục tiêu của luận án:

• Xác định tỷ số đồng phân thực nghiệm của một số hạt nhân trung bình và nặng hình dạng cầu hoặc biến dạng trong phản ứng (γ, n) và (n, γ) tương ứng gây bởi bức xạ hãm và nơtron nhiệt-trên nhiệt.

•.Đánh giá một số hiệu ứng ảnh hưởng tới tỷ số đồng phân như năng lượng kích thích, sự sai khác về spin, sự truyền mô men xung lượng, cấu hình nucleon và hiệu ứng kênh.

•.Luận án đã sử dụng phương pháp thực nghiệm để đo tỷ số tiết đồng phân bằng phương pháp kích hoạt và đo phổ gamma kết hợp tính toán tỷ số đồng phân theo lý thuyết trong phản ứng (γ, n) bằng việc sử dụng mã TALYS 1.95 và công cụ GEANT4.

Các phương pháp nghiên cứu thực nghiệm là phương pháp truyền thống, có độ chính xác và tin cậy. Có thể kết luận luân án có **tính cần thiết, thời sự, ý nghĩa khoa học và thực tiễn.**

II. **Sự không trùng lặp của đề tài nghiên cứu so với các công trình, luận án đã công bố ở trong và ngoài nước; tính trung thực, rõ ràng và đầy đủ trong trích dẫn tài liệu tham khảo:**

Đối tượng nghiên cứu của luận án và nội dung của luận án không trùng lặp với các công trình, luận án đã công bố ở trong và ngoài nước. Luận án có 209 tài liệu tham khảo, các tài liệu tham khảo, luận án đã trích dẫn trung thực rõ ràng và đầy đủ.

III. **Sự phù hợp giữa tên đề tài với nội dung, giữa nội dung với chuyên ngành và mã số chuyên ngành:**

Nội dung luận án phù hợp với tên đề tài và nội dung trình bày trong luận án. Nội dung nghiên cứu của luân án là một trong những hướng nghiên cứu của chuyên ngành Vật lý nguyên tử và hạt nhân.

IV. **Độ tin cậy và tính hiện đại của phương pháp đã sử dụng để nghiên cứu:**

Luận án đã nghiên cứu các phản ứng quang hạt nhân và phản ứng bắt nơtron bằng phương pháp kích hoạt hạt nhân và đo phổ gamma off-line. Nguồn photon hãm và nơtron được tạo ra từ việc sử dụng máy gia tốc điện tử MT-25 của phòng thí nghiệm phản ứng hạt nhân Flerov (FLNR), JINR, Dubna, Nga. Luận án đã tiến hành tính toán tỷ số IR theo các mẫu lý thuyết dựa trên mã TALYS 1.95 và công cụ mô phỏng GEANT4, để so sánh với kết quả thực nghiệm.

Phần thực nghiệm của luận án được thực hiện tại phòng phòng thí nghiệm hiện đại: Phòng phòng thí nghiệm phản ứng hạt nhân Flerov (FLNR), JINR, Dubna, Nga. Phương pháp nghiên cứu thực nghiệm và tính toán lý thuyết là những phương pháp truyền thống và hiện đại có độ tin cậy cao. Các kết quả của luận án đã được công bố trong 9 công trình khoa học trên các tạp chí quốc tế và trong nước có uy tín. Vì vậy có thể kết luận phương pháp nghiên cứu và kết quả công bố trong luận án có **độ tin cậy và tính hiện đại**

V. Kết quả nghiên cứu mới của tác giả:

5.1. Đã tiên hành xác định bằng thực nghiện sự phụ thuộc vào năng lượng của tỷ số đồng phân trong phản ứng (γ, n) trong vùng năng lượng cộng hưởng khổng lồ trên các đồng vị Hg, Eu, Cd, Ce, Se và Pd. Luận án đã nhận diện được 7 cặp đồng phân và tính toán tỷ số đồng phân của $^{195m,g;197m,g}$Hg, ^{152m1,m2}Eu, ^{115m,g}Cd, ^{137m,g}Ce, ^{81m,g}Se và ^{109m,g}P d. ***Tỷ số đồng phân thực nghiệm của ^{195m,g}Hg từ 14 - 24 MeV, ^{197m,g}Hg từ 18 - 24 Mev và ^{152m1,m2}Eu tại 19, 21 và 23 Mev lần đầu được công bố.***

5.2. Đối với phản ứng (n,γ) trên các đồng vị của Pd, Cd, Ce và Se gây bởi neutron nhiệt và cộng hưởng, luận án đã nhận diện được sáu cặp đồng phân và tính tỷ số đồng phân bao gồm $^{109m,g;111m,g}$P d, $^{115m,g;117m,g}$Cd, ^{137m,g}Ce và ^{81m,g}Se. Tỷ số đồng phân của $^{115m,g;117m,g}$Cd và $^{109m,g;111m,g}$P d gây bởi nơtron hỗn hợp nhiệt và cộng hưởng và tỷ số đồng phân của ^{111m,g}P d gây bởi nơtron cộng hưởng lần đầu được công bố. Đặc biệt kết quả nổi bật nhất của luận án này là sự đóng góp các dữ liệu thực nghiệm mới của ^{nat}Eu(γ, n)^{152m1,m2}Eu, ^{nat}Hg(γ, n)$^{195m,g;197m,g}$Hg, ^{nat}Pd(n, γ)^{109m,g}Pd, và ^{nat}Cd(n, γ) $^{115m,g;117m,g}$Cd. đã đóng góp vào thư viện dữ liệu phản ứng hạt nhân thực nghiệm (EXFOR) của Cơ quan Năng lượng Nguyên tử Quốc tế (IAEA). Đây là đóng góp có ý mới của Luận án.

5.3. Luận án đã nghiên cứu một số hiệu ứng ảnh hưởng tới tỷ số đồng phân, bao gồm năng lượng kích thích, cấu hình nucleon, sự sai khác về spin và hiệu ứng kênh phản ứng. Luận án đã nghiên cứu phản ứng đối ngẫu (γ, n) và (n, γ) tạo ra các cặp đồng phân với cùng năng lượng kích thích sản phẩm để thấy được ảnh hưởng của xung và mômen xung lượng coi như là một phần của hiệu ứng kênh.

5.4. Luận án đã tiến hành sử dụng công cụ GEANT4 để mô phỏng phổ bức xạ hãm phát ra từ gia tốc điện tử MT-25 của phòng thí nghiệm phản ứng hạt nhân Flerov

Dubna Nga, kết hợp với mô hình lý thuyết sử dụng mã TALYS 1.95 để tính tính toán tỷ số IR trong phản ứng (γ, n) với năng lượng bức xạ hãm từ 10 - 25 MeV trên bia Se, Pd, Ce, Eu và Hg. Luận án cũng đã khảo sát hàm kích thích với sáu mẫu mật độ mức và tám hàm lực gamma. Xu hướng phụ thuộc vào năng lượng của các kết quả tính toán lý thuyết tương tự đối với kết quả thực nghiệm. Ngoài ra, hiệu ứng cấu hình nucleon cũng được xác nhận trong trường hợp của Hg.

VI. Ưu điểm và nhược điểm về nội dung, kết cấu và hình thức của luận án:

Luận án được viết bằng tiếng Anh, có bố cục rõ ràng hợp lý văn phong dễ hiểu. Luận án có nội dung phong phú, đã tiến hành xác định bằng thực nghiệm kết hợp tính toán lý thuyết tỷ số nhiều cặp đồng phân từ hạt nhân trung bình đế hạt nhân nặng, hạt nhân chẵn – lẻ, hạt nhân lẻ - lẻ và hạt nhân xa đường cong bền, biến dạng cầu. Kết quả thu thu được đều đã được lý giải, bình luận chặt chẽ và so sánh với các kết quả của các tác giả khác.

VII. Nội dung luận án đã được công bố trên tạp chí, kỷ yếu hội nghị khoa học nào và giá trị khoa học của các công trình đã công bố:

1. Bui Minh Hue Tran Duc Thiep. Isomeric ratios in neutron capture reaction, induced by thermal, resonant and mixed thermal-resonant neutrons on ^{114}Cd and ^{116}Cd nuclei. NIM, B 502, pp. 46- 53 (2021).
2. Bui Minh Hue, Tran Duc Thiep.. The isomeric ratios in (n, γ) neutron capture reactions on ^{108}Pd and ^{110}Pd nuclei, Journal of Radioanalytical and Nuclear Chem- istry 326, no. 1, 503-509 (2020).
3. Tran Duc Thiep, Truong Thi An, Phan Viet Cuong, Bui Minh Hue. Isomeric yield ratios of ^{195m,g}Hg and ^{197m,g}Hg in the ^{196}Hg(γ, n) and ^{198}Hg(γ, n) reactions induced by bremsstrahlung energy within giant dipole resonance region, Nuclear Inst. and Methods in Physics Research, B. 457, 4-9 (2019).
4. Tran Duc Thiep, Truong Thi An, Phan Viet Cuong, Nguyen The vinh, Bui Minh Hue, Le Tuan Anh, A. G. Belov. Isomeric yield ratio of ^{152m1}Eu(8-) to ^{152m2}Eu(0-) produced from ^{153}Eu (γ, n) ^{152}Eu reaction in the giant dipole resonance region, J. Radioanal. Nucl. Chem., 317, 1263–1271 (2018).
5. Bui Minh Hue, Tran Duc Thiep. Theoretical consideration of isomeric ratios in some photonuclear reactions induced by bremsstrahlung with endpoint energy in giant dipole resonance region using Talys 1.95 code, Nuclear Science and Technology, Vol.12, No.1, pp. 21–31 (2022).
6. Tran Duc Thiep, Truong Thi An, Bui Minh Hue, Phan Viet Cuong, Nguyen Hong Ha, A. G. Belov, S. Mitrofanov. Investigation of the same isomeric pair, produced from different nuclearreactions, Nuclear Science and Technology, Vol.10, No. 1, pp. 01-10 (2020).
7. Tran Duc Thiep, Truong Thi An, Bui Minh Hue, Phan Viet Cuong, A. G. Belov, S. Mitrofanov. The nuclear channel effect in the isomeric ratio of the reaction products, Nuclear Science and Technology, Vol.9, No. 1, pp. 09-20 (2019).
8. Bui Minh Hue, Tran Duc Thiep, Isomeric Ratios in Several Inverse (γ, n) and (n, γ) Reactions, Proceedings of 28th International Seminar on Interaction of Neutrons with Nuclei, Website: http://isinn.jinr.ru/proceedings/isinn- 28/pdf/HueBui.pdf, (2021).

9. Bui Minh Hue, Tran Duc Thiep, Isomeric Ratios in Inverse (γ, n) and (n, γ) Reactions on Ce, Cd, Pd and Se targets, Proceedings of the 7th Academic Conference on Natural Science for Young Scientist, Master and PhD. Student from ASEAN Countries (CASEAN-7), p388-396 (2021).

Trong 9 công trình trên có 4 công trình đăng trên tạp chí thuộc hệ thống ISI có chỉ số IF cao, 3 công trình đăng trên tạp chí chuyên ngành trong uy tín và 2 báo cáo tại 2 Hội nghị khoa học chuyên ngành. Trong đó tác giả đứng đầu hoặc là tác giả chính của 5 công trình.

Kết luận chung: Bản luận án có chất lượng tốt, Bản luận án đáp ứng tốt các yêu cầu đối với một luận án tiến sĩ chuyên ngành. Bản tóm tắt luận án phản ánh trung thành cơ bản nội dung của luận án.Luận án có thể đưa ra bảo vệ cấp Học viện để nhận học vị tiến sĩ.

Hà Nội, ngày 16 tháng 1 năm 2023

Người nhận xét

PGS.TS. Bùi Văn Loát

Xác nhận của cơ quan công tác

TRƯỜNG ĐẠI HỌC KHOA HỌC TỰ NHIÊN XÁC NHẬN:

Chữ ký của ông bà

PGS. TS. Bùi. Văn. Loát....

Hà nội, Ngày 16. tháng 01. năm 2023.

T/L. HIỆU TRƯỞNG

P. TRƯỞNG PHÒNG

ĐẠI HỌC QUỐC GIA HÀ NỘI
TRƯỜNG ĐẠI HỌC KHOA HỌC TỰ NHIÊN

TS. Nguyễn Thị Hồng Doan

(Mẫu 22-HV-Giải trình sau bảo vệ cấp Học viện)

CỘNG HOÀ XÃ HỘI CHỦ NGHĨA VIỆT NAM
Độc lập – Tự do – Hạnh phúc

BẢN GIẢI TRÌNH CÁC ĐIỂM BỔ SUNG, SỬA CHỮA SAU BẢO VỆ LUẬN ÁN TIẾN SĨ CẤP HỌC VIỆN

Họ và tên NCS: Bùi Minh Huệ

Tên luận án: "Nghiên cứu tỷ số đồng phân và các hiệu ứng liên quan trong phản ứng quang hạt nhân và phản ứng bắt neutron".

Tên tiếng anh: "Study of isomeric ratio and related effects in photonuclear and neutron capture reactions".

Chuyên ngành: Vật lý Nguyên tử và Hạt nhân

Mã số: 9440106

Người hướng dẫn Khoa học: 1. GS. TS. Trần Đức Thiệp

2. TS. Sergey Mikhailovich Lukyanov

Sau phiên họp đánh giá luận án tiến sĩ cấp Học viện, NCS đã chỉnh sửa luận án theo những nội dung sau:

STT	Nội dung đề nghị bổ sung, chỉnh sửa	Nội dung đã bổ sung, chỉnh sửa
1	Một số câu văn chưa rõ nghĩa và vẫn còn lỗi chính tả.	NCS đã chỉnh sửa các câu văn của luận án rõ ràng, dễ hiểu hơn và đã sửa lỗi chính tả.
2	Trong Bảng 3.3 (trang 59) nên cấu trúc lại để có thể thấy rõ ràng hơn những kết quả đóng góp mới của luận án.	NCS đã sửa lại cách trình bày các kết quả đo được và so với các tác giả khác trong Bảng 3.3 cho rõ ràng và sáng sủa.
3	Cần giải thích các đại lượng khi thảo luận (VD: E_u và E_d trong trang 12).	Các đại lượng vật lý sử dụng trong luận án đã được trình bày trong danh sách các đại lượng vật lý trang viii và ix.
4	Mục 1.3 và 1.3.3 có tên trùng nhau.	NCS đã sửa tên mục 1.3.3. Photonuclear reaction (γ, n) thành 1.3.3. (γ, n) reaction.
5	Một số ký hiệu nên được điều chỉnh phù hợp (VD: L nên chuyển thành ΔL trong nhãn của hình 1.4).	NCS đã sửa L thành ΔL trong nhãn của hình 1.4.

6	Nên trình bày tốt hơn ở một số chỗ (VD: trang 27 chỉ có 1 hình 1.6. hay còn nhiều khoảng trống tại các trang 53, 58, 60, 72, 78, 79, 92).	NCS đã chỉnh sửa lại hình thức trình bày cho đẹp hơn, không còn những khoảng trống thừa.
7	Phần hình nhỏ (inset) trên hình 2.2 nên được giải thích.	Phần hình nhỏ trong hình 2.2 là phổ bức xạ hãm đã được chú thích thêm vào tên nhãn của hình.
8	Còn lỗi chính tả (VD: trang 44, 46, 49, 52, 68, 76, 81, 93, và 99).	NCS đã sửa các lỗi chính tả.
9	Nên chỉnh nhãn của hình 2.7 từ "Gamma Vision Software" thành "The user interface of Gamma Vision Software".	NCS đã sửa tên nhãn của hình 2.7 thành "The user interface of Gamma Vision Software".
10	Nên thống nhất cách trích dẫn đến công thức là cho trong ngoặc (VD: công thức (2.20)).	NCS đã sửa lại cách trích dẫn số công thức vào trong ngoặc.
11	Nên thống nhất cách kí hiệu các đồng vị để đứng (VD: không nghiêng ^{115m,g}Cd).	NCS đã sửa lại tất cả tên đồng vị đều viết bình thường không nghiêng.
12	Phụ lục A không được nhắc đến trong luận án, nên trích dẫn trong phần 2.2.1.	NCS đã sửa trích dẫn Phụ lục A trong phần 2.2.1.
13	Cách diễn đạt câu có chỗ chưa rõ ràng, không đúng bản chất vật lý (VD: trang 56 "Spherical and deformed shapes of ^{151,153}Eu are characterized by one peak and two peaks respectively of the total photoneutron cross sections in Fig. 3.26").	NCS đã bỏ câu này do đã đề cập tới hình dạng cầu của hạt nhân ^{151}Eu và biến dạng của hạt nhân ^{153}Eu trước đó.
14	Trang 98. Vibrational motion là một biến dạng do dao động tập thể. Nên cần tra lại khái niệm neutron valence trong câu: "and ^{74,82}Se and ^{110}Pd are vibrational even nuclei owing to the residual interaction among the valence nucleons resulting vibrational motion in nuclei".	NCS đã sửa lại Vibrational motion là một biến dạng do dao động tập thể và không đề cập tới valence nucleons trong trường hợp này nữa.
15	Từ trang 99-115 chỉ nên trình bày một số đặc trưng cơ bản của trạng thái hạt nhân như chẵn-lẻ, năng lượng kích thích và mật độ mức. Không nên liệt kê các tham số trong file output để người đọc tự hiểu.	NCS thấy cần thiết đưa ra một số tham số quan trọng liên quan tới việc tính toán mẫu để những độc giả quan tâm có thể tham khảo hoặc dùng để hiệu chỉnh cho các tính toán khác.

16	Trong mục 2.1.5 của luận án có trình bày về Hiệu chỉnh trùng phùng tổng (Coincidence summing corrections) và phương pháp hiệu chỉnh, về nội dung này cần trình bày rõ cả hai trường hợp: (1) suming out và (2) summing in cũng như phương pháp hiệu chỉnh cho từng trường hợp.	NCS đã trình bày hiệu chỉnh cho trường hợp summing out trong luận án và đã bổ sung thêm phần hiệu chỉnh cho trường hợp summing in.
17	Khi trình bày về đo hoạt độ của mỗi đồng vị phóng xạ cần nói cụ thể (những) tia gamma đã được sử dụng.	NCS đã trình bày các tia gamma sử dụng để đo hoạt độ trong các bảng 3.1, 3.5, 3.9, 3.13 và 3.19.
18	Phần tổng quan khá dài và chi tiết, có thể phân bổ lại để sử dụng một phần làm nội dung cho phần 2.	Phần tổng quan của luận án chiếm 36 trang, phần 2 là phương pháp thực nghiệm và tính toán lý thuyết chiếm 15 trang. Còn phần 3 là kết quả và thảo luận chiếm 60 trang. NCS thấy sự phân bổ này là hợp lý và đúng theo quy định của Học viện.

Hà Nội, ngày 06 tháng 03 năm 2023

Đại diện tập thể hướng dẫn

Trần Đức Thiệp

Nghiên cứu sinh

Bùi Minh Huệ

Thư ký

Ngô Hải Tân

Chủ tịch

Nguyễn Văn Đỗ

Xác nhận của Cơ sở đào tạo

KT. GIÁM ĐỐC

PHÓ GIÁM ĐỐC

HỌC VIỆN KHOA HỌC VÀ CÔNG NGHỆ

VIỆN HÀN LÂM KHOA HỌC VÀ CÔNG NGHỆ VIỆT NAM

Nguyễn Thị Trung

VIỆN HÀN LÂM
KHOA HỌC VÀ CÔNG NGHỆ VN
HỌC VIỆN KHOA HỌC VÀ CÔNG NGHỆ

CỘNG HÒA XÃ HỘI CHỦ NGHĨA VIỆT NAM
Độc lập - Tự do - Hạnh phúc

Hà Nội, ngày 22 tháng 02 năm 2023

DANH SÁCH CHỮ KÝ THÀNH VIÊN HỘI ĐỒNG BẢO VỆ LUẬN ÁN TIẾN SĨ CẤP HỌC VIỆN

Nghiên cứu sinh: Bùi Minh Huệ

Tên đề tài tiếng Việt **Nghiên cứu tỷ số đồng phân và các hiệu ứng liên quan trong phản ứng quang hạt nhân và phản ứng bắt neutron**

Tên đề tài tiếng Anh: **Study of isomeric ratio and related effects in photonuclear and neutron capture reactions**

Chuyên ngành: Vật lý nguyên tử và hạt nhân
Mã số: 9 44 01 06.

Ngày bảo vệ: 22/02/2023

Số Quyết định thành lập Hội đồng: 2304/QĐ-HVKHCN ngày 29/12/2022 của Giám đốc Học viện Khoa học và Công nghệ.

Số TT	Họ và tên, học hàm, học vị	Chức danh trong Hội đồng	Chữ ký
1	GS.TS. Nguyễn Văn Đỗ	Chủ tịch	
2	PGS.TS. Nguyễn Trung Tính	Phản biện 1	
3	PGS.TS. Nguyễn Quang Miên	Phản biện 2	
4	TS. Lê Xuân Chung	Phản biện 3	
5	GS.TS. Lê Hồng Khiêm	Ủy viên	
6	PGS.TS. Bùi Văn Loát	Ủy viên	
7	TS. Ngô Hải Tân	Thư ký	